C A N A D A /FEDERAL REPUBLIC OF G E R M A N Y

SCIENCE & TECHNOLOGY COOPERATION AGREEMENT

SUMMARY REPORT OF THE

WORKSHOP ON

REMOTE SENSING OF FLUORESCENCE SIGNALS

COORDINATED BY
HOWARD EDEL and HELMUT BIANCHI

OTTAWA, OCTOBER 14-17, 1986

Canada

Fisheries and Oceans | Pêches et Océans

C A N A D A /FEDERAL REPUBLIC OF G E R M A N Y
SCIENCE & TECHNOLOGY COOPERATION AGREEMENT

SUMMARY REPORT OF THE

WORKSHOP ON

REMOTE SENSING OF FLUORESCENCE SIGNALS

COORDINATED BY
HOWARD EDEL and HELMUT BIANCHI

OTTAWA, OCTOBER 14-17, 1986

Canada

Fisheries and Oceans | Pêches et Océans

C A N A D A /FEDERAL REPUBLIC OF G E R M A N Y

SCIENCE & TECHNOLOGY COOPERATION AGREEMENT

SUMMARY REPORT OF THE

WORKSHOP ON

REMOTE SENSING OF FLUORESCENCE SIGNALS

OTTAWA, OCTOBER 14-17, 1986

Canada

Executive Summary

The Canada/Germany workshop in Ottawa, from October 14-17, 1986 was held to strengthen the bilateral collaboration building on the joint FLUREX campaigns and Fluorescence Line Imager oceans monitoring program. The respective industrial capabilities have matured to a stage where a consortium led by Messerschmidt-Boelkow-Blohm (MBB) of Germany and Moniteq of Canada is prepared to propose an imaging spectrometer system for the Earth Observation Program of the European Space Agency.

The results of the workshop can be summarized into five items for cooperation.

1. Scientists of Canada and Germany plan to continue joint scientific studies and applications development of imaging spectrometers. Respective new projects will be prepared for May 1987 discussion.

2. The priorities for a scientific program concerning the marine environment were identified as development of spectral data bank, determination of productivity from observed fluorescence, development of algorithms to correct the atmospheric influence and finally exploration of the use of expert systems for an enhanced spectral image analysis tool.

3. The area of cooperative scientific projects using imaging spectrometers is recommended to be expanded to include forest stress monitoring, cloud height determination, cloud optical depth, water vapour column content and spectral snow albedo.

4. The respective industries of Canada and Germany are encouraged to develop a framework for cooperative development of future space borne imaging spectrometers. To ensure that requirements of the users are met, close cooperation with the scientific team is suggested. The plan implies the commercialization of government supported technologies.

5. The coordinators will report workshop results to their respective governments and prepare a coordinated report to the European Space Agency.

GERMANY/CANADA SCIENCE AND TECHNOLOGY AGREEMENT
WORKSHOP
ON REMOTE SENSING OF FLUORESCENCE SIGNALS

Ottawa

October 14 - 17, 1986

---

1. Background and Present State of Cooperation

1.1 Under the umbrella agreement on cooperation in research and technology, signed by the governments of the Federal Republic of Germany and Canada in 1971, a project is being carried out, focussing on the measurement of chlorophyll "a" in the sea. Within the course of the project experts from both sides established close personal links and joint experiments were carried out. For example the FLUREX 1982 campaign over the Baltic and North Sea provided synchronized imaging from space and aircraft with sea truth measurement from German research vessels and from the German North Sea research platform. Several German sensors along with a Canadian spectrometer, were flown yielding valuable scientific results concerning methodology to map the plankton distribution in coastal waters. Besides the joint activities, each side continued scientific investigations on its own initiative, developing a high level of expertise and international recognition.

1.2 Within Canada's national programme a Fluorescence Line Imager (FLI) was developed and flown for various applications, not only in the marine environment for sensing plankton and bathymetric purposes but also for terrestrial applications, mainly in forest stress monitoring.

A high resolution "Reflective Optics System Imaging Spectrometer (ROSIS)" was studied on the German side for space application. An airborne version will be built and tested in the forthcoming months.

1.3 Both the German and Canadian partners have a distinct interest in being involved in the development and application of a space borne fluorescence imaging spectrometer.

1.4 Due to their expertise German and Canadian scientists involved in the FLUREX campaigns were contracted by the European Space Agency (ESA) to conduct a study on the chlorophyll measurement in the sea. Results of their investigations, also including those of the Canadian Scientists within the joint FLUREX 1982 campaign, will be reported in a special ESA meeting in France in November 1986.

1.5 The joint German/Canadian project has reached a stage of maturity justifying the need to evaluate results accomplished by now and to agree on priorities for future work. A workshop was considered the appropriate means. It was organized by Helmut Bianchi and Howard Edel with valuable assistance from Jim Gower and Heinz van der Piepen.

The workshop was held in Ottawa, from October 14 to 17, 1986 and was attended by 41 participants from Germany and Canada (Annex 1). The programme of the workshop (Annex 2) comprised 26 presentations .

The workshop was judged to be very successful. A unique opportunity was offered to experts of both countries concerned with the theory and application of chlorophyll fluorescence spectroscopy.

The lively and constructive discussions between scientists, representatives of industry, university and government agencies led to a number of conclusions and suggestions which are detailed in section 2.

2.0 Conclusion/Suggestions

2.1 General Conclusions

2.1.1 The presentations given at the workshop will be compiled and made available to the participants and others interested in high spectral resolution imaging.

2.1.2 Similar workshops should be held from time to time. These could focus on more specific topics of mutual interest. It will be decided on a case-by-case basis to what extent scientists from other countries should also be invited.

2.1.3 Cooperative work in the ongoing project should be continued with close contacts between users and manufacturers.

2.1.4 Any further joint action is to match with the respective national priorities and should comply with international efforts. Basic work with regard to the understanding of mechanisms as well as the application of remote sensing techniques should be encouraged.

2.2 Future Scientific Cooperation

The participating scientists including the joint FLUREX group expressed their considered direct wishes and requirements for future work and action as follows:

2.2.1 Scientific activities in the area of phytoplankton related to chlorophyll fluorescence were ordered according to the following priorities.

- High spectral resolution study of atmosphere effects in the fluorescence region leading to optimized algorithms.
- Study effects of interfering substances by applying inverse modelling to corrected data.
- variations in fluorescence yield: inference of productivity.

- other potential targets in water: establishment of a library of verified spectra of inherent optical coefficients and upward radiances.

These priorities will be taken into account in the continuation of the bilateral cooperation in remote sensing fluorescence signals in the sea. Respective new well defined projects (proposals) detailing the specific objectives, project partners, work plan, mile stones etc. will be submitted to the coordinators by the end of 1986.

- Data bank
  Spectra, optional parameters, concentrations of substances and pigments drawn from:
  - existing data
  - new data
  Groups involved: IOS, GKSS, UNIV. OLDENBURG
  Project may be started soon

- Expert system based image processing with an interface to the Data bank including additional data such as typical value for areas, seasons etc.
  Groups involved: MEDS, IOS, GKSS, DFLR
  Project needs a longterm cooperation

- Fluorescence - Chlorophyll - Productivity
  ie. compare blue/green, fluorescence, fluorescence regression slope applying fast productivity measuring techniques.
  Requirement: new comparative algorithms must be developed.
  new experiments in case 1 waters.
  Groups involved: IOS, BIO, GKSS, UNIV. OLDENBURG
  Project needs a longterm cooperation

- Atmosphere's influence and inverse techniques using full reflective spectrum.
  Groups involved: IOS, GKSS
  Project to be started soon.

Some of the new projects will start immediately and be of shorter duration, some of them will demand work over years.

The FLUREX group recognized the need for additional expertise concerning the relation between fluorescence and productivity. Since the Marine Environmental Laboratory of the Bedford Institute of Oceanography has established expertize in this area, it is suggested that this group be encouraged to participate in joint studies.

With respect to the development of an expert system for the improved interpretation of ocean colour data, the participation of the Canada Centre of Remote Sensing should be promoted.

An equivalent group of experts has to be identified on the German side.

Any scientific contribution from any other group would be welcome.

Roland Doerffer (GKSS-Research Center, Geesthacht) and Jim Gower (Institute of Ocean Sciences, Patricia Bay) were confirmed as coordinators of the scientific programme. The coordinators, Bianchi and Edel, should be kept informed of progressing developments.

2.2.2 It has been recognized that an imaging spectrometer is also a valuable tool for other areas of research such as forestry and meteorology. It is suggested that the coordinators of the workshop take action with regard to requesting other user groups to set their priorities and requirements for a space borne imaging spectrometer and to ask for their support concerning construction and operation of such a device. The areas of forestry, cloud height determination, cloud spectral snow albedo are of utmost interest.

As far as environmental monitoring is concerned, reference is also made to the German/Canadian cooperation in this area. The coordinators of that programme will be approached.

2.3 Cooperation of and with industry and the European Space Agency (ESA).

As far as definition and promotion, as well as design development and operation of a suitable instrument is concerned the following conclusions were drawn:

2.3.1 The scientists expressed their considered requirement for a high spectral resolution imaging spectrometer. The integration of such device in a polar platform is highly desired. Appropriate actions are to be taken to submit a proposal to ESA within the Earth Observation Programme (EOP).

2.3.2 The German and Canadian industries, having carried out extensive research and development and/or built an imaging sensor devise (compare item 1.2), are requested to come to an agreement on the cooperation aiming at the joint development of a space-borne high resolution spectrometer and to integrate competent firms from other European countries. This consortium is encouraged to submit a proposal to ESA under the EOPP.

The FLUREX group will provide its expertise to advise the industrial development of the instrument, in support of any industrial cooperation which may finally be agreed and accepted by ESA.

2.3.3 The coordinators of the workshop are requested to take appropriate action aiming at a special presentation to ESA to fulfill their wish of being familiarized with the results and conclusions of the workshop.

The coordinators are also requested to report to their respective governments and to ask for their coordinated support in relation to ESA.

It is understood that any action is to match with the respective national concerns and priorities.

3. General Actions

This summarizing report of the coordinators of the workshop will be presented to all participants, to the governmental departments which are responsible for German/Canadian operations and to ESA.

A special report will be given and new project sheets to will be tabled for the next round of consultations on bilateral cooperation in science and technology, planned for May 1987.

Ottawa, October 22, 1986

Helmet Bianchi
German Coordinator for the
Bilateral Cooperation in
Science and Technology

Howard Edel
Remote Sensing Coordinator
of the Canadian Department
of Fisheries and Oceans

October 14-15, 1986

ATTENDEES

Name	Affiliation	Telephone No.
Helmut Bianchi	GKSS	04752/12-675
Heinz van der Piepen	DFVLR	08153-28878
Bernd Kunkel	MBB	(89)-6000-4761
Gary Borstad	Borstad Associates	(604) 656-5633
Nigel Denyer	CCRS	(613) 993-5012
Dick MacLoed	Consult.	(613) 224-2519
Jim Gower	DFO/IOS	(604) 656-8258
Herbert Winkenbach	DFVLR	02203/601-2863
Dawson Truax	Apocalypse Ent.	(604) 388-4520
Hartmut Grassl	GKSS	00494-152/12833
Dave Kendall	Space Division/NRC	990-0790
John Hall	Oceans Newsmagazine	(613) 733-4335
Jack Gibson	CCRS	(613) 998-9060
Susan Till	CCRS	(613) 998-9060
Fabian McDougall	DSS	(613) 997-7348
Maynard Dokken	DSS	(613) 997-7340
Roger Buxton	Moniteq	(416) 669-5334
Ian Ross	OCRS/Toronto	(416) 965-8411
Tom Alföldi	CCRS	(613) 993-9890
M-C Mouchot	CCRS	(613) 993-9900
R.A. Neville	CCRS	(613) 998-9060
T. Platt	DFO/BIO	(902) 426-3793
Richard Swann	M.D.A.	(604) 278-3411
Parvez Kumar	NRC/Space Division	(613) 990-0787
Allan Hollinger	Moniteq	(416) 669-5334
Roger Buxton	Moniteq	(416) 669-5334
Dave McLaughlin	OME	(416) 965-4516
Ken Yuen	DFO/OSD	(613) 990-0311
John Miller	York University	(416) 736-2100
Nelson Freeman	Radarsat	(613) 998-6735
Brenda Topliss	DFO/BIO	(902) 426-8353
Roland Doerffer	GKSS	04752/12-675

October 17, 1986

ATTENDEES

Name	Affiliation	Telephone No.
Howard Edel	DFO/OSD	(613) 990-0314
Bernd Kunkel	MBB	(89)-6000-4761
Roger Buxton	Moniteq	(416) 669-5334
Brenda Topliss	DFO/B.I.O.	(902) 426-8353
Kurt P. Günther	University Oldenburg	0441-798-3518
Heinz van der Piepen	DFVLR	08153-28878
Jim Gower	DFO/IOS	(604) 656-8258
Rainer Reuter	University Oldenburg	441-798-3522
Allan Hollinger	Moniteq	(416) 669-5334
Richard Swann	M.D.A.	(604) 278-3411
Robert M. Vaive	M.O.S.S.T.	(613) 998-8656
R. O'Neil	CCRS/DAD	(613) 998-9060
Helmut Bianchi	GKSS-1B	04152/12-675
Maynard Dokken	DSS	997-7340
Jürgen Fischer	GKSS	04152 12 851
S.L. Britton	Ontario International Corp. (Ontario Government)	(416) 965-3013
Gary Borstad	Borstad Associates	(604) 656-5633
R.A. Neville	CCRS	(613) 998-9060
C.D. Anger	ITRES Res/Un. of Calgary	(403) 274-7440
Hartmut Grassl	GKSS	00494-152/12833
Herbert Winkenbach	DFVLR	02203/601-2863
Nigel Denyer	CCRS	993-5012
Bob Neville	CCRS	998-9060
M-C Mouchot	CCRS	993-3295
Joseph Cihlar	CCRS	993-9883
Norm O'Neill	Cartel (Un. de Sherbrooke)	(819) 821-7000 ext. 3273
D. Bradford	DFO/OSD	990-0308
Ken Yuen	DFO/OSD	990-0311
Ben Gailor	External Affairs	995-8783
Ralph Baker	CCRS	(613) 952-0770
Roland Doerffer	GKSS	04152/12-675

CANADA-GERMANY WORKSHOP ON IMAGING SPECTROMETRY

PROGRAM

Day 1: Tuesday October 14

INTRODUCTION, HISTORY AND COOPERATIVE FRAMEWORK

0900-0915 Welcome/Introduction/Purpose
Bill Doubleday

0915-0930 History (1974-1984) of water colour work in Canada
Jim Gower

0930-1000 Overview of German water colour work
Roland Doerffer/Heinz Van der Piepen

1000-1020 The German-Canadian 'agreement on technical cooperation'
Doug Bradford/Helmut Bianchi

break

THE FLUORESCENCE LINE IMAGER

1040-1100 The Fluorescence Line Imager, a conceptual overview
Jim Gower

1100-1120 Optics aspects of the FLI (design, alignment, and calibration)
Al Hollinger

1120-1140 Designing a flexible sensor; Electronics and software design of the FLI
Cliff Anger

1140-1200 FLI data handling software written at IOS
Dawson Truax

lunch

PHYTOPLANKTON CHLOROPHYLL FLUORESCENCE, 1^{o} PRODUCTION + AIRBORNE SURVEYS

1330-1350 Biophysics of chorophyll fluorescence
Kurt Gunther

1350-1410 Measurement of chlorophyll fluorescence in water
Roland Doerffer

1410-1430 Measurement of chlorophyll fluorescence in water
Brenda Topliss

1430-1450 Using chlorophyll fluorescence to estimate primary production
Trevor Platt

break

1510-1530 Airborne phytoplankton surveys of in vivo chlorophyll fluorescence, the Canadian experience
Gary Borstad

1530-1550 Airborne remote sensing of chlorophyll fluorescence signals
Heins Van der Piepen

1550-1610 Extraction of chlorophyll fluorescence signals from atmospheric effects in the red spectral region
Jurgen Fischer

1610-1630 Yellow substance monitoring
Rainer Reuter

Day 2: October 15

APPLICATIONS OF HIGH SPECTRAL RESOLUTION IMAGING

0900-0920 DFO water colour applications of the FLI
Gary Borstad

0920-0940 Use of the FLI for forest stress detection
John Miller

0940-1000 Use of the FLI for forest species identification
Don Leckie

1000-1020 Use of the FLI for passive hydrography
Norman O'Neill

break

1050-1110 Use of the FLI for aquatic vegetation mapping
Marie-Catherine Mouchot

1110-1130 Possible further applications of imaging spectrometers for earth observations
Hartmut Grassl

1130-1150 A working group study of optical sensors for a Polar orbiter platform
Susan Till

Lunch

LOOKING FORWARD TO THE NEXT GENERATION OF REMOTE SENSING SYSTEMS

1400-1420 Reflective Optics System Imaging Spectrometer (ROSIS)
Bernd Kunkel

1440-1500 The Viking CCD imager (title uncertain)
Cliff Anger

break

1530-1550 Open discussion and workshop summary
Jim Gower/Hartmut Grassl

Day 3: Thursday, October 16

TECHNICAL VISITS, time table on separate sheet

Canada/Germany Workshop

Visiting Schedule

Thursday, 16 October 1986

9:00 - 9:45	Visit NRC Space Vision System Mr. Richard Hughes - 993-5647
10:00 - 10:45	Coffee & bus ride to CRC
10:45 - 12:15	Visit David Florida Lab. Dr. Rolf Mamen - 998-2383
12:30 - 13:30	Lunch
14:00 - 15:00	Visit CCRS Woodward Drive Dr. David Goodenough
15:30 - 17:00	Visit CCRS Limebank Road Hunt Club - Dr. R. O'Neil Dr. L. Gray Dr. R. Neville

M.C. Mouchot

Engineer degree in Geodesy 1982 - France

M.Sc. Remote Sensing 1984 - Quebec

Working with CCRS/Application Division since 1985 for applications in oceanography.

Involved with SST recognition with NOAA-AVHRR and Landsat TM, seaweed mapping with MEIS and FLI and sediment mapping with TM.

Gary Borstad

1978 Ph.D. - phytoplankton biology western tropical Atlantic (Barbados)

- large area distributions got him interested in remote sensing (Apollo-Soyuz project)

- Came to West Coast, began to work with Jim Gower in 1978 on development of fluorescence technique for survey purposes.

- His work has taken him to Arctic several times with the air borne spectrometer.

- Also involved in analysis of FLI data for water applications.

Don Leckie

Project Leader: Digital Remote Sensing Project
Petawawa National Forestry Institute
Canadian Forestry Service
Chalk River, Ontario

B.Sc. Engineering, University of Manitoba

Ph.D. (Remote Sensing), University of British Columbia

Employed at PNFI since 1980

Interests:

- Use of airborne sensors for determining forest stand parameters.

- Use of airborne and satellite remote sensing techniques for forest damage assessment.

Dr. Susan M. Till joined the Sensor Development Section of the Canada Centre for Remote Sensing in 1981, as research scientist, and has worked since then on the design, development and evaluation of active and passive electro-optical systems for remote sensing. These systems have included the airborne laser fluorosensor, for marine pollution detection, the lidar bathymeter, for water depth measurement, and the multispectral pushbroom imager, MEIS II. She is a member of the Radarsat optical working group, and has been acting Head of Sensor Development Section since 1985.

She received the degrees of MA and PhD from the University of Cambridge, where she carried out research in laser spectroscopy and interferometry. She continued her research in spectroscopy at the Herzberg Institute of the National Research Council of Canada, and then joined the electro-optical systems section of Barringer Research Ltd., Toronto, where she was project scientist on the ground support equipment for the Haloe Shuttle experiment.

Trevor Platt

Head of Biological Oceanography in the Marine Ecology Laboratory at the Bedford Institute of Oceanography, Dartmouth, Nova Scotia.

Interested in physiological ecology of phytoplankton; structure and function of pelagic ecosystem; CO_2 budget of the ocean on global scale; extraction of ecologically-useful information from remotely-sensed ocean colour data.

Dr. Brenda J. Topliss

B.Sc.	:	Physics, University of Durban, U.K.
M.Sc.	:	University College of North Wales, U.K. in Physical Oceanography
Industry	:	Marine Investigation Sources Ltd., North Seal Oil Surveys, effluent dispersal and oil spill modelling.
P.G.D. 1977	:	Physical Oceanography (study in Optical Oceanography) U.C.N.W. Banger, Wales, U.K.
University: Researcher 1977-1979		Multi-disciplinary research group. Study of discontinuities in Liverpool Bay at U.C.N.W.
Visiting Fellow (Canada)	:	Optics for sedimentalogy/remote sensing & image analysis. Atlantic Geoscience Centre, Geological Survey of Canada at Bedford Institute of Oceanography.
Research Scientist 1982	:	Remote Sensing for Department of Fisheries and Oceans at B.I.O. in Atlantic Oceanographic Laboratory.

Present work consists of remote sensing for physical: working infra-red satellite data for physical oceanography studies; at present working on upwelling studies (with B. Petrie, AOL).

Geology: sediment mapping at high latitude using satellite and aircraft data (with C. Amos, AGC).

Biology: ocean colour algorithm development; fluorescence studies linked to FLI development (with T. Platt, MEL).

Much of the remote sensing work consists of working with different disciplinary groups or research workers tackling specific problems connected with either remote sensing or image analysis.

Analysis of Test and Flight Data from the Fluorescence Line Imager

About the Authors

Gary Borstad was born on September 3, 1948 in Sexsmith, Alberta. He obtained a bachelor's degree at the University of Alberta in 1970, a master's (C4) in oceanography at the University of Paris, France, and a Ph.D. in Marine Science at McGill University in 1978. His Ph.D. thesis was on plankton biology in the tropical Atlantic. He has since worked on biological oceanography on the west coast of Canada and in the Canadian Arctic, with a particular emphasis on the application of remote sensing techniques. Recent projects include analysis of satellite ocean thermal and colour imagery, and airborne spectroscopic data to study phytoplankton, fish, and whale ecology.

Howard Edel was born on February 6, 1945 in Grandview, Manitoba. He obtained a diploma in Electronic Technology from the Northern Alberta Institute of Technology in 1965 and a bachelor's degree in Electrical Engineering at the University of Ottawa in 1972. He has worked as a computer systems analyst and implemented special hardware and software interfaces to digital computers at the National Research Council of Canada and the Canada Centre for Remote Sensing. Since joing the Department of Fisheries and Oceans he has been responsible for departmental remote sensing policy and applications project coordinator. Recently he has led the development of the imaging spectrometer instrument and coordination of international cooperation on satellite optical sensor systems development.

Jim Gower was born on July 25, 1940 in Beer, Devon, England. He obtained a bachelor's degree at the University of Cambridge, England in 1962, and a Ph.D. in radio-astronomy at the same university in 1966. In England and at the University of British Columbia after his move to Canada in 1967, he has worked in astronomy. In 1971 he joined the newly formed Institute of Ocean Sciences, Sidney, B.C., as the head of the remote sensing group. He has been involved with several NASA satellite projects, such as Seasat, which carried radar sensors, and Nimbus 7, which carries the Coastal Zone Color Scanner. Recently, he has concentrated on development of improved techniques for mapping phytoplankton concentrations from aircraft and satellites.

Allan B. Hollinger is Chief Scientist at Moniteq Ltd. where he has been responsible for the development of electro-optic systems. He received his degrees in physics from McGill University and the University of Toronto. He is a member of the Optical Society of America and the Canadian Association of Physicists.

John R. Miller

Associate Professor of Physics, York University, Toronto

- Received a B.E. in Engineering Physics, M.Sc. and Ph.D. (1969) in Space Physics from the University of Saskatchewan, Saskatoon, Saskatchewan.

- Spent 2 years at the Herzberg Institute, National Research Council of Canada in Ottawa as a Post Doctoral Fellow.

- Served as a Project Scientist at York University on instrumentation development for Remote Sensing for two years.

- Joined York University faculty in 1974. Current active research interests include water colour interpretation, bathymetry using passive remote sensing, atmospheric correction methodology, spectral geobotany.

- Involvement with the FLI began with participation in the CCUSS feasibility study that culminated in the design and construction of FLI.

- Specification of FLI configuration to study the vegetation red reflectance edge for flights in Vermont, Ontario in 1985 and in Europe in 1986 to study vegetation stress. Recent work includes the development, in collaboration with Moniteq Ltd., of analysis software to deduce images of red edge variations.

Dawson Truax

(Apocalypse Enterprises, Victoria)

Software support at IOS since 1973

Satellite software (CFCS, NOAA)

IOS Spectrometer Software

IOS Image Processing System

FLI software

Dr. H. van der Piepen

Dr. Ing. Heinz van der Piepen studied Physics and Electrical Engineering at the Technical Universities in Munich and in Berlin. He worked 15 years in the field of applied spectroscopy and remote sensing at the CSIR in South Africa and at NASA in the U.S.A. In 1978 he joined the Institute for Optoelectronics of the DFVLR in Oberpfaffenhofen. His main interest is the remote sensing, technology and interpretation of ocean color. In context with this activity he is also member of ESA's Ocean Color Working Group.

Roland Doerffer

University of Hamburg study of Biology, Hydrobiology and Fishery Research, Biochemistry

1972 : Degree Diplom Biologe

1978 : Doctor degree in Biology

1974-1978: Scientist Sonderforschungsbereich Meeresforschung (Marine Research) University of Hamburg, Remote Sensing of Sea Water Constituents

Since 1978: Scientist GKSS Forschungszentrum Geesthacht, Institute of Chemistry

Since 1983: Head of the Department of Applied Remote Sensing in the GKSS Institute of Physics

Dr. Juergen Fischer

GKSS-FORSCHUNGSZENTRUM GEESTHACHT GMBH
Institute of Physics
Department of Optical Remote Sensing
Max-Planck-Str.
D-2054 Geesthacht

Education: M.Sc. in Meteorology, University of Berlin
Ph.D. in Meteorology, University of Hamburg

Dr. Juergen Fischer has been working in the field of remote sensing, especially of modelling the radiative transfer in ocean and atmosphere. Before he joined GKSS in 1982, he worked at the Max-Planck-Institute of Meteorology. During the last two years he concentrated on the evaluation of aircraft and C Z C S measurements, on the development of inverse modelling techniques for the separation of different water substances from spectral measurements, and on the modelling of the sun stimulated chlorophyll fluorescence.

Dr. Kurt P. Günther

University: Oldenburg
FB 8-Physics
Department of Applied Optics
Car v. Ossietzky Str.
P.O. 2503
D-2900 Oldenburg

Function : Project Manager, Research Scientist
Responsibility: Research
- development of airborne laser fluorosensors
- field experiments with aircraft
- lidar data processing and interpretation
- laboratory research concerning chlorophyll a fluorescence of phytoplankton and terrestrial plants

Education
- lessons for graduate level
- supervision of diploma

Education : M.Sc. in Physics, University of Munich
Ph.D. in Physics, University - Oldenburg

Dr. K.P. Günther has been working since 1978 in the field of remote sensing. His special interest was dedicated to the development of airborne laser fluorosensors to monitor the concentration of artificial dyes (e.g. Rhodamine), of yellow substance and chlorophyll a. He participated in several regional oceanographic experiments as FLUREX '82 and '85, ADRIA '84, ARCHIMEDES 'I and 'II, partly as coordinator of subprograms. Beside the development of the lidar systems he was engaged in modelling the variable fluorescence efficiency of phytoplankton chlorophyll a to get a better understanding of in situ and airborne fluorosensor data. New activities grew up with the successful application of the concept of variable fluorescence by monitoring forest decline with airborne lidar systems.

Bernd Kunkel

Messerschmitt-Bölkow-Blohm GmbH
MBB-ERNO Space Systems Group
Space Instrumentation Dep.
Postbox 80 11 69
D-8000 Muenchen 80

Education : Diploma in Physics, University of Marburg/F.R.G. in 1969

Age : 44

Professional Career :

- since 1969 with M.B.B. Ottobrunn/Munich, Space Systems Group
- since 1971 main activities in remote sensing studies (systems, instrumentation mainly)
- since 1978 specialised in optoelectronics instrumentation, emphasis (but not exclusively) on push-broom instruments (MOMS, SWIR-MOMS), matrix CCD systems, laser sensors, essentially IR sensors, as project manager
- since 1979 studying imaging spectrometer concepts; in 1985 study manager of "Chlorophyll Scanner for Spaceborne Fluorescence Measurements", leading to the ROSIS concept; responsible project manager for ROSIS development
- several publications on preceding activities, 2 papers on ROSIS: ISPRS/Stuttgart and IGARSS/Zürich, September 1986.

Dr. Herbert Winkenbach

DFVLR
5000 Köln 90

Scientific/Professional Background

1952 : Diploma thesis in the field of Solid State Physics at University of Stuttgart

1952-1960: Scientific research in Nuclear Physics for doctor thesis at University of Göttingen

1960-1970: Project Engineer/Manager for Plasma Physics equipments; Nuclear Heated Thermionics and Incore Thermionic Reactors for space power units at BBC firm, Mannheim

1970 -

up to now: Management within DFVLR for Federal Ministry for Research and Technology (BMFT) sponsored scientific and technical projects, mainly in the field of Extraterrestrical Physics and since 1981 Remote Sensing.

Rainer Reuter

University of Oldenburg
Physics Department
Fed. Rep. Germany

1969-1975: Studies in Physics and Oceanography at the Universities of Heidelberg and Kiel.

Feb. 1979: Ph.D. degree in physics from University of Kiel. Thesis concerned the investigation of marine suspended matter with in situ light scattering methods.

1978-1979: GKSS Forschungszentrum Geesthacht. Development and realization of a sensor system for monitoring of river water quality, particularly of thermal plumes; including current measurements from moving boats.

Since 1980: University of Oldenburg. Areas of work include development of the airborne laser fluorosensor, investigation of hydrographic parameters with optical methods, and teaching in physics, oceanography and remote sensing.

Since 1982: Head of the Remote Sensing Working Group at the Physics Department. Projects in laser remote sensing of the sea, particularly the investigation of hydrographic frontal systems, of marine pollution monitoring, and of satellite ground truth collection.

Professor Hartmut Grassl

Director of the Institute of Physics
GKSS-Research Centre
MS in Physics from Munich University
Ph.D. in Meteorology Much University

Present Fields of Research:

- Remote Sensing of Ocean and Atmosphere
- Climate Modelling
- Estuarine Research

Helmut Bianchi

Finished studies in engineering and economy at the Technical University of Berlin in 1963.

Since 1963 working for GKSS-Research Center Geesthacht.

Now heading the International Bureau and in this capacity responsible for the coordination on the German side for the bilateral S&T agreement.

Doug Bradford

Mr. Bradford is Chief of Intergovernmental Ocean Science Affairs in DFO.

He has been involved in the coordination of the Canada-FRG Bilateral S&T Agreement since 1974.

He has an MA in physical geography from the University of Waterloo, Ontario.

Fisheries and Oceans | Pêches et Océans

C A N A D A /FEDERAL REPUBLIC OF G E R M A N Y

SCIENCE & TECHNOLOGY COOPERATION AGREEMENT

SUMMARY REPORT OF THE

WORKSHOP ON

REMOTE SENSING OF FLUORESCENCE SIGNALS

COORDINATED BY
HOWARD EDEL and HELMUT BIANCHI

OTTAWA, OCTOBER 14-17, 1986

Canada

FLI Workshop

The Canada-Federal Republic of Germany Bilateral Agreement on Scientific and Technological Cooperation and Its Relationship to the Remote Sensing of Fluorescence Signals

J.D. Bradford
Oceanographic Sciences Directorate
Department of Fisheries and Oceans
Canada

H. Bianchi
G.K.S.S.
Federal Republic of Germany

We are pleased to welcome you to the joint Canada/Federal Republic of Germany workshop on Remote Fluorescence Spectroscopy. It is very gratifying to have so many participants from Germany and we sincerely hope that you enjoy your visit to Canada.

Cooperation in measuring ocean colour is one of approximately 100 joint projects which are being carried out under the Canada-Federal Republic of Germany Bilateral Agreement on Scientific and Technological Cooperation. I would like to take a few minutes of your time, before the more technical discussions begin, to talk about the bilateral agreement and its relationship to the cooperation in the remote sensing of oceanographic fluorescence data.

The Bilateral Agreement was signed over 15 years ago, in April 1971 to be exact. It is interesting to look at the original wording. In the preamble, for example, it states that the two governments:

> "Desirous of strengthening the close and friendly ties between them,
> Wishing to broaden the scope of all aspects of scientific and technological cooperation between the two states for peaceful purposes and for their mutual benefit,
> Recognizing the beneficial effects that such cooperation can have on the quality of life and economic well being of their respective peoples,
> Have Agreed as follows:"

Ten articles are then listed which spell out the terms and conditions of cooperation. For the purposes of this workshop I would like to focus only on Article I which reads as follows:

> "The contracting parties undertake, in accordance with the laws and regulations in force in each of the two states, to facilitate and to encourage scientific and technological cooperation and exchanges of information and personnel between the agencies, organizations and enterprises in the public and private sectors of the two states."

If we look back over the Agreement we see that oceanography and in particular the development of oceanographic sensors has been a cornerstone of the cooperation. As early as 1973, a joint Canada-Germany workshop had been convened at Bedford Institute and scientists from the Metrology Division of BIO were working closely with their counterparts at the University of Kiel in Germany on several joint projects aimed at producing superior sensors and instrumentation for oceanographic research. Since then, over 25 projects covering a broad range of oceanographic interests have been identified under the Agreement. It is safe to say that as far as the marine sciences are concerned, over the years scientific and technological cooperation have been encouraged and facilitated and a steady two-way flow of exchanges of information and personnel has taken place.

In general terms, compared to other bilateral S and T agreements, the Canada/FRG Agreement has been a front runner. In Canada it is used as the yardstick by which other Agreements are measured. Until the 1980s, core activities for S and T cooperation were mainly in the marine sciences, fisheries and the geosciences with some exploratory interest in energy projects. Today, a review of all the activities taking place under the Agreement indicates the emergence of a well-rounded portfolio covering all phases of the technological innovation process, that is, exploratory fundamental research, applied research, and developmental R and D with joint work on prototypes, field trials and demonstration technologies. Much of the cooperation now has significant commercial potential.

Turning to the remote sensing of the sea, cooperation under the Agreement began in 1981 with a proposal from Dr. Jim Gower to develop a technique for measuring and mapping phytoplankton concentrations in the sea from satellites by using the fluorescence signals of chlorophyll. This led quickly to a full-fledged joint field experiment called FLUREX in which the Canadian-designed and built spectrometer, together with German sensor devices, was flown over the North Sea & Baltic in a German aircraft with ground truthing carried out by German surface vessels. The latest cooperative effort took place last July when the FLI was taken to Germany for performance tests over the Black Forest.

At the moment we seem to be at a turning point in the Cooperation. It seems to be ready to expand from the scientist-to-scientist type of collaboration which we have enjoyed so far to an industry-to-industry arrangement aimed at producing a marketable instrument. This is not to say that the scientific cooperation will be reduced in priority. On the contrary we would hope that many opportunities would arise for joint research projects leading to a second-generation space borne, high resolution imaging spectrometer. Nor would the government-to-government involvement necessarily be diminished. Instead we would hope that our respective governments would continue to work through the Agreement to encourage and facilitate the industrial side of the instrument development.

To sum up, it is clear that the Canada/FRG Bilateral Science and Technology Agreement has been extremely useful in fostering cooperation on imaging spectroscopy. It is equally clear that the Agreement will be needed just as much in the future if the new fluorescence sensors are to realize their full potential as environmental sensors.

Thank you for your attention and good luck with the Workshop.

Ladies and Gentlemen:

Let me join in the wish for a good success of the workshop. But let me also outline some additional aspects of the cooperation, emphasizing a bit more the German view of it.

Indeed, it was the Canadian side which made the first step towards the development of joint bilateral efforts in sensing the fluorescence signal of chlorophyll "a" from space.

It is an old wish of the oceanographers to sense the constituents of coastal waters not as a total but differentiated with respect to chlorophyll and other materials like suspended minerals and dissolved organics.

The sunlight induced characteristic fluorescence signal of chlorophyll and its narrow banded sensing offered opportunities to fulfill the wish of the researchers. When we started our discussion on the cooperation it was for us, from the coordinating side, not too difficult to marry the scientists, because they were engaged already - which essentially meant, that they knew each other, so that a solid basis for a fruitful cooperation was existing. As we heard from Mr. Bradford, a well coordinated joint action, took place within the FLUREX 1982 campaign which indeed demanded a well synchronized organization between satellite orbit and actions from aircraft, ships and the research platform in the North Sea. Several sensors were flown, one of them was the FLI.

According to my information, the results justified the efforts. Regrettably the Canadian partners were not able to join the FLUREX 1985 campaign.

The first spin-off result of the cooperation was the formation of the work sharing FLUREX group, comprising scientists with different expertise from different German institutes.

Another spin off was the contract offered by the European Space Agency ESA to conduct a study on chlorophyll measurement from space, which may be considered as an appreciation of profound work on the theoretical bases on the interpretation of spectrometer data, the optical properties of substances in the sea and the receipt of satellite data. These theoretical works were supplemented by a feasibility study on a space borne version of a high resolution imaging spectrometer which was financially supported by the German Federal Ministry for Research and Technology, the BMFT. The new concept of the ROSIS, the Reflective Optics System Imaging Spectrometer, will find its realization within the next 18 months.

The workshop to be held during the next few days is being attended by experts concerned with theoretical and practical work, by users and manufacturers of remote sensing devices. It will offer a unique opportunity to assess the scientific results yielded to date, it will also offer the opportunity to elucidate the theoretical designs of imaging spectrometers.

It is still the declared wish of oceanographers to have satellite images available, giving differentiated information of the constituents in coastal waters. Because of the high cost involved, the realization of a space borne fluorescence imaging spectrometer necessarily leads to the discussion of international cooperation. And this will not only focus on sensing the oceanographic environment but will cover also its application in other subjects. The last day of our workshop is devoted to the discussion of continuing the scientific cooperation and to broadening it to industry-industry links.

I would like to express my distinct hope, that our workshop will bring us a remarkable step forward. To achieve this, I wish you, I wish us a good success.

Joint Canadian / German Workshop on High Spectral Resolution Imaging for Land and Ocean Remote Sensing

Ottawa, 14 - 17 October 1986

REMOTE SENSING OF OCEAN COLOR/FLUORESCENCE FROM SPACE - INTERESTS, ACTIVITIES AND GOALS IN THE FEDERAL REPUBLIC OF GERMANY

H. van der Piepen

Institut für Optoelektronik, DFVLR, Oberpfaffenhofen, FRG

REMOTE SENSING OF OCEAN COLOR/FLUORESCENCE FROM SPACE - INTERESTS, ACTIVITIES AND GOALS IN THE FEDERAL REPUBLIC OF GERMANY

1. INTRODUCTION

1.1 Water color and oceanography from space

The visible portion of the sunlight may penetrate the water body to a certain depth. Through processes like absorption, fluorescence and scattering caused by natural and by man-made suspended and dissolved substances as well as by the water itself, it is modulated in intensity and spectral composition. The backscattered portion of the light as observed by a remote sensor may thus render information on the type, distribution and concentration of many biochemical and physical water parameters.
This phenomenon of ocean color/fluorescence developed originally from the field of optical oceanography and has become an important and integral part of modern oceanography.

1.2 Observation methods and sensor technologies

The relatively low albedo of water (in comparison to land), the interaction with the atmosphere and the necessity to avoid direct sun glint impose special requirements on suitable multispectral sensors especially if operated from space. These are essentially:

- Narrow spectral channels from the blue to the near i.r. range
- High sensitivity and signal/noise ratios
- High radiometric resolution and data recording
- High pixel co-registration
- Tilt capability
- Relatively large swath width (in comparison to land)
- Low polarization.

These special requirements have been the cause for the development of specific multispectral sensors for water color/fluorescence monitoring. Furthermore, they resulted in the development of special atmospheric correction methods and bio-algorithms for the data interpretation.

1.3 Fields of applications

The monitoring of ocean color/fluorescence basically allows investigations in the following areas:

- Marinebiology and ecology
- Fisheries resources
- Pollution and sediment transport
- Ocean dynamics
- Climatology (carbon cycle, energy balance).

These application thus include observations in lakes, estuaries, coastal zones, open oceans and polar regions. The requirements in regard to instrument technologies, resolution, coverage and repeat cycles may differ accordingly.

1.4 Space systems

In view of these different applications, it is important to ensure not only the launch of advanced spaceborne monitoring sensors, but also ensure and encourage the systematic transition from experimental into operational systems.

After the termination of the CZCS programme, investigations into suitable follow-on sensors have been undertaken on both sides of the Atlantic.
In the U.S.A. present candidates are the Ocean Color Imager (OCI) to be re-considered for the flight on a NOAA satellite upon special request of the NASA Administrator, and the Moderate Resolution Imaging Spectrometer (MODIS) which is an integral part of the NASA Earth Observation System (EOS) which most likely will make use of the polar orbiting platforms of the Space Station.
In Europe the Ocean Color Monitor (OCM) originating from the Coastal Oceans Monitoring Satellite System (COMSS) and later from the ESA Remote Sensing Satellite (ERS-I), the socalled Advanced OCM (a pushbroom-type imaging spectrometer) are possible candidates for EURECA, an Advanced Ocean/Ice Mission and for a later ERS follow-on system.

2. OCEAN COLOR-RELATED RESEARCH IN THE FRG

2.1 History

Activities in context with optical oceanography and remote sensing of ocean color date back till 1976. Based on laboratory and ship investigations, it started first at near-shore research institutes but spread soon to other organizations especially in context with atmospheric modelling, aircraft monitoring and digital data processing. Joint experiments first on a national, later on an international level (e.g., FMP, FLEX, MARSEN, FLUREX) supported strongly the formation of an active user community within the FRG and Europe.

Government-funded agencies as for instance the GKSS Research Centre in Geesthach and the DFVLR Research Centre in Oberpfaffenhofen became directly involved in these activities with their respective technical and research facilities. Within the FRG, both organizations have nowadays become a nucleus for ocean color/fluorescence work and relevant future planning.

2.2 Present activities

2.2.1 Science

As a result of the shipborne, airborne and spaceborne data analysis in the past, the request for an improved mapping of water constituents in coastal zones lead to the present emphasis on investigating the natural fluorescence as an alternative to the "traditional" absorption method. This takes place essentially within the socalled FLUREX group, this is a group of scientists, which first began to conduct relevant investigations jointly during the FLUREX Experiment in 1982. It also involves investigations with airborne laser systems. Furthermore, the modelling of the radiative transfer in the water and in the atmosphere has become an essential part of the present work.

2.2.2 Technological developments

Technical developments during the past concentrated on shipborne radiometers on the one hand, and airborne radiometers and multispectral sensors on the other hand. The latter were basically of the mechanically scanning types.

The present development of airborne sensors concentrates on the implementation of pushbroom-type detectors.

After the successful conduct of a (BMFT-sponsored) study of a spaceborne color/fluorescence scanner based on an imaging spectrometer with a matrix CCD detector, the research organizations GKSS, DFVLR and the MBB/ERNO company started with the joint development of an aircraft prototype which will permit not only a thorough test of the feasibility of the instrument but also will open new applications (including land) because of the narrow spectral bands involved.
Furthermore, DFVLR operates and applies a high resolution spectrometer incorporating a linear CCD detector array. Sofar this instrument has been used on ships, however, it is planned to incorporate it together with the imaging spectrometer into one of the DFVLR aircraft.

2.3 Application programmes involving ocean color/fluorescence

The basic research and technological developments and the verification by means of ground truth mentioned above, have been combined with more application-oriented tasks and projects supported by different sections of the government. Typical examples are:

- Investigations of frontal systems in the North Sea
- Monitoring programme of the Baltic Sea
- Eutriphication of rivers and lakes
- Warm water eddies of the North Atlantic
- Climatology-related processes in the atmosphere, hydrosphere, cryosphere
- Elbe monitoring programme
- Adria monitoring programme.
- EUREKA/EUROMAR

This indicates, that the remote sensing activities in the FRG are a combination of scientific resaearch, technological developments and applications.

2.4 Scientific and user communities

From the described situation it is evident that the user community in the FRG as in other countries is rather complex and basically consists of:

- **Scientific users**
  These are at universities, other research institute and government-funded agencies. They are mainly involved in modelling and in the development, test and verification of water color/fluorescence methods and processing algorithms.

- **Applied science users**
  These are also at universities, other research institutes and government-funded agencies, but are involved in research programmes which need the derived products (e.g. chlorophyll map, sediment sinks, carbon fixation numbers etc.) as an input into their investigations.
- **Users**
  These are mainly federal and provincial government ministeries, public services and commercial entreprises which need a processed end product on an operational base.

3. GOVERNMENT ACTIVITIES

3.1 General

The German government supports oceanographic research and associated remote sensing activities on different levels and through different programmes (compare section 2.3).

The responsibility of the Ministry for Research and Technology (BMFT) lies in general in the *pre-operational* support of scientific research and technological developments on national and (bi-lateral) international levels, in the support of government-funded agencies (e.g., DFVLR, GKSS) and in the support of ESA programmes as one of the member countries. The German Research Foundation (DFG) sponsors special sectors of interdisciplinary research at universities and mainly in the field of basic research.
Contrary, the *operational* use and practical application of remote sensing involves partially other ministeries and public services with special tasks as e.g. environmental monitoring, pollution control, fish stock estimates etc.) but also commercial enterprises.

3.2 User requirements

The user requirements in regard to a spaceborne ocean color/fluorescence monitoring system can be summarized as follows:

Short-term requirements:
a.) There is a strong interest to continue the global data collection as has been obtained from the Nimbus-7/CZCS for a period of 8 years. The emphasis here lies on large and medium scale monitoring.

b.) There is a growing interest to provide an advanced research tool for both, new sciences and new technologies in particular for investigations of the potential of sun-stimulated fluorescence for the mapping of natural and man-made water constituents. The emphasis here lies in medium and small scale monitoring, in particular of coastal zones.

Long-term requirements:
Long-term interests require an operational system which is suitable to respond to the user requirements on all scales in open ocean and coastal zones especially for the monitoring of

biomass, pollution and climatology-related topics like carbon fixation.

3.3 Potential of German industry

Based on the technological facilities and many years of experience in space activities, German industry has a high potential in participating in any ocean color/fluorescence space project. In context with this topic and in accordance with the EOPP Procurement Plan (ESA/PB-RS (86)31) this applies especially to the fields of

- Optical instrument development
- Mechanical structures
- Electrical and data handling
- Ground segments.

German industry is in many cases supported by research institutes and government-funded agencies in the fields of

- Modelling
- Laboratory and aircraft tests of detectors and sensors
- Measurement campaings including ground truth
- Data processing in general
- Verification of methods and algorithms.

Besides this general experience, specific experience has been developed during the past from the handling of many studies and projects like MOMS, AOCM, ROSIS and others.

In view of the ongoing activities and the above-mentioned potential, the various German organizations have a strong foothold in this field and are interested to participate further in related ESA activities.

3.4 Participation in the ESA Earth Observation Programme

Besides the various national activities (compare section 2), the German participation in future spaceborne ocean color/fluorescence sensor systems is essentially based on the ESA Earth Observation Programme (EOP). The objectives of this programme which is also supported by the FRG are to

- prepare operational systems in polar orbits tailored to the needs of ocean, ice, coastal zones and meteorological applications
- provide research tools for scientific and user communities

- prepare potential future missions by advanced systems and instrument studies and by dedicated instrument developments.

The programme elements of the EOP include ERS-1/2 (1990-1995) and the polar platforms missions.

As part of the EOP, the FRG and other member countries signed during the course of this year the Earth Observation Preparatory Programme (EOPP).
One key element of the EOPP is the the preparation of an Advanced Ocean/Ice/Mission which could make use of the polar orbiting platforms of Columbus. The payload of such a mission is not only based on instruments derived from ERS-I but also on those which had to be deleted from this mission (e.g., OCM, IMR). Furthermore, the platform will provide space for a set of research/science-oriented sensors. Thus there is a strong probability that a suitable ocean color/fluorescence sensor will be integrated into this mission. The FRG will support this.

Because of the earlier mentioned potential and interest of various organizations within the FRG, it is expected that these will participate in special tasks of the EOPP such as

- mission concept and system studies
- instrument and feasibility studies
- measurement campaings involving aircraft and ships
- pre-development of critical technologies
- other related topics.

3.5 Bilateral cooperation with other countries

Beside the participation in the ESA programme, the FRG has a number of bilateral cooperation agreements with other countries (including ESA member or associated member countries).
In the field of remote sensing, the German interests are properly reflected by the ESA programme; national programmes are closely related to these or complementary. Typical examples are the cooperation with Canada (DFO, CCRS), Spain (INTA) and with Indonesia (LAPAN). This cooperation has also been the base of participation in international experiments as for instance OSTA-I/OCE (Spain, USA), the Alboran Sea Experiment (Spain, USA and others), SNELLIUS II (Indonesia, The Netherlands), FLUREX (Canada).

4. CONCLUSIONS AND RECOMMENDATIONS

Remote sensing of ocean color/fluorescence provides a base for the monitoring of a variety of ocean and costal processes and thus is of interest to many disciplines.
It is considered absolutely essential that the experience and the associated technologies which have been developed during the past from laboratory, ship and aircraft investigations but also from space are pursued further as a key element in the ESA Earth Observation Programme.

It is expected that all the member countries and associated members will support this development. Further more it is expected that ESA will consider these requirements in the elements of the EOPP and in negotiations with other countries participating in the preparation and operation of future polar platform missions.

5. LIST OF ACRONYMS

AOCM .... Advanced Ocean Color Monitor
BMFT .... Bundesministerium für Forschung und Technologie
COMSS ... Coastal Oceans Monitoring Satellite System
CZCS .... Coastal Zone Color Scanner
DFG ..... Deutsche Forschungsgemeinschaft
EOP ..... Earth Observation Programme
EOPP .... Earth Observation Preparatory Programme
EOS ..... Earth Observation System
ERS ..... ESA Remote Sensing Satellite
EURECA .. European Retrievable Carrier
FLEX .... Fladenground Experiment
FLUREX .. Fluorescence Experiment
FMP ..... Flugzeugmeßprogramm
GKSS .... GKSS Forschungszentrum
MARSEN .. Marine Rem. Sens. Experiment in the North Sea
MODIS ... Moderate Resolution Imaging Spectrometer
OCG ..... Ocean Color Working Group
OCI ..... Ocean Color Imager
OCM ..... Ocean Color Monitor
OCS ..... Ocean Color Scanner
ROSIS ... Reflectice Optic System Imaging Spectrometer

ESA/GKSS/DFVLR Contract No. 55315/V8537

The use of chlorophyll fluorescence measurements from space for separating constituents in water

CONTRIBUTIONS FROM IOS B.C. CANADA

J.F.R. Gower

Institute of Ocean Sciences, P.O. Box 6000,
Sidney, B.C., V8L 4B2, Canada

August 1986.

ESA/GKSS/DFVLR Contract No. 55315/V8537

The use of chlorophyll fluorescence measurements from space for separating constituents in water

This document represents the final report due under the sub-contract between GKSS, Federal Republic of Germany, and IOS, Canada. It consists of a general introduction, followed by contributions to sections of the report compiled under the above contract. At the end are a list of general conclusions and the references.

J.F.R. Gower

Institute of Ocean Sciences, P.O. Box 6000,
Sidney, B.C., V8L 4B2, Canada

August 1986.

Introduction.

In 1974 the Institute of Ocean Sciences, Sidney, B.C., Canada (IOS) took delivery of a custom designed silicon diode array, multichannel spectrometer, (the "IOS spectrometer") which digitally records the intensities of light dispersed onto the 256 elements of a Reticon photodiode array (Walker et al., 1974,1975). This was incorporated into a airborne observing package, designed to view the water surface through a polarizer at the Brewster angle, so as to reduce surface reflected light and make observations possible when flying under cloud.

Technical specifications of the instrument are as follows:

I.F.O.V.	0.7 X 0.2 degrees
View direction	
up-welling radiance	53 degrees incidence Any azimuth
down-welling irradiance	By mirror to opal diffuser
Spectral resolution	14 nm
Spectral coverage	400 - 800 nm (polarized) 400 - 1060 nm (total)
Quantization	12 bits
Response time	.1 sec (minimum) 2 sec (typical)
Signal to noise	2000/1 (typical)
Data recording	Computer compatible tape

The instrument is calibrated between flights with a white card in sunlight, and produces spectra of reflectance factors (Lu^+/Ed^+), which should equal the irradiance reflectance multiplied by a constant factor of about 0.6 (Austin, 1980).

In the first test observations in April 1975 (Neville and Gower, 1977), the spectra showed a small increase in intensity centred at a wavelength of about about about about 685 nm and with a width of about 25 nm, easily resolved by the spectrometer resolution of 14 nm. Previous observers had used photomultiplier detectors, which rapidly lose sensitivity at wavelengths longer than about 650 nm.

The 685 nm peak showed a good correlation with the near surface chlorophyll concentration, and on the basis of this, and its position and width, it was ascribed to fluorescence of chlorophyll a stimulated by ambient (sun and sky) light (Neville and Gower, 1977). The signal was also reported at about the same time in under-water measurements (Morel and Prieur, 1977).

It had earlier been suggested that a combination of chlorophyll absorption at 670 nm, with reflectance and water absorption at longer wavelengths could explain such a peak (Gordon, 1974). Gordon (1979) later showed that the intensity of the signal is, however, consistent with expected fluorescence efficiencies. At IOS we used tests with DCMU, and varying intensities and colours of

illumination in the sea and a large outdoor tank to assure ourselves that fluorescence was a major, if not the only, source.

Observations of this fluorescence can be applied to remote sensing surveys of near surface phytoplankton. Such surveys are usually based on radiance or reflectance measurements at blue and green wavelengths (green to blue ratio), to monitor the effects of chlorophyll absorption and associated backscatter in phytoplankton. The relatively narrow bandwidth of the fluorescence line and its position at the red end of the spectrum, where atmospheric radiance is low, should give advantages to remote sensing measurements using passive fluorescence.

Disadvantages would be expected from the relatively low signal available, and the varying fluorescence efficiency of different phytoplankton species in different physiological states. A number of field experiments were undertaken in the period 1977 - 1980, particularly along the B.C. coast and in the Canadian Arctic, to evaluate the technique further. It was found that the method had definite advantages in operational survey conditions for mapping near-surface chlorophyll.

The value of the more conventional "green to blue ratio" technique, making use of chlorophyll absorption effects, was demonstrated in satellite observations starting in 1978. Improvements are, however, needed for coastal (Case 2) waters, and it is here that a satellite instrument capable of (passive) remote fluorescence measurements should prove of especial value. It has also been noted that remote measurements of in-vivo chlorophyll fluorescence, combined with absorption data, can help determine the rate of phytoplankton productivity (Topliss and Platt, 1986).

Development of a satellite sensor capable of imaging the distribution of the fluorescence emission was undertaken starting in 1981 (Borstad et al., 1985). The airborne prototype, the Fluorescence Line Imager, (FLI) is an imaging spectrometer with dual (spectral and spatial) operating modes and programmable band selection. It has been flown on a wide variety of remote sensing missions over both land and sea targets, starting in 1984.

A field experiment "FLUREX" was undertaken in 1982 in cooperation with German scientists who have also been developing the passive fluorescence technique for studying local North Sea and Baltic waters. The IOS spectrometer was used on both an aircraft and a ship during April 20 to 28, i.e. during the spring bloom period, with a view to studying the fluorescence technique in these waters, and evaluating the problems of making such measurements from a satellite.

The remainder of this report is in the form of contributions to specific sections of the GKSS/DFVLR Report, based largely on FLUREX data.

4.6 Measurements from multiple altitude aircraft flights for studying atmospheric effects on the fluorescence signal.

Most Flurex flights were arranged to give data at several low altitudes (typically 1500, 1000 and 500 ft) over the same area, to allow extrapolation of the airborne results to the sea surface. However, on two occasions multiple altitude observations were made to above 10,000 ft, once over the North Sea, and once over the Baltic. These were on April 20th over the North Sea tower, when the surface chlorophyll level was measured to be 1.0 $mg.m^{-3}$, and on the 25th over the Alkor at station 2 in the Baltic when the chlorophyll level was 2.5 $mg.m^{-3}$.

Reflectance spectra are shown plotted on the same scale for the April 20 and 25 data in figures 4.6.1 (a) and (b). These reflectances are for observations at the Brewster angle of incidence (53 degrees). Values increase rapidly to a form close to the theoretical $(wavelength)^{-4}$ for Rayleigh scattering. Absorption features appear near 700 nm at the higher altitudes. Near the chlorophyll fluorescence wavelength, reflectance has increased by a factor of 8 to 10, between the lowest and the highest altitude.

The form of the absorption that will affect fluorescence measurements in Flurex can be calculated using the uncalibrated irradiance spectra observed from the aircraft (viewing upwards through the opal diffusing glass in the top of the aircraft). Figure 4.6.2 shows the spectra observed at the lowest altitude (500 ft) and at the highest (12000 ft) on April 20. The two curves are very similar, but their ratio (plotted over the range 0.75 to 1.00 in figure 4.6.2) shows absorption features centred at 692.4 nm (oxygen and water vapour), 724.3 nm (water vapour), 762.1 nm (oxygen), and 821.9, 902.6 and 944.1 nm (water vapour).

At shorter wavelengths Rayleigh scattering causes a relatively smooth reduction in signal at the lower altitude. Absorption at higher altitudes, such as that due to ozone in the stratosphere, or in the sun's atmosphere such as that due to sodium at 598 nm or hydrogen at 656 nm will not affect the observed irradiance ratio, or the observed reflectances, although the solar features are visible in the uncalibrated irradiance spectra of figure 4.6.2.

Figure 4.6.3 shows the result of adding Gaussian curves to fill the line shapes at the centre wavelengths listed above. At the resolution of the IOS spectrometer (14 nm), some of the lines are blended together, and in these cases the deeper line was filled first. The total, after the additions, is shown dashed. The 762 nm oxygen feature consists of many lines in a 7.5 nm range, corresponding to a half power width of about 3.5 nm. The observed width of this absorption feature (14.6 nm) is therefore very close to the resolution of the IOS spectrometer (14nm).

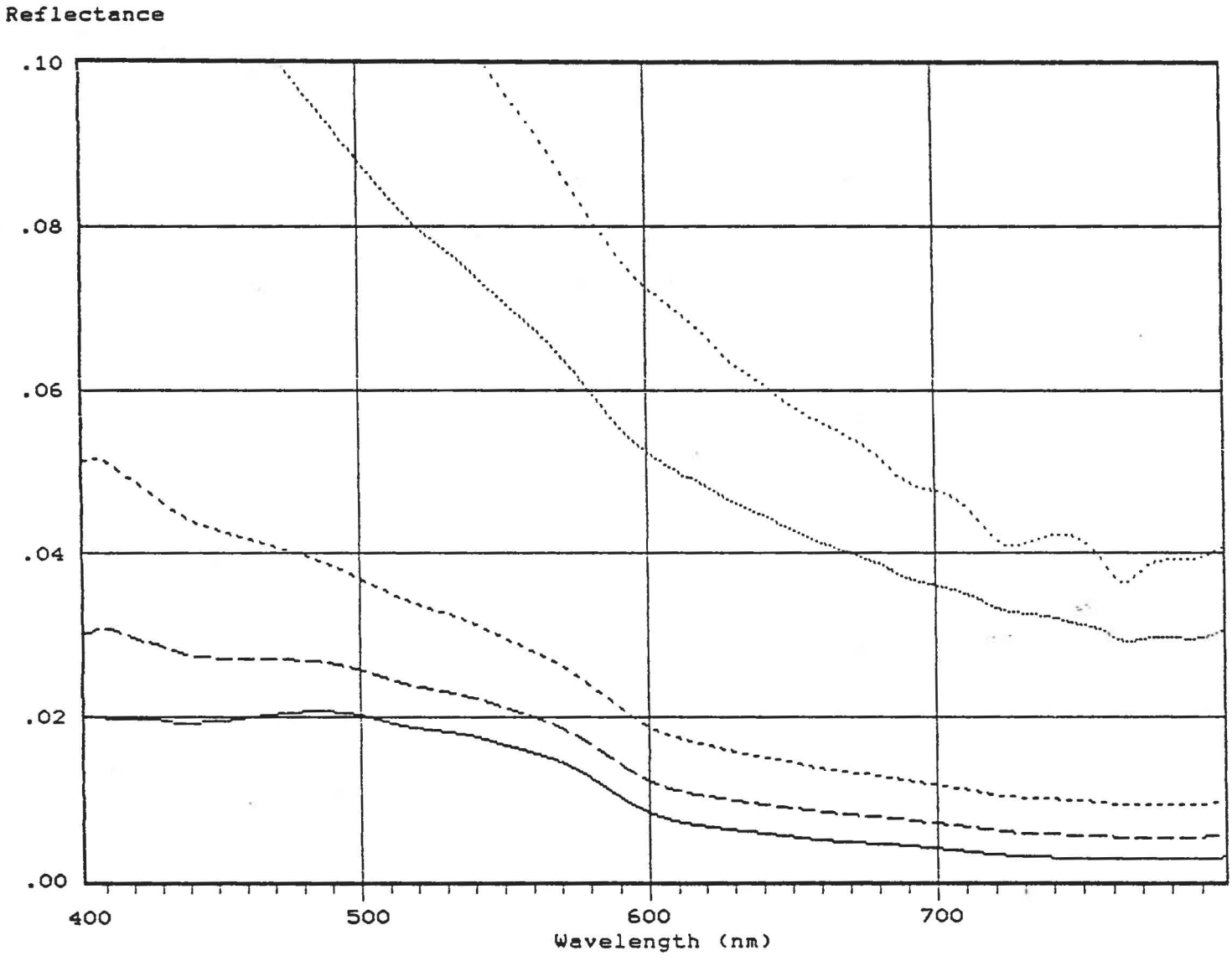

Figure 4.6.1(a) Variation of computed reflectance spectrum with altitude April 20 1982, over the North Sea tower. Increasing atmospheric back-scatter is apparent at 500, 1000, 2000, 5000 and 12000 ft respectively.

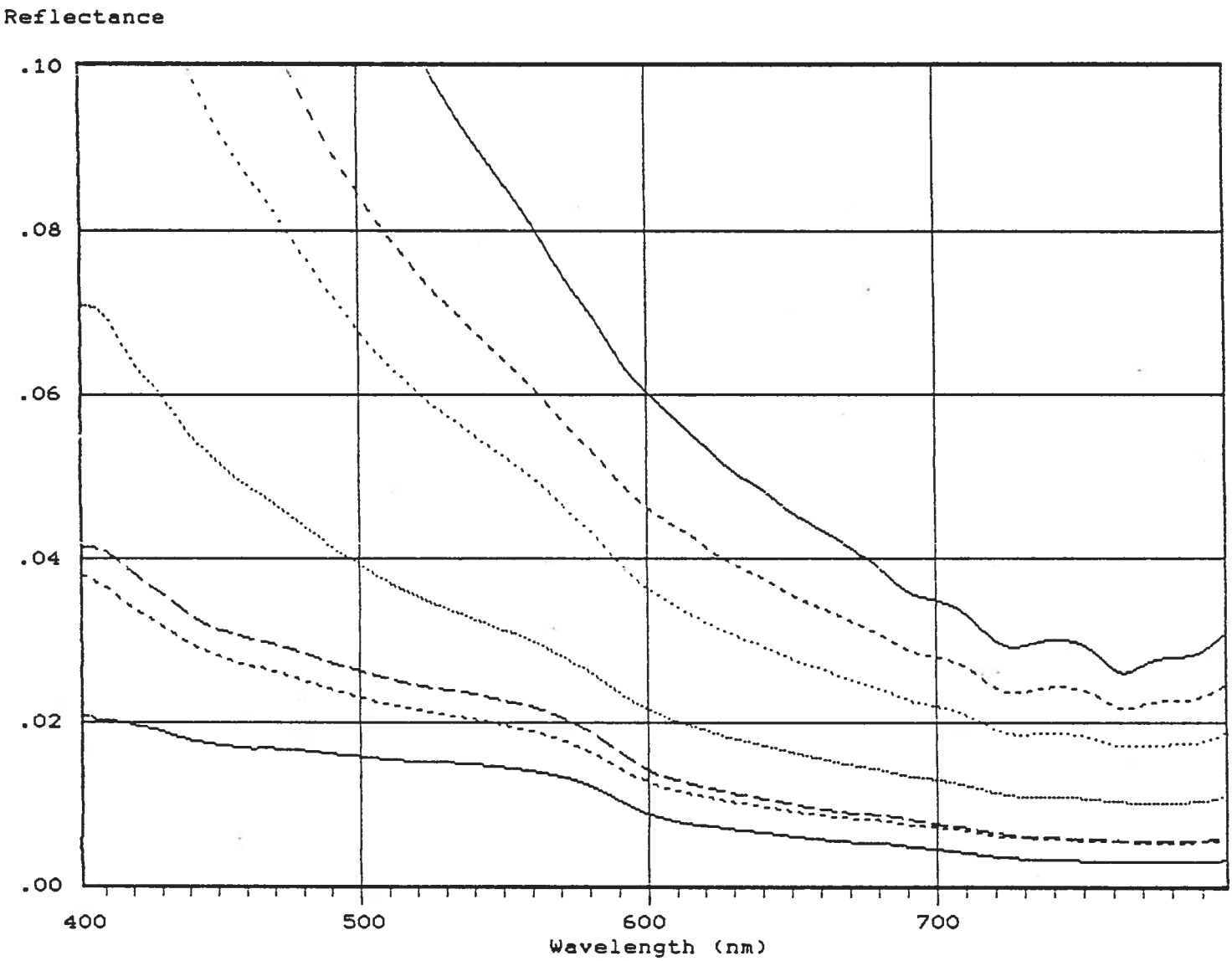

Figure 4.6.1(b) Variation of computed reflectance spectrum with altitude April 25 1982, over the Baltic. Increasing atmospheric back-scatter is apparent at 500, 1000, 1500, 3000, 5000, 10000 and 14000 ft respectively.

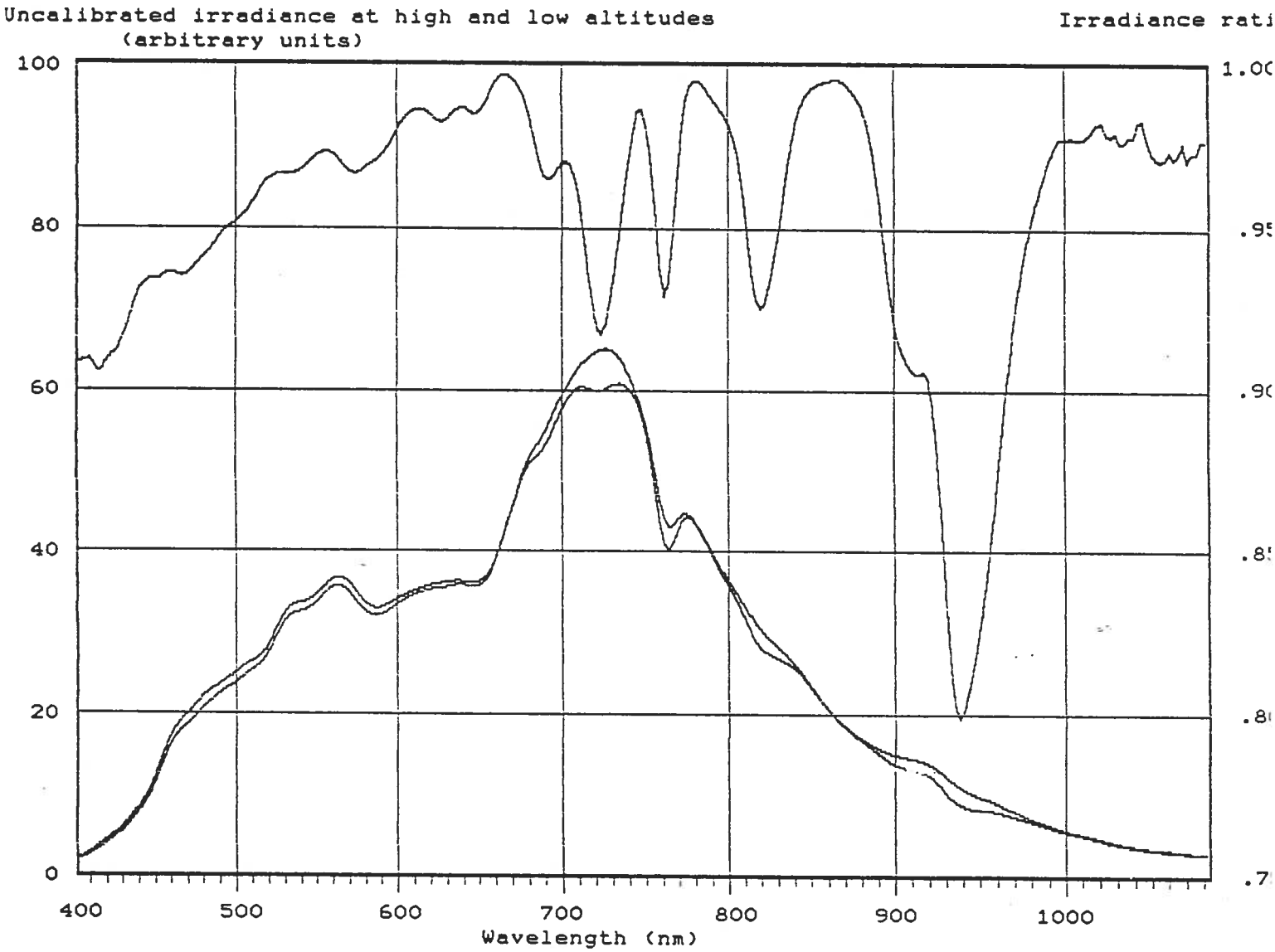

Figure 4.6.2 Irradiance spectra observed at 500 and 12000 ft on April 20 (lower curves). The ratio of these spectra showing atmospheric absorption (upper curve).

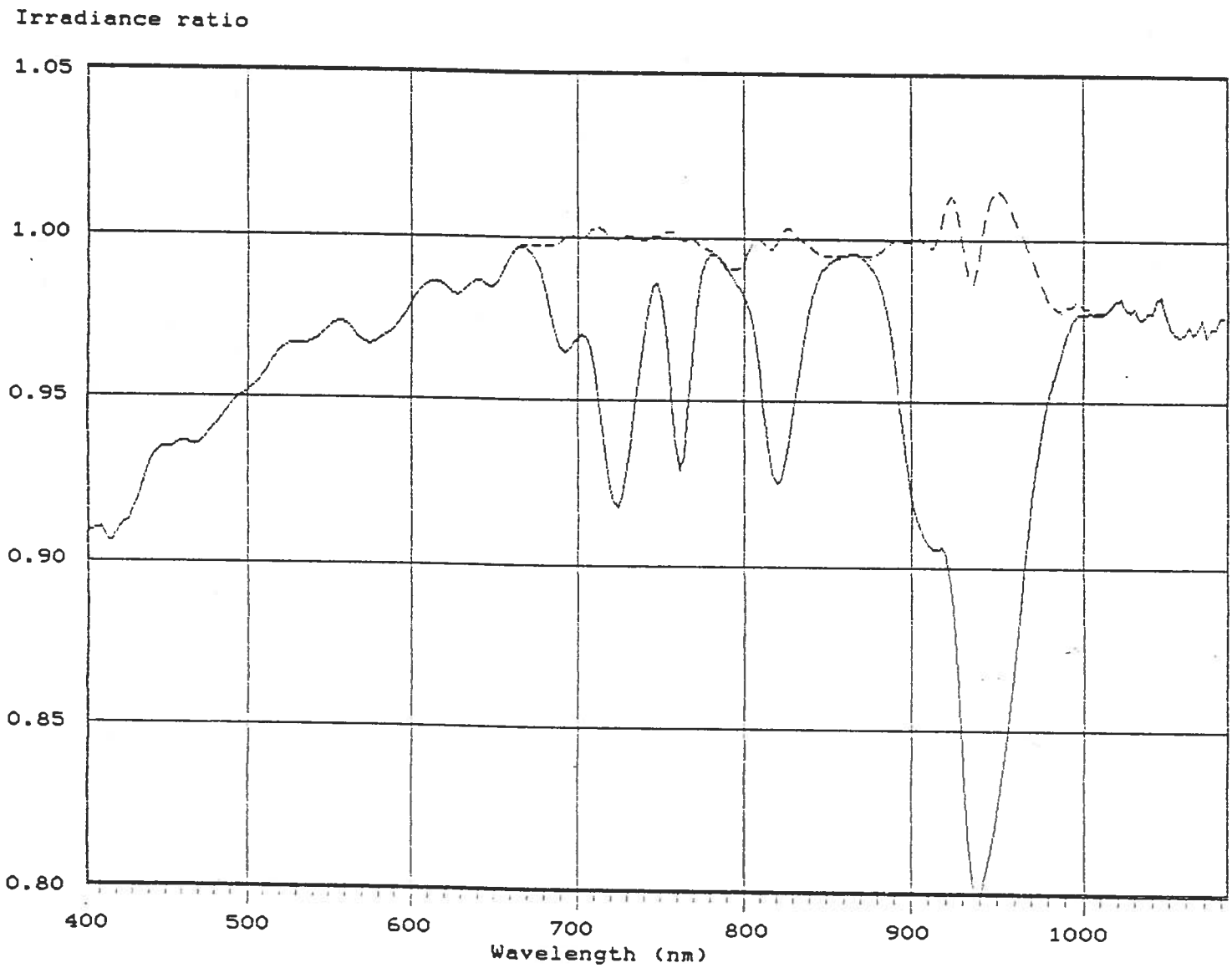

Figure 4.6.3 Atmospheric absorption effects as observed with the IOS spectrometer, fitted with Gaussian line shapes, as listed in the text. Dashed curve shows residual.

Centre wavelengths, widths to half depth, depths (absorption difference between 500 and 12000 ft) and absorbing gases for the lines or bands in figure 4.6.3, are as follows:

Wavelength	Width	Depth	Gas
692.4	19.7	.033	O_2,H_2O
724.3	26.3	.082	H_2O
762.1	14.6	.071	O_2
821.9	25.8	.075	H_2O
902.6	24.7	.066	H_2O
944.1	45.0	.201	H_2O

For observations with the IOS spectrometer, the 692 nm and 724 nm absorption features will affect the long-wave side of the observed fluorescence peak. At low altitudes, where atmospheric absorption has a very small effect on measured reflectance, we have calculated the FLH as the excess reflectance at 684.3 (diode 152) above a linear baseline that intersects the reflectance curve at 652 and 716.5 nm (diodes 164 and 140). For the April 20 data the line height at 500 ft is 12.4×10^{-5}, and for April 25, 27.4×10^{-5}. These values are in the same ratio as the surface measurements of 1.0 and 2.4 $mg.m^{-3}$. The appropriate conversion factors are discussed in sections 8 and 9.

Because of increasing absorption at wavelengths in the 650 to 720 nm region, the line height calculated in this way changes with altitude as shown in figures 4.6.4 (a) and (b) for April 20 and 25 respectively. Except for the anomalous point at 12000 ft on April 20, the apparent reduction with altitude is the same in both cases.

The reason for this change can be seen in figure 4.6.5 (a) and (b). These are plots showing the structure of the reflectance spectra, for the altitudes plotted in figure 4.6.1 (a) and (b), in the region of the fluorescence line. For this purpose, a linear baseline of reflectance, intersecting these spectra at 652.1 and 716.5 nm has been subtracted. The absorption feature at 724 nm is seen to affect the long wave side of the base line, while the feature at 692 nm affects the peak directly. Because both baselines wavelengths are on the steeply sloped sides of these features, the form of the variation with altitude depends critically on the exact shape, and relative depth of the lines. This will vary with the relative concentration of water vapour in the atmosphere below the aircraft, as indicated by the anomalous point on April 20 (Figure 4.6.4(a)).

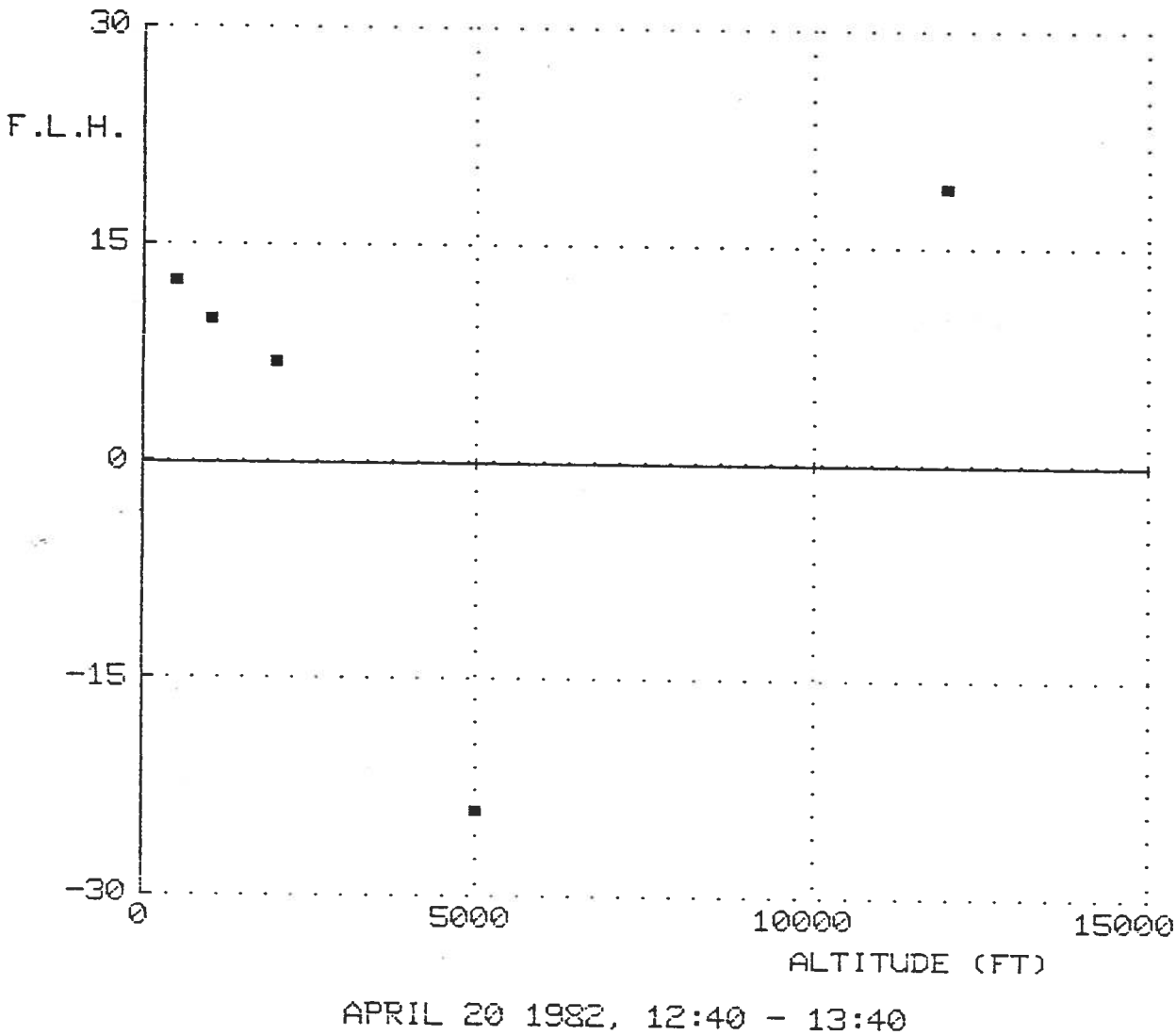

Figure 4.6.4 (a) Variation of observed fluorescence line height at 685 nm with altitude on April 20.

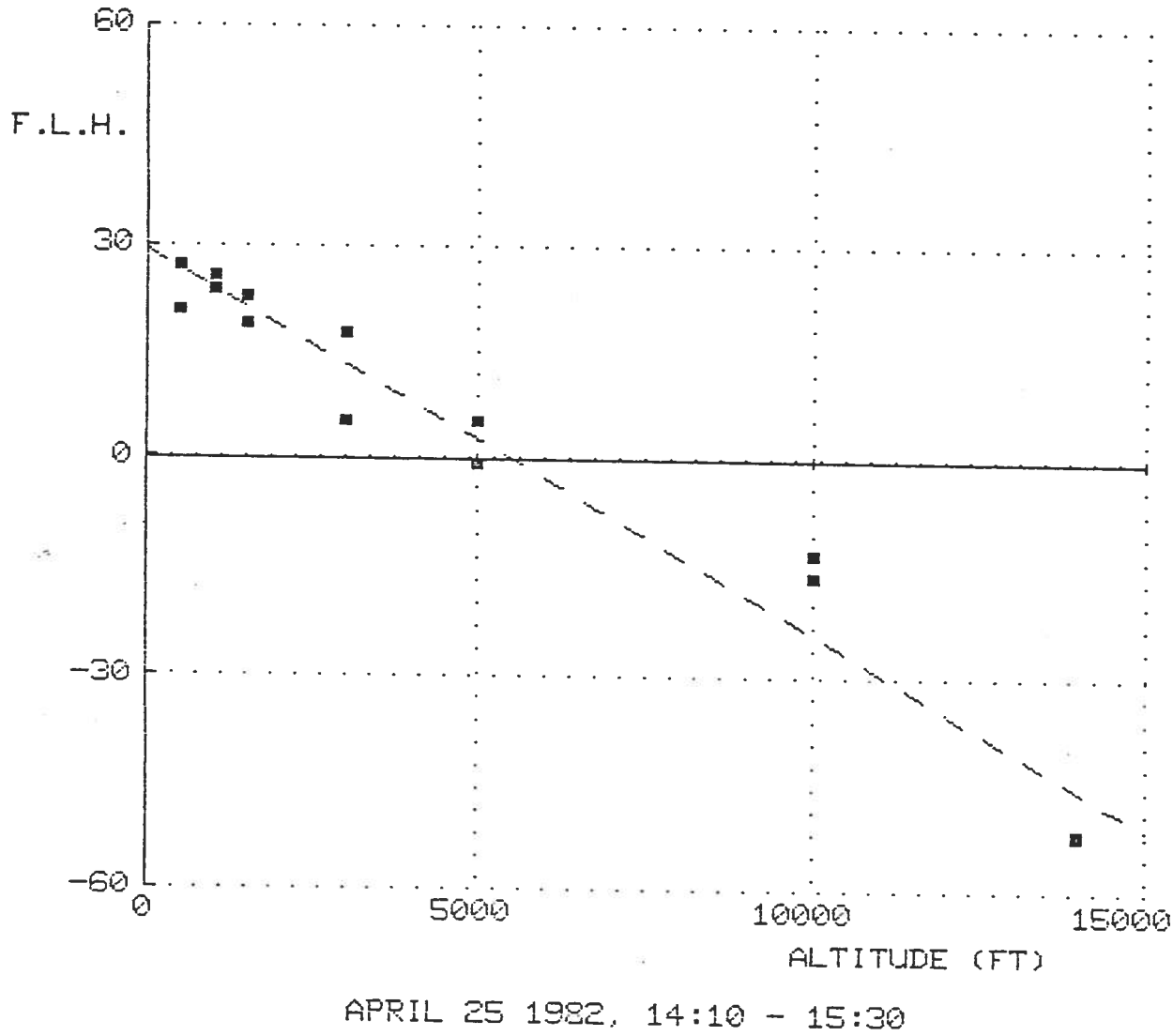

Figure 4.6.4 (b) Variation of observed fluorescence line height at 685 nm with altitude on April 25.

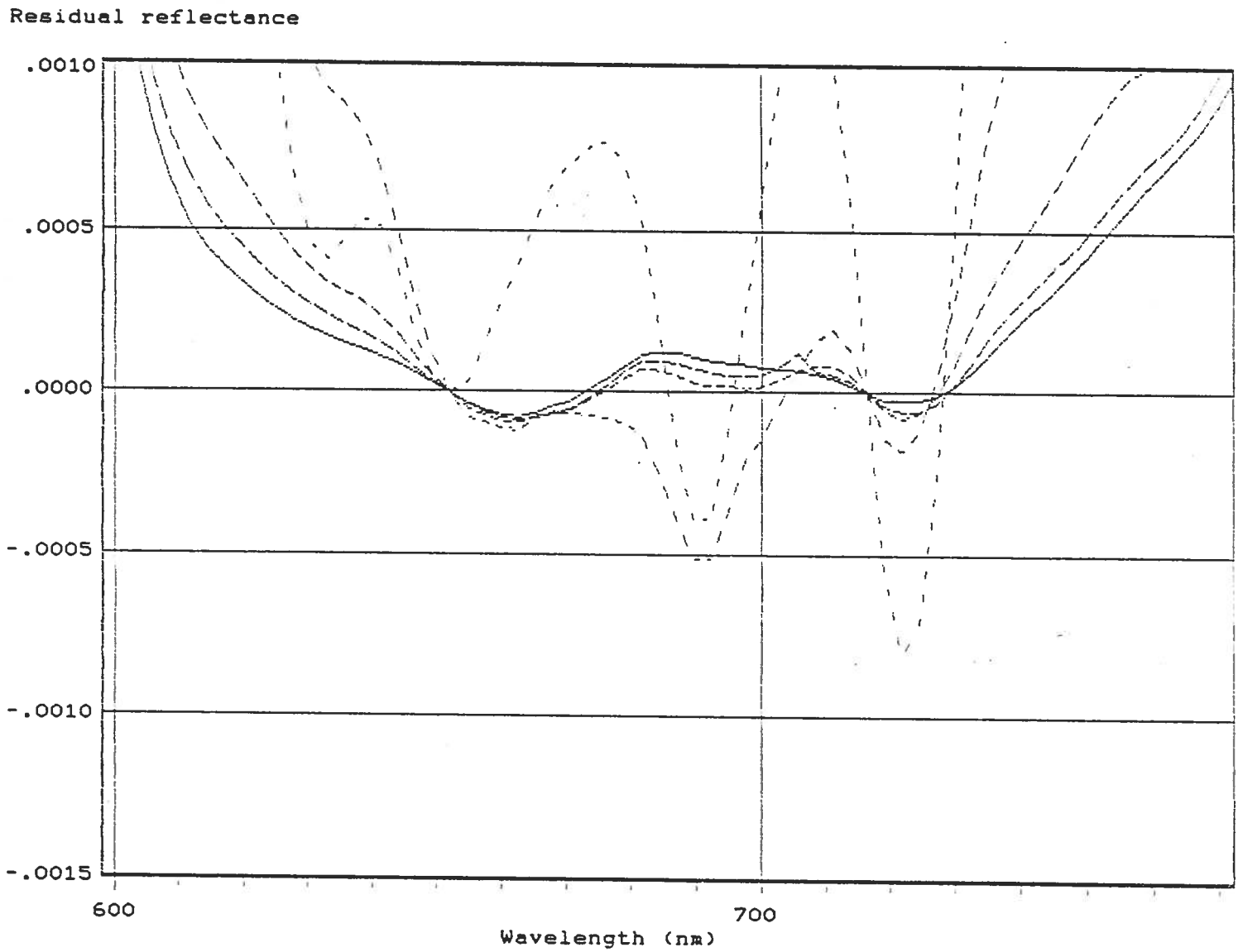

Figure 4.6.5 (a) Variation of the shape of the residual reflectance spectra on April 20 after subtraction of a linear baseline through the curve at 652.1 and 716.5 nm.

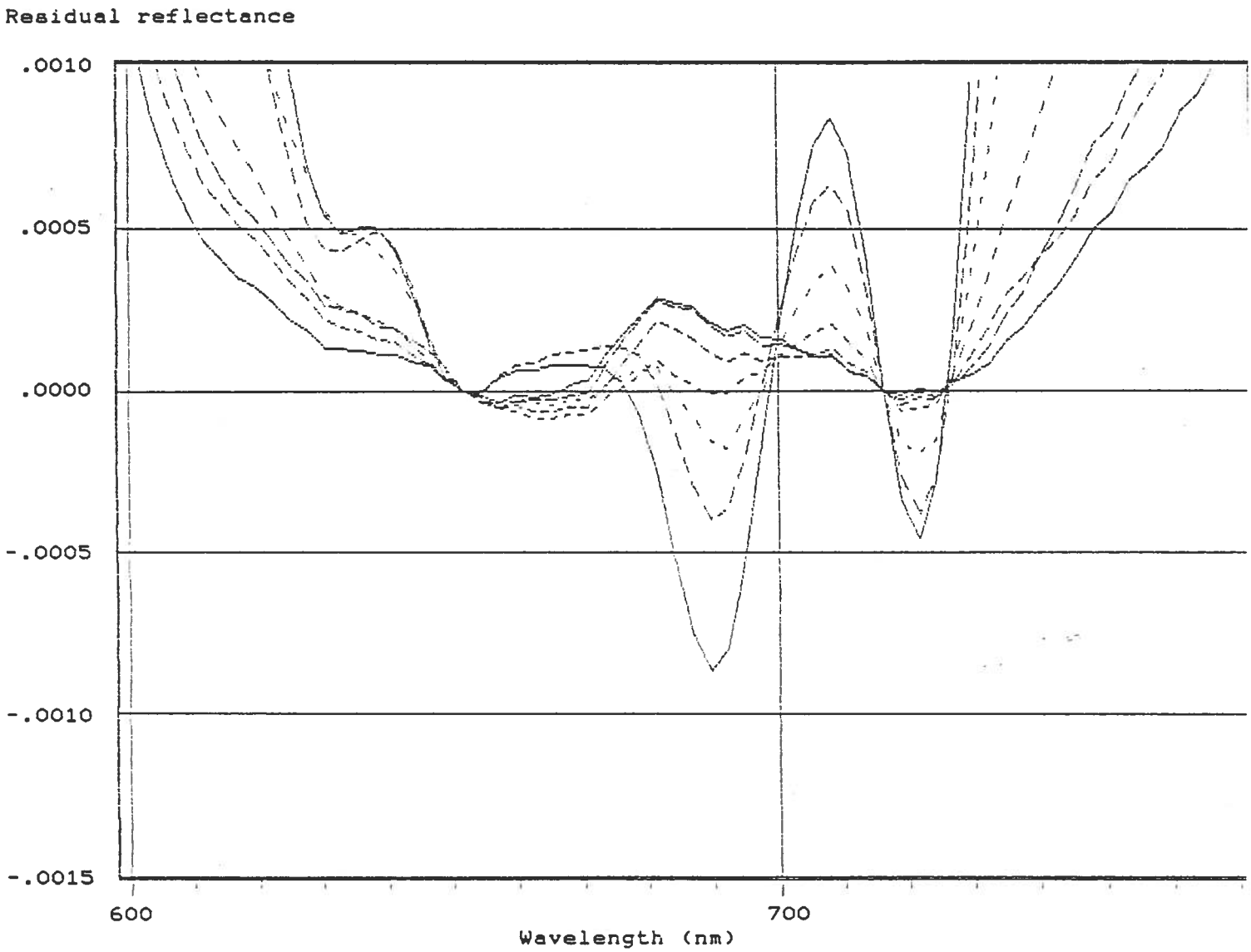

Figure 4.6.5 (b) Variation of the shape of the residual reflectance spectra on April 25 after subtraction of a linear baseline through the curve at 652.1 and 716.5 nm.

4.8 Possibilities for atmospheric correction from satellite and ground-based data.

For correcting the observed variation with altitude shown in figures 4.6.4(a) and (b), three options are available: (a) constructing a linear or curved baseline through wavelengths that are less affected by atmospheric absorption, (b) modelling or measuring and correcting the absorption, or (c) using a spectrometer or other sensor with sufficient spectral resolution as to allow the absorption lines to be avoided.

(a) Use of an improved baseline algorithm.

The wavelengths of the baseline used in surveys with the IOS spectrometer are selected for use in low altitude reflectance measurements, where the effects of atmospheric absorption are reduced to very low levels. For spectra in which the absorption is stronger, more appropriate wavelengths can be chosen from the data shown in figure 4.6.2. A curved baseline that passes through the observed reflectance curve at 609, 665 and 746 nm is one such possibility. Figure 4.8.1 shows the result of using this subtraction at the altitudes plotted in Figure 4.6.1.

The long wave baseline wavelength has now been moved to between the absorption features at 724 and 762 nm. The additional shortwave point introduces a curvature that increases the apparent fluorescence peak at the low altitudes. The point at 665 nm needs to be moved to about 670 nm to ensure that all features appear as drops in reflectance due to absorption. However this would cut into the fluorescence signal.

It can be seen that the shape of the residual reflectance curves are now roughly constant for the lower 3 altitudes, i.e. up to about 2000 ft. This represents an improvement over Figure 4.6.5. However, above this altitude, strong variations, different on the two days, again occur.

The major problem shown here is that for data with this spectral resolution, the absorption features have obscured the fluorescence signal. Improved spectral resolution, for example 2.5 nm as chosen for the FLI, or at least placement of sharp band edges with this precision, is therefore needed for measurements from high altiudes or from space.

(b) Modelling of atmospheric absorption.

The effect of this atmospheric absorption can in principal be modelled, if enough is known about its exact form. The amount of oxygen absorption should be relatively stable. Effects due to absorption by the more variable concentration of water vapour will be a more serious problem for a satellite sensor.

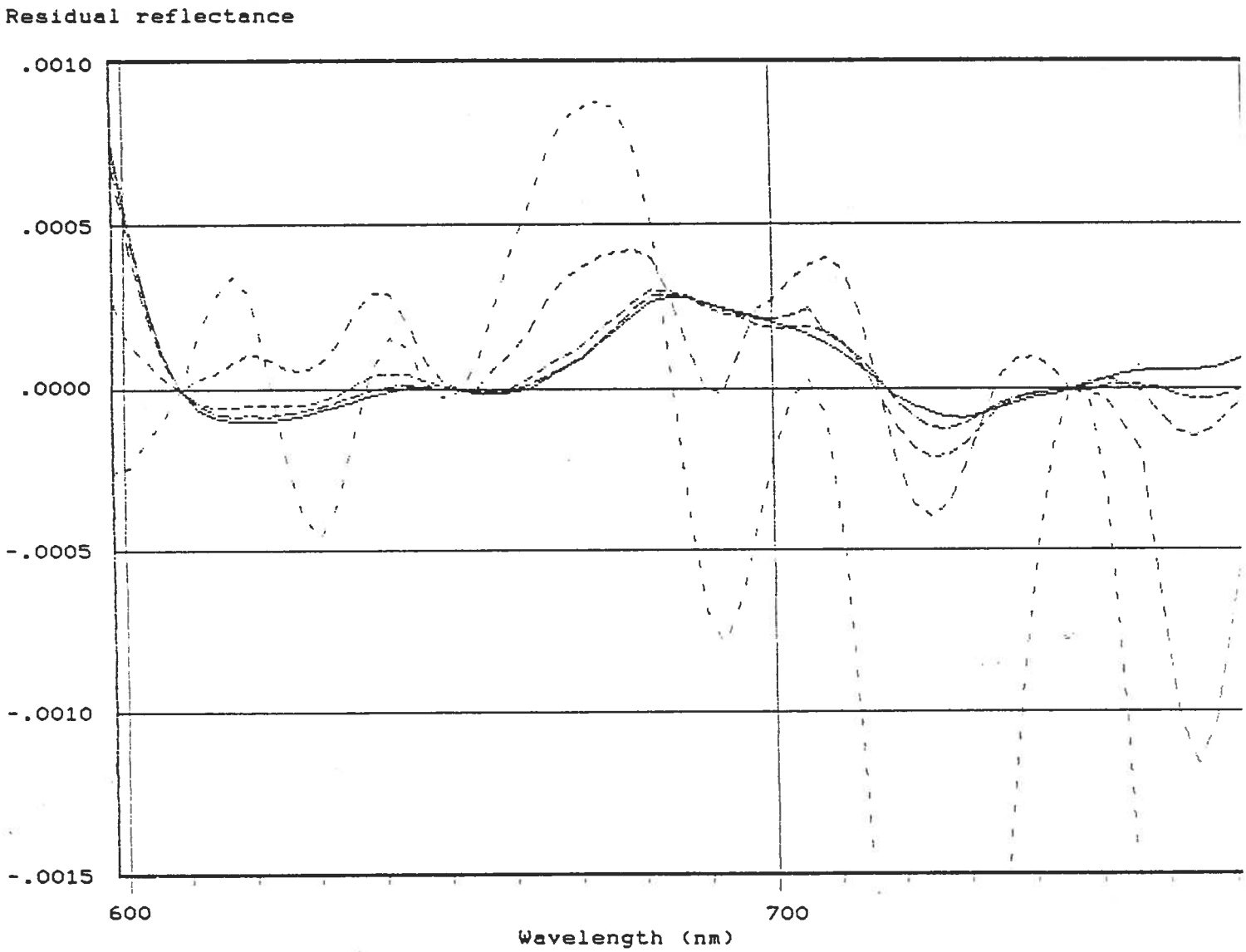

Figure 4.8.1 (a) Variation of the shape of the residual reflectance spectra on April 20 after subtraction of a curved (parabolic) baseline intersecting at 609, 665 and 746 nm.

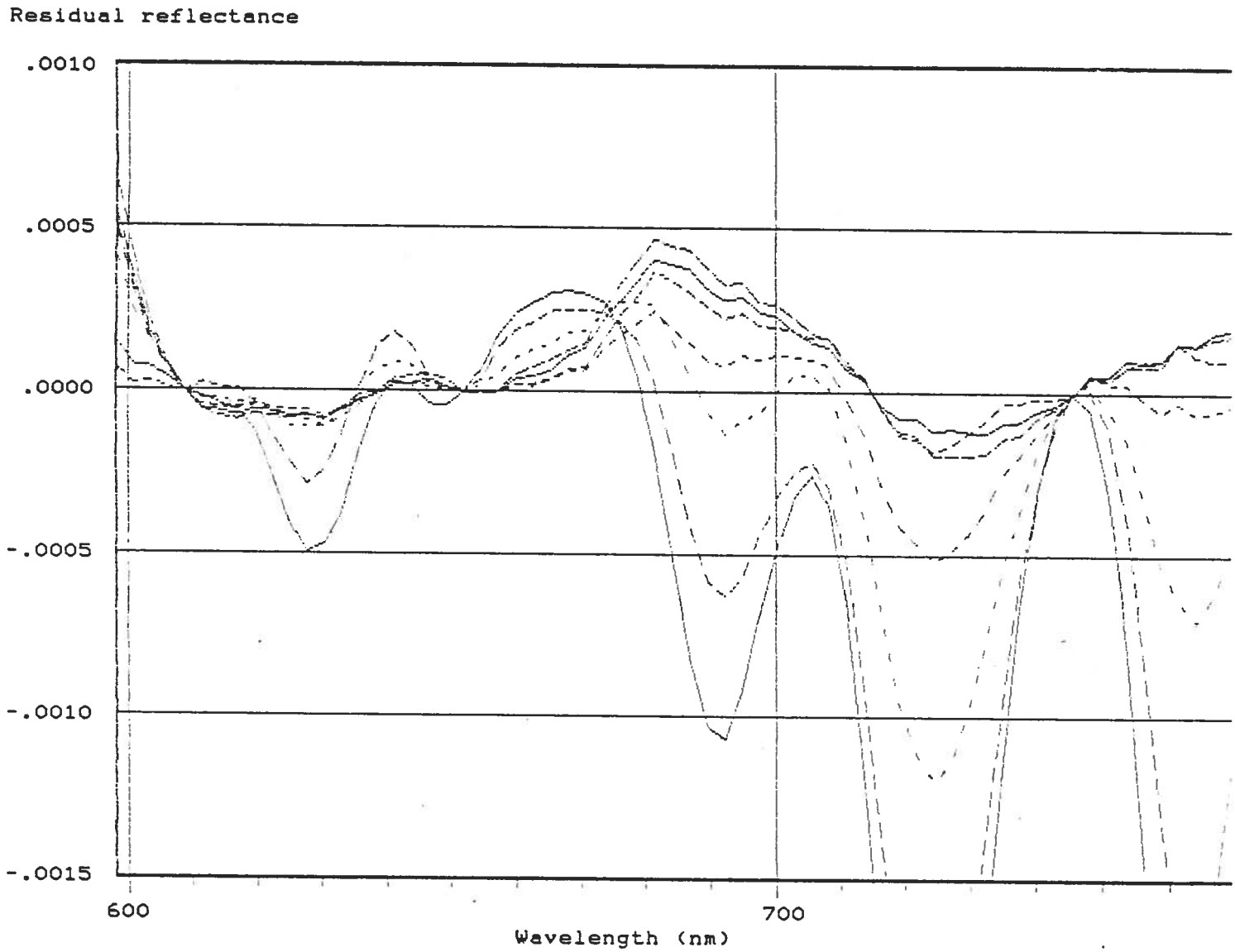

Figure 4.8.1 (b) Variation of the shape of the residual reflectance spectra on April 25 after subtraction of a curved (parabolic) baseline intersecting at 609, 665 and 746 nm.

It is significant that between the April 20 and 25 observations, and in other measurements made over the Mediterranean in March 22 1979, the absorption features are sufficiently different as to produce different variations with altitude of the apparent fluorescence line.

(c) A sensor with improved spectral properties.

The best solution to the problem would appear to be in placing well enough defined spectral bands of a satellite imager so as to minimize these effects. The Fluorescence Line Imager was designed as an imaging spectrometer that would test and demonstrate this capability. Figure 4.8.2 shows a reflectance curve measured with the FLI over shelf water off the east coast of the USA in December 1984. It can be seen that the 2.5 nm resolution of this instrument allows measurement between the absorption features that are merged in figure 4.6.2. In its imaging mode the FLI sets the wavelengths of spectral bands in steps of 1.3 nm. Figure 4.8.2 also shows, as vertical shaded strips, the positions of these bands as chosen in recent flights, which avoid these absorption features. Band combinations 3,4,5 and 4,5,6 are presently being evaluated for chlorophyll fluorescence imaging.

5.4 Scales of the horizontal variability of chlorophyll / phytoplankton as indicated from remote sensing measurements.

For addressing the resolution requirements of an ocean colour scanner, the average properties of ocean and coastal areas must be considered. To illustrate the problem, satellite images, numerical models and average measurements of ocean dynamics can be used. In many ocean and coastal areas, the scales of water colour patterns will reflect the scale of ocean mesoscale turbulence, forming patterns such as that shown in Figure 5.4.1, which represents a Landsat image 180 Km across.

The range of scales in such patterns is extremely wide (Gower et al., 1980), extending in a continuous spectrum from the scale of the generating weather patterns (order of 1000 Km) down to scales where molecular diffusion is important (order of a few centimeters). Over this entire range, increasing sensor resolution will lead to increased detail on the resulting images. However, for a satellite with a minimum re-visit time of 1 day, the finer detail will be uncorrelated, and cannot be used to follow water movements or evolution of dynamic events. One criterion in selecting a sensor resolution, is therefore to observe the finest details that remain correlated over a one day interval.

The results of a numerical model can be used to illustrate this. Figure 5.4.2 (a) shows modelled patterns formed by a passive tracer under the influence of a two-dimensional oceanic turbulence field. Tracer concentrations are constrained to be higher in the

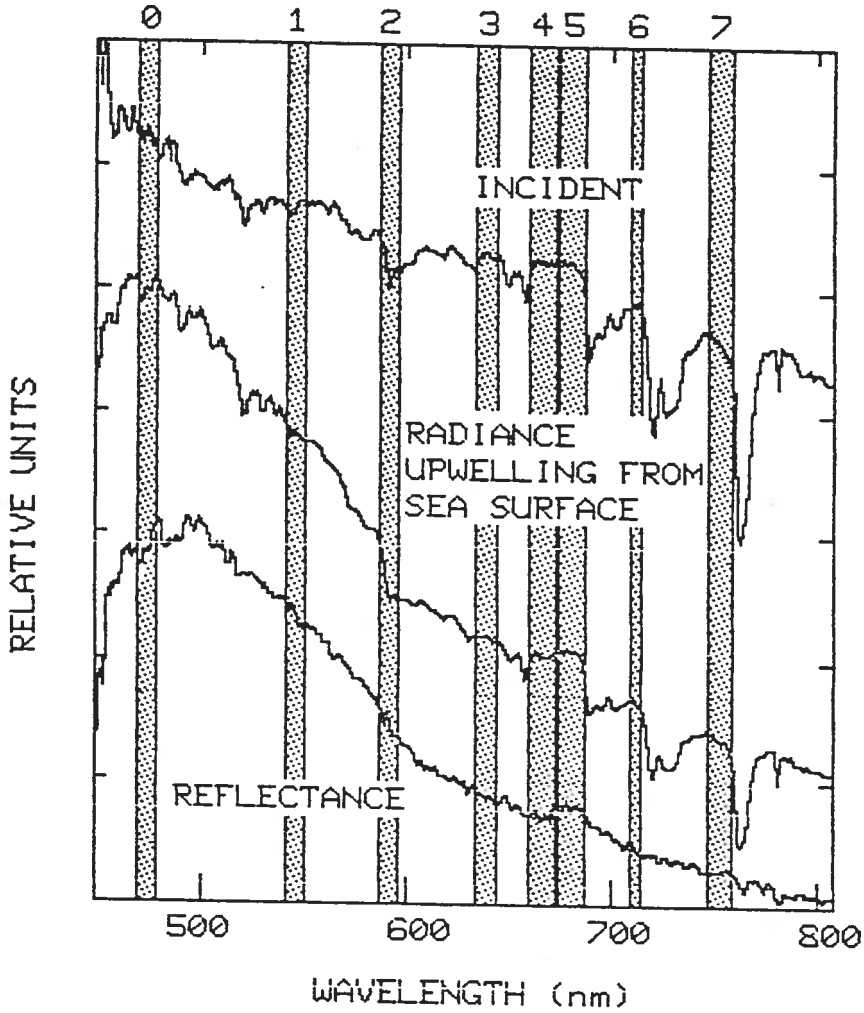

Figure 4.8.2 Ed+ (top) and Lu+ spectra (centre) observed with the FLI imaging spectrometer showing the computed reflectance (bottom), and one of the spectral band configurations (shaded columns) selected for water colour imaging.

top right and lower in the bottom left. The image can be taken to represent an area 400 Km across. Figure 5.4.2(b) shows the computed pattern after a 1 day time interval. Features are highly correlated on spatial scales down to about 10 - 20 Km. In figures 5.4.2 (c), (d) and (e) the time interval is increased to 4, 10, and 20 days. Correlation is apparent for the 40 - 50 Km scales in (c) and larger (say, 50 - 80 Km) scales in (d), but except for the fixed mean gradient, is absent in (e).

Because the spatial variability is represented by a continuous, linear energy / wave number spectrum, the same images also represent the patterns expected on other spatial scales. The above scales for the images are appropriate to an area with r.m.s. eddy velocities of about 0.1 $m.s^{-1}$. Scaling to maintain this same velocity, means that if the images are taken to represent, for example, real scenes 100 Km across, then the time intervals between (a) and (b), (c), (d) and (e) are 1/4, 1, 2.5 and 5 days respectively.

Images (a) and (c) can therefore show the pattern change expected over a one day interval in a scene 100 Km across. Similarly, pairs (a) and (d) and (a) and (e) may be used to represent 1 day variations in scenes 40 and 20 Km across respectively.

When interpreting the images in this way the scales for which correlation is apparent should be constant for all 4 pairs. The numbers estimated above translate to 10 - 20 Km, 10 - 12.5 Km, 5 - 8 Km, i.e. a roughly constant value in the 7 - 15 Km range. No correlation would be expected between (a) and (e).

Motions on this scale should be typical of many ocean and coastal regions. According to this model, only scales larger than about 10 Km in these areas can be correlated over a 1 day interval. A satellite sensor with 1 Km resolution, such as the CZCS, is already capable of imaging this range, with some resolution in hand to cover lower energy areas. Justification for instruments with higher resolutions must therefore be made in other terms: more precise single images, imaging of smaller areas or lakes, more exact correlation with ship measurements, or measurement capability through small gaps in cloud.

Data bandwidths and processing complexity are also important factors. The 1 km resolution of the AVHRR and CZCS represent a reasonable compromise which was followed in designing the FLI instument.

6.4 Radiance profiles from low flying aircraft in remote sensing surveys, and as ground truth for satellite data evaluation.

Figure 5.4.1 Landsat image showing scales of horizontal variability of phytoplankton in an intense bloom in the Atlantic ocean south of Iceland on 19 June 1976. (Gower et al., 1980)

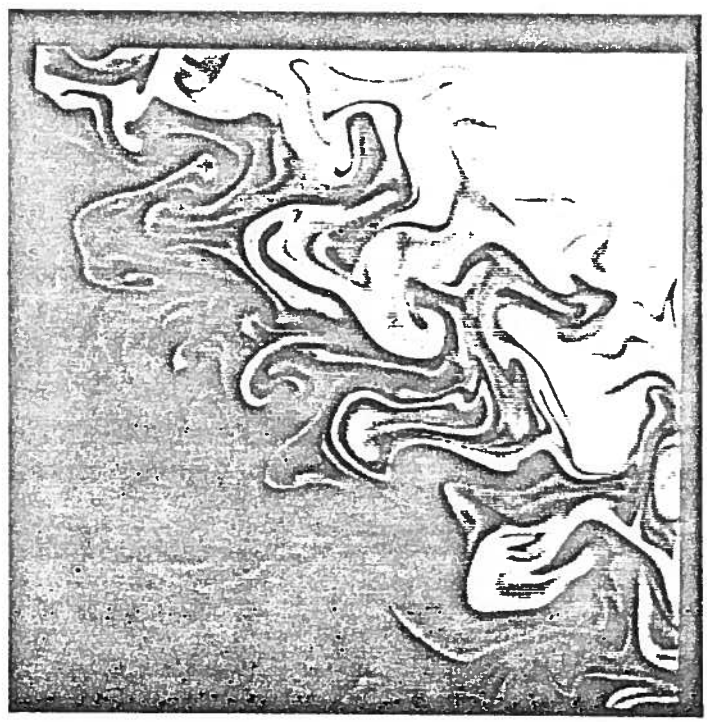

Figure 5.4.2 (a) Time 0.

Figure 5.4.2 (a) to (d) Numerically modelled images of horizontal variability of phytoplankton, showing changes with increasing time intervals in the ratio 1 to 4 to 10 to 20.

Figure 5.4.2 (b) Time 1.

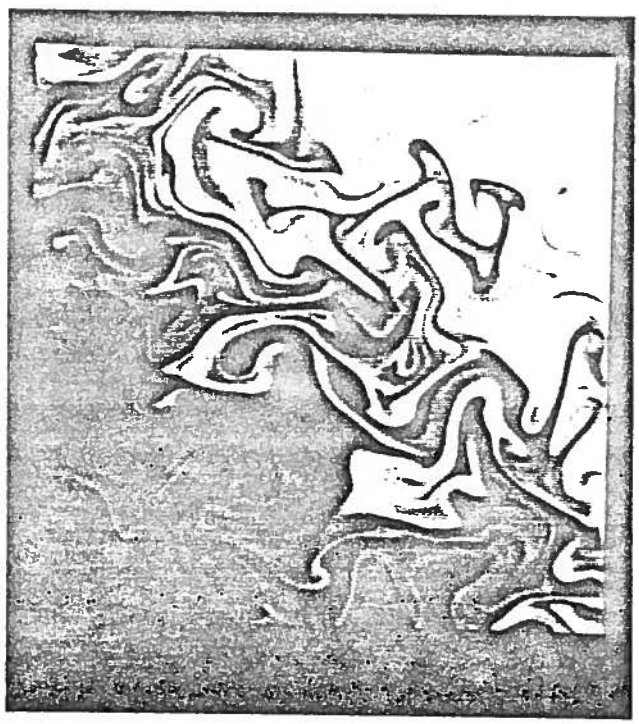

Figure 5.4.2 (c) Time 4.

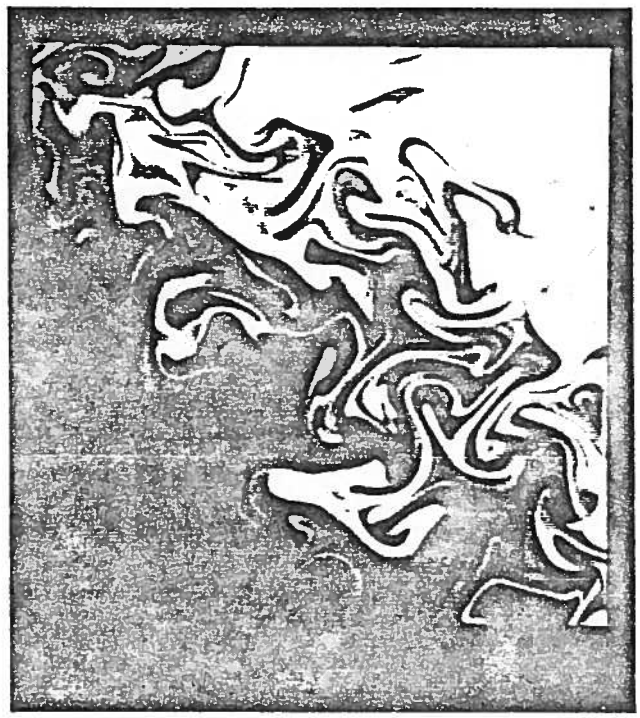

Figure 5.4.2 (d) Time 10.

Figure 5.4.2 (e) Time 20.

Figure 6.4.1 shows (dashed curve), a spectrum taken at 500 ft over the North Sea Tower on April 20 in Flurex (lowest curve in Figure 4.6.1(a)). From the similar spectrum taken at 1000 ft altitude, the reflectance increase due to 500 ft of atmosphere can be calculated (dotted curve), and a corrected spectrum can be derived, by linear extrapolation, for the zero altitude case (solid curve). This will still contain a contribution from surface reflection, though in these observations, this was minimized by observing through a polarizing filter. Water radiance is low at wavelengths longer than 750 nm, but the polarizer becomes inefficient after about 780 nm. Radiance observations beyond 800 nm are used only to indicate possible residual surface reflection. Water reflectance spectra in this report are often zeroed at 780 nm to suppress atmospheric and surface reflection effects.

Further analysis of this data is illustrated in figure 4.6.5(a) and 4.8.1(a). It can be seen that, even though the atmosphere contributes most of the radiance in the region of the fluorescence line, the shape of the reflectance curve converges rapidly to its surface form at the lower altitudes. Computation of accurate in-water radiances from airborne data requires more careful corrections, but airborne chlorophyll surveys can be carried out using both the fluorescence line and the green to blue ratio methods. Such surveys can extend the speed and area of coverage of measurements well beyond the capabilities of a ship.

One demonstration of this was undertaken with the IOS spectrometer in the eastern Canadian arctic in 1979 (Borstad and Gower, 1984). Chlorophyll and surface temperature were measured from the air to produce maps in good agreement with ship measurements. In three flights the aircraft was able to equal the number of line miles covered by the ship in 12 days of observing. In this case the aircraft had the distinct advantage of not being restricted in its track by sea ice, though the spectrometer requires open water areas at least 100 meters across to make a measurement.

7.1 Variability of radiance spectra from case 2 water.

Figures 7.1.1(a) and (b) show spectra measured with the IOS spectrometer in flights and ship operations in B.C. and during FLUREX. With the exception of the lake spectrum in Figure 7.1.1(b), they have been adjusted vertically to give zero reflectance at 780 nm. They illustrate the variability caused by suspended sediment and high levels of phytoplankton. In Figure 7.1.1(a) suspended sediment causes an increase in reflectance over the range 400-600 nm, and a smaller increase at longer wavelengths which tilts the baseline for fluorescence, but does not prevent measurement of the line height.

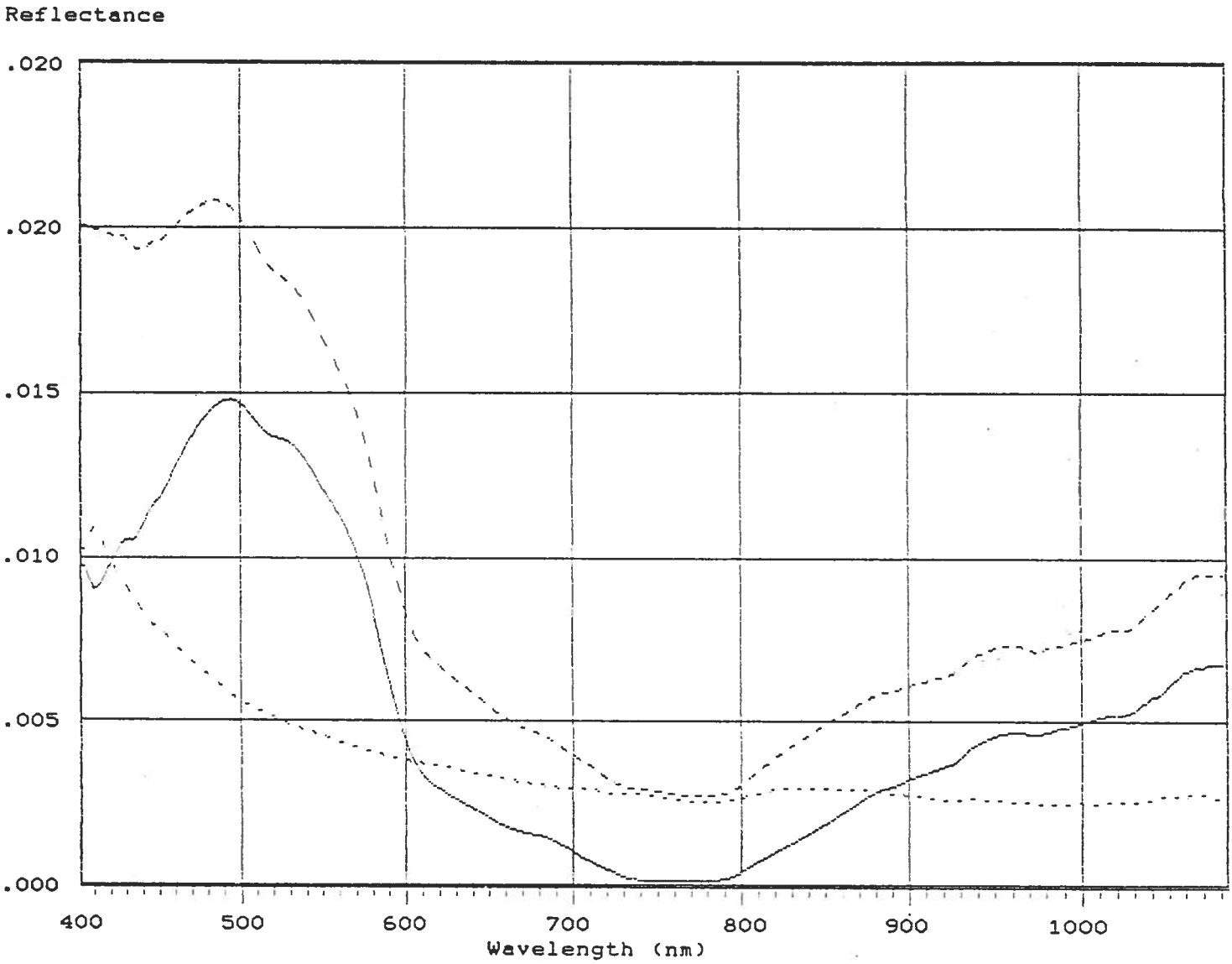

Figure 6.4.1 Reflectance spectra observed at 500 ft (dashed). A correction for the atmospheric component (dotted) allows computation of a near surface spectrum (solid line) which can be used as ground truth for satellite observations.

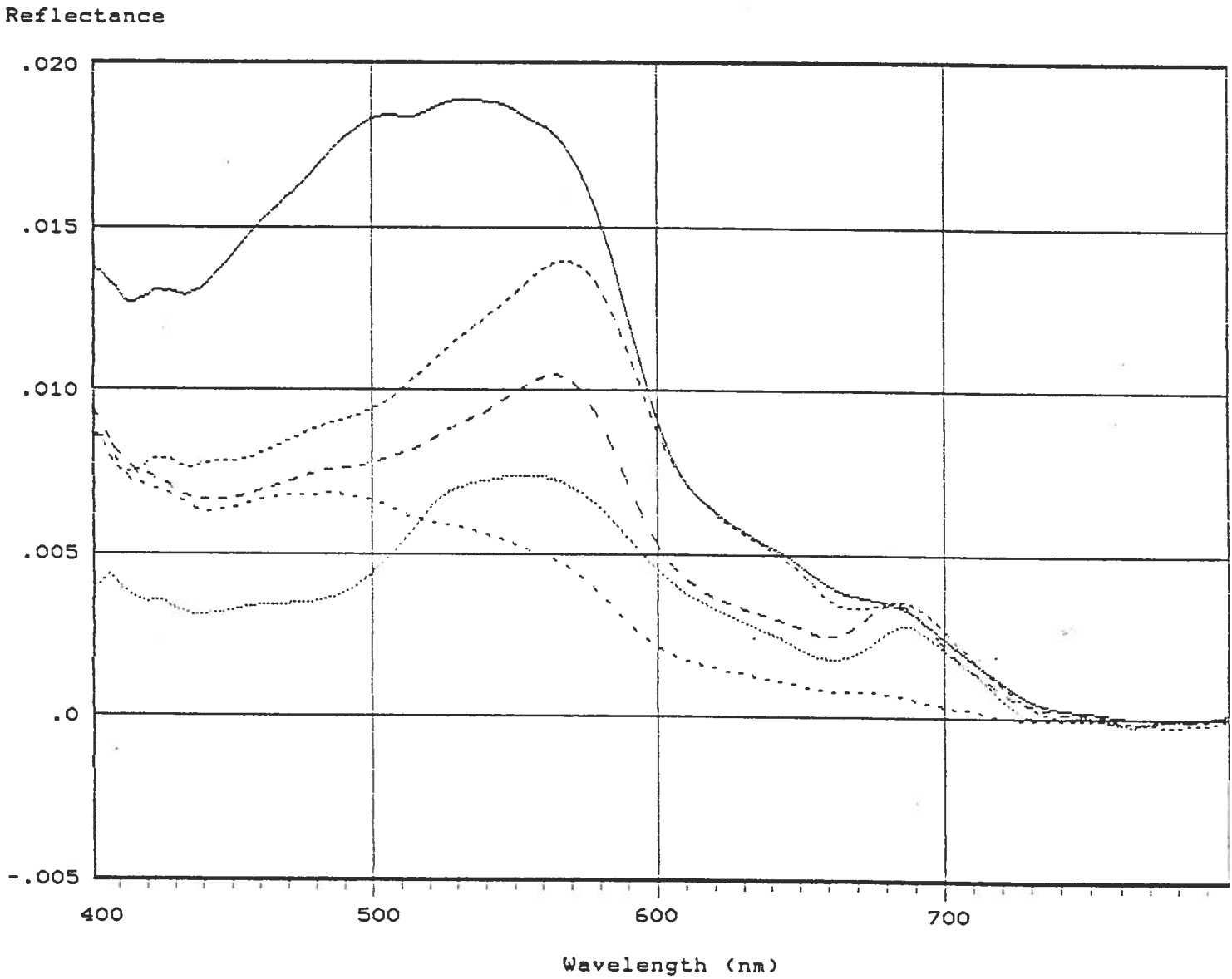

Figure 7.1.1(a) Reflectance spectrum showing increased back-scatter from suspended inorganic material (solid line) compared to the reflectance spectra observed in case 1 waters (dashed lines). (Observations along the B.C. coast and in FLUREX)

Under anomalous conditions of high phytoplankton concentration (Figure 7.1.1 (b)), the peak of the fluorescence line is observed to be shifted to 700-710 nm (Lin et al., 1984). The overall reflectance varies with the relative scattering of the phytoplankton species involved, but is generally low shortward of 500 nm. The upper short dashed spectrum is form a lake near Station 11 in FLUREX. These spectra suggest that chlorophyll absorption at 670 nm is an important factor in determining the form of the observed fluorescence.

Other factors were also observed to affect the spectra collected in FLUREX. Figure 7.1.2 shows the effect of an apparent change in fluorescence efficiency in water crossed by the Alkor in a time interval of 3 minutes. The difference between the two spectra shows that most of the change was in the height of the fluorescence line. Accurate measurement of such a difference spectrum give a precise measurement of the position and width of the line, and demonstrates that the feature is caused by fluorescence, rather than by a combination of absorption and reflectance.

Another cause of variation in observed water reflectance spectra will be the effect of a reflectance contribution from the sea bottom, or from near-bottom re-suspended material. Figure 7.1.3 shows a series of water reflectance spectra measured at a height of 500ft on a flight line over the Baltic. These have been adjusted vertically to give zero reflectance at 780 nm. The lower solid curve shows a typical reflectance contribution from the 500 ft of atmosphere beneath the aircraft on this flight, deduced by extrapolation from a pass at 1500 ft. Variations in low-level haze or surface reflection appeared to be affecting the data, and a correction was therefore applied by scaling this atmospheric contribution so that, after its subtraction, the remaining reflectance at 408 nm is zero. The results are shown in figure 7.1.4.

The time sequence is illustrated in figure 7.1.5. The flight is from FLUREX station 3 to 8 to 9, passing over shallow water near the coast near Falhoeft at 3 minutes into the flight, and over the Stoller Grund at 12 minutes. The increase in reflectance at 3 minutes is shown in figure 7.1.6. This has a strong effect on the green to blue ratio as shown in figure 7.1.5, but is clearly a bottom effect as indicated by the narrow spectral peak, centred on 570 nm, close to the expected wavelength for minimum absorption in coastal waters, and the absence of any fluorescence signal. Figure 7.1.7 shows the forms of reflectance increases at other times. They evidently fall into two types: those due to near surface phytoplankton, and those due to bottom reflectance.

In shallow waters the limited depth penetration of the fluorescence method is a clear advantage in avoiding confusion with bottom effects.

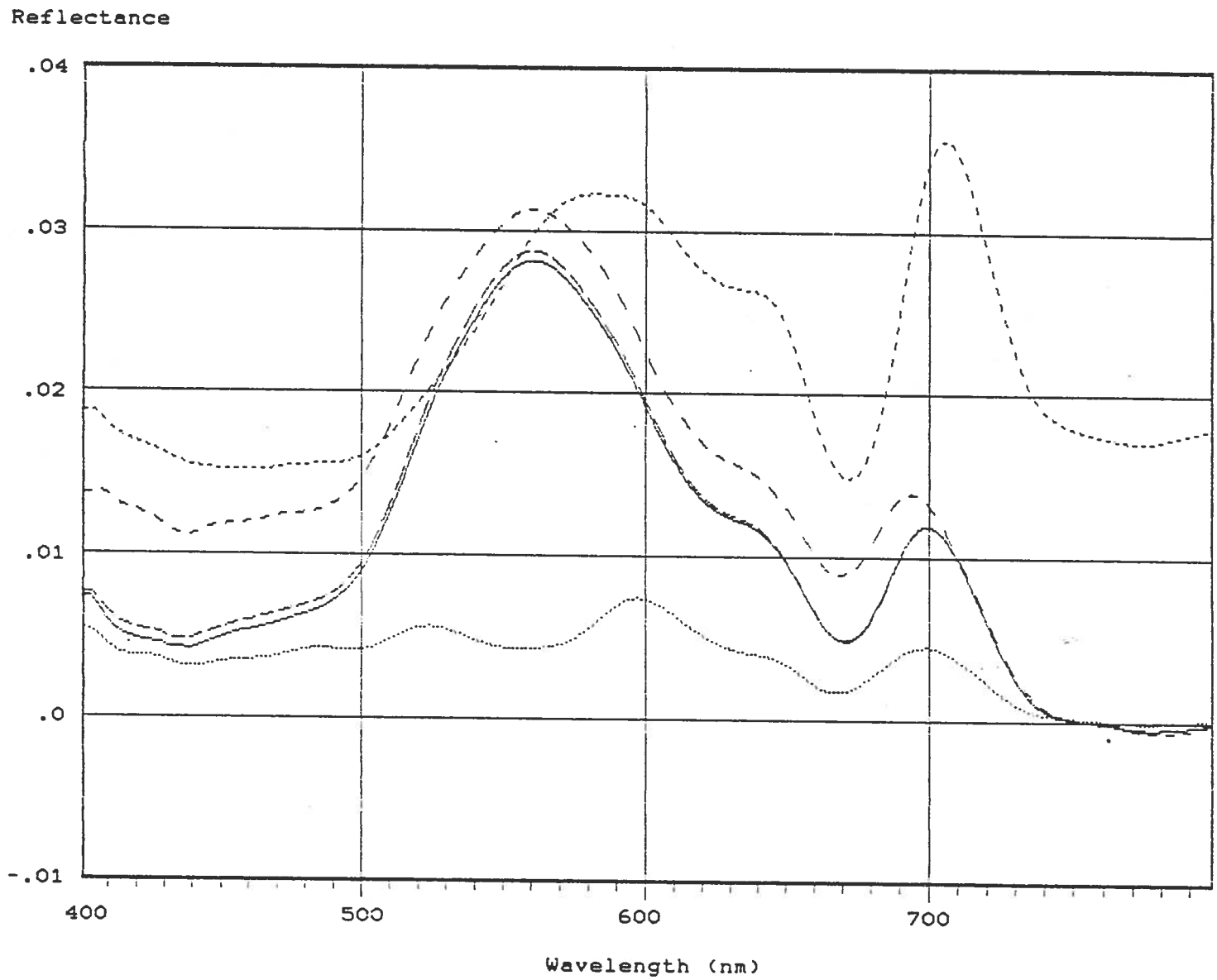

Figure 7.1.1(b) Reflectance spectra showing high and anomalous values due to large amounts of phytoplankton. Solid and long dashes, spectra in Schlei. Medium dashes, leaving Schlei (14:50 after Tonne 23). Short dashes, upper curve, lake observed near Kiel, Station 11. Dotted, lower curve, Mesodinium Rubrum bloom in B.C. coastal inlet.

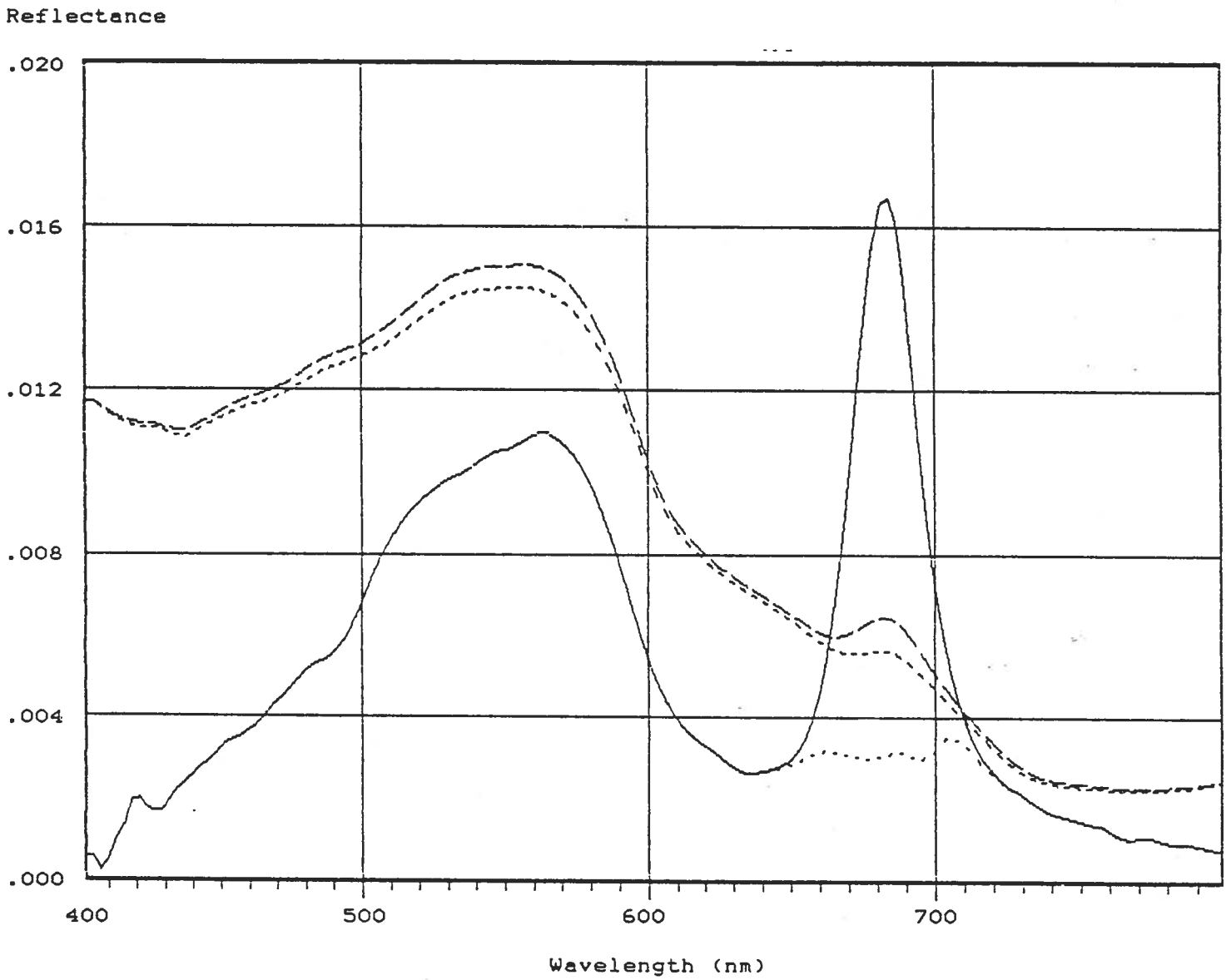

Figure 7.1.2 A reflectance increase (solid curve, at 20 times scale) observed from the deck of a ship in the entrance to Kiel Harbour, between spectra (dashed) taken at two locations roughly 300 m apart. The dotted line is the residual after subtracting a Gaussian line shape centred at 683.5 nm and 24 nm wide at half height.

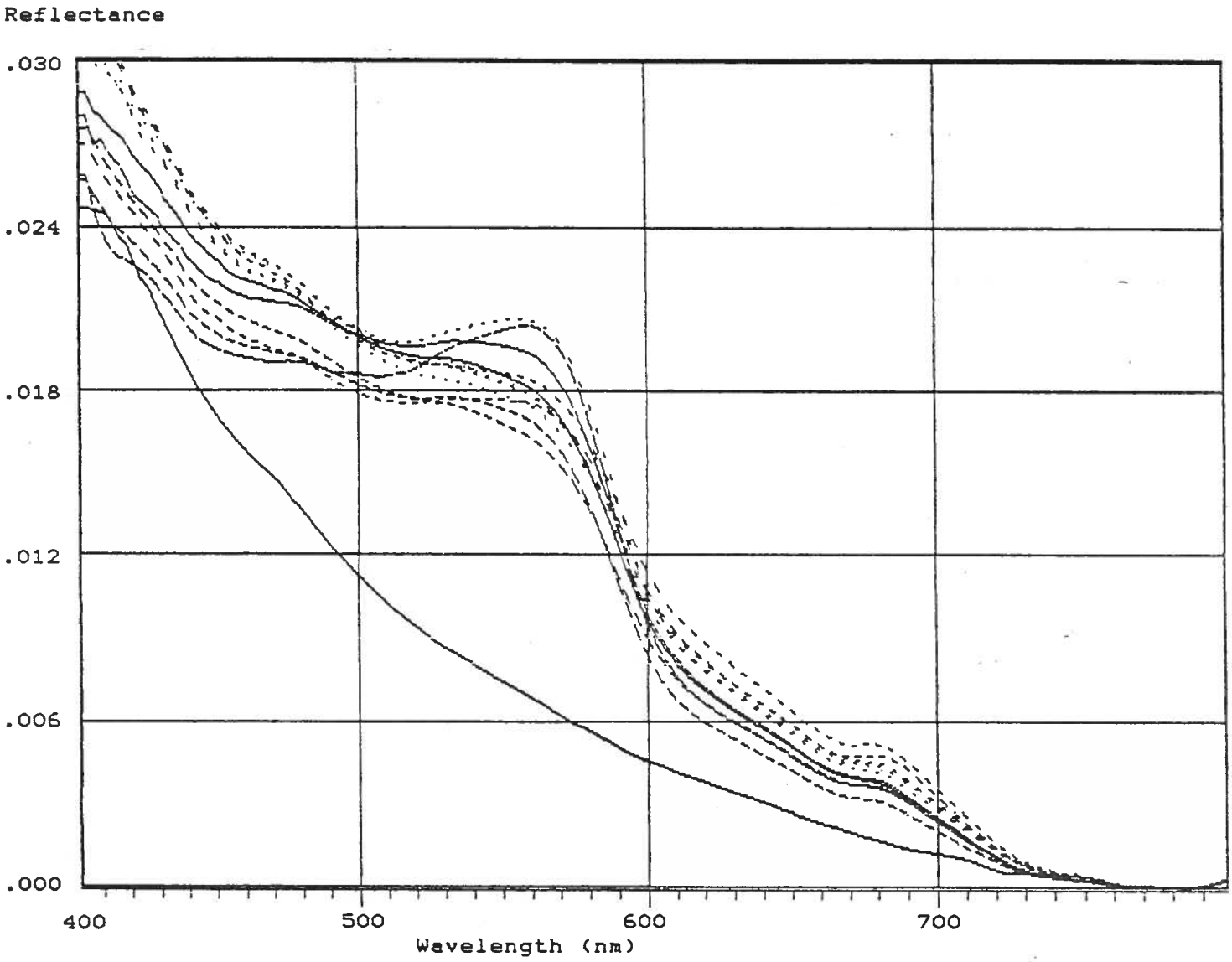

Figure 7.1.3 Reflectance spectra observed over the baltic at 500 ft altitude on a line crossing FLUREX stations 3,8, and 9. All are adjusted to zero reflectance at 780 nm. The lower solid line shows mean atmospheric back-scatter.

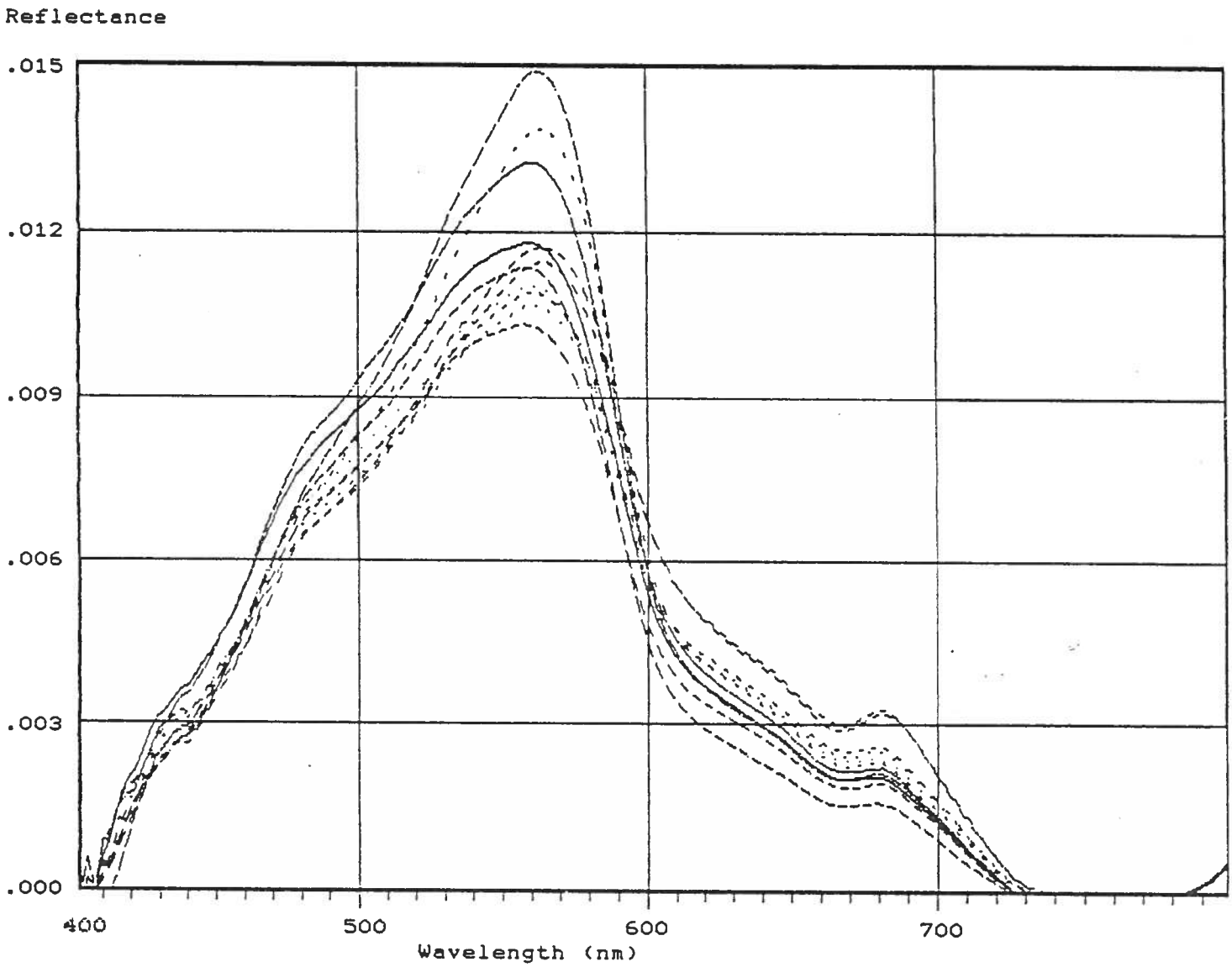

Figure 7.1.4 Reflectance spectra of Figure 7.1.3 adjusted to zero reflectance at 408 nm.

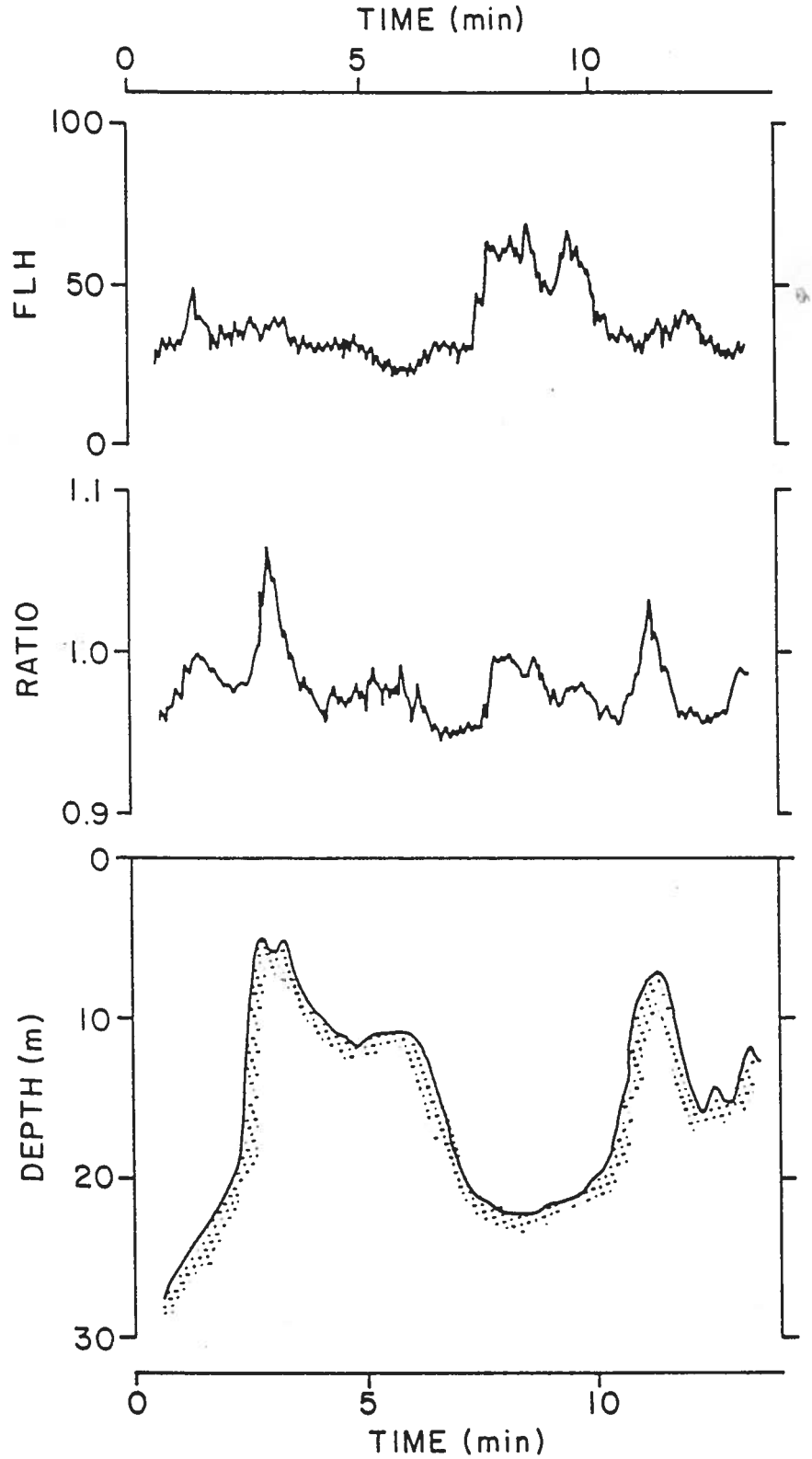

Figure 7.1.5 A plot of fluorescence and green/blue ratio indicators of chlorophyll, against time in a flight over the Baltic during FLUREX (top 2 plots). Two peaks in the ratio plot that do not coincide with increases in fluorescence, correlate with shallow water (bottom plot).

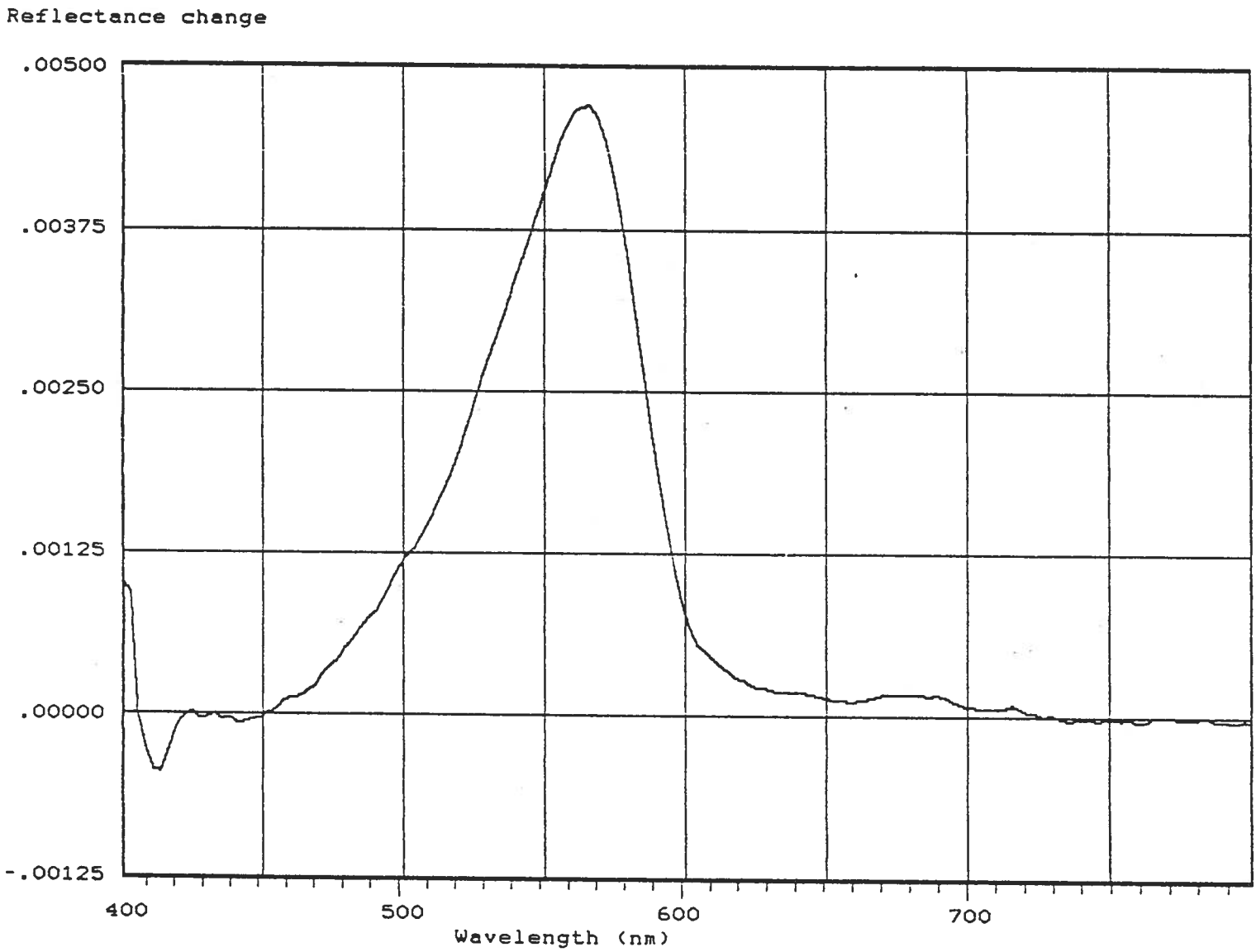

Figure 7.1.6 The spectral form of the reflectance increase at the sharp peak in the ratio plot of Figure 7.1.5 at a time of 5 minutes.

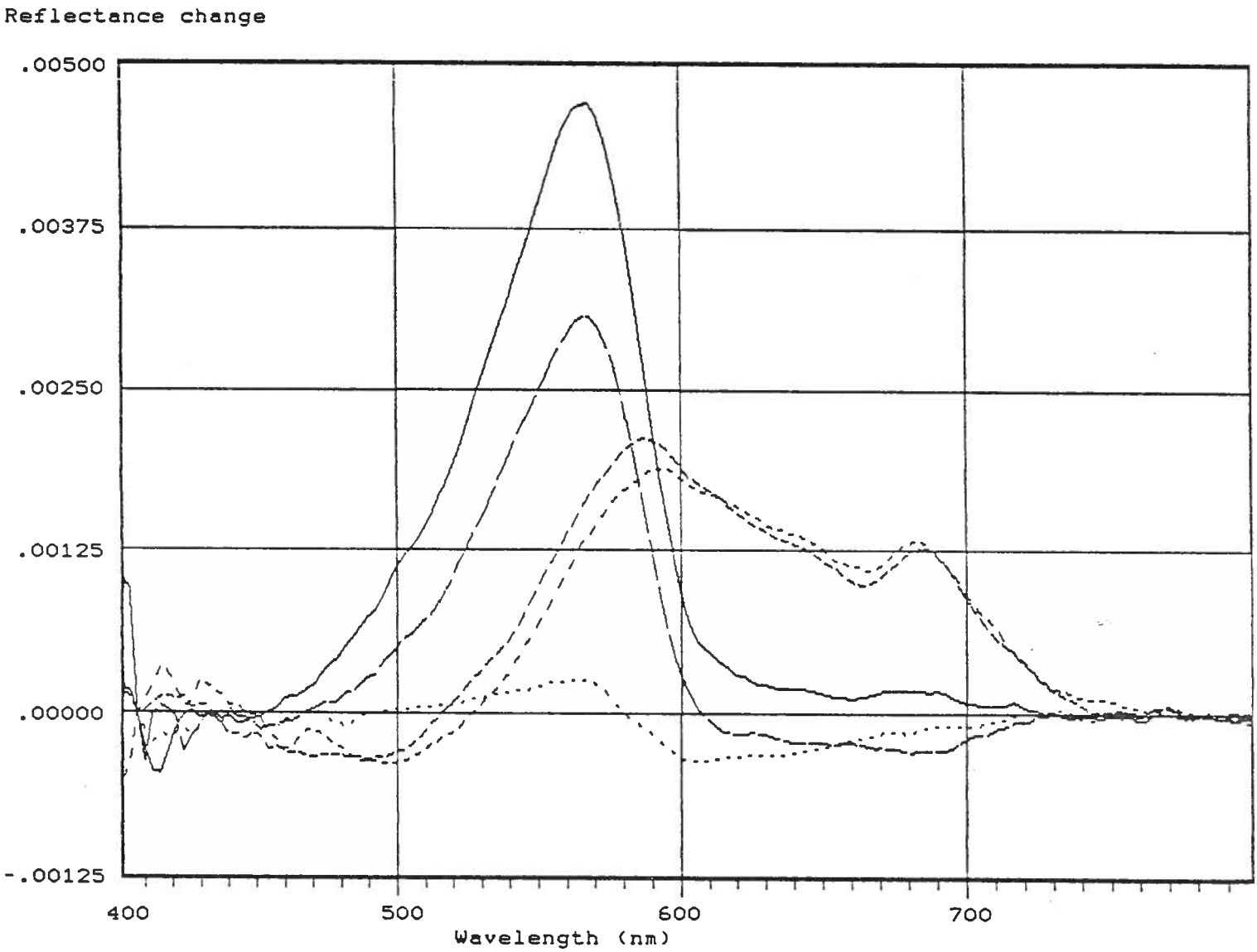

Figure 7.1.7 The spectral form of the reflectance increases at the two sharp peaks in the ratio plot of Figure 7.1.5 (time = 5 minutes, solid line, 11.5 min, long dashes), at the two peaks in the fluorescence plot (8.5 and 9.5 min, longer and shorter medium dashes), and over the 10 meter depth water at 5 min (short dashes).

7.2 Determination of spectral bands related to chlorophyll by means of factor analysis.

In order to test the utility of the fluorescence and the green to blue ratio methods of chlorophyll mapping, observed or modelled spectra can be analysed by characteristic vector or factor analysis to search for additive component spectra, covering the full wavelength range, that contribute significantly to the total variance (Doerffer, 1981, Gower et al., 1984, Fischer et al., 1986).

Gower et al. used a series of spectra observed from a boat, from which simultaneous measurements of near surface chlorophyll *a* were also made. The characteristic vectors are as shown in Figure 7.2.1. All spectra were zeroed at 780 nm to remove the (approximately white) contributions from surface reflection, which amounted to .1 to .5 percent. The mean spectrum shows the increase to 1 percent below 550 nm and the fluorescence emission at 685 nm. the first 4 eigenvectors accounted for 86, 11, 2, and 0.6 percent of the variance about this mean. In Figure 7.2.1 these have been weighted by their contributions to the total variance. The first eigenvector has the form expected for varying near-surface backscatter. The second has the form for suspended phytoplankton, (blue chlorophyll pigment absorption, backscattering in the blue/green and green and fluorescence centred on 685 nm), while the third still shows fluorescence, but indicates a different response at short wavelengths.

The spectral bands needed for measurement of the spectral variations present in this data are evident from the Figure. Suspended sediment can be detected with a single band in the 500-550 nm range. Chlorophyll detection needs a shorter wave band at 400-450 nm for use of the green to blue ratio, and bands spaced across the fluorescence line for the line height method. Precise positions of these latter bands must be determined by atmospheric absorption effects (Section 4.6).

7.3 Comparison of signal/noise ratio of different chlorophyll related spectral bands.

Linear combinations of the relative weights of these eigenvectors can be fitted to the measured chlorophyll values, and the resulting correlation can be used to evaluate the potential accuracy for determining chlorophyll *a* concentrations from spectral data. The analysis can be restricted to wavelength ranges covering the green and blue (appropriate to the ratio method) or to the red (fluorescence). Results in B.C. coastal waters are discussed by Gower et al., (1984). For this data the correlation between remote sensing and ship measurements was improved when the longer wavelength data alone was used, that is, when fluorescence, rather

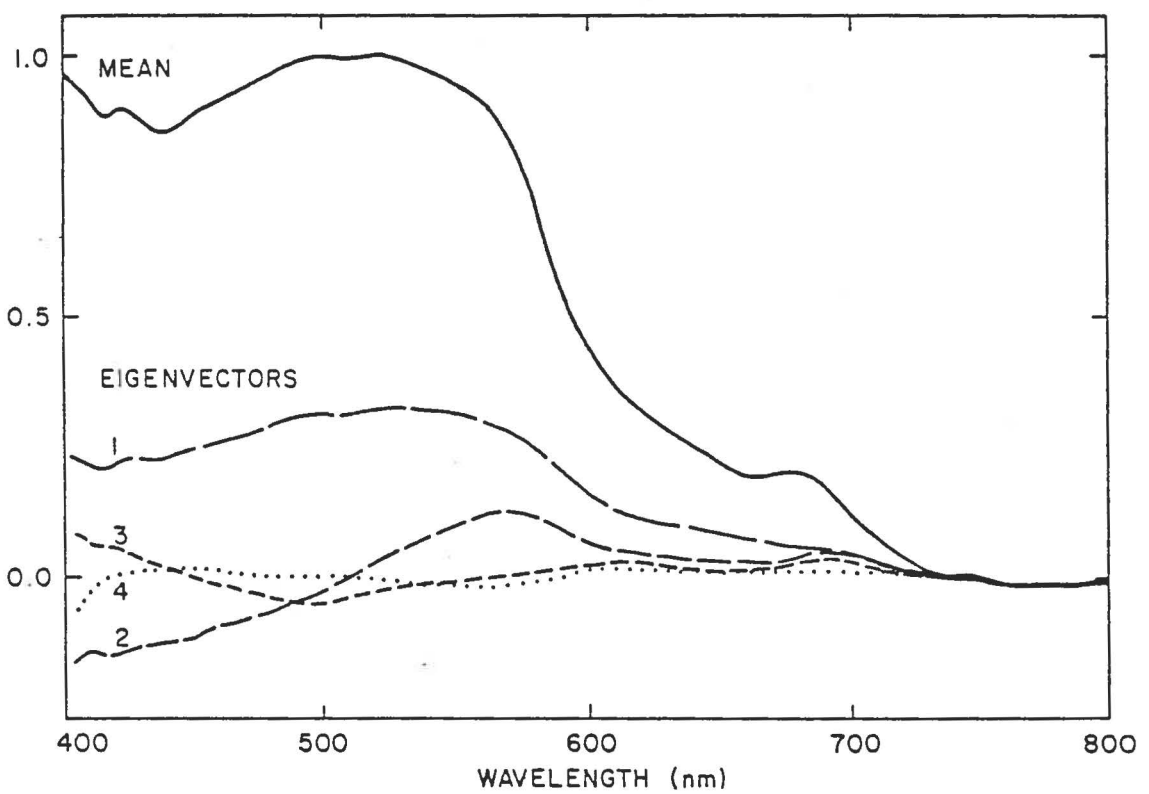

Figure 7.2.1 Characteristic vectors derived from a series of 47 above-surface water reflectance spectra collected over a 4 month period (July - October 1981) in B.C. coastal waters.

than absorption (green/blue ratio) was used to measure chlorophyll. Fischer et al (1986) reach a similar conclusion using model spectra.

Since the fluorescence signal has a linear response to chlorophyll, and gives a specific narrow spectral signature. It would be expected to give improved measurements in coastal or "case 2" waters where concentrations are high (.5 $mg.m^{-3}$ and above), and other suspended or dissolved material can influence the optical water properties, especially at shorter wavelengths. For lower chlorophyll concentrations in less complicated, "case 1", off-shore water the green to blue ratio, with its sensitivity for concentrations down to .02 $mg.m^{-3}$ should give improved results.

7.4 Derivation and test of fluorescence algorithms.

The fluorescence measuring algorithm normally applied with the IOS spectrometer makes use of the fact that a reflectance spectrum measured at a low flying altitude gives a smooth and nearly linear background near 685 nm (i.e. 640 - 730 nm). This allows the reflectance increase due to fluorescence to be easily measured. Peak reflectance near 550 nm is in the 1 to 2% range, dropping to 0.1 to 0.2% near 685 nm. The fluorescence signal gives typically about a 0.1% increase for a chlorophyll concentration of 5 $mg.m^{-3}$, and therefore represents a significant increase even at concentrations near 1 $mg.m^{-3}$.

Figure 7.4.1 shows the uncalibrated upwelling radiance (long dashes) and downwelling irradiance (short dashes) measured at 500 ft altitude over the North Sea tower on April 20 1982. Both curves are affected by the spectral response of the spectrometer, and by the absorption features described in section 4.6. The reflectance curve, calculated as the ratio of these (with corrections for differing light paths in the aircraft installation, dotted curve) is shown as the solid curve.

The effects of atmospheric absorption features are sufficiently reduced in this, reflectance curve, that chlorophyll fluorescence can be measured as the excess reflectance above a linear baseline, as discussed in section 4.6. Further analysis of this data is shown in figures 4.6.5 (a) and 4.8.1 (a).

7.5 Comparison with green/blue algorithm.

A statistical comparison with the green to blue algorithm is discussed in sections 7.2 and 7.3. Green and blue reflectance data are routinely measured with the IOS spectrometer, and both indicators are used in survey operations. Corrections for

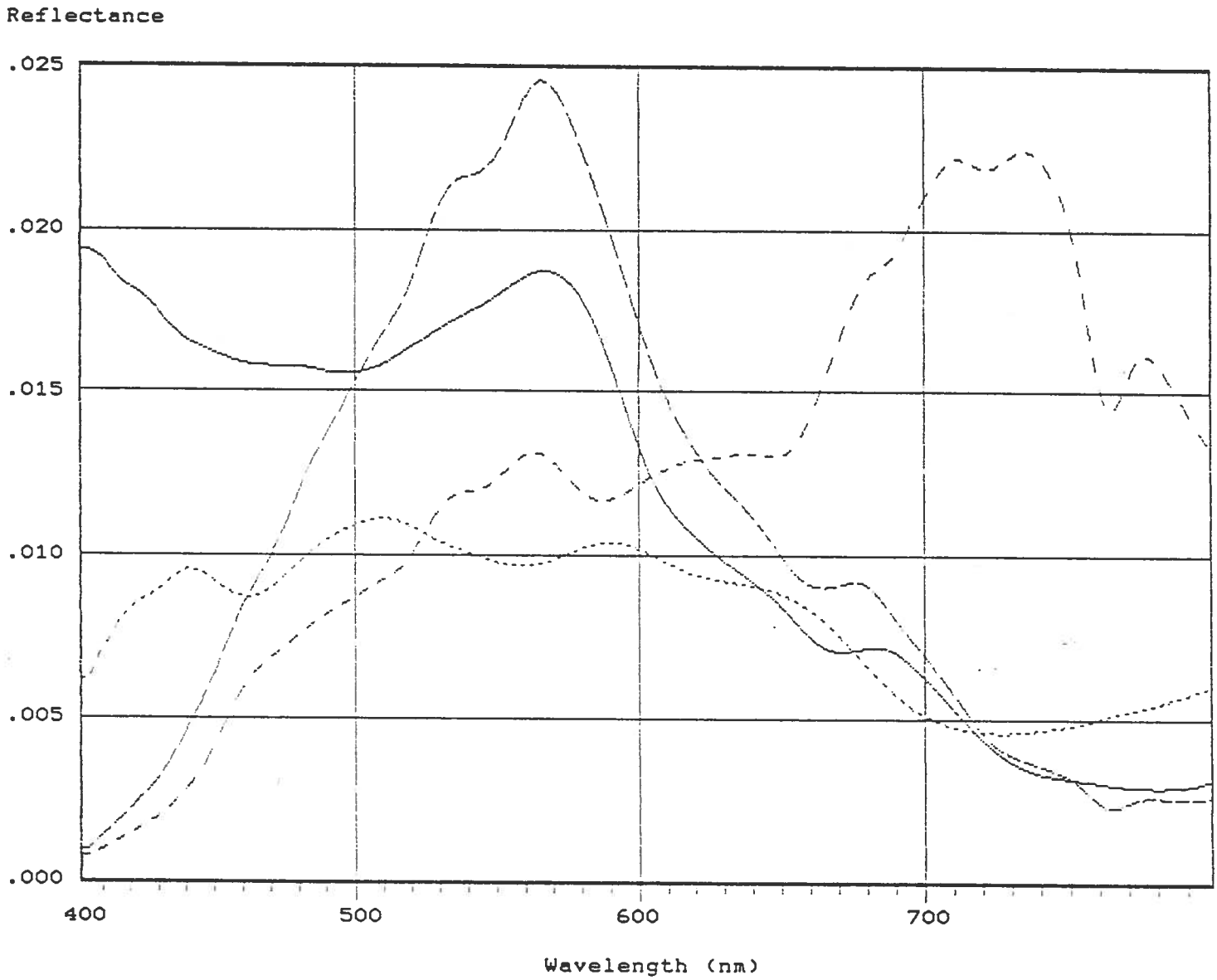

Figure 7.4.1 Spectra showing reflectance calculation and calibration with IOS spectrometer data (FLUREX, April 20, North Sea tower). Long dashes: uncalibrated radiance, short dashes: uncalibrated irradiance, dotted: correction for spectrometer light paths, solid line: computed reflectance.

atmospheric and surface effects are much more important for green and blue results, and this complicates observations under cloud, and in other difficult but common conditions.

For a specific comparison, Figure 7.5.1 shows data from a 22 minute section of one of the airborne flight lines over the mouth of Lancaster sound in the Canadian Arctic in August 1979. From top to bottom, these show the variation of the fluorescence line height at 685 nm, the reflectance at 780 nm, the green (560 nm) to blue (440 nm) reflectance ratio, the temperature and the down-welling (sun and sky) irradiance.

Although the fluorescence and the ratio indicators of chlorophyll are clearly responding to the same physical boundaries at the water surface, the values of the changes suggest different fluorescence efficiencies in different geographical areas. The correlation between the ratio and the fluorescence indicators of chlorophyll is shown in the scatter diagram of figure 7.5.2. This suggests that at least two different efficiencies were encountered, though varying observing conditions will cause some spread in the points.

Individual spectra from this line are plotted in figure 7.5.3. Spectrum (a) is from the first patch of elevated chlorophyll (Time = 12:27 on Figure 7.5.1) shows higher short-wave reflectance (indicating a higher ratio of backscatter to absorption) than in the second patch (Sectrum (c) at 12:41). Spectrum (b) was observed at 12:30, between patches. Spectra collected near (a) show relatively low fluorescence, and form the lower branch on figure 7.5.2.

The correlation observed in these and similar profiles has since spurred the development of the Fluorescence Line Imager as a satellite sensor. The capability of mapping the fluorescence efficiency of the phytoplankton, which is known to vary with its rate of productivity, is a further advantage that needs to be explored in more detail.

8 Aircraft data application test: Verification of algorithms including correction procedures with aircraft spectrometer and scanner data.

8.1 FLUREX data description and examples.

In the FLUREX operation the IOS spectrometer collected water spectra from a range of altitudes in a DFVLR Do-28 research aircraft in the period April 20-25 1982 over the North Sea and Baltic, while surface measurements were made on the Research Vessel

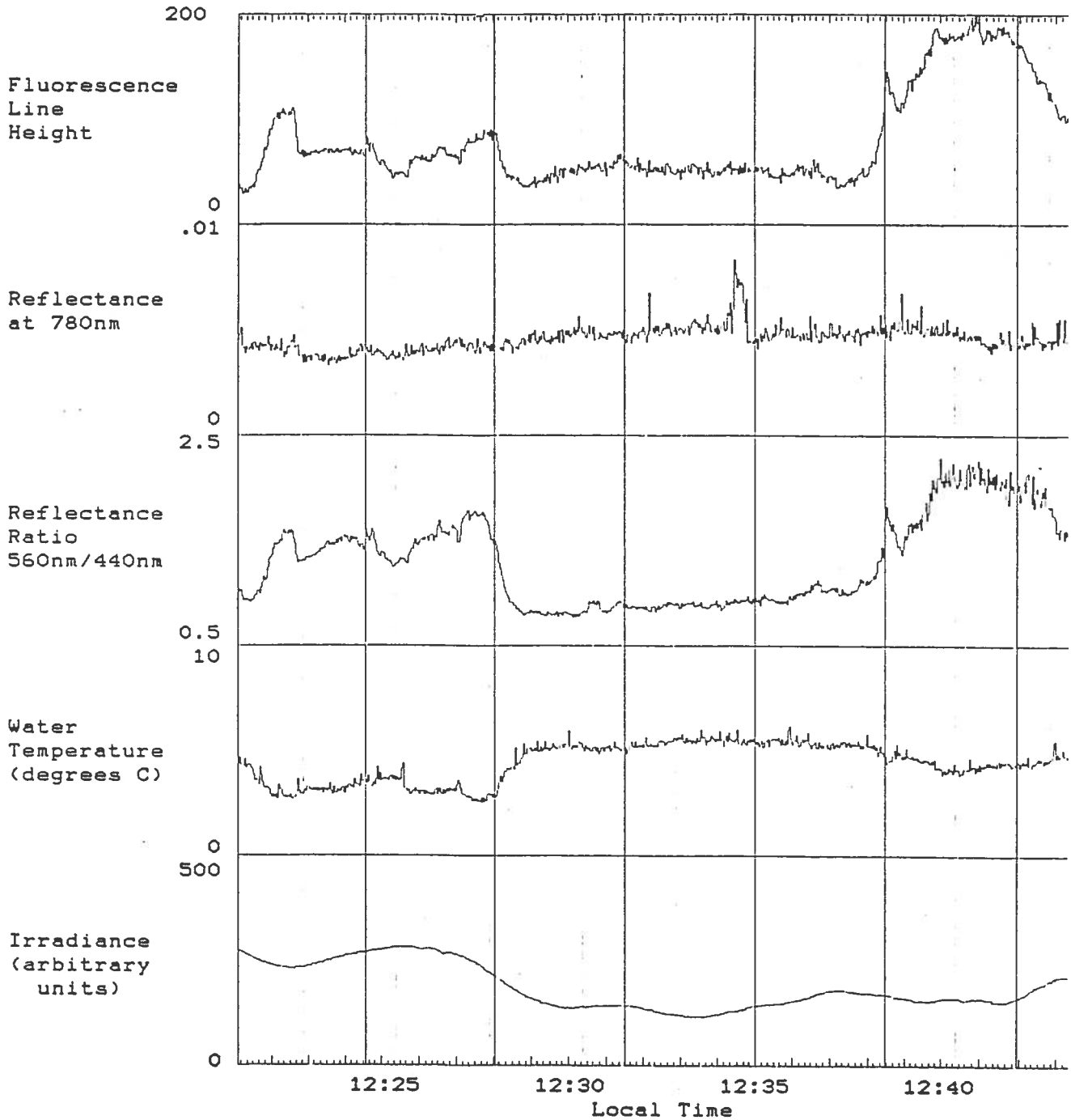

Figure 7.5.1 Data extracted from airborne spectral measurements over the eastern entrance of Lancaster Sound, August 26 1979, showing the correlation between fluorescence and ratio indicators of phytoplankton pigments, and a negative correlation with water temperature.

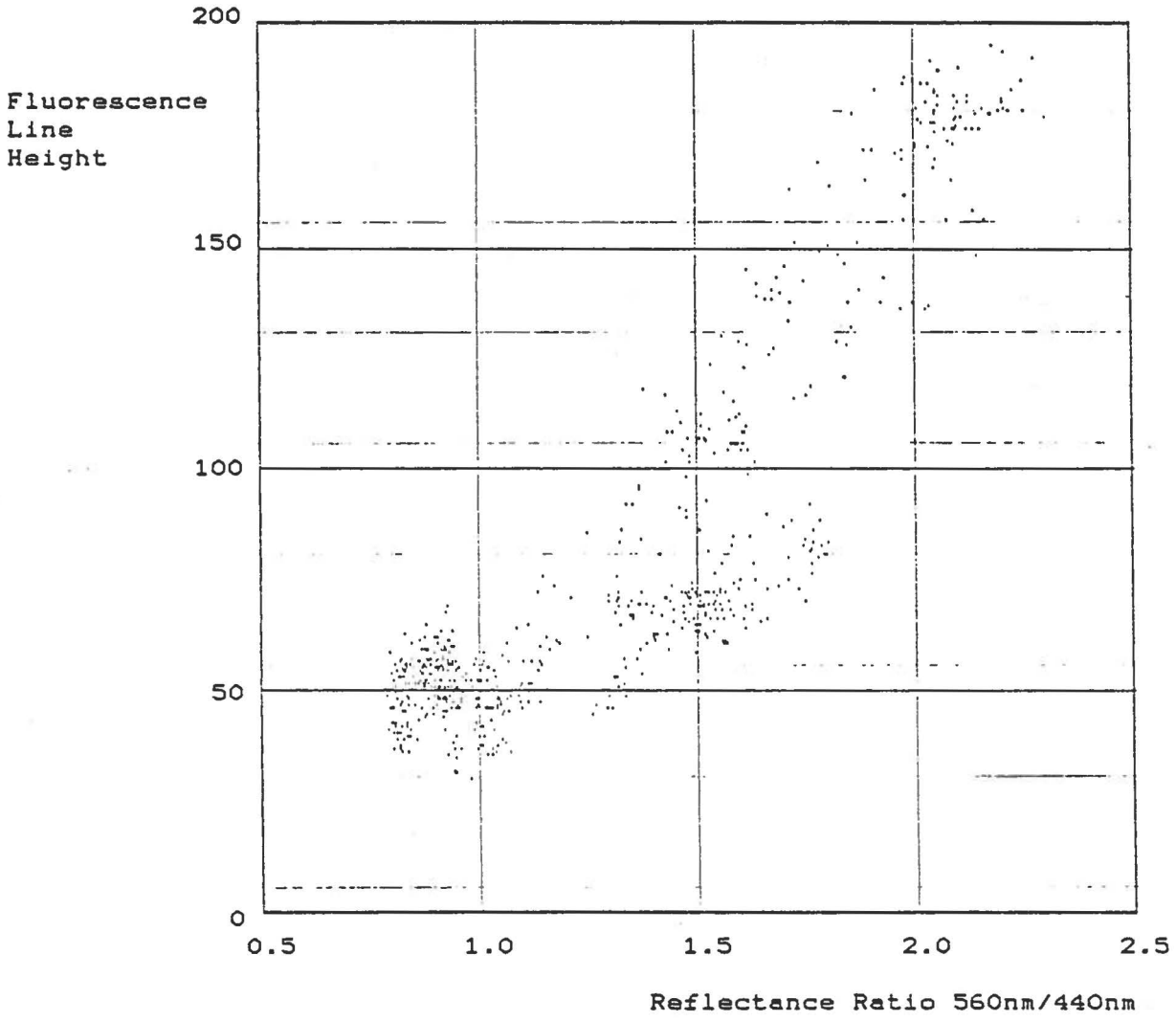

Figure 7.5.2 Scatter plot showing the correlation between fluorescence line height and reflectance ratio for the data in figure 7.5.1.

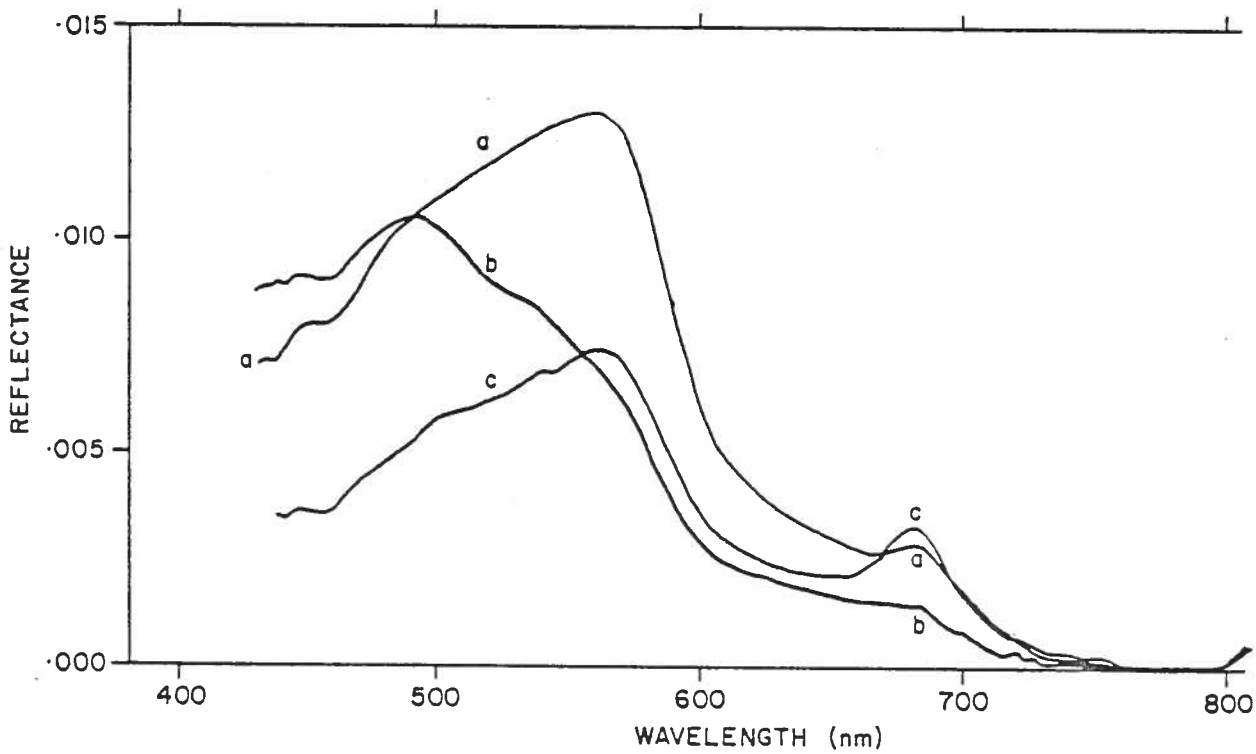

Figure 7.5.3 3 water reflectance factor spectra taken from a low flying (500 ft) aircraft in the Canadian arctic.

Alkor. The spectrometer was then transferred to the Alkor for the period April 26-28 for further near surface measurements.

Figures 8.1.1, 8.1.2 and 8.1.3 show comparisons of fluorescence line height, with measured chlorophyll concentration in the near surface sea water for the available cases in FLUREX. In figure 8.1.1 the North Sea points do not correlate well, and are perhaps affected by presence of suspended sediment. The regression line fitted to all points (heavy dashed line) passes close to the origin and has a similar slope to the average observed in B.C. (section 9). Airborne data are expected to scatter more than ship data, because of the differences in averaging and positioning. With the exception of 3 representative points, ship data from April 27 is plotted separately in Figure 8.1.3.

In figure 8.1.2 the data from the Schlei gives a reasonable correlation with chlorophyll measurements, with evidence of more scatter from the airborne data. In this case the fluorescence line algorithm (peak and baseline) is shifted to longer wavelengths by 19 nm, corresponding to a centre wavelength of 702.3 nm. The regression constrained to pass through the origin is close to the best fit to the data in Figure 8.1.1, showing that the same fluorescence yield applies in the Schlei. This is surprising in that the spectra suggest that self-absorption is occurring there.

The data for a single station that was occupied from 08:00 to 17:30 local time on April 27, Figure 8.1.3, shows a much better correlation, even though the variation during the day (a smooth minimum centred on noon) is only over a narrow range.

8.2 Atmosphere in Flurex

Figure 8.2.1 shows the reflectance increase due to 500 feet of atmosphere, calculated from the tower overflights on April 20. The contribution is roughly constant between 500 and 2000 ft, greater between 2000 and 5000 ft and lower above this, suggesting a low haze layer, with a maximum density in the 2000 to 5000 ft range.

Figure 8.2.2 shows the result of subtracting a scaled $(\text{wavelength})^{-4}$ reflectance increase from the measured reflectances at 500, 1000, 2000, 5000 and 12000 ft. Scaling is by the pressure increase in a standard atmosphere. Apart from the anomalous 5000 ft data, the remaining reflectance can be interpreted as due to water, plus atmospheric aerosol or haze below 5000 ft as in figure 8.2.1. The haze appears to have a featureless and flat spectrum. The FLUREX data suggests that the only problem posed by the atmosphere for measurement of fluorescence from space are the absorption effects, discussed in section 4.

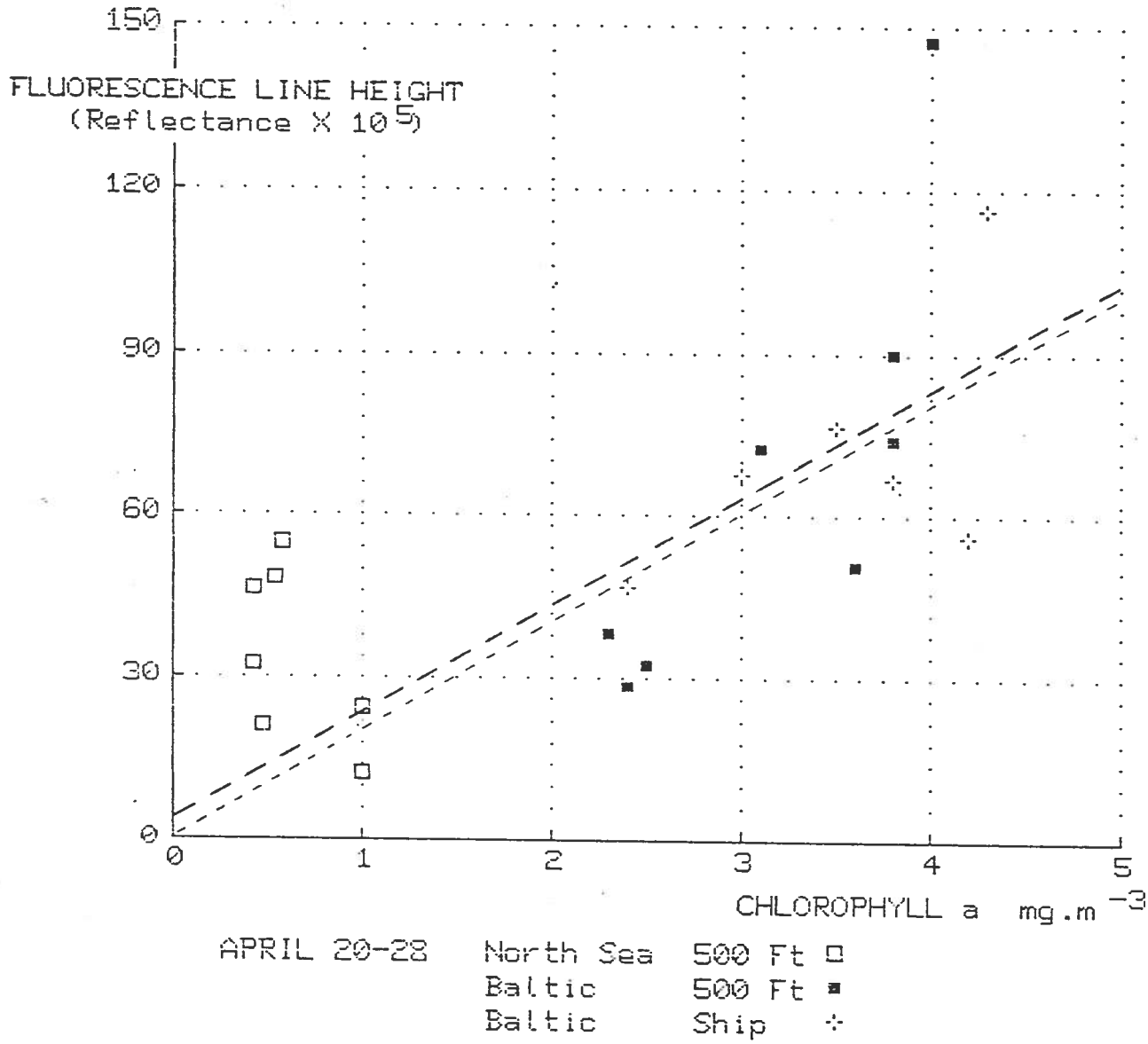

Figure 8.1.1 Observed fluorescence line heights plotted against chlorophyll values in the North Sea and Baltic. The long dashed curve is the best fit to the data. The short dashed curve is the best fit to the Schlei data (Figure 8.1.2), constrained to pass through the origin. Only 3 points from April 27 (Figure 8.1.3) are plotted.

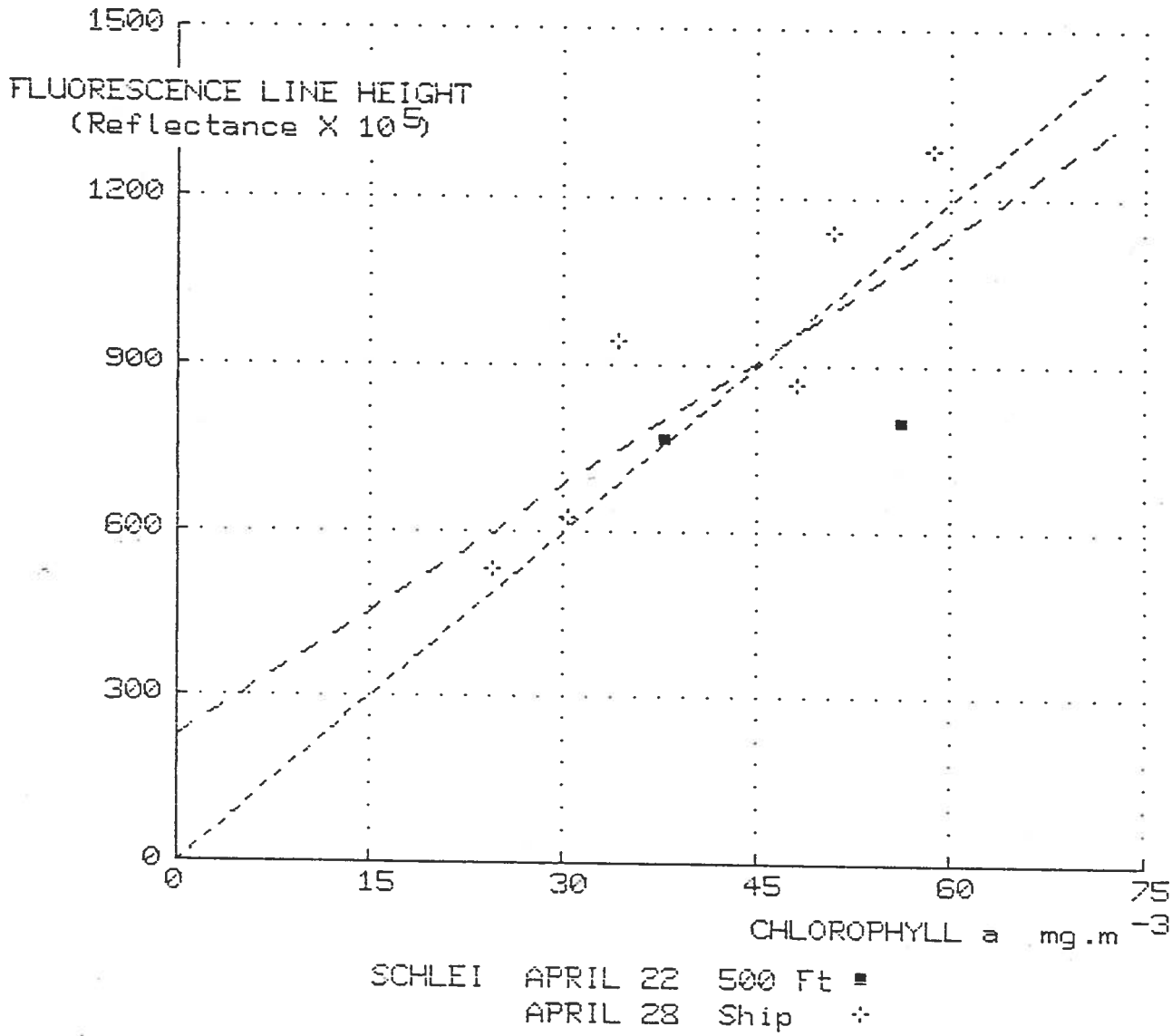

Figure 8.1.2 Observed fluorescence line heights plotted against chlorophyll values in the Schlei inlet off the Baltic. Long dashed line is regression fit to the data. The short dashed line is the fit constrained to pass through the origin.

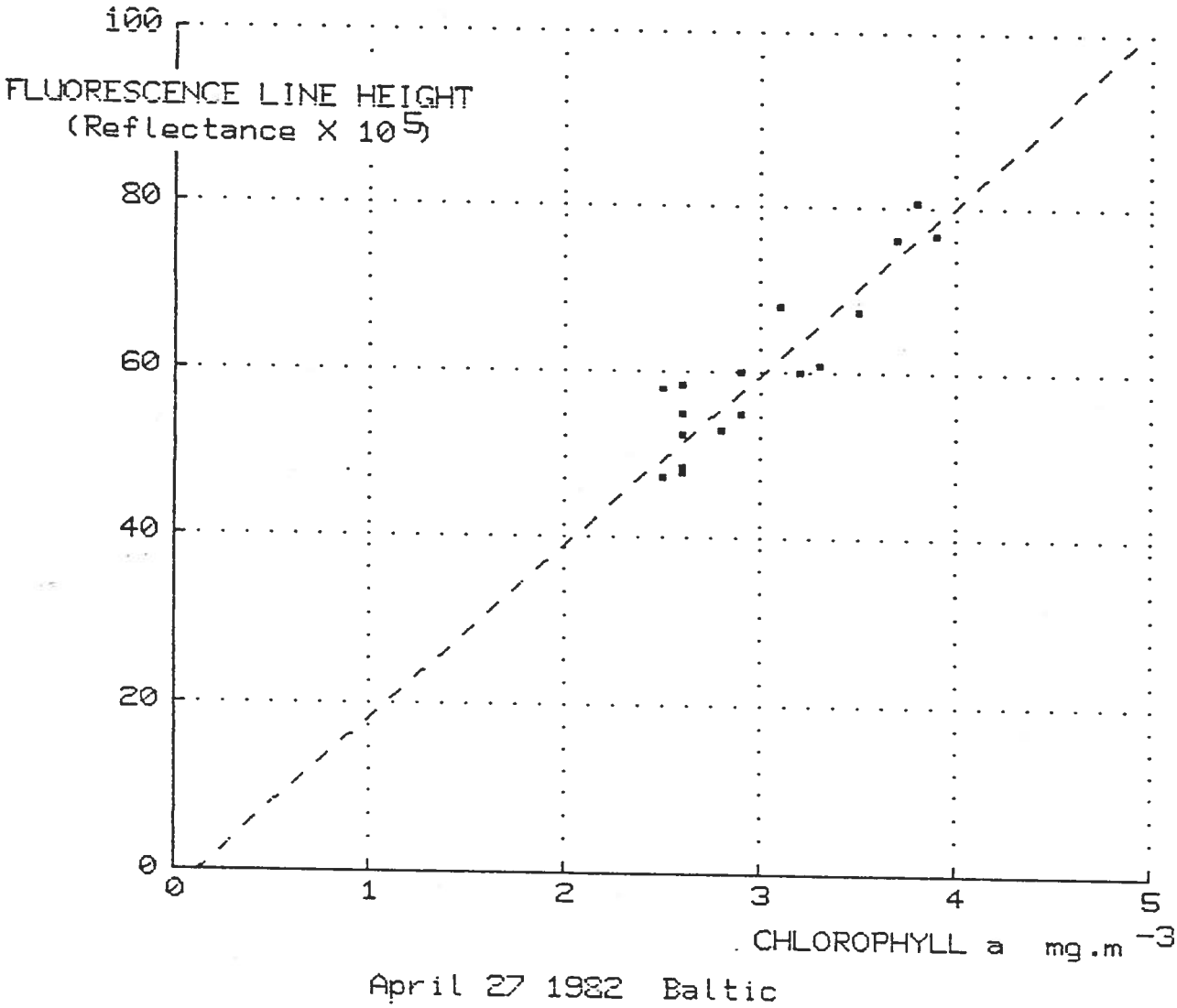

Figure 8.1.3 Observed fluorescence line heights plotted against chlorophyll values for the station occupied at position 11 in the Baltic from 09:00 to 17:00 on April 27 1982.

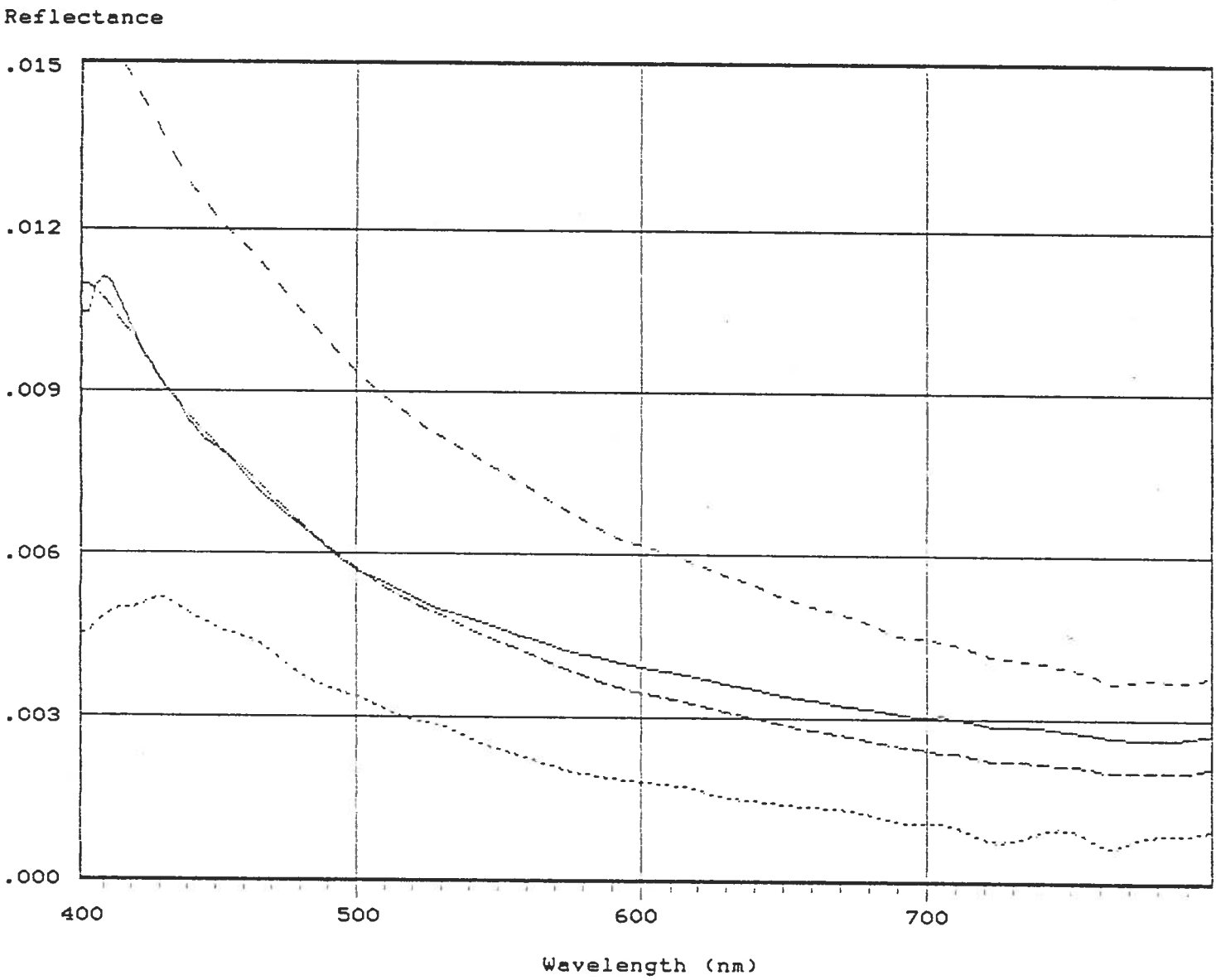

Figure 8.2.1 Reflectance increase due to 500 ft of atmosphere computed from observations at 500 and 1000ft (solid line), 1000 and 2000 ft (long dashes), 2000 and 5000 ft (medium dashes), and 5000 and 12000 ft (dotted). Pressure scaling assumes a standard atmosphere.

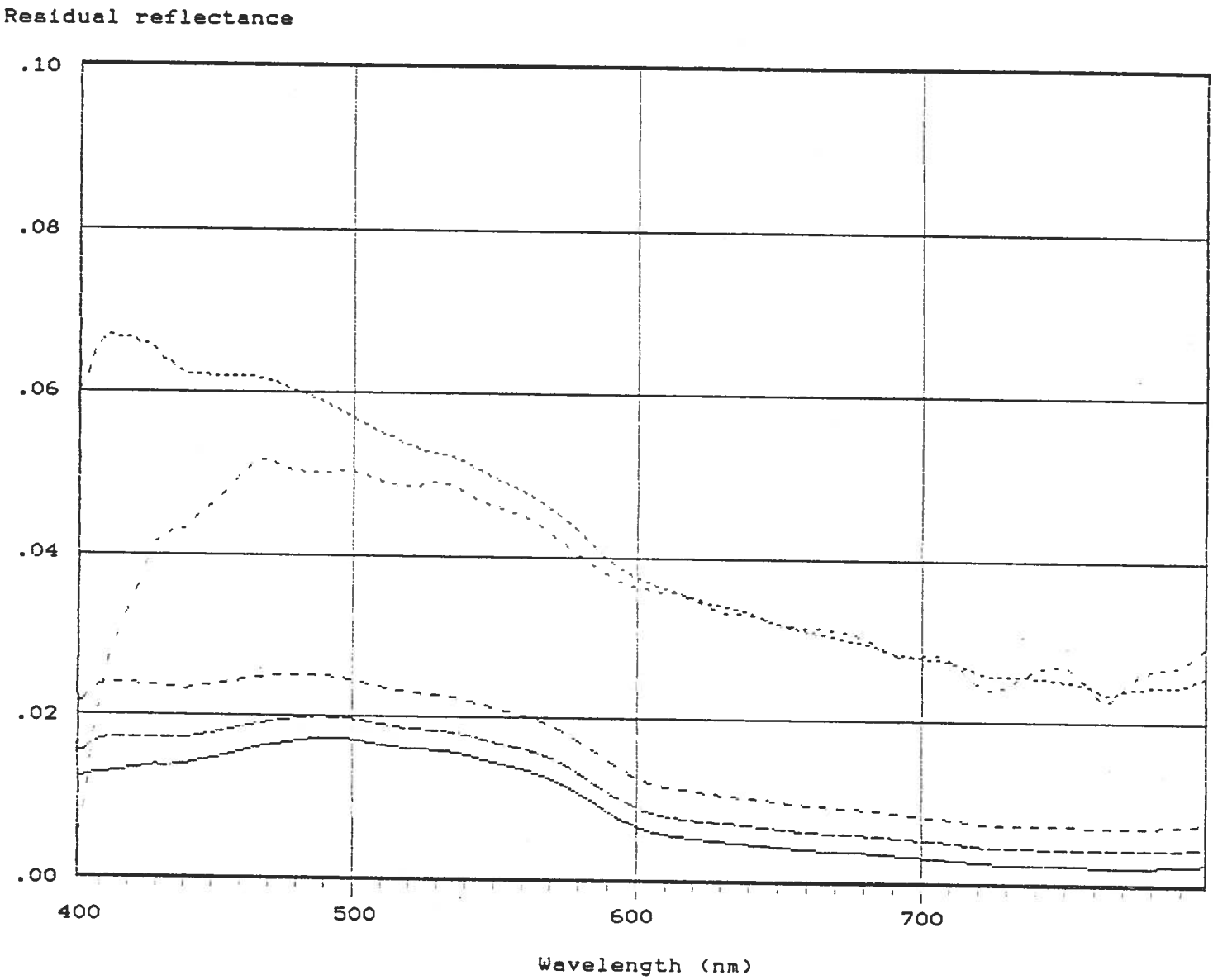

Figure 8.2.2 Residual (aerosol) scattering contributions to observed reflectances at 500, 1000, 2000, 5000 and 12000 ft after subtracting a pressure-scaled Rayleigh (wavelength^{-4}) term. Higher altitude curves are plotted with diminishing dash length.

9. Comparison with the results from other areas.

Many examples of FLUREX data are given in other sections of this report. In general the spectra are similar to those observed elsewhere, both in broad shape and in details of the fluorescence emission. Figure 9.1 shows a spectrum taken over position 11 and corrected for the 500 ft flying altitude, compared with two spectra observed in B.C. coastal waters.

Relations between fluorescence line height and measured chlorophyll in FLUREX are plotted in Figures 8.1.1 to 8.1.3. In general the slopes of fitted lines shows reasonable agreement. Apparent variations in fluorescence efficiency (output per unit chlorophyll) are, however, expected and have been observed in other surveys undertaken with the IOS spectrometer for which sufficient comparison data is available. Figure 9.2 shows the slopes of the best fit lines on a linear scale, over the indicated chlorophyll ranges on 9 different occasions from 1975 to 1982, all but one in western Canada coastal waters. These are:

(a)	Apr 16 1975	B.C. Saanich Inlet
(b)	Jun/Jul 1976	B.C. Saanich Inlet
(c)	Jun 1-8 1976	B.C. Saanich Inlet
(d)	Jul 23-26 1979	B.C. Coastal inlets (CFOX)
(e)	Aug 7-10 1979	B.C. West coast (CFOX)
(f)	Aug 11 1979	B.C. West coast
(g)	Jun 25 1981	B.C. West coast
(h)	Jul/Aug 1981	B.C. Coastal inlets
(i)	Apr 27 1982	Baltic (FLUREX)

It can be seen in Figure 9.2 that with the exception of (a), (b) and (f), the lines have slopes in the range 17 X 10^{-5} to 33 X 10^{-5} of reflectance increase per $mg.m^{-3}$ chlorophyll *a*. Results from the Canadian arctic (Borstad and Gower, 1984) also suggest a mean relation with a slope of about 20 X 10^{-5} in these units. It would be tempting to ascribe the slopes of lines (a) and (b) to poor calibration of the early measurements, but these sequences of spectra show roughly the same range of water reflectances as the others.

In summary, Figure 9.2 shows a mean fluorescence output proportional to chlorophyll *a*, equal to 24 X 10^{-5} of reflectance, per $mg.m^{-3}$ of chlorophyll *a*, with an rms variation by a factor of about 1.8 on each side of this value. If cases (a) and (b) are excluded, then the rms variation is by a factor of 1.3.

Variations in fluorescence efficiency over at least a 4:1 range are observed from fluorometer results (e.g. Kiefer, 1973). However, these observations make use of stimulating light that differs in intensity and spectrum from natural illumination. They also represent a range of depths, light intensities and sample

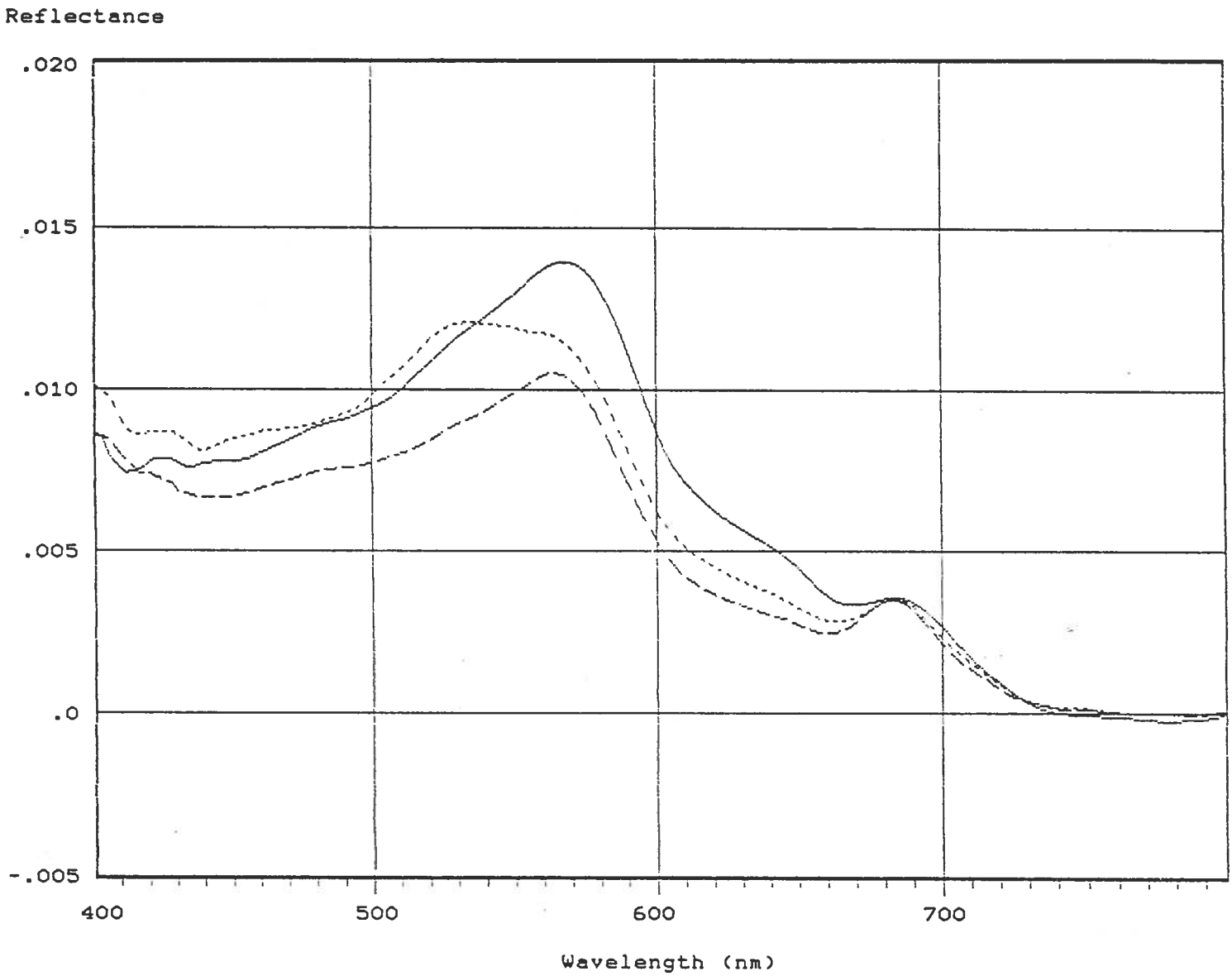

Figure 9.1 Reflectance curve from FLUREX (April 20, 500 ft altitude over position 11, with correction for altitude) compared with 2 spectra observed in B.C. coastal waters. (Saanich Inlet dashed, Satellite Channel dotted).

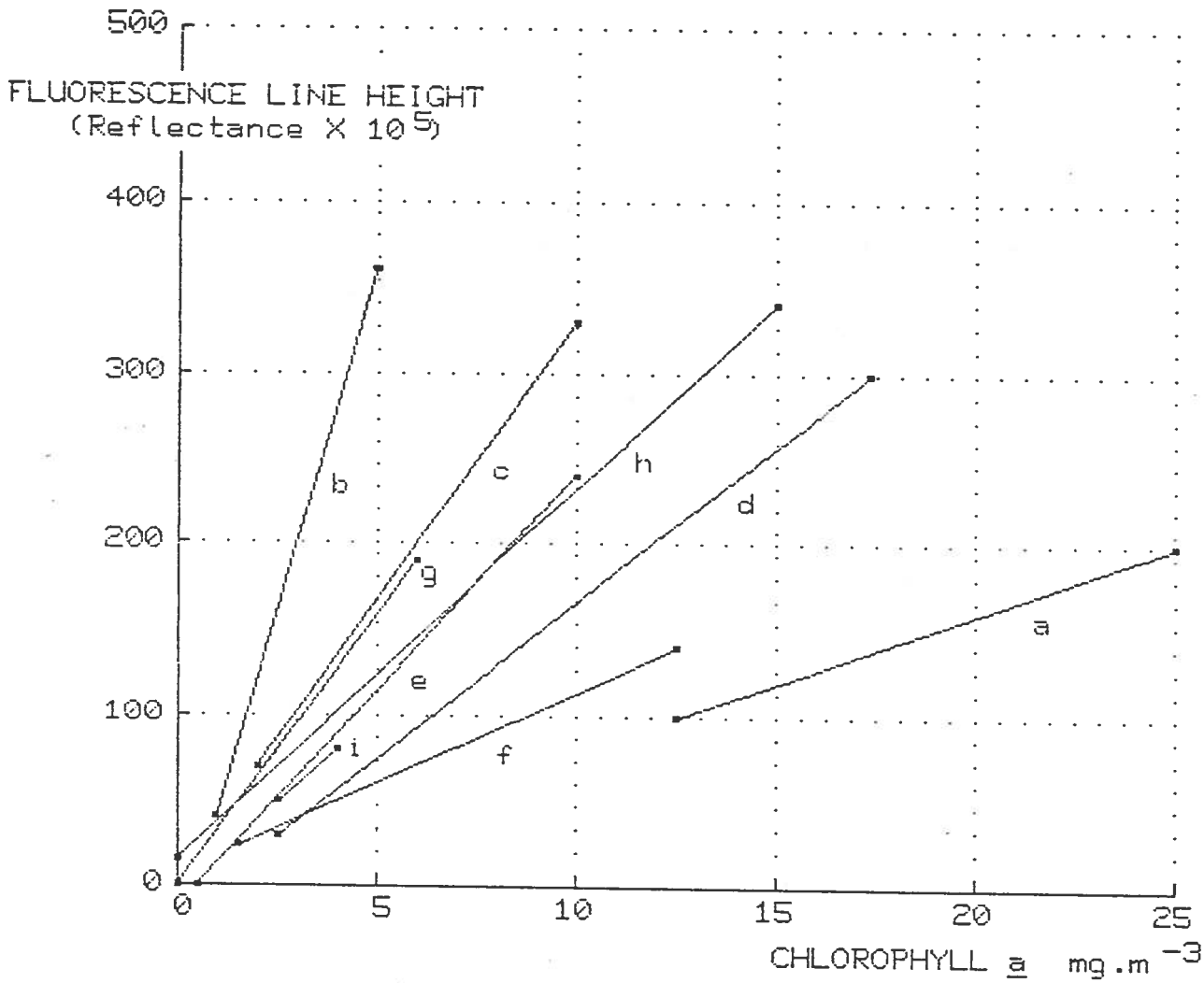

Figure 9.2 Mean relations between fluorescence and chlorophyll concentration observed on 9 occasions, as listed in the text and plotted individually in Figure 9.3.

treatments, so they may not be directly comparable to the variations shown in Figure 9.2.

As part of the July/August 1981 experiment, we also measured in vivo fluorescence with a Turner designs fluorometer. This correlated as well with measured chlorophyll as did the remotely sensed measurements (r^2 = 0.88), but the two fluorescence measurements correlated less well with each other (r^2 = 0.78). This tends to confirm this difference in the two fluorescence measures.

The lines in Figure 9.2 represent close correlations (r^2 0.8 - 0.9) passing close to the origin, both for areas of order 100 Km on a single day, and, at a single point, during a day and for periods of up to 10 days. Individual plots are presented in Figures 9.3(a) to (i) as listed above.

10. Requirements for a satellite borne fluorescence scanner.

Successful work on fluorescence measurements has spurred the development of an imaging spectrometer capable of mapping the spatial distribution of fluorescence emission from sea water. The instrument is named the Fluorescence Line Imager (FLI) (Borstad et al., 1985). It was designed as an airborne prototype for a satellite instrument, with the same spatial resolution as the CZCS or its airborne equivalents (about 2000 pixels over a 70 degree swath, equivalent to 1 Km resolution from orbit). The spectral range was designed to be 430 to 805 nm, with 2.5 nm resolution.

The FLI uses 5 CCD cameras with a total of 550,000 sensing elements. Data rates are reduced to manageable proportions by combining either the spectral elements into 8 bands or the spatial elements into 40 directions. In the first mode the FLI acts as a push-broom scanner with about 1900 pixels per line, and with band spectral properties (positions and widths) under computer control in steps of 1.3 nm. In the second it acts as 40 spectrometers providing low spatial resolution imagery in 288 bands. Figure 4.8.2 shows an example of spectral data from this instrument.

The instrument has been flown in a number of exercises, and is slowly being improved for routine operations. Over water, the first examples of fluorescence mapping are now being produced. The FLI's high spectral resolution and flexibility has led to its being applied for many other purposes, such as for coastal water bathymetry, and aquatic vegetation surveys. It also finds many applications over land, particularly in mapping leaf chlorophyll reflectance changes in response to plant stress. It is anticipated that flexible instuments of this type will be used as the standard optical remote sensor for any appiication where spectral resolution of target properties is important.

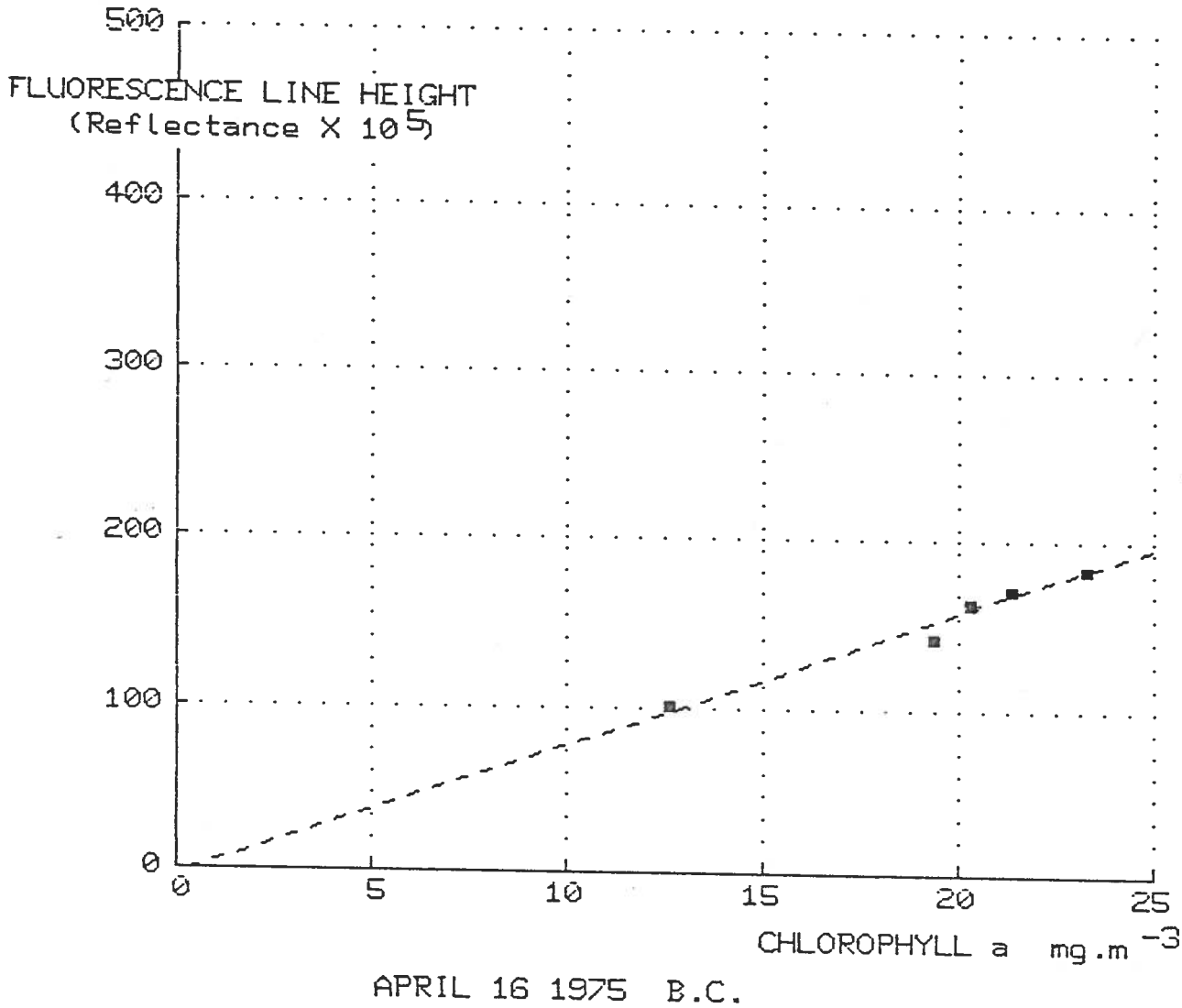

Figure 9.3 (a)

Figure 9.3 (a) to (i) Plots of fluorescence line height against chlorophyll concentration observed on 9 occasions, as listed in the text and plotted in Figure 9.2.

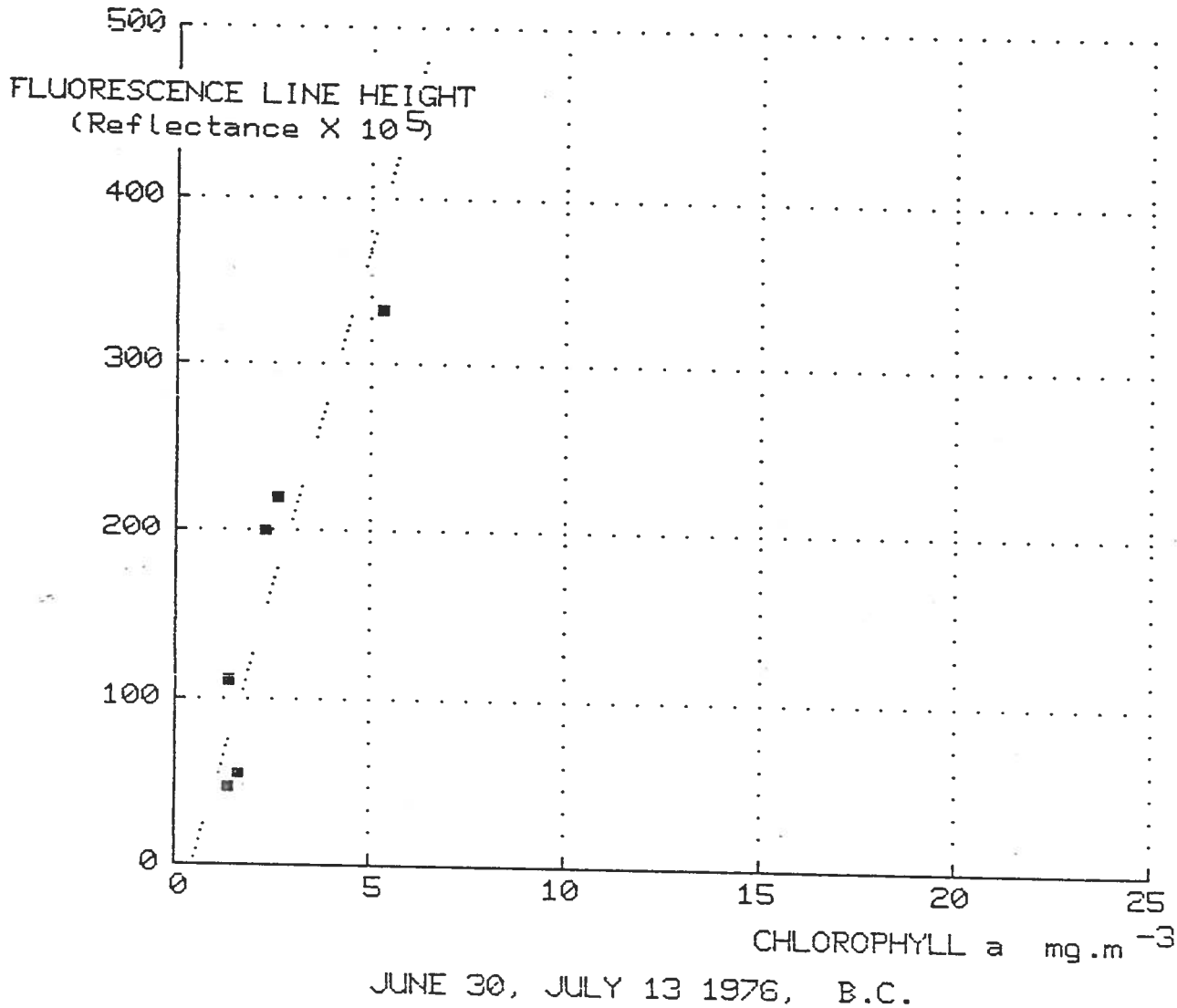
500
FLUORESCENCE LINE HEIGHT
(Reflectance X 10 5)
400
300
200
100
0
0
5
10
15
20
25
CHLOROPHYLL a mg.m -3
JUNE 30, JULY 13 1976, B.C.

Figure 9.3 (b)

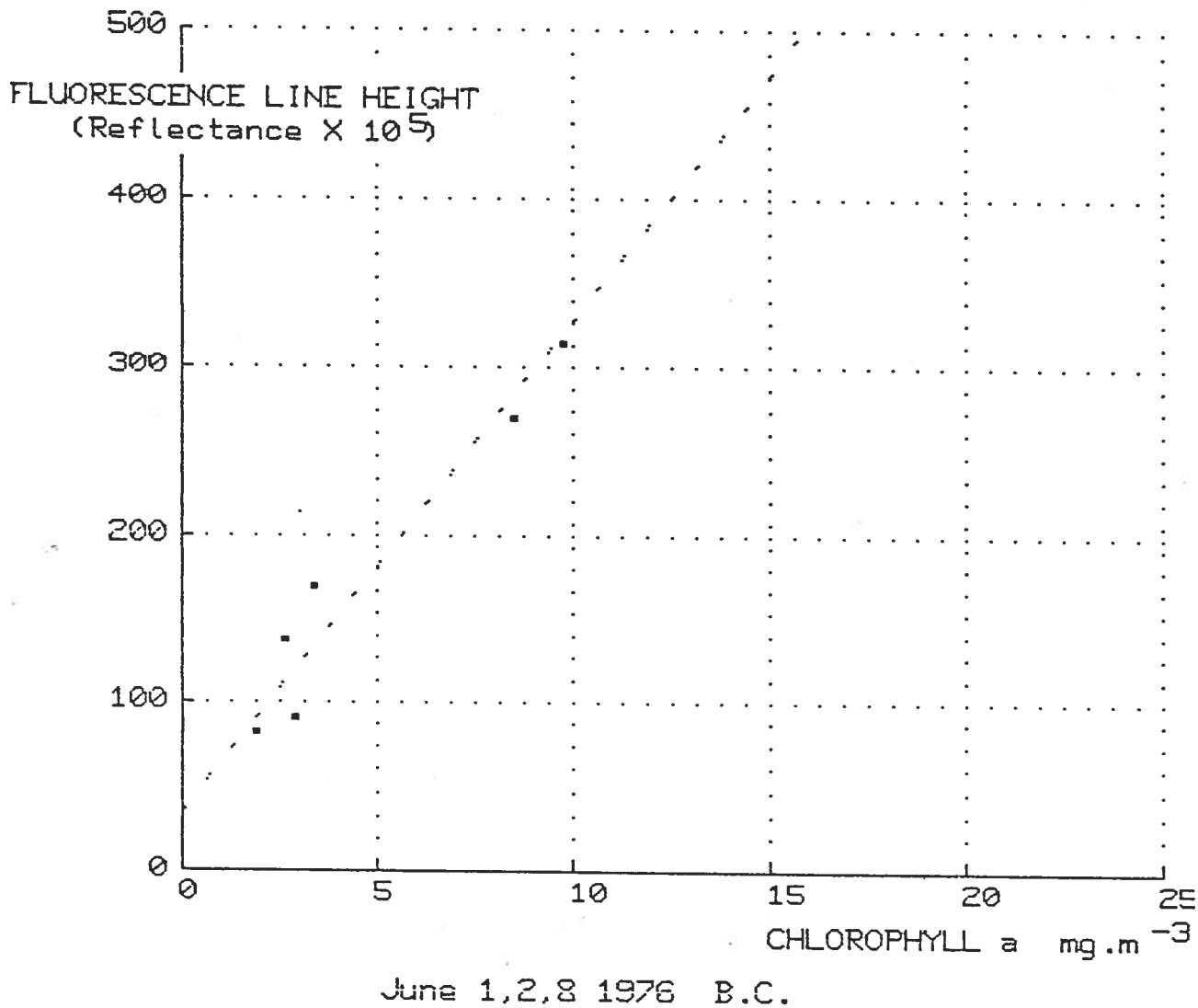
500
FLUORESCENCE LINE HEIGHT
(Reflectance X 10 5)
400
300
200
100
0
0
5
10
15
20
25
CHLOROPHYLL a mg.m -3
June 1,2,8 1976 B.C.

Figure 9.3 (c)

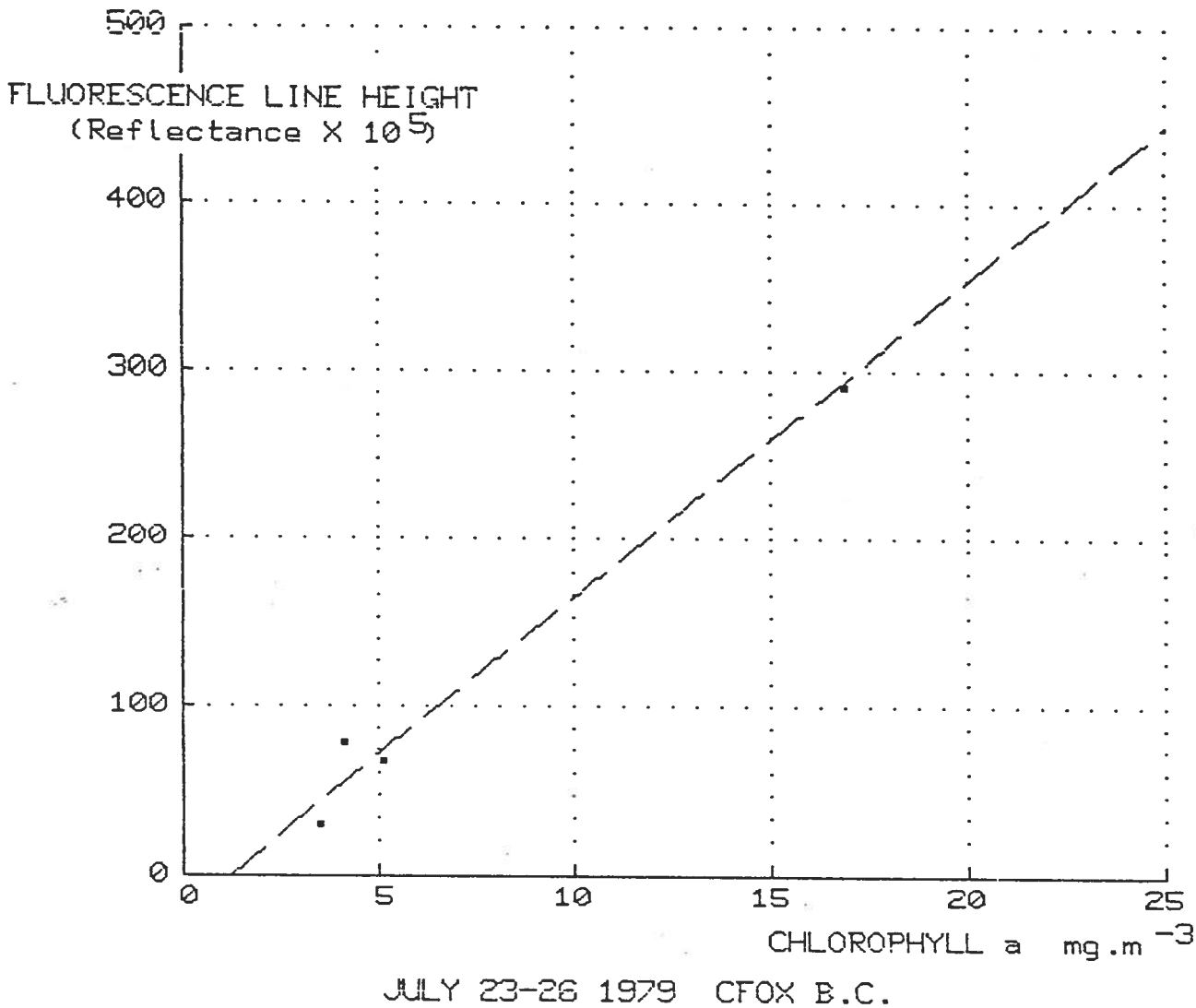
500
FLUORESCENCE LINE HEIGHT
(Reflectance X 10 5)
400
300
200
100
0
0
5
10
15
20
25
CHLOROPHYLL a mg.m -3
JULY 23-26 1979 CFOX B.C.

Figure 9.3 (d)

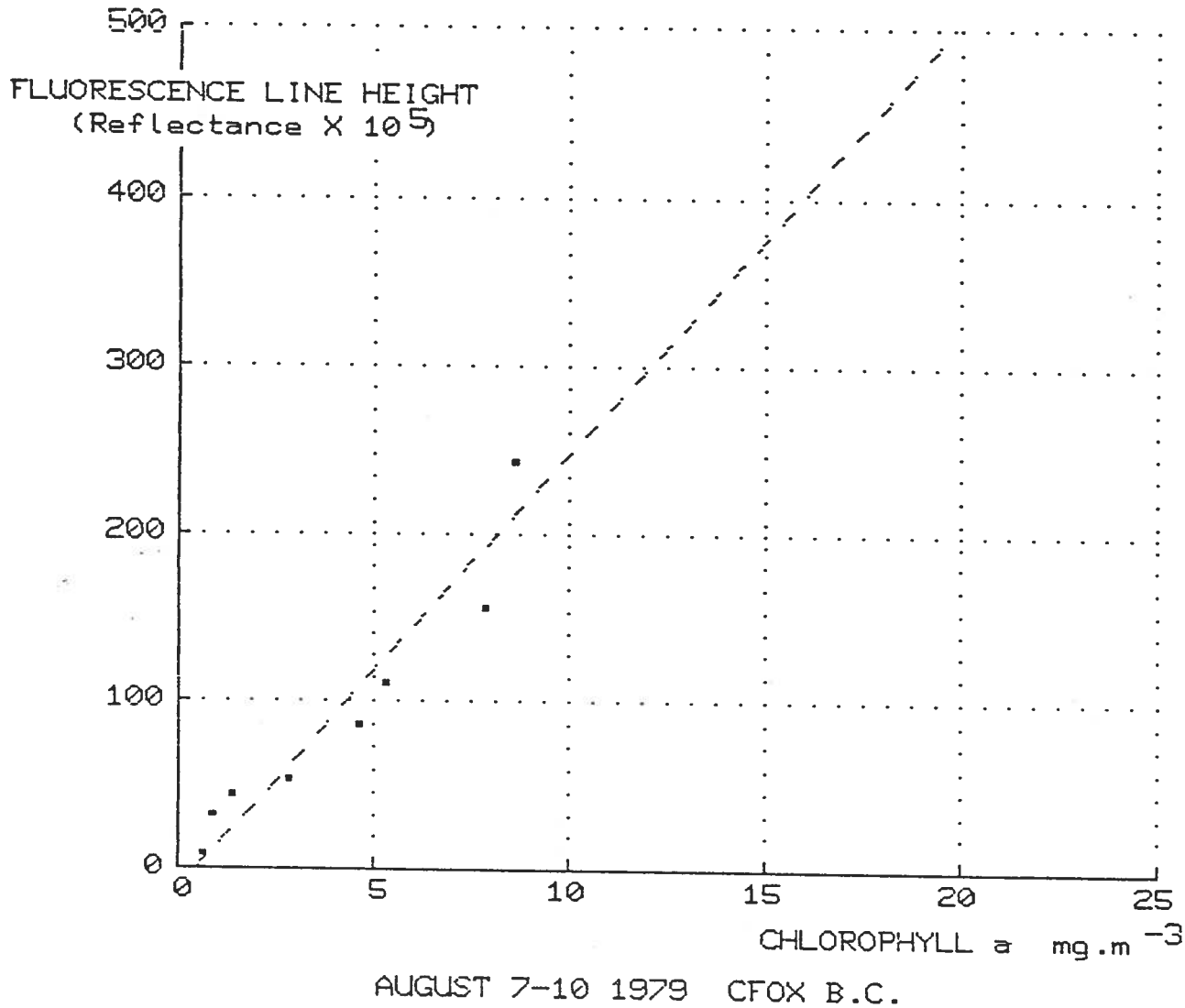
500
FLUORESCENCE LINE HEIGHT
(Reflectance X 10 5)
400
300
200
100
0
0
5
10
15
20
25
CHLOROPHYLL a mg.m -3
AUGUST 7-10 1979 CFOX B.C.

Figure 9.3 (e)

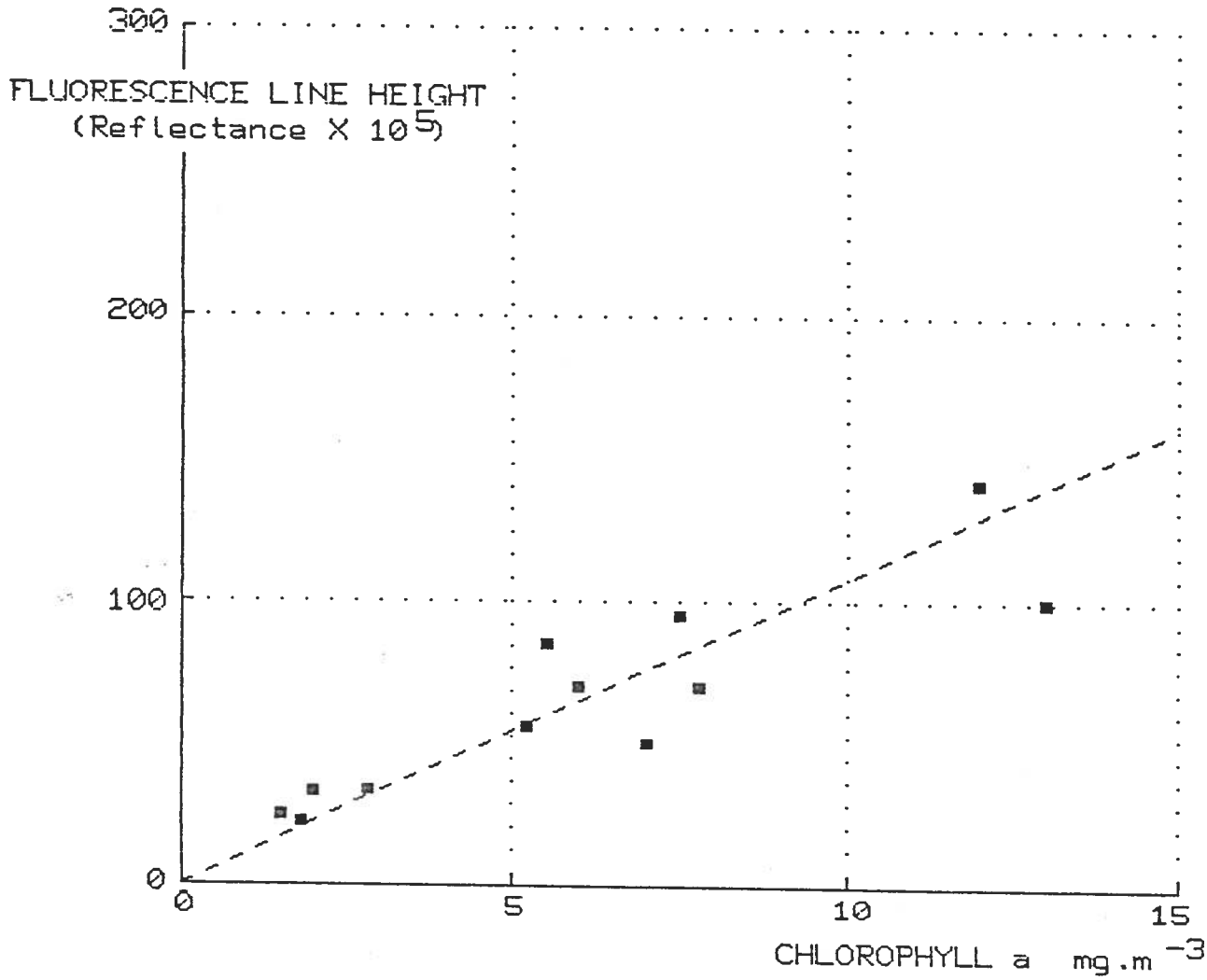
300
200
100
0
FLUORESCENCE LINE HEIGHT
(Reflectance X 10 5)
0
5
10
15
CHLOROPHYLL a mg.m -3
AUGUST 11 1979 B.C.

Figure 9.3 (f)

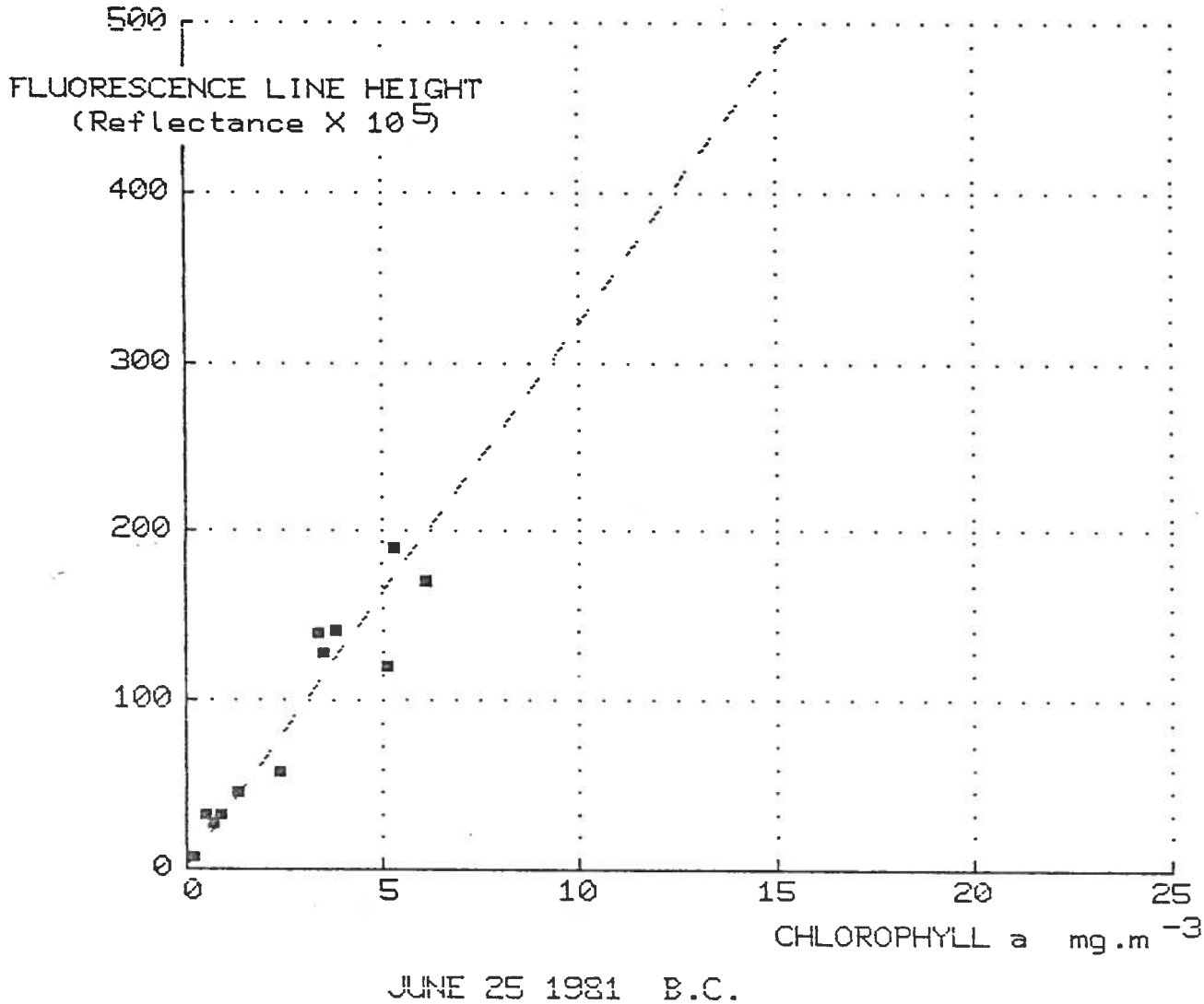
500
FLUORESCENCE LINE HEIGHT
(Reflectance X 10 5)
400
300
200
100
0
0
5
10
15
20
25
CHLOROPHYLL a mg.m -3
JUNE 25 1981 B.C.

Figure 9.3 (g)

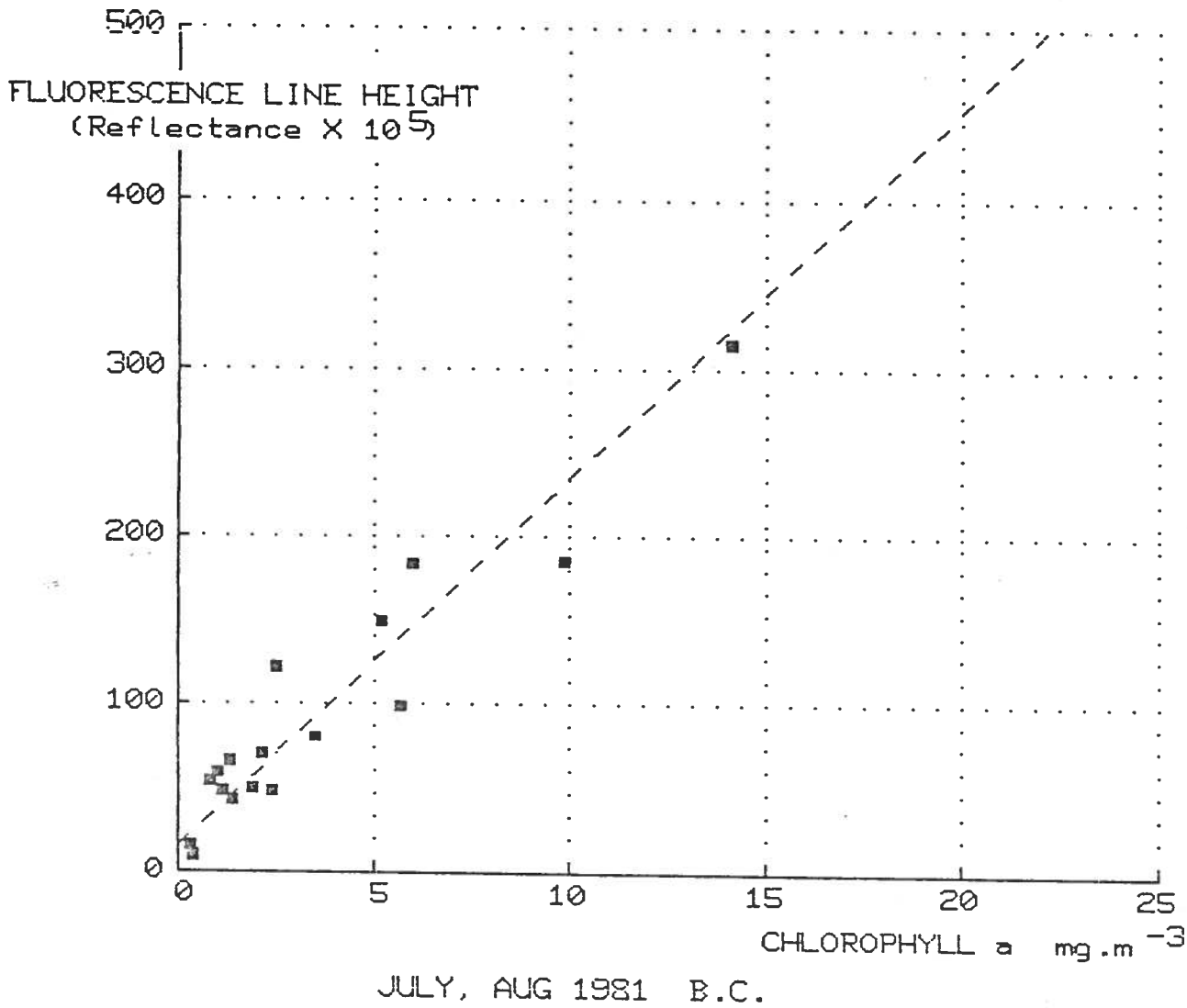
500
400
300
200
100
0
FLUORESCENCE LINE HEIGHT
(Reflectance X 10 5)
0
5
10
15
20
25
CHLOROPHYLL a mg.m -3
JULY, AUG 1981 B.C.

Figure 9.3 (h)

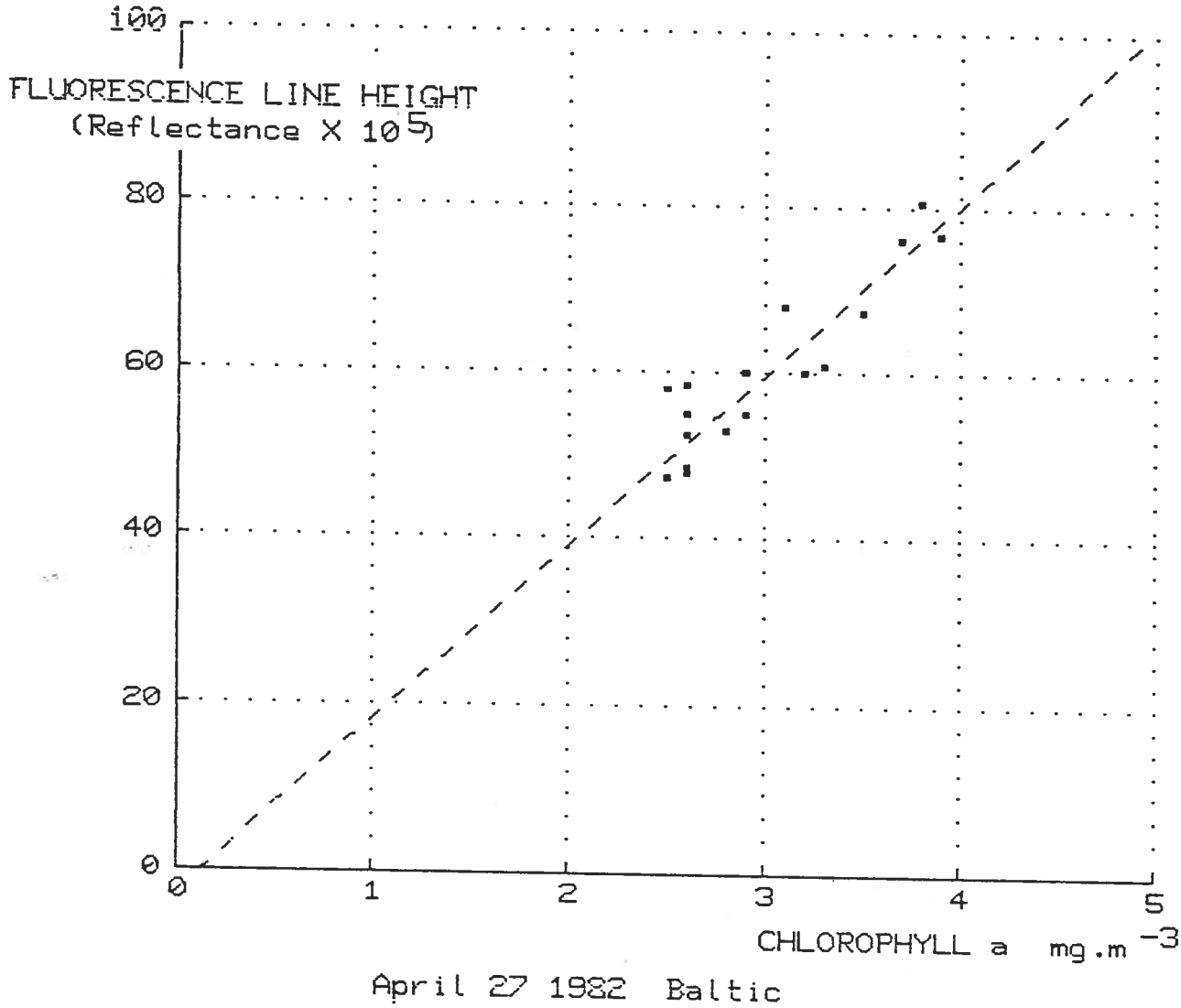
100
FLUORESCENCE LINE HEIGHT
(Reflectance X 10 5)
80
60
40
20
0
0
1
2
3
4
5
CHLOROPHYLL a mg.m -3
April 27 1982 Baltic

Figure 9.3 (i)

CONCLUSIONS

1. Mapping of the naturally stimulated fluorescence from chlorophyll a appears to provide a useful adjunct to measurements of absorption and scattering effects, especially in coastal waters. Waters encountered in FLUREX presented no special problems, though shifted fluorescence peaks, such as those observed in the Schlei, will be differently affected by atmospheric oxygen in satellite observations. Shapes of reflectance spectra, and the value of the fluorescence yield are similar to those observed in Canadian waters.

2. Recent developments in two dimensional array image sensors make feasible the sensitivity and spectral resolution required of a satellite sensor capable of providing naturally stimulated fluorescence data, as well as the broader band green and blue radiances needed for measurement of chlorophyll by its absorption effects.

3. An important goal of satellite water colour mapping is the measurement of primary productivity. This is known to vary with the fluorescence efficiency of the phytoplankton (Topliss and Platt, 1986), suggesting an important application of the fluorescence technique.

4. The fluorescence technique showed the expected operational advantages associated with use of a narrow band chlorophyll signature at long optical wavelengths, and also demonstrated an advantage for observations in shallow waters.

REFERENCES

Borstad, G.Å., and J.F.R. Gower, 1984, "Phytoplankton chlorophyll distribution in the eastern Canadian Arctic", Arctic, 37, 224-233

Borstad, G.A., H.R. Edel, J.F.R. Gower, and A.B. Hollinger, 1985, "Analysis of test and flight data from the Fluorescence Line Imager", Canadian Special Publication of Fisheries and Aquatic Sciences, 83, 38pp.

Doerffer, R., 1981, "Factor analysis in ocean color interpretation", in Oceanography from Space, J.F.R. Gower, (Ed), Plenum, New York, pp339-345.

Fischer, J., R. Doerffer and H. Grassl, 1986, "Factor analysis of multispectral radiances over coastal and open ocean water based on radiative transfer calculations", Applied Optics, 25, 448-456

Gordon, H.R., 1974, J.Opt. Soc. Am., 64, 773.

Gordon, H.R., 1979, "Diffuse reflectance of the ocean: the theory of its augmentation by chlorophyll a fluorescence at 685 nm", Applied Optics, 8, 1161-1166.

Gower, J.F.R., K.L. Denman and R.J. Holyer, 1980, "Phytoplankton patchiness indicates the fluctuation spectrum of mesoscale ocean structure", Nature, 288, 157-159.

Gower, J.F.R., S. Lin and G.A. Borstad, 1984, "The information content of different spectral ranges for remote chlorophyll estimation in coastal waters", Int. J. Remote Sensing, 5, 349-364.

Kiefer, D.A., 1973, "Fluorescence properties of natural phytoplankton populations", Marine Biology, 22, 263-269.

Lin, S., G.A. Borstad and J.F.R. Gower, 1984, "Remote sensing of chlorophyll in the red spectral region", in "Remote sensing of shelf seas hydrodynamics", J.C.J. Nihoul, Ed, 317-336.

Morel, A. and L. Prieur, 1977, "Analysis of variations in ocean color", Limnol. Oceanog., 22, 709-722.

Neville, R.A., and J.F.R Gower, 1977, "Passive remote sensing of phytoplankton via chlorophyll a fluorescence", J. Geophys. Res. 82, 3487-3493.

Parsons, T.R., and R.J. LeBrasseur, 1968, "A discussion of some critical indices of primary and secondary production for large scale ocean surveys", Calif. Mar. Res. Comm., CalCOFI Report, 12, 54-63.

Topliss, B.J. and T. Platt, 1986, "Passive fluorescence and photosynthesis in the ocean: implications for remote sensing", Deep Sea Research, in press.

Tully, J.P., 1961, "Assessment of temperature structure in the eastern subarctic Pacific Ocean", Fisheries Research Board of Canada, Manuscript Report Series, (Oceanographic and Limnological), No. 103, 40pp.

Walker, G.A.H., V.L. Buchholz, D.Camp, B. Isherwood, J. Glaspey, R. Coutts, A. Condal, and J.F.R. Gower, 1974, "A compact multichannel spectrometer for field use", Rev. Sci. Instrum., 45, 1349-1352.

Walker, G.A.H., V.L. Buchholz, D.Camp, B. Isherwood and J.F.R. Gower, 1974, "A silicon diode array spectrometer for ocean colour monitoring", Canadian Journal of Remote Sensing, 1, 26-30.

FLI historical summary

The following two tables show the financial history of the airborne spectrometer program, and the FLI imaging spectrometer construction and testing program.

The airborne spectrometer, built in 1974, showed the potential of remote sensing for mapping near surface phytoplankton distributions in low altitude airborne surveys. The multichannel, silicon detector used made it possible to derive sensitive and accurate measurements of chlorophyll fluorescence emission near 685 nm wavelength, and to use these as a measure of phytoplankton concentration. The spectrometer has been used in coastal surveys off the B.C. coast, in the Arctic and in Europe. DSS contributed to development of survey techniques, and the spectrometer is being used in commercially funded surveys by Borstad Associates Ltd.

A program to extend these measurements from airborne, low level non-imaging, to a satellite-borne imaging mode, started with the CCUSS feasibility study in 1981 which concluded that:

> A suitable sensor could be built based on CCD imaging technology
>
> An airborne prototype should be built first to evaluate the design, define atmospheric problems, and demonstrate the imaging spectrometer concept
>
> Canadian industry had the capability and experience to produce such an instrument

Joint funding of the construction was arranged between DFO and ICS in 1981-83 at a total cost of $940,000. Subsequent improvements have added about $250,000. Flight tests over a wide variety of targets have been carried out, representing the remaining costs shown. Significant additional contract work has been carried out by Moniteq Ltd, and the instrument is presently being operated on a commercial basis by them.

The FLI program has from the beginning had the idea of an eventual space sensor designed for water colour and (low spatial resolution) land sensing. Elements of the flight testing and design work have been aimed specifically at this.

Note: All listed expenditures are by IOS unless noted.
DSS (U.P.) money supported the work of G.A. Borstad at Seakem Ltd and Borstad Associates Ltd.

Total IOS	$224,500
DFO marine pollution funds	$ 40,000
DFO (FLI project)	$ 20,000
DFO (Nanaimo)	$ 10,000
DFO (Winnepeg)	$ 12,000
DIAND	$ 5,000
DSS (U.P. funds)	$199,000
International (Govts)	$178,000
Borstad Associates	$ 11,000
Other commercial	8,000
Grand Total	$727,500

Above does not include IOS personnel (30% of a scientist, plus 50% of a technician, 1975-1986)

FLI Design Evolution

CCUSS Phase 1 Feasibility and Baseline Design:

(Contributors: York University
ITRES Research
Moniteq
University of Calgary
University of British Columbia)

Multiple cameras to cover 70-90° field of view

ISA Holographic grating flat field spectrograph*

RCA 211 CCD detector 320 X 256 X 2 (frame transfer arrays)

2000 to 1 signal to noise in 600 to 800 nm

Atmospheric signal appears smooth in 660 - 686 nm*

Software controlled readout to allow change of readout mode

CCUSS Phase 2 study, Space sensor, data processor, + (*)

(Contributors as before with: PhD Associates
A. Lyle Broadfoot
Harvey Richardson)

Transmission optics chosen over holographic grating
- Simple, fast, transmission grating design
- Higher efficiency

Atmospheric analysis inconclusive
- Existing data not suitable
- Need for airborne measurements with FLI

Space sensor (3 camera design) estimates:
- Weight: 20 Kg
- Volume: 42 Lt (equiv. to 35cm cube)
- Power: 54 W

VAX image processor with video disc archiving recommended

TABLE 1. FLUORESCENCE LINE IMAGER SPECIFICATIONS

SPATIAL MODE: 70 degree swath, with 5 cameras giving a total of 1925 pixels. Pixel size 0.65 mR. Spatial resolution 1.3 mR. Spectral pixels are grouped to form 8 bands (push-broom images) each 1925 pixels wide. Spectral bandwidth and position are programmable.

SPECTRAL MODE: 430-800 nm range using 288 detector elements. Pixel size 1.4 nm. Spectral resolution 2.5 nm. Spectra are recorded from 40 different detectors across the swath (8 per camera). Look directions are programmable.

INTEGRATION TIMES: 40 msec minimum, typically 90 msec in spatial mode, 150 msec in spectral mode.

DETECTORS: Five 385 by 288 element EEV P8600 arrays

SENSITIVITY: Maximum 1900:1 S/N for a band of 16 detector elements at full signal, which is set for ambient levels over water.

DIGITIZATION: 12 bits. Summation is to 16 bits after readout.

OPTICS: Transmission grating with F1.4 Nikon lenses.

DATA RECORDING: Bell and Howell 14 track HDDT. 8 X 875 Kbit.s^{-1} recorded.

POWER: Head and aquisition units: 450 W.
Thermal cooling unit: up to 1 KW.

AIRCRAFT MOUNTINGS: DC-3, Falcon Fan-Jet, Piper Navaho, Dornier-28

SIZE, WEIGHTS:

Head	66 X 48 X 38 cm	70 Kg.
Data aquisition	48 X 35 X 60 cm	26 Kg.
Cooling unit	38 X 42 X 54 cm	41 Kg.

(No real-time display at present).

The FLI - Optical Design, Alignment, Calibration and Deployment

A.B. Hollinger
Moniteq Ltd.

A brief review of the optical design of the Fluorescence Line Imager (FLI) was given along with a brief deployment history.

The CCIISS study had recommended a reflective holographic optical system operating at a focal ratio of about f/2. However, a review of the design indicated that stray light in such a design could not be easily controlled since there can be direct paths between the slit and detector which do not disperse the optical radiation falling on the entrance slit.

A transmissive system (Fig. 1) would avoid this problem since all radiation must pass through the diffraction grating. In addition, the proposed transmissive concept was believed to provide a more compact optical system. The focal ratio was decreased to f/1.4 to compensate for some of the transmissive losses in the system.

The FLI design study had suggested the minimum requirements were for a 1500 pixel swath covering a 70° field of view. The FLI is based on a multiple module concept for two fundamental reasons:

i) the large swath angle (70°) would lead to unacceptably large distortion in a single module

ii) a single module containing more than one CCD would require either an expensive, customized focal plane array or the use of a beam combiner which would necessitate a more complicated optical design.

The FLI uses a spectrograph design with a magnification of less than 1 between the slit and focal plane array. This design concept minimizes the aperture of the collimator and telescope relative to a unity magnification design.

Figure 2/3 is a schematic/photograph of the FLI optical module. Each module is approximately 7.5 x 7.5 x 30 cm in size. The module incorporates a shutter for recording dark signals and an iris to increase the dynamic range for land operation.

Figure 4 shows the five modules of the FLI. Each module is set 14.2 degrees away from its neighbour. The entire housing can be tilted fore and aft relative to the nadir to avoid sun glint during deployment.

The FLI underwent its first flight test in December of 1983. Since that time, the FLI has been used to collect data for a variety of applications. These are summarized in Table 1. These of course include chlorophyll fluorescence work over lakes in the Eastern Townships, a joint DFO/NASA Wallops experiment off Chesapeake Bay, and work off Yarmouth, Nova Scotia. The sensor has been used for two batnymetric studies - one in the Gulf of Mexico off Panama City, Florida, and a second near the Bruce Peninsula.

The FLI has also been used for a variety of land use applications beginning with some studies over the Petawawa National Forest Institute. In subsequent years, studies of botanical stress were conducted over Camel's Hump, Vermont and over many different sites in Ontario. In addition, a number of sites of geological interest were also examined in Algonquin Park and near Hemlo. Moniteq has also conducted a test study of hydrocarbon seeps in Michigan. This data is available as part of a proprietary set.

At this time Moniteq has just completed a survey in West Germany examining a variety of land and water applications.

The FLI has been deployed in five different aircraft. Most of the work for DFO has been conducted using the CCRS Falcon, although some early work was done in the CCRS DC-3. The work in Ontario made use of the OCRS Navajo Chieftain, while the recently completed German surveys utilized two DFVLR aircrafts - the Dornier 228 and 28.

We would like to acknowledge the scientific and technical support of H. Edel and J. Gower of DFO, the support of R. O'Neil, J. Granot, S. Till and G. Fitzgerald of CCRS. We also acknowledge the support of I. Ross, V. Singhroy and V. Zsilinszky of OCRS. Finally, we are pleased to acknowledge the technical support of M. Schroeder, V. Amman and G. Krittikos of DFVLR.

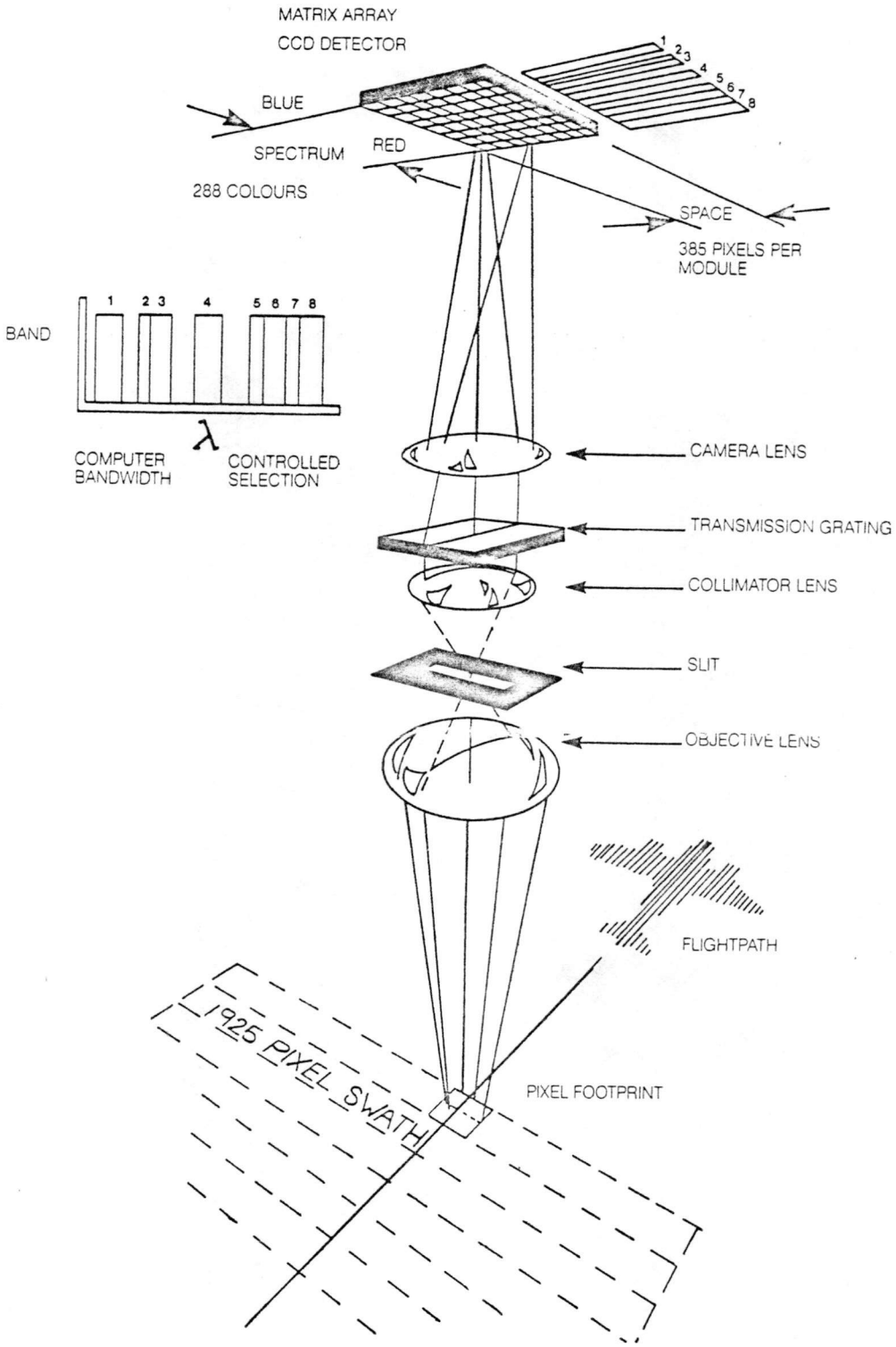

FIG. 1. A conceptual diagram of the DFO Fluorescence Line Imager (from Moniteq 1984b).

ELI MISSION HISTORY SUMMARY

LAKE ONTARIO (KINGSTON, ONTARIO)

JUNE 20/84	FULL SPATIAL FULL SPECTRAL	CHLOROPHYLL MAPPING

EASTERN TOWNSHIP LAKES (SHERBROOKE, QUEBEC)

JUNE 21/84	FULL SPECTRAL	CHLOROPHYLL MAPPING

ST. LAWRENCE RIVER (MONTREAL, QUEBEC)

JUNE 21/84	FULL SPATIAL	

WINCHESTER AGRICULTURAL AREA (SE. of OTTAWA, ONT.)

JUNE 22/84	FULL SPECTRAL	AGRICULTURAL CLASSIFICATION

PANAMA CITY (FLORIDA)

SEPT 26 /OCT 2/84	FULL SPATIAL FULL SPECTRAL	BATHYMETRY/BOTTOM CLASSIFICATION

WALLOPS IS./CHESAPEAKE BAY (W. VA) JOINT EXP'T NASA

DEC 12-15/84	FULL SPATIAL FULL SPECTRAL	CHLOROPHYLL MAPPING

CAMELS HUMP (VERMONT)

AUG 4/85	FULL SPATIAL FULL SPECTRAL	FOREST STRESS/ACID RAIN INDUCED CONIFER

YARMOUTH (NOVA SCOTIA) overflying GEORGES BANK, GRAND MANAN IS, BAIE de CHALEUR

JULY 25- AUG 1/85	FULL SPATIAL FULL SPECTRAL	CHLOROPHYLL MAPPING

BRUCE PENNINSULA (SOUTHERN ONTARIO)

JULY 24/85	FULL SPATIAL FULL SPECTRAL	BATHYMETRY
AUG 4/85	FULL SPATIAL FULL SPECTRAL	BATHYMETRY

CAMELS HUMP (VERMONT)

AUG 4/85	FULL SPATIAL FULL SPECTRAL	FOREST STRESS/ACID RAIN INDUCED CONIF

BISSET LAKE (SOUTHERN ONTARIO)

AUG 5/85	FULL SPATIAL FULL SPECTRAL	FOREST STRESS/GEOCHEMICAL INDUCED DECIDUOUS TREES
SEPT 14/85	FULL SPATIAL FULL SPECTRAL	FOREST STRESS/GEOCHEMICAL INDUCED DECIDUOUS TREES

HEMLO (ONTARIO)

AUG 26/85	FULL SPATIAL FULL SPECTRAL	FOREST STRESS/GEOCHEMICAL INDUCED CONIFER TREES

THUNDER BAY (ONTARIO)

AUG 26/86	FULL SPATIAL FULL SPECTRAL	FOREST STRESS/MOE CONTROL SITE

BARBARA LAKE (ONTARIO)

AUG 31/85	FULL SPECTRAL	FOREST STRESS/ACID RAIN INDUCED

COWIE LAKE (ONTARIO)

AUG 31/85	FULL SPATIAL FULL SPECTRAL	FOREST STRESS/ACID RAIN INDUCED HUMIC SUBSTANCES IN LAKES

NATAL LAKE (ONTARIO)

AUG 31/85	FULL SPATIAL	FOREST STRESS/GEOCHEMICAL INDUCED
SEPT 13/85	FULL SPATIAL FULL SPECTRAL	FOREST STRESS/GEOCHEMICAL INDUCED

MAGNETAWAN (ONTARIO)

SEPT 13/85	FULL SPATIAL FULL SPECTRAL	FOREST STRESS/ACID RAIN INDUCED

GIBSON INDIAN RESERVE (ONTARIO)

SEPT 14/85	FULL SPATIAL FULL SPECTRAL	FOREST STRESS/ACID RAIN INDUCED

PETAWAWA (ONTARIO)

JUN 22/84	FULL SPECTRAL	FOREST CLASSIFICATION
OCT 3/85	FULL SPATIAL FULL SPECTRAL	FOREST CLASSIFICATION

GOOSE LAKE (MICHIGAN)

OCT 2/85	FULL SPATIAL FULL SPECTRAL	VEGETATION STRESS/HYDROCARBON MICROSEEPAGE INDUCED

METROPOLITAN TORONTO WATERFRONT (ONTARIO)

OCT 11/85	FULL SPATIAL	SEDIMENT TRANSPORT/CIRCULATION

86-10-12

NOTES ON FLI INSTRUMENT DESIGN

C. D. ANGER

ITRES RESEARCH LTD., Calgary 403-274-7440 and
DEPT. OF PHYSICS, Univ. of Calgary 403-220-5391

NOVEL FEATURES OF THE FLI DESIGN WERE:

1. Use of a multi-disciplinary team from government, university, and industry to develop specifications and basic design concepts for the instrument. In this way both scientific and instrument design tradeoffs could be made in order to develop the best overall approach.

2. The imaging spectrograph concept, based on 2-d CCD array sensors and compact transmission grating spectographs.

3. Flexibility in choice of wavelength information to be recorded from the scene, with choices effected electronically, without moving parts.

4. Schemes for achieving rapid readout of the array sensor (s), preserving information from only the wavelength regions of interest (up to 8 spectral bands), thereby keeping the data rate to a minimum while maximizing the frame rate.

5. An alternate operating mode (software selectable) which provided full spectral information from a limited set of spatial regions.

6. Design features intended to achieve precision of .05% in individual intensity measurements, including
   (a) precise temperature regulation of array temperatures, based on individually controlled thermoelectric cooling of the CCD's
   (b) high speed 12-bit A-D conversion of CCD outputs
   (c) low noise analog circuit design employing Correlated Double Sampling of each CCD output.
   (d) provision for both on-chip and off-chip summation of values obtained from within a specified spectral band to provide up to 16 bit precision for each band intensity value.
   (e) a fast spectrograph design to provide nearly full exposure of each CCD pixel (approx. 300,000 electrons) per frame.

7. Built in real-time correction for dark current and non-uniformity of the arrays and spectrographs.

8. Complete in-flight interactive control and monitoring of all instrument functions, combined with real-time display of selected bands. An in-line high speed stack-based programmable "calculator" provides real-time display of arbitrary linear combinations and ratios of band intensities for each pixel.

CONCLUSIONS RELATING TO A FUTURE SATELLITE VERSION OF THE FLI

1. CCD array sensors work well in space and lend themselves to very compact, high sensitivity, wide dynamic range designs. Excellent geometrical stability and very broad spectral range are inherent qualities, along with stability of response. In space applications, attention to radiation protection is required, but this is less of a problem in relatively low altitude orbits.

2. CCD sensors, when combined with a flexible readout system, make it possible to achieve arbitraryand interactive trade-offs between spatial and spectral resolution and coverage, as required to achieve a given objective, and to maintain compatibility with available telemetry rates.

3. Interactive real-time control of instrument mode and operating parameters, based on real-time data, has been proven to be a feasible and extremely powerful way of operating a satellite imager. It can easily pay for itself through simplifications in flight instrument design and increases in overall reliability and adaptability.

4. Design of the analysis system needs to be done in parallel with design of the instrument and interactive control system, as part of one overall system design. This was done with Viking and represented one of the strongest aspects of the programme. Because of the commitment to interactive control, much of the software developed for flight operations was directly usable for scientific analysis almost immediately after launch.

5. Calibrations, both pre-flight and in-flight need to be part of the overall design effort from the outset. Even though a great deal of effort was put into this with Viking, it turned out that most of it was devoted to attempting to understand a new instrument and convince ourselves that it was operating correctly. As a result, we are still (9 months after launch) attempting to resolve some uncertainties in the calibration.

6. The lesson from point (5) is probably the most significant of all because it is the easiest to overlook: Technological backup for the development of any new instrument is essential. If all the technology in a space instrument is thoroughly understood at the outset, it is almost certainly obsolete! If you want to avoid spending a year or more understanding your instrument after it goes into orbit, then you had better plan to spend a year or more on the ground before launch understanding the technologies employed in that instrument and the instrument itself. This need not delay the instrument development, since it is best done in parallel with that development.

86-10-12

EXPERIENCE FROM THE VIKING SATELLITE IMAGER PROGRAMME

C. D. Anger
Dept. of Physics,
University of Calgary.

BACKGROUND:

A Canadian instrument to carry out global imaging of ultraviolet aurora was launched on the Swedish Viking Satellite in February, 1986. The instrument employed an intensified CCD array sensor and fast optics to provide images at the rate of one every 20 seconds at very low light levels. Two electronic cameras gave digitized images at far-UV wavelengths where reflected sunlight from the atmosphere is weak and does not prevent imaging of the aurora even in full sunlight.

Some of the design features of the instrument are:

1. Two element wide angle f/1 reflective optics (inverse Cassegrain configuration).

2. Curved focal plane matched to a curved single-stage open microchannel plate intensifier.

3. Intensifier coupled to an EEV CCD array sensor through reducing and distortion-correcting fibre optics.

4. Electronic spin compensation to provide one second exposure times for each pixel from a spacecraft spinning at 18 degrees persecond. Cameras contain no moving parts.

5. Exposure and electronic pointing control based on earth-limb crossing or sun pulse provided by the spacecraft. Electronic control of region to be imaged, image size and shape, exposure parameters, gain and high voltage parameters,and on-chip charge summation (to obtain better sensitivity and/or spatial coverage without degrading temporal resolution for a fixed telemetry rate).

6. Real-time data recording and analysis facility at the receiving station in Kiruna, Sweden, with full interactive control of instrument based on images dispayed in near real-time.

The Development of Fluorescence Line Imager (FLI) Software at IOS

D. N. Truax

1.0 Overview

The present software for analysing FLI data on the IOS image processing system represents approximately three years of development effort. During this time the software has undergone several modifications as user options have been added and new software has replaced old.

The early software was written to display FLI CCT and calibration data and to verify the FLI uniformity correction algorithm. More recent software performs an actual radiance calibration calculation thus producing spectra and/or imagery in scaled radiance units. The recent software also maintains the full 16 bit precision of the FLI data.

As both early and recent FLI software is available to users at IOS, a description of both is presented.

2.0 Current Hardware Environment

DEC PDP 11/44 minicomputer system with 2 megabytes main memory plus cache memory and floating point arithmetic processor.

Adage (Ikonas) 512 by 512 pixel image display system with graphics overlay option, digitizing tablet and video camera input, and high resolution RGB display.

Approximately 1000 megabytes of online disk storage.

Several interactive CRT user terminals.

Magnetic tape drives with 800, 1600 or 6250 bpi capabilities.

Lineprinter with graphics option.

Floppy disk drive.

2.1 Hardware Limitations

Software task size is limited to 65 kilobytes due to 16 bit address size of the PDP-11/44 computer. This necessitates cumbersome overlaying of many task subprograms.

PDP-11/44 processor is too slow for some applications.

3.0 FLI Data Sources and Products

3.1 FLI Data Sources

LGSOWG CCTs which are generated on the CCRS Airborne System from the aircraft FLI HDDTs.

Floppy disks which are the output of the FLI calibration software.

3.2 FLI Data Products

Calibrated and geometrically corrected FLI LGSOWG CCTs.

35mm photographic prints and slides of the image display.

Lineprinter hardcopy of image display graphics.

4.0 Image Processing Software

Written in DEC FORTRAN IV PLUS.

Operates under DEC RSX11M operating system.

Uses the OVAAC8 software to communicate through the PDP 11/44 to an Adage (Ikonas) image display.

4.1 Early FLI Software

4.11 Calibration Data Display Software

This software allows calibration files to be viewed on the image display system thus permitting visual inspection of the FLI CCD array responses. Bad CCD elements can be identified and the overall response of each CCD to the calibration light source of known brightness can be evaluated.

Calibration files which are received on floppy disks are first copied to main disk storage. The display software then sorts each calibration file from the CCD readout order to spectral and spatial pixel order and scales the 16 bit CCD counts to 8 bits for display.

4.12 Uniformity Correction Software

These programs were written to evaluate the Itres uniformity correction software.

At each stage of the procedure an intermediate disk file is produced which is compatable with a corresponding Itres file. These files can then be compared visually and numerically using the calibration file display software.

The end product of this software is a file containing band uniformity correction factors for a particular FLI band configuration.

4.13 FLI CCT Data Display

These programs read FLI spectral and/or spatial data directly to the image display while optionally applying band uniformity corrections. Data may be selected from a FLI CCT by record number and/or aquisition time. Options are also provided for displaying spectral data as low resolution spatial imagery and displaying fluorescence line height or green/blue ratio imagery. A geometrical correction which removes FLI camera overlap and eliminates known bad pixels is also available for spatial imagery . A status log of the CCT can also be produced.

4.14 FLI CCT Copy

This software copies a FLI CCT to another CCT in LGSOWG format. Options for applying band uniformity and geometrical corrections are also provided.

4.15 Limitations of Early FLI Software

FLI CCT data must be written to the image display before it can be written to disk using other IOS software.

FLI CCT data once on disk is limited by the 8 bit resolution of the image display system.

4.2 Recent FLI Software

4.21 FLI Floating Point Calibration Software

The floating point calibration software in one step creates a single calibration file which contains a floating point correction factor for each pixel of each FLI CCD array. Each calibration coefficient is normalized to an integration time of one millisecond. Other software then uses this calibration file to form spectral or spatial band calibration arrays which are then used to convert CCD counts into calibrated radiance units.

4.22 FLI CCT to Disk Storage

This software reads FLI spectral or spatial data from CCT into standard disk files.

FLI CCT data may be read unaltered to disk, or alternately may be corrected to true radiances using the floating point calibration file.

Once calibrated, pixels are multiplied by a power of 10 in order to scale them to 16 bit integer disk format. These disk image files can then be read to the image display or processed using other IOS software.

All the options which were available in the earlier FLI CCT to image display programs have been retained.

4.23 FLI CCT Calibrated Tape Copy

This program copies a FLI CCT to another CCT in LGSOWG format with options for applying the radiance calibration and/or geometrical correction.

4.24 FLI Spectral CCT Reformat

This program copies a FLI spectral mode CCT to another CCT in LGSOWG format while resorting the data from spectral order to spatial order.

5.0 Other IOS Software

Once FLI data has been read into the image display or into standard IOS disk files it is then available to other IOS software. This software includes programs for characteristic vector analysis (eigenvectors), Fourier analysis, statistical analysis and a wide assortment of image enhancements and graphical representations of image data.

Biophysics of the daily cycle of in vivo chlorophyll a fluorescence stimulated by artificial light sources

K.P. Günther

University Oldenburg
2900 Oldenburg,FRG

1. Introduction
2. Kautsky curve
3. In vivo fluorescence
4. In vivo excitation and emission spectra
5. Bipartite model of Butler and Kitajima
6. Expanded "bipartite model"
7. Experimental results of FLUREX '82
8. Discussion of the FLUREX '82 results
9. Experimental results of FLUREX '85
10. Conclusion

1. Introduction.

According to the present knowledge, photosynthesis and in vivo chlorophyll a fluorescence of algae and higher plants occur in the cellular organelles called chloroplasts of typical dimension of 3 - 10 m. Within this structure, pigments embedded in membranes, called thylakoids (Figure 1), absorb the visible light energy . Common to all oxygen producing algae and higher plants is chorophyll a, which acts in the membrane as light - harvesting protein complexes and in special chlorophyll a protein complexes as reaction centers. At the reaction centers the excitation energy is transformed to photochemical energy and used for photosynthesis.

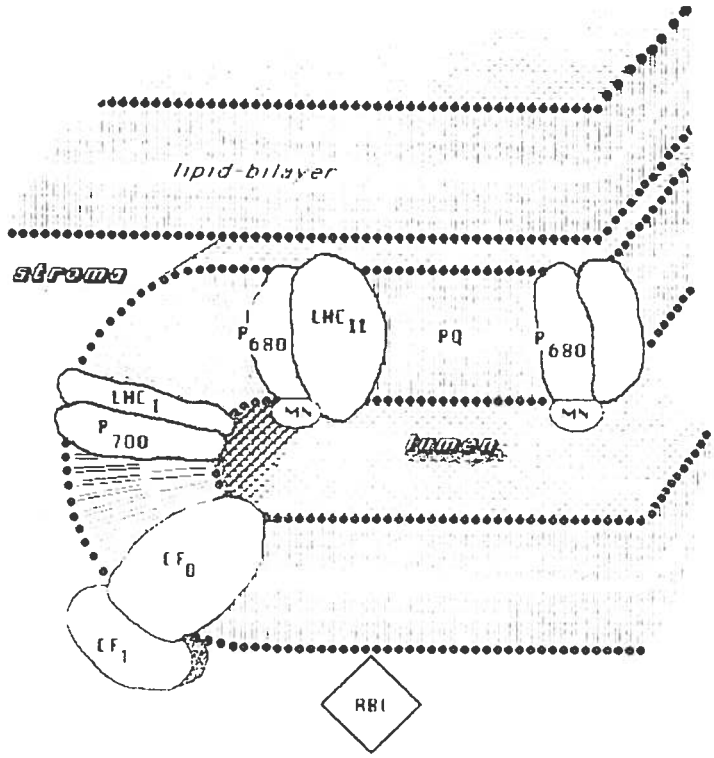

Figure 1: Schematic view of the thylakoid membrane. The polar nature of the double layer lipid membrane is indicated by the black dots representing the hydrophobic end of the lipids and the tails indicating the hydrophilic end

P700	reaction center I
LHC I	light harvesting complex I
P680	reaction center II
LHC II	light harvesting complex II
PQ	plastoquinone pool
MN	oxygen evolving complex
CF0	coupling factor
CF1	coupling factor

The typical absorption bands of in vivo chlorophyll a are found in the blue at 440 nm and in the red at 670 nm. Other pigments found in the thylakoids as chlorophyll b and c, biliproteins (phycoerythrin, phycocyanin and allo-phycocyanin) and carotinoids (carotenes and xanthophylls) enhance the spectral absorption in the range from 480 to 660 nm.

The excitation energy from the accessory pigments is fed to two different photochemical reaction centers (P680 and P700) via exciton transfer. This energy transfer can be described by a resonant dipol-dipol interaction (Förster 1948). The Förster-mechanism shows a strong dependence on the distance of the two interacting molecules and on the relative orientation of the dipols. Calculations show that for efficient energy transfer the typical distance is less than 10 nm. Assuming an increase of the typical distance of 10% , the energy transfer efficiency is decreased by 60 % . The typical time constant for exciton transfer to the trapping center is in the picosecond range.

At the reaction center P680 and P700 the transformation of excitation energy into photochemical energy occurs by charge separation. At present, one assumes that the reaction center is a molecular complex consisting of the chlorophyll a molecule accepting the excitation energy and of an electron donor and acceptor, respectively. The electron acceptor of reaction center II is termed Q (for quencher) which is a bound plastoquinone molecule incorporated in the reaction center polypeptide. The electron donor of reaction center II is the water splitting complex sometimes cited as oxygen evolving complex. The photochemical energy from photosystem II is transported by redox reactions to photosystem I. The electron donor for reaction center I is usual a plastocyanin molecule,while the electron acceptor is possibly a bound iron-sulfur protein or a flavoprotein. The photochemical energy from photosystem I is brought to the Calvin cycle to drive the biochemical formation of ATP,the universal energy transmitting adenosin-triphosphate, in the cyclic and NADPH, the necessary reduction equivalents nicotinamid-dinucleotid-phosphate, in the non cyclic electron transport.

A simplified, schematic diagram of the photosynthetic unit (PSU) is shown in Figure 2. The PSU is divided in the light harvesting chlorophyll proteins (LHCP), the antenna pigments of photosystem I and II, the photochemical reaction centers I (P700) and II (P680) and the electron transport chain, connecting the two reaction centers. Only one substructure of the electron transport chain is shown, the so called plastoquinone pool,which stores the electrons coming from reaction center II. The plastoquinone pool has a regulatory function, concerning the state of the thylakoid membrane (Horton and Black 1980). The highly reduced state of plastoquinone induces an encymatic reaction, the phosphorylation of the light harvesting chlorophyll proteins. Due to the phosphorylation the structure of

the thylakoid membrane is changed (Barber 1983) and thus the distance between the accessory pigments and the reaction centers. A model given by Barber (1983) and shown in Figure 3 relates changes in the phosphorylation of LHCP with changes in the energy transfer from P680 to P700 and with changes in the degree of thylakoid stacking. The mechanism of thylakoid stacking is not important in phytoplankton but in higher plants. Regarding the sensitive regulation mechanism with respect to exciton transfer, the energy transfer to reaction

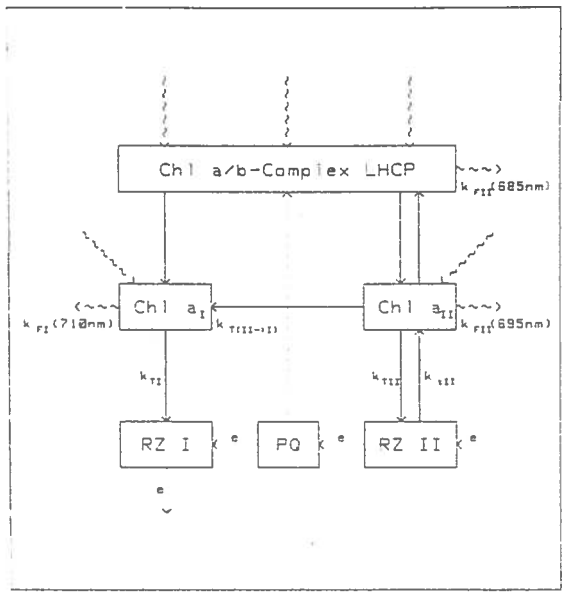

Figure 2: Schematic, simplified representation of the structure and organization of a photosynthetic unit.

chl a/b - complex : light harvesting chlorophyll protein (for most marine algae the chl b is substituted by chl c) fluorescence at 685 nm

chl a_I, chl a_{II} : antenna chlorophylls of reaction center I, II fluorescence at 730nm, 695nm

RZ I, RZ II : reaction center I and II (P700 and P680)

PQ : plastoquinone pool

k_{FI}, k_{FII} : rate constants for fluorescence of antennae I, II

k_{TI}, k_{TII}, k_{tII} : rate constants for energy transfer from antennae to reaction center I, II and vice versa

$k_{T(II-->I)}$: spillover rate constant

Wavy lines indicate photons. The dotted line indicates the photo-phosphorylation due to the reduced state of the plastoquinone pool.

center II is reduced with increasing distance between the molecules. Due to the fact that the coupling between reaction center I and the light harvesting chlorophyll proteins is very weak (Andersson and Anderson 1980) the transfer of excitation energy to the reaction center I is nearly unaffected.

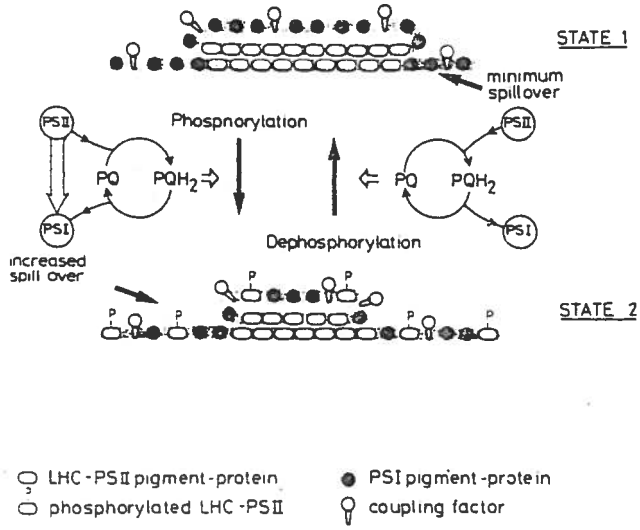

Figure 3: A model relating the changes in phosphorylation of LHCP with changes in the energy transfer from P680 to P700. The membrane kinase responsible for the phosphorylation is activated by the reduced plastoquinone pool (PQH_2).
(Adopted from Barber (1983)).

In total, the input of electrons from reaction center II to the plastoquinone pool is reduced while the demand of electrons by reaction center I remains nearly constant. This change of energy transfer affects the in vivo chlorophyll a fluorescence as well as the rate of photosynthesis.
The time constant for this reversible process is in the minute range and can be observed with dark adapted phytoplankton by the fluorescence induction curve, the so called Kautsky effect, after the onset of continuous light (Kautsky and Hirsch 1931; Kautsky et al. 1960; Franck et al. 1969).

2. The Kautsky curve

After an extended dark-period (> 5 minutes) all elements of the electron transport chain are in an oxidized state. Upon the onset of continuous illumination the in vivo fluorescence shows a characteristic fluorescence induction called Kautsky curve (Kautsky et al. 1931). The almost immediate rise from the zero (dark) level to O (Figure 4) reflects the "dead" or "constant" fluorescence, a contribution which does not change with increasing photosynthetic turnover. The rise from O to P is largely influenced by the increasing reduction of the primary electron acceptor Q (Fig. 2). If Q is reduced the drain of the electrons from P680 to Q and the plastoquinone pool PQ decreases and the share of fluorescent transitions increases. Reasons for the "dip" (I,D) are still in discussion including the onset of PS I activity and cooperative phenomena between different subspecies of Q. The decrease after P occurs when reactions behind PQ, particularly the Calvin cycle, are turned on. The difference between P and the steady state level S are often discussed as a measure for photosynthetic turnover. This difference becomes low in senescent populations and vanishes after blocking the transport chain artificially e.g. with the herbizide 3-(3,4-dichlorophenyl)-1,1-di-methylurea (DCMU).

The fluorescence induction curve of DCMU treated chloroplasts and algae show a biphasic structure giving evidence for the hypothesis of two primary quencher Qa and Qb as acceptors operating in parallel rather than in series i.e. there are two types of rection centers, the α- and ß-centers. For higher plants, this heterogeneity of photosystem II is well documented (Melis and Homann, 1975,1976; Melis and Anderson, 1983).

Results of Owens (1986) analysing the kinetics of photosystem II fluorescence in marine diatom Phaeodactylum tricornutum treated with DCMU show the biphasic nature of fluorescence induction suggesting that the heterogeneity of photosystem II is a general consequence of thylakoid membrane appression.

For a detailed interpretation of the complex behaviour of the fluorescence induction curve, Christoffers (1986) presented a mathematical model taking into account the interplay between the primary electron acceptors of P680 and the excitons created in the light harvesting complex and the antenna. Assuming that α- and ß-centers operate in parallel and compete for the excitons in a statistical pigment bed, he could exactly deduce measured fluorescence induction curves of DCMU treated algae from a two quencher model.

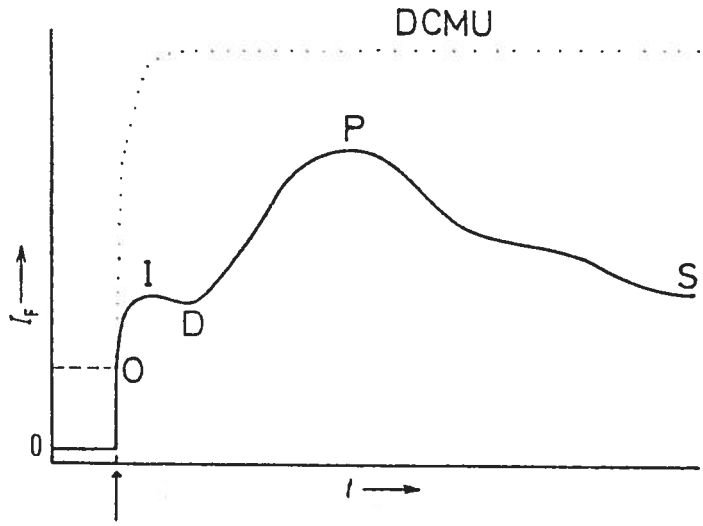

Figure 4: Typical fluorescence induction curve of dark adapted phytoplankton (Kautsky curve) after the onset of continuous light (solid line).
The dotted curve represents the typical induction curve of phytoplankton treated with DCMU.
The arrow indicates the onset of the light.

O	:	dark adapted fluorescence
I	:	first fluorescence maximum
D	:	first depression
P	:	main fluorescence maximum
S	:	stationary fluorescence

3. In vivo fluorescence.

Regarding the widely used in vivo chlorophyll a fluorescence method to monitor the phytoplankton distribution, to determine the biomass or to relate chlorophyll fluorescence to photosynthesis, it is important to understand where the observable fluorescence originates and how the observed fluorescence can be related to the mechanism of photosynthesis in terms of oxygen evolution or carbon uptake.
The analysis of fluorescence spectra of chloroplasts of higher plants at 77 K (Goedheer 1964) and of measurements of the in vivo fluorescence decay of algae in the pico to nanosecond range (Moya and Garcia 1983; Haehnel et al. 1983) leads to the conclusion that at least three different chlorophyll a proteins act in the photosynthetic units.

The fluorescence emission of the light harvesting chlorophyll proteins has its maximum at 685 nm, while that of the antenna chlorophylls of photosystem II and I are at 695 nm and 730 nm, respectively. At physiological temperatures the in vivo fluorescence spectra of algae show only one maximum at 685 nm with a typical bandwidth of about 10 nm and a shoulder at 730 nm, corresponding to the weak fluorescence of the antenna of photosystem I. However, the fluorescence has lower intensity at environmental temperature. One possible explanation for this observation is given by the cyclic electron flow.The electrons shuttled to ferredoxin may go in a second way,the cyclic electron flow, to the plastoquinone pool. They produce a proton gradient and supply energy for ATP synthesis without producing NADPH.

A typical in vivo fluorescence spectrum of marine phytoplankton is shown in Figure 5. The measured data are indicated by crosses.

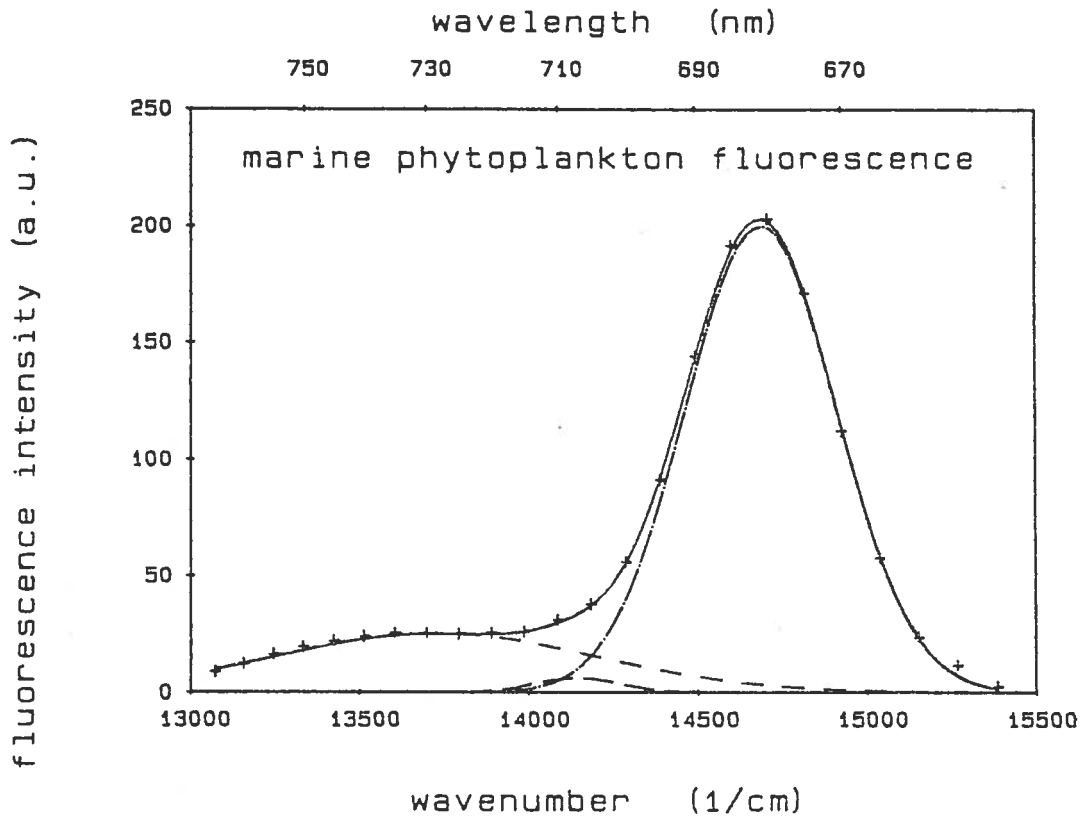

Figure 5: Fluorescence emission of marine phytoplankton on an energy linear scale. The data adopted from Haardt and Maske appendix 15 of this issue are analysed numerically, assuming three spectral emissions of Gaussian shape.
Deviation of the fit is smaller than 1%.

crosses : meassured data
broken lines : fitted Gauss-curves
solid line : sum of the fitted curves

Assuming that the fluorescence spectrum given on an energy linear scale can be described by a linear superposition of spectral bands in accordance with the three chlorophyll protein complexes mentioned above a numerical fit was executed using symmetrical Gauss curves. The measured data could be fitted with a deviation of less than 1%. The parameter set describing the Gauss curves is presented in Table 1, showing the central wavelength, the full width at half maximum (FWHM) and the relative intensity of the spectral component.

Table 1: Fitted Gauss curve parameters of the data presented in Figure 5.

central wavelength(nm):	681	707	728
FWHM (nm):	24	15	59
rel. intensity (%):	75	2	23

4. In vivo excitation and emission spectra.

Algae show specific absorption and fluorescence spectra due to their pigment composition. The fluorescence excitation (and consequently the photosynthetic action spectra) depend on the in-vivo absorption spectra of the specific pigments and the exciton transfer efficiency from these pigments to the reaction centers (Fig. 2). Assuming constant pigment composition and transfer efficiency the diversity in pigment composition of algae might provide for a certain population analysis based on absorption or fluorescence excitation and emission spectra. As indicated in Figure 6 there are some characteristic differences in the fluorescence spectra. Due to the biliproteins (phycoerytrin and phycocyanin) acting as accessory pigments in the thylakoid membrane of blue-green and red algae a typical fluorescence emission is observed at 580 nm as well as the fluorescence emission at 685 nm common to all phyla.

The practical application of monitoring the diversity of marine phytoplankton is limited by the fact that the dominating phyla (Bacillariophyta, Haptophyta and Dinophyta) show very similar excitation and emission spectra. On the other hand this limitation is an advantage for active and passive remote sensing techniques monitoring the fluorescence emission at 685 nm.

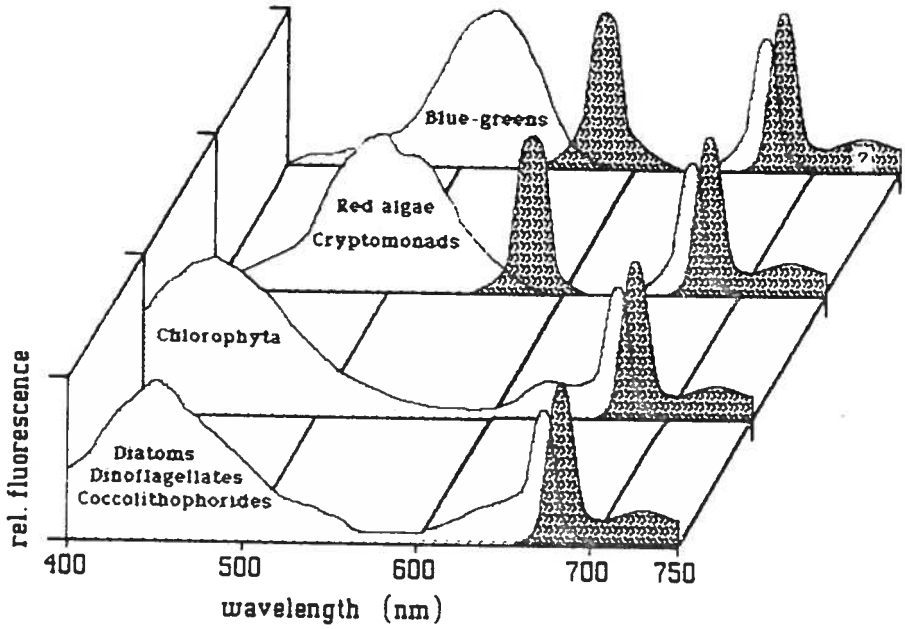

Figure 6: Representative excitation (light shade) and emission spectra (dark shade) of marine plankton phyla (adopted from Yentsch and Phinney, 1985 and extended). The fluorescence at about 730 nm of blue-green algae, indicated with a question mark, is not yet observed.

The common absorption features in the blue and red portion of the spectrum and the common fluorescence emission at 685 nm indicate that the fluorescence efficiency of in-vivo chlorophyll a for the dominating marine phyla is to a first approximation independent of the species.

In Table 2 a set of in-vivo chlorophyll a fluorescence efficiency data deduced form the literature is presented.Different methods were used from conventional cw broad band excitation (spectral fluorometer SF) to specific laser line excitation by cw or pulsed systems (LA). Additional, fluorescence efficiencies are mentioned which are deduced from a comparison of radiative transfer calculations of solar stimulated fluorescence with measured data. Fitting the experimental data to the model is done by adjusting the fluorescence efficiency for optimal agreement. These "fitted" fluorescence efficiencies are noticed in Table 2 by RT. The fluorescence efficiencies range from 0.15% to 10.1% converging to a mean value of 0.35%.

Recent results of Soo Hoo et al. (1986) confirm that variations due to phyla composition are minor than the spectral variations due to adaptation. It is not known to what extend this variation in spectral character is due to changes in pigment composition or energy transfer efficiency.

Table 2:

In - vivo chlorophyll a fluorescence efficiencies

Author		[%]	Method
Vermeulen,Wassink,Reman	(1937)	0.15-0.3	SF
Latimer,Bannister,Rabinowitch	(1956)	1.5-2.8	SF
Friedman,Hickman	(1972)	0.29-0.6	LA
Mumola et al.	(1975)	0.15-0.3	LA
Farmer et al.	(1979)	0.2-0.6	LA
Gordon	(1979)	0.66-0.79	RT
Kim	(1980)	0.35-1.2	LA
Poole,Venable,Campbell	(1981)	0.25	SF
Klein-Hennig	(1981)	0.15-0.45	LA
Kattawar,Vastano	(1982)	0.44-0.53	RT
Günther	(1985)	0.3-0.4	LA
Carder,Steward	(1985)	0.84-10.1	RT
Topliss	(1985)	0.96-2.4	RT
Fischer,Doerffer,Grassl	(1986)	0.3-0.4	RT

Abbreviations for methods:

SF: spectral fluorometer
LA: laser excitation
RT: radiative transfer model

Applying the in vivo chlorophyll a fluorescence method to oceanographic or limnological purposes, one can write for the observed chlorophyll a fluorescence F_m per concentration unit, in general:

$$F_m = I_{abs} * \Phi_{fII} \qquad (1)$$

where I_{abs} is the absorbed light intensity emitted by an in situ fluorometer, an airborne laser or the sun. Φ_{fII} is a variable fluorescence efficiency, depending on environmental parameters.

Under nutritional stress, in vivo chlorophyll a fluorescence shows an increase up to a factor of 2-4 (Kiefer 1973 b,c; Blasco 1975; Slovacec et al. 1977). In contrast, the reduction of the in vivo fluorescence efficiency due to high light is a well known phenomenon since the work of Loftus et al. (1975), Kiefer (1973 a,b), Heaney (1978), Abbott et al. (1982) and Rabbani (1985).This photoinhibition can be observed clearly in stratified water masses with low turbulent mixing and nearly constant chlorophyll a concentration with depth by profiling the fluorescence and the downwelling irradiance. Additional, photoinhibition is reflected by the daily cycle of the chlorophyll a fluorescence or by the response of phytoplankton fluorescence to rapid variations in light (Abbott et al. 1982).

To get a quantitative understanding of photoadaption of phytoplankton to fluctuating light, three different approaches are possible.

- Laboratory or in situ data are normalized to constant chlorophyll a concentration and then analyzed using numerical methods e.g. fit procedures giving an empirical understanding of what happens with the molecular fluorescence efficiency with increasing light.

- Second, time series of light and fluorescence are investigated by calculating the coherence spectrum and its confidence interval using fast Fourier transformation (Abbott et al. 1982) assuming a linear relationship between light and fluorescence.

- Third, based on a comprehensive photochemical model of the photosynthetic apparatus the reduction of the fluorescence efficiency due to photosynthetic active radiation is described in terms of physical rate constants and other photosynthesis related parameters (Günther 1985,1986).

5. Bipartite model of Butler and Kitajima.

For the quantitative description of the in vivo chlorophyll a fluorescence Butler and Kitajima (1975) developed the "tripartite model" of a photosynthetic unit, indicating that the system is divided functionally in the light harvesting complex, the antenna associated with the reaction centers I and II respectively and the reaction centers themselves.

For physiological temperatures the "tripartite model" can be reduced to the simplified "bipartite model" described below. The simplification of the "bipartite model" with respect to the "tripartite model" is done in combining the light harvesting complex and the antenna to form one light absorbing complex ignoring the interaction of the light harvesting complex with the antenna. For this compact photochemical model the following assumptions are made:

1) The light harvesting chlorophyll proteins and the antenna of reaction center II are considered as one combined complex, fluorescent at 685 nm. The fluorescence is described by a rate constant k_{FII}.

2) The reaction centers are nonfluorescent.

3) The reaction centers influence the variable fluorescence efficiency by their state. The open state is the reduced ground state, where the reaction center can accept excitation energy from the antenna for charge separation. The closed state is termed the oxidized state where excitation energy is transfered back to the antenna with a rate constant k_{tII}. This process enhances the probability for fluorescence, for thermal desactivation or for the so called spillover.
   For an ensemble of reaction centers in the thylakoid membrane the relative number of open reaction centers is described by the parameter A_{II}, while the number of closed centers is described by $(1 - A_{II})$. The parameter A_{II} can range from 0 to 1. If A_{II} is 0, all centers are in the closed state. In this limit, the photosynthetic unit shows the maximum fluorescence while photosynthesis is inhibited.

4) Open reaction centers do not feed back the excitation energy, described by a rate constant for charge separation k_P. In general, it holds that k_P is greater than the rate constant k_{tII}.

5) Spillover is a process describing the transfer of excitons from the antenna of photosystem II to the antenna of photosystem I. This process reduces the fluorescence of photosystem II.

To describe the possible interactions of photosynthetic units in the thylakoid membrane Butler et al. (1975) developed a separate package model (SP model) and a matrix model (M model). Within the separate package model no interaction between the photosynthetic units is regarded. In contrast, for the matrix model excitation transfer between photosynthetic units is assumed.

6. Expanded "bipartite model".

Assuming that the absorbed intensity I_{abs} given in Eq. (1) is constant for a model phytoplankton cell and does not change with environmental factors, photoadaptation with regard to the chlorophyll a fluorescence can be described by a general formula for the variable in vivo chlorophyll a fluorescence efficiency f_{II}:

$$f_{II} = \beta * f_{II} * f(A_{II}) \qquad (2)$$

β is the amount of absorbed light energy going to photosystem II, f_{II} is a constant fluorescence efficiency depending on the desexcitation rate constants of the fluorescing antenna chlorophyll a molecules and $f(A_{II})$ a model function describing the connection of the photosynthetic units in the thylakoids. The parameter A_{II} represents the relative number of open reaction centers as mentioned above.

The model of Butler et al. (1975) can explain the fast increase of the chlorophyll a fluorescence of dark adapted cells after the onset of continuous light due to closed reaction centers (fluorescence induction or Kautsky effect). The difference of the maximum fluorescence and the ground fluorescence where all reaction centers are open is well correlated with the photosynthetic efficiency.

The reduction of the fluorescence due to high light, the above mentioned photoinhibition, is not included in the "bipartite model". Günther (1985,1986) introduced a light intensity dependent energy distribution parameter β describing the light dependent state of the thylakoid membrane, and an intensity dependent parameter A_{II} to model the photoadaptation in a quantitative way ignoring the time dependence (Figure 7).

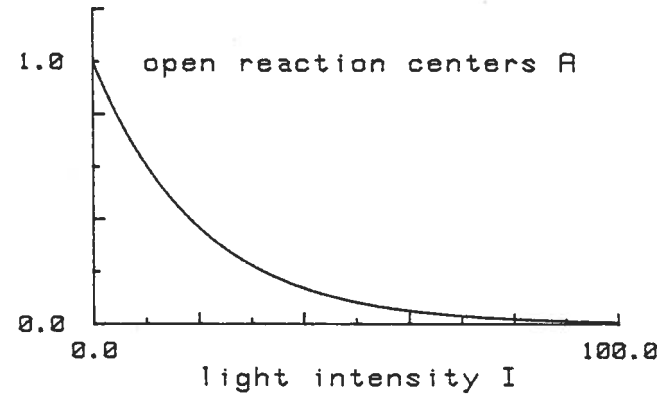

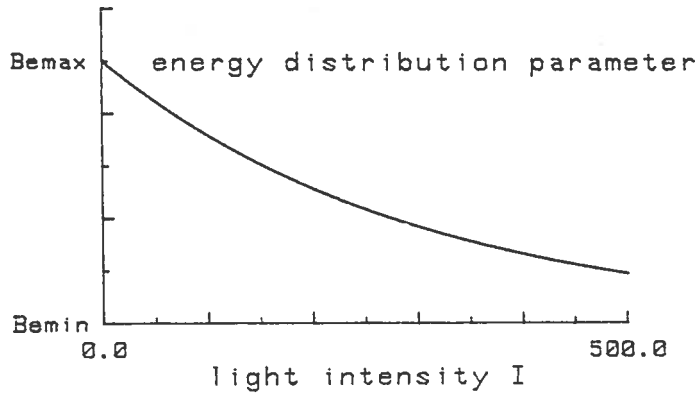

Figure 7: Schematic representation of the function $\beta(I_{Phar})$ and $A_{II}(I_{Phar})$.
β the dimensionless energy distribution parameter can vary between β_{max} and β_{min}.
A_{II} the relative number of open reaction centers can vary between 1 and 0.
I_{Phar} symbolizes the photosynthetic active radiation restricted to the wavelength band from 350 to 750 nm

The idea of modeling the parameter β and A_{II} as light dependent is based on the findings of Horton(1980) and Allen et al. (1981) that the membrane state is regulated by the redox state of the plastoquinone pool. As mentioned above the redox state of the plastoquinone pool controlled by the amount of light absorbed by the cell induces an encymatic reaction the phosphorylation. This in turn changes the distance between the light-harvesting pigment complexes and the reaction centers and thus the parameter β.

Assuming that $\beta(I)$ decreases from a maximum level β_{max} under low light conditions to a minimum level β_{min} with increasing light exponentially, an intensity parameter I_1 is introduced determining the light state of the membrane.
The light dependence of A_{II} modeled by an exponential increase with increasing light gives a light parameter I_0, indicating the adaptation of the reaction centers according to the growth conditions, e.g. shade or light adapted cells.

Applying these assumptions to the "bipartite model" one can calculate the relative variation of the fluorescence efficiency due the so called photosynthetic active radiation. It is important to note that the light influencing phytoplankton is restricted to a wavelength band from 350 nm to 750 nm.

The relative decrease of the fluorescence efficiency with increasing light according to the expanded "bipartite model" is shown in Figure 8. The dark value of the fluorescence efficiency is set to 1. Knowing the absolute fluorescence efficiency of marine phytoplankton measured as the dark level in accordance with open reaction centers one has to multiply this value with the data given in Figure 8 to get the actual fluorescence efficiency during day.

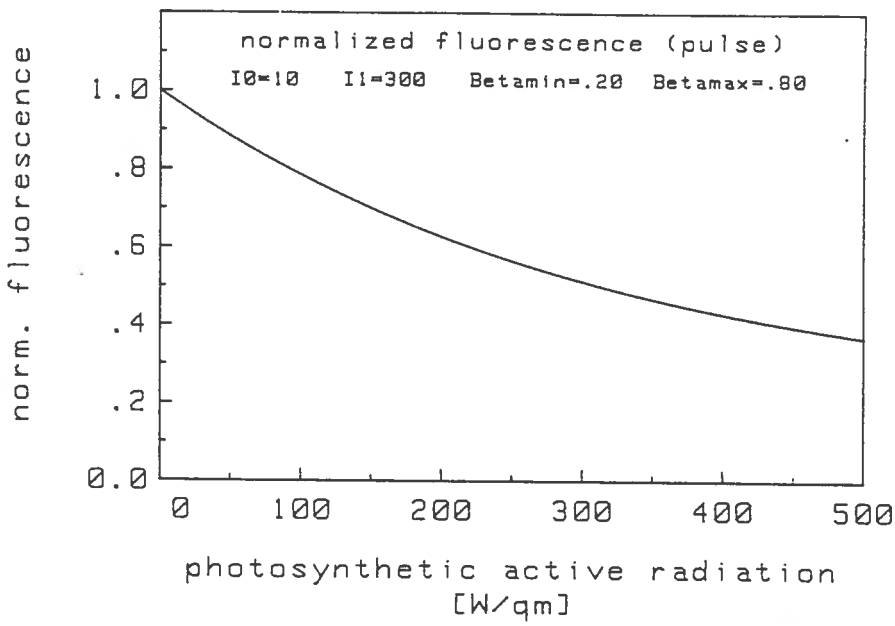

Figure 8: Dark normalized fluorescence efficiency φ_{fII}, depending on the photosynthetic active radiation (Phar) according to the expanded "bipartite model". The parameters (given on top of the figure) are chosen in agreement with the experimental findings.

7. Experimental results of FLUREX '82.

The experiments presented in this section were performed during the Fluorescence Remote Sensing Experiment FLUREX '82. The data are published elsewhere in detail (Günther and Reuter 1983; Günther 1985; Günther 1986a). For completeness, a review is given here.

Continuous grund truth measurements with an in situ fluorometer and an in situ attenuation meter, held at constant water depth, were performed at the research platform NORDSEE to investigate the daily cycle of the fluorescence efficiency due to the impact of photosynthetic active radiation. Additional, a two channel fluorescence lidar system was installed at the top of the research platform to monitor the chlorophyll a fluorescence. The system, described by Gehlhaar et al. (1981), was modified for the specific detection of the in vivo chlorophyll a fluorescence at 685 nm and the water Raman scattering at 650 nm. The excitation wavelength of the flashlamp pumped dye laser was adjusted to 532 nm with pulse energies of about 350 mJ. The lidar signals gave the depth integrated chlorophyll a fluorescence and an effective water attenuation coefficient. This parameter can be deduced from the water Raman scattering signal influenced by the beam attenuation at laserwavelength and by the diffuse attenuation at Raman scattering wavelength.
At regular intervals, ground truth water samples were collected. A subsample was used for chlorophyll a extraction according to the method of Whitney et al. (1979). The rest of the water samples was used to determine the total beam attenuation coefficient over the spectral region from 400 to 800 nm with a laboratory photometer.The cuvette length was one meter. The detector solid angle was 0.27° with a spectral bandwidth of 5 nm. In a second step, the attenuation due to dissolved organic matter (yellow substance) was determined after filtration with 0.2 m filters. Bidestilled water was used as reference standard.

A first analysis of the fluorescence data showed a high correlation of the Raman corrected fluorescence lidar signals and the in situ fluorescence readings over the whole experimental period with a correlation coefficient of 0.97. Both fluorescence data varied by a factor of 4 in time while the analysis of the extracted chlorophyll a values revealed a relativly constant chlorophyll a concentration indicating that the in situ and the lidar signals were both affected by environmental factors.

To analyse the influence of daylight on the fluorescence efficiency in detail, the continuously recorded in situ fluorescence data were normalized to constant chlorophyll a concentration taking into account the results of the analysis of the water samples and of the continuously recorded in situ attenuation data at 670 nm. With a good approximation the influence

of yellow substance on the diffuse attenuation coefficient at 670 nm could be neglegted due to yellow substance concentrations of less than 0.74 mg/l. Additional, the influence of particulate matter on the attenuation was nearly constant in time and less than 0.1 m^{-1}. With these findings the continuous in situ attenuation data could be considered to be proportional to the chlorophyll a concentration. Assuming that the in situ fluorescence data were proportional to the chlorophyll a concentration and the fluorescence efficiency the normalization of the fluorescence readings could be accomplished by dividing the fluorescence data by the water and suspended sediment corrected attenuation values.

With this approximation, the normalized fluorescence data in relative units could be regarded as a measurement of the fluorescence efficiency. The mean squared error of the normalized fluorescence was approximately 18 %.
For two days, April 22 and 23, Figures 9 and 10 show the daily cycle of fluorescence efficiency together with the daily cycle of the photosynthetic active radiation given by the dotted lines. The solid line shows the result of the expanded photosynthetic model.

The model parameters β_{min}, β_{max}, I_0 and I_1 were fitted by a computer program. For all days including those which are not presented here, only the parameter β_{min} had to be changed from 0.2 to .3 to describe the observed photoinhibition with a high correlation.

For April 22, the weather was partly cloudy with short clear ups similar to April 21, showing a maximum irradiance of about 470 Wm-2. The fluorescence efficiency showed a daily cycle due to the influence of the photosynthetic active radiation again. Although the maximum irradiance on April 22 was higher compared to April 20, the fluorescence efficiency was reduced to about 50 % compared to 60% , suggesting that the short clear ups at noon had minor influence due to an internal regulation mechanism with time constants greater than the shortest increase of the light during this day (Figure 9).

The best approximation of the model to the in situ data could be achieved by increasing the parameter β_{min} to 0.3. For April 23, the same parameter set as for April 22 was found to minimize the deviation of the model and the measured data. A good correlation between photosynthetic active radiation and fluorescence efficiency was observed until the afternoon. The increase of the global irradiation in the late afternoon was not seen in a comparative decrease of the measured fluorescence efficiency. Due to a nonconsistent increase of the night values up to 1.2 it was assumed that a systematic error was introduced (Figure 10).

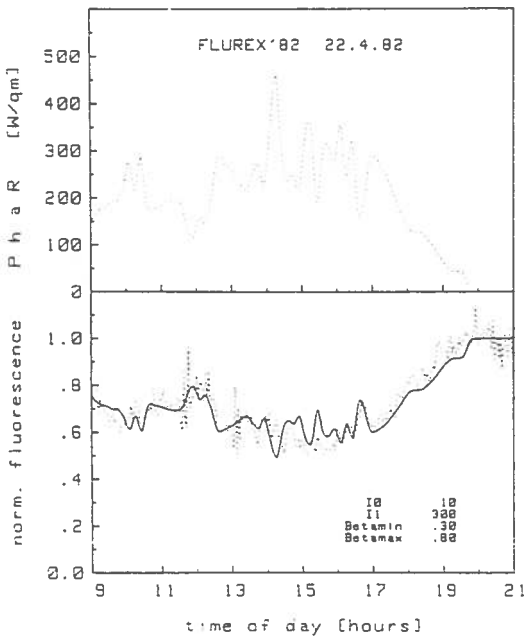

Figure 9;
Daily cycle of the relative chl a fluorescence efficiency and the photosynthetic active radiation on April 22,1982.
dotted line:measured data
solid line:results of the expanded "bipartite model"

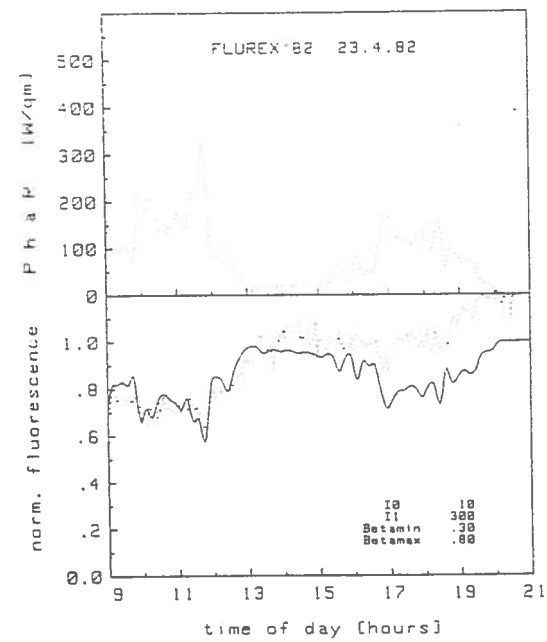

Figure 10:
Daily cycle of the relative chl a fluorescence efficiency and the photosynthetic active radiation on April 23,1982.
dotted line:measured data
solid line:results of the expanded "bipartite model"

8. Discussion of the FLUREX '82 results.

For the interpretation of the model parameters introduced to expand the bipartite model of Butler et al. (1975) for a quantitative description of the in vivo fluorescence reduction due to high light a sensitivity study was made with respect to the fluorescence and the photosynthesis efficiency. The parameter I_0, describing the light dependence of the state of the reaction center II, can range from $1 Wm^{-2}$ to $30 Wm^{-2}$ giving an error of about 2% with respect to the fluorescence reduction.

Regarding the influence of I_0 on the efficiency of photosynthesis, which can be deduced by the bipartite model, it can be seen, that I_0 determines the light value for maximum photosynthesis. A comparison with the empirical formula of Steele (1962) for the description of photosynthesis efficiency P given in Eq. (3) shows that the free parameter a of Steele is reciprocal related to I_0 and describes the light value of maximum photosynthesis too.

$$P = P_{max} * I * a * e^{(1-a*I)} \qquad (3)$$

P_{max} is the maximum for photosynthesis efficiency, I is the light intensity and a a free parameter. The free parameter a determines the position of the maximum for photosynthesis efficiency, as well as the linear region of the P-I curve. It can be shown that

$$I_0 = 1/a \qquad (4)$$

Additional, the investigations of Ryther et al. (1959) confirm that for shade adapted algae the maximum of photosynthesis is typical at $10 Wm^{-2}$ and for sunadapted algae at $70 Wm^{-2}$. With $I_0 = 30 Wm^{-2}$, the maximum is in the range observed by Ryther indicating that the algae population under investigation during FLUREX '82 is assumed to be shade adapted (Figure 11).

To optimize photosynthesis with regard to the light conditions phytoplankton can change the size of the photosynthetic units (Perry et al. 1981) on a long time scale. The number of chlorophyll molecules per reaction center P700 increases with decreasing light.

The parameter I_1 determines the fluorescence reduction due to high light levels. Varying I_1 in the range from $200 Wm^{-2}$ to $400 Wm^{-2}$, the normalized fluorescence efficiency changes by about 12 % compared to $I_1 = 300 Wm^{-2}$. According to the analysis, the parameter I_1 describes the light adapted state of the membrane and can be related to the threshold level for photoinhibition introduced by Kiefer (1973a), Heaney (1978) and Vincent (1979). The parameter I_1 is nearly insensitiv to the efficiency of photosynthesis.

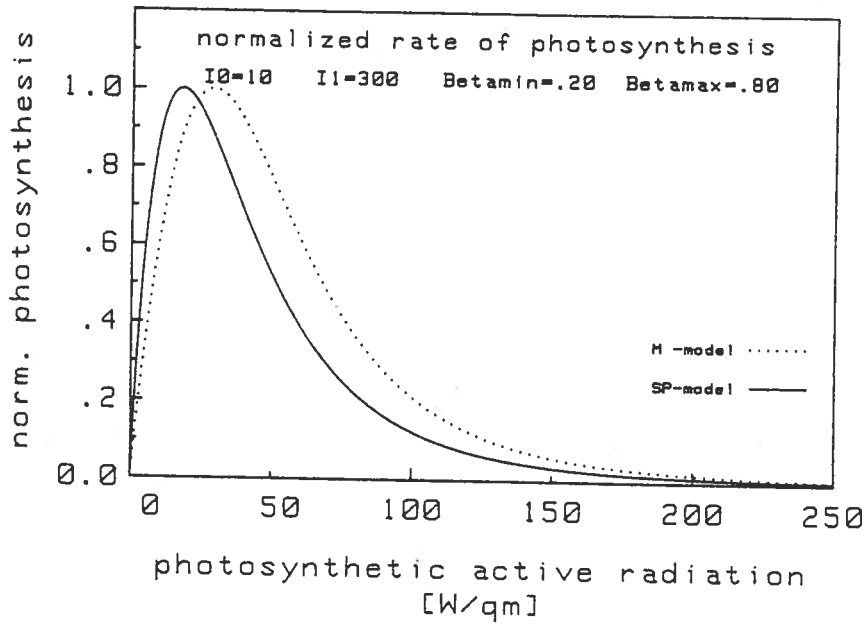

Figure 11: Normalized rate of photosynthesis depending on the photosynthetic active radiation. The parameter are choosen in agreement with the findings of the FLUREX '82 campaign.
solid line: separate package model
broken line: matrix model

To analyze the influence of β_{min} and β_{max} on the normalized fluorescence efficiency F_n, an approximation can be given, assuming I_0 and I_1 as constant for the time of investigation. This approximation holds for light intensities I greater than the parameter I_0.

$$F_n \sim \beta_{min}/\beta_{max} + (\beta_{min}/\beta_{max} - 1) * \exp(-I_{phar}/I_1) \qquad (5)$$

where I_{phar} is the intensity of the photosynthetic active radiation. The approximation shows, that F_n is determined by the ratio of β_{min} to β_{max}. A variation of β_{min} and β_{max} with fixed ratio reveals that the approximation of F_n compared to the exact evaluation is within an error of 2%.

Analyzing the influence of β_{min} and β_{max} on the efficiency of photosynthesis, one can show that β_{max} determines the light level of maximum photosynthesis, while the maximum value of photosynthesis is to a first approximation independent of β_{min}. Assuming that the ratio β_{min} to β_{max} describes the physiological state of the membrane due to phosporylation, an increase of this ratio is equivilant to a minor decrease of photoinhibition at high light levels. In the limit of $\beta_{min} \sim \beta_{max}$, no photoadaptation is expected according to the expanded bipartite model.

The data of Kiefer (1973a,1973b) and Blasco (1975) as well as own investigations confirm that under nutritional stress the photoinhibition of algae is reduced compared to algae in the exponential growth phase resulting in a higher fluorescence efficiency.

Investigating the fluorescence induction curve (Kautsky effect) of phytoplankton treated with the herbizide DCMU one can observe a steep increase of the fluorescence after the onset of light. No decrease, or photoadaptation occurs due to the fact that DCMU inhibits the flow of electrons from the reaction center P680 towards the plastoquinone pool. In the frame of the expanded "bipartite model" the redox state of the plastoquinone pool is not changed. Thus the encymatic reaction for phosphorylation is not initiated, resulting in a constant $\beta(I_{Phar})$.

Thus, it can be assumed that the ratio β_{min} to β_{max} depends on the nutrient availability and environmental stress factors.

In conclusion, the four parameters introduced by the proposed expanded "bipartite model" can be reduced to two parameters determining the photoadaptation of phytoplankton with respect to the fluorescence efficiency due to high light.

9. Experimental results of FLUREX '85.

From March 25 to 31, 1985, a second Fluorescence Remote Sensing Experiment FLUREX '85 was performed to continue the experiments of FLUREX '82 regarding the variable fluorescence efficiency of phytoplankton influencing remote sensed chlorophyll fluorescence. Different sensors operated from ships and aircrafts in the German Bight and the Baltic near Kiel. It was intended to combine ground truth data with active and passive remote sensing data. Due to bad weather situation a reduced experimental program was performed.

First preliminary results are reported concerning the photoadaptation of phytoplankton measured with an in situ fluorometer. For this purpose the "Kieler Multisonde" of the Institute for Applied Physics, University of Kiel, was operated from board of the research vessel "Alkor" of the "Institut fur Meereskunde", Kiel. This multifunctional profiling system measured pressure, temperature, salinity, down- and upwelling irradiance, attenuation at 670 nm and fluorescence at 685 nm.

Investigating the photoadaptation of phytoplankton by inspecting in vivo chlorophyll a fluorescence, the raw data of fluorescence and attenuation were processed similar to the procedure mentioned above for the FLUREX '82 campaign to get concentration normalized fluorescence data. Applying Eq. (5) to the normalized fluorescence emission data and the downwelling irradiance data a least squares fit was performed to extract the ratio β_{min} to β_{max}, indicated in Figure 11 as β, and the intensity value I_1.
In Figure 12, one typical result of a depth profile measured on march 25, 1985, at position 54° 37.4' E, 10° 21.8'N is presented. The typical exponential decrease of the normalized fluorescence with increasing downwelling irradiance is seen comparable with the results obtained during FLUREX '82 where the daily cycle of the fluorescence emission was investigated. In the surface layer where the downwelling irradiance was about 200 Wm^{-2}, a reduced fluorescence efficiency of about 70% is seen compared with the fluorescence efficiency at 8 meter depth, the 1% light level.

Comparing the result of β= 0.29 with the results of FLUREX '82 where β increased from 0.25 to 0.37 during the experimental period, a good agreement is seen, indicating that the physiological state of the thylakoid membrane seems to be comparable.

The measurements in 1982 and 1985 were performed during plankton blooms resulting in a decreasing nutrient availability.During FLUREX '82 the experimental period started at the end of a plankton bloom reflected with regard to the fluorescence emission by an increase in β. During FLUREX '85 the plankton bloom was still in progress, reflected by a low β.

The parameter I1, discussed as representative for the photo-adaptation of phytoplankton with respect to the available light is reduced comparing the result of FLUREX '82 (I1 = 300 Wm-2). One possible explanation for the observed difference is the lower mean light level at the end of March 1985 compared to the light level at the end of April 1982 indicating a different adaptation.

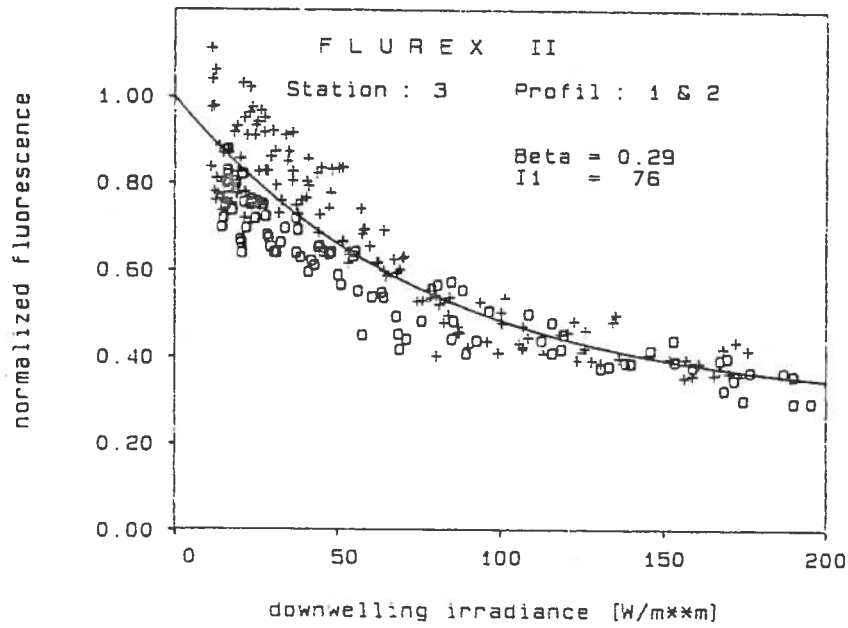

Figure 12 : Light dependent normalized fluorescence efficiency $f_{II}(I_d)$ measured by depth profiling downwelling irradiance I_d and fluorescence excited by short pulses. The data β and I_1 are in accordance with the expanded "bipartite model".
Crosses indicate the results of a pull up profile and rings of a pull down profile.

10. Conclusion.

Concluding the results obtained during FLUREX '82 and '85, the fluorescence efficiency shows a light dependent behaviour which can be described by the expanded "bipartite model" quantitatively.

Performing in vivo chlorophyll a fluorescence experiments with artificial light sources, one has to take into account the photoadaptation of phytoplankton. The results show that the fluorescence efficiency is reduced in high light.

Regarding remote sensing techniques as .g. airborne lidar systems or radiometers operating during day at light levels greater than about 200 Wm^{-2} one can assume to a good approximation that the phytoplankton in the upper water layer is photoadapted and has reduced the fluorescence efficiency. Remembering Figure 1 one can see that a variation of irradiance comparable with daily variations of global irradiance around a mean day light level is weakly reflected by the fluorescence efficiency.

To demonstrate this fact with respect to solar stimulated fluorescence application Figure 13 shows the result of a calculation regarding a constant phytoplankton concentration. For this calculation a variable fluorescence efficiency according to the expanded "bipartite model" was assumed. Figure 12 demonstrates the nonlinear increase of the fluorescence emission

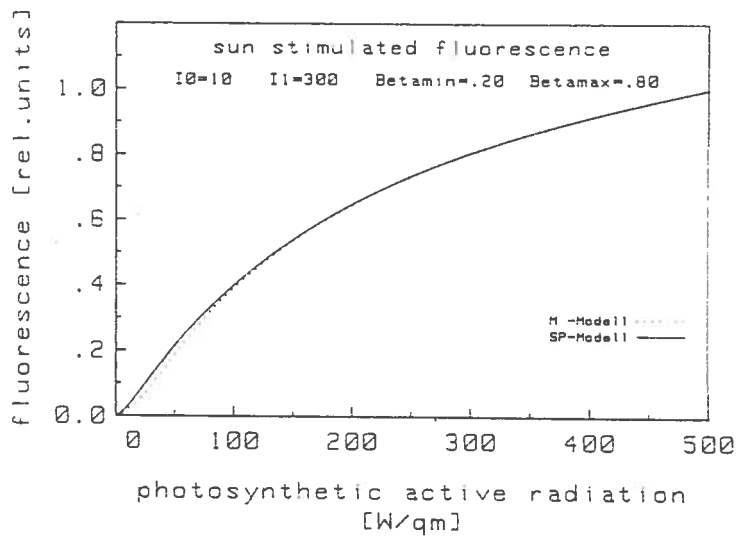

Figure 13 : Solar stimulated fluorescence signal depending on the photosynthetic active radiation assuming a variable fluorescence efficiency f_{II} according to the expanded "bipartite model".
dotted line : matrix model
solid line : separate package model

with increasing irradiance. The light level is varied from dark to full sun.Regarding typical remote sensing applications with irradiances of more than 150 - 200 Wm-2, the increase of the fluorescence signal with increasing irradiance can be approximated linearly. Thus, the fluorescence efficiency can be regarded as constant for this irradiance range remembering the reduction compared to low irradiance. This finding is in good agreement with the fluorescence efficiency of 0.3% which is used fitting radiative transfer models (Fischer et al. 1986) for solar stimulated fluorescence to measured data. Assuming that this value is correct for high light levels, the fluorescence efficiency will increase to about 1% for dark adapted phytoplankton.

Acknowledgement:
The experiment FLUREX '82 performed at the research platform NORDSEE was financed by a grant from the Bundesministerium für Forschung und Technologie.
Many thanks for participating and supporting this experiment to my collegues K. Loquay and R.Reuter.
Many thanks to my collegues R. Grosse and H.-M. Henning for profiling during FLUREX '85.

Literature:

ABBOTT, M.R., P.J. RICHERSON, AND T.M. POWELL. 1982. In situ response of phytoplankton fluorescence to rapid variations in light. Limnol. Oceanogr. 27: 218-225.

ALLEN, J. F., J. BENNETT, K. E. STEINBACK, AND CH. J. ARNTZEN. 1981. Chloroplast protein phosphorylation couples plastoquinone redox state to distribution of excitation energy between photosystems. Nature 291: 25-29.

ANDERSSON, B., AND J.M. ANDERSON. 1980. Lateral heterogeneity in the distribution of chlorophyll-protein complexes of the thylakoid membranes of spinach chloroplasts. Biophys. Biochim. Acta 593: 427-440.

BARBER, J. 1983. Membrane conformational change due to phosphorylation and the control of energy transfer in photosynthesis. Photobiochem. Photobiophys. 5: 181-190.

BLASCO, D. 1975. Variations of the ratio in vivo-fluorescence/ chlorophyll and its application to oceanography. Effects of limiting different nutrients, of night and day and dependence on species under investigation. NASA Technical Translation, TTF-16: 317 pp.

BUTLER, W.L., AND M. KITAJIMA. 1975. A tripartite model for chlorophyll fluorescence. In: Proc. Third Int. Congress Photosynth. Ed.: M.AVRON. Elsevier. Amsterdam. 13 pp.

CARDER, K.L., AND R.G. STEWARD. 1985. A remote-sensing reflectance model of a red-tide dinoflagellate off west Florida. Limnol.Oceanogr. 30: 286-298.

CHRISTOFFERS, D. 1986. On the theory of in vivo chlorophyll fluorescence. Computer simulation of primary photosynthetic reactions. Photochem. Photobiophys. 11: 101-113.

FARMER, F.H., C.A. BROWN,Jr., O. JARRETT,Jr., J.W. CAMPBELL, AND W. STATON. 1979. Remote sensing of phytoplankton density and diversity in Narragansett Bay using airborne fluorosensor. In: Proceedings, Thirteenth International Symposium on the Remote Sensing of the Environment. Vol. 3. 1793-1805.

FISCHER, J., R. DOERFFER, AND H. GRASSL. 1986. Factor analysis of multispectral radiances over coastal and open ocean water based on radiative transfer calcultions. Appl. Opt. 25:448-456.

FÖRSTER, Th. 1948. Zwischenmolekulare Energiewanderung und Fluoreszenz. Annalen der Physik 2: 55-75.

FRANCK, U.F., N. HOFFMANN, H. ARENZ, AND U. SCHREIBER. 1969. Chlorophyllfluoreszenz als Indikator der photochemischen Primarprozesse der Photosynthese. Berichte der Bunsengesellschaft 73: 871-879.

FRIEDMAN, E.J., AND G.D. HICKMAN. 1972. Laser induced fluorescence in algae. A new technique for remote detection. NASA Contractor Report CR 62090.

GEHLHAAR, U., K.P. GÜNTHER, AND J. LUTHER. 1981. Compact and highly sensitive fluorescence lidar for oceanographic measurements. Appl. Opt. 20: 3318-3320.

GOEDHEER, J.C. 1964.Fluorescence bands and chlorophyll a forms. Biophys. Biochim. Acta 88: 304-317.

GORDON, H.R. 1979. Diffuse reflectance of the ocean: the theory of its augmentation by chlorophyll a fluorescence at 685 nm. Appl. Opt. 18: 1161-1166.

GÜNTHER, K.P., AND R. REUTER. 1983. Optical measurements at the research platform "Nordsee" during FLUREX'82. Data report FLUREX'82.

-------, K.P. 1985. Die Abhängigkeit der in vivo Chlorophyll a Fluoreszenz marinen Phytoplanktons von der Globalstrahlung -Ein Beitrag zur Interpretation von Fluoreszenzfernerkundungssignalen- Thesis, University of Oldenburg.

--------,K.P. 1986a. A quantitative description of the chlorophyll a fluorescence reduction due to global irradiation in the surface layer. In: Marine Interfaces Ecohydrodynamics. Ed.: J.C.J. Ninoul. Elsevier, Amsterdam. 603-617.

--------,K.P. 1986b. Photoinhibition of chlorophyll a fluorescence and its influence to remote sensing techniques.In: Proc. Int. Geoscience and Remote Sensing Symposium. IGARRS 86. Zurich, 8 - 11. Sept. 1986,ESA SP-254 (Vol. III).

HAEHNEL, W., A.R. HOLTZWARTH, AND J.WENDLER. 1983. Picosecond fluorescence kinetics and energy transfer in the antenna chlorophylls of green algae. Photochem. Photobiol. 37: 435-443.

HEANEY, S.I. 1978. Some observation on the use of the in vivo fluorescence technique to determine chlorophyll a in natural populations and cultures of freshwater phytoplankton. Freshwater Biol. 8: 115-126.

HORTON, P., AND M.T. BLACK. 1980. Activation of adenosine 5' triphophate-induced quenching of chlorophyll fluorescence by reduced plastoquinone. The basis of state I - state II transitions in chloroplasts. FEBS Lett. 119:141-144.

KATTAWAR, G.W., AND J.C. VASTANO. 1982. Exact I-D solution to the problem of chlorophyll fluorescence from the ocean. Appl. Opt. 21: 2489-2492.

KAUTSKY, H., AND A. HIRSCH. 1931. Neue Versuche zur Kohlensäureassimilation. Naturwissenschaften 19: 964-970.

-------, H., W. APPEL AND H. AMANN. 1960. Chlorophyllfluoreszenz und Kohlensäureassimilation. Biochemische Zeitschrift 332: 277-292.

KIEFER, D.A. 1973a. Fluorescence properties of natural phytoplankton population. Mar. Biol. 22: 263-269.

------, D.A. 1973b. Chlorophyll a fluorescence in marine centric diatoms: responses of chloroplasts to light and nutrient stress. Mar. Biol. 23: 39-46.

------, D.A. 1973c. The in vivo measurements of chlorophyll by fluorometry. In:The Belle W. Baruch Library in Marine Science: Estuarine Microbial Ecology. Ed.: L.H. STEVENSON AND R.R. COLWELL. University of South Carolina Press.

KIM, H.H. 1980. A laser fluorosensing study - supplementary notes. In: Ocean remote sensing using lasers. Ed.: H.R. GORDON, NOAA Tech. Memo. ERL PMEL-18.

KLEIN-HENNIG,A. 1981. Ein Messystem für in vivo Fluoreszenzwirkungsquerschnitte von Phytoplankton. Diploma. University Oldenburg.

LATIMER, P., T.T. BANNISTER, AND E. RABINOWITCH. 1956. Quantum yields of fluorescence of plant pigments. Science, 124: 585-586.

LOFTUS, M.E., AND H. SELIGER. 1975. Some limitations of the in vivo fluorescence technique. Chesapeak Sci. 16: 79-92.

MELIS, A., AND P.H. HOMANN. 1975. Kinetic analysis of fluorescence induction in 3-(3,4-dichlorophenyl)-1,1-dimethylurea poisoned chloroplasts. Photochem. Photobiol. 21: 431-437.

-----, A., AND P.H. ------. 1976. Heterogeneity of the photochemical reaction centers in system II of chloroplasts. Photochem. Photobiol. 23: 343-350.

-----, A., AND J.M. ANDERSON. 1983. Structural and functional organization of the photosystem in spinach chloroplasts. Antenna size, relative electron - transport capacity and chlorophyll composition. Biochim. Biophys. Acta 724: 473-484.

MOYA, I., AND R. GARCIA. 1983. Phase fluorimetric lifetime spectra. I. In algal cells at 77 K. Biophys. Biochim. Acta 722: 480-491.

MUMOLA, P.B., O. JARRETT, AND C.A. BROWN. 1975. Multiwavelength lidar for remote sensing of chlorophyll a in algae and phytoplankton. The use of lasers for hydrographic studies. NASA SP-375. 137-145.

OWENS, T.G. 1986. Photosystem II heterogeneity in the marine diatom *Phaeodactylum tricornutum*. Photochem. Photobiol. 43: 535-544.

PERRY, M.J., M.C. TALBOT, AND R.S. ALBERTE.1981. Photoadaptation in marine phytoplankton: Response of the photosynthetic unit. Mar. Biol. 62: 91-101.

POOLE, L.R., D.D. VENABLE, AND J.W. CAMPBELL. 1981. Semianalytic Monte Carlo radiative transfer model for oceanographic lidar systems. Appl. Opt. 20: 3653-3656.

RABBANI, M.M. 1984. Untersuchungen zum Fluoreszenzwirkungsgrad des Phytoplanktons und der damit assoziierten morphologischen und physiologischen Adaptionsmechanismen. Thesis. Christian-Albrechts- Universitat, Kiel.

RYTHER, J.H., AND D.W. MENZEL. 1959. Light adaptation by marine phytoplankton. Limnol. Oceanogr. 4: 492-497.

SLOVACEK, R.E., AND P.T. HANNAN. 1977. In vivo fluorescence determination of phytoplankton chlorophyll a. Limnol. Oceanogr. 22: 919-925.

SOO HOO, J.B., D.A. KIEFER, D.J. COLLINS, AND I.S. McDERMID. 1986. In vivo fluorescence excitation and absorption spectra of marine phytoplankton: I. Taxonomic characteristics and responses to photoadaptation. J. Plankton Res. 8: 197-214.

STEELE, J.H. 1962. Environmental control of photosynthesis in the sea. Limnol. Oceanogr. 7: 137-150.

TOPLISS, B.J. 1985. Optical measurements in the Sargasso Sea: solar stimulated chlorophyll fluorescence. Oceanclogica Acta. 8: 263-270.

VERMEULEN, D., E.C. WASSINK, AND G.H. REMAN. 1937. On the fluorescence of photosynthesizing cells. Enzymologia 4: 254-268.

VINCENT, W.F. 1979. Mechanisms of rapid photosynthetic adaption in natural phytoplankton communities. I. Redistribution of excitation energy between photosystem I and II. J. Phycol. 15: 429-434.

WHITNEY, D.E., AND W.M. DARLEY. 1979. A method for the determination of chlorophyll a in samples containing degradation products. Limnol. Oceanogr. 24: 183-186.

YENTSCH, C.S., AND D.A. PHINNEY. 1985. Spectral fluorescence: an ataxonomic tool for studying the structure of phytoplankton populations. J. Plankton Res. 7: 617-632.

The effect of short term illumination changes on the sun light stimulated fluorescence of phytoplankton

R.Doerffer

GKSS Forschungszentrum Geesthacht

1. Introduction

It has been demonstrated in appendix 2 and 3 of the study, that illumination changes due to sun elevation can be neglected for remote sensing purposes. Another effect, which might change the fluorescence efficiency are short term illumination changes caused by clouds which shade the water surface. For satellite remote sensing it is important to know, if after a cloud passage the fluorescence has the same value as before the passage assuming no concentration change.

The influence of light changes on biophysical processes in the algae cell is discussed in appendix 1, in KIEFER(1973), RABBANI (1974) and in GÜNTHER (1984).

During the Fluorescence Experiment FLUREX'82 we had the opportunity to observe this situation but only for one case. The fluorescence signal was extracted from spectral radiance measurement as described in Annex 2. Simultaneously the downwelling irradiance was recorded with the same multichannel radiometer.

2. Results

The observation was made at April 25 , 16:30 h, in the Kiel Bight, Baltic Sea, at the end of a clear day when some small cirrus and cumulus clouds appeared. Chlorophyll concentrations ranged from 2 - 4 mg m^{-3}, suspended matter dry weight was ~2 mg/l.

The radiances were measured while the ship was slowly drifting.

Fig.1 shows the downwelling irradiance at 445 nm, where chlorophyll has its absorption maximum. The upper level in the time series indicates the irradiance for clear sky, while the minima indicate passages of single small clouds, which reduce the irradiance up to 50%. The larger cloud passage (at 200 s) lasted for about 100 seconds.

The corresponding radiances for 645 nm and 685 nm are represented in fig.2. In general both radiances are correlated. Of interest are the events when the light level is changing. At the beginning of the first cloud

passage (time: 170 s) L(645) changes as rapidly as the downwelling irradiance while the slope of L(685) is flatter. Both radiances reach the same relative level lateron. Another interesting event can be observed at time 400 s: L(685) has an invers trend compared to L(645).

These events are much more evident when applying the fluorescence algorithm on the radiance data (fig.3). The applied algorithm normalizes the fluorescence line height by the height of the baseline (s. appendix 2) in order to take into account the variable irradiance:

fluor.norm = fluor.line height / baseline height

3. Discussion and Conclusions

Before and after the passage of a cloud the fluorescence does not show any difference. The average value and the fluctuations of the fluorescence signal correspond (according to the calibration appendix 2) to chlorophyll densities of 1.5 ± 0.5 mg m^{-3}, also proven by the direct measurements from water samples.

The maximum in the fluorescence signal right at the beginning of the first cloud passage is caused by the different temporal response to the rapid change in irradiance. The slow change in L(685) with a time constant of about 15 seconds must be related to biophysical and biochemical processes. These in turn are reflected by a fluorescence efficiency change, explainable by the induction or transient process (KAUTZKY effect, s.Appendix 1), which has also a time constant of the same order. The same process is presumably also responsible for the inverse trend in fluorescence (time 400 s in fig.3); in this case the algae react with less fluorescence to a sudden increase in irradiance. Similiar effects were also observed by ABBOTT et al. (1982) in time series of fluorescence with an in situ fluorometer (with artificial light source).

Do these effects have an influence on remote sensing of chlorophyll fluorescence from space? For this question we have to consider a scenario where a cloud free pixel was shaded just before the satellite passes. Assuming a wind speed of 10 m/s a cloud can move about 1oo - 200 m during the above adaptation process. In the neighbourhood of a cloud windside pixels may be partly contaminated by this effect. However, pixels in the vicinity of a cloud should be excluded from interpretation of water colour anyhow.

References

Abbott,M.R., P.J.Richerson, T.M.Powell (1982): "In situ response of phytoplankton fluorescence to rapid variations in light", Limnol.Oceanogr., 27(2),, 218-225

Günther,K. (1984): "Die Abhängigkeit der in vivo Chlorophyll a Fluoreszenz marinen Phytoplanktons von der Globalstrahlung", Dissertation Universität Oldenburg

Kiefer,D.A. (1973): "Chlorophyll a fluorescence in marine centric diatoms: Responses of chloroplasts of light and nutrient stress" Mar. Biol. 23, 39-46

Rabbani,M.M. (1984): "Untersuchungen zum Fluoreszenz-wirkungsgrad des Phytoplanktons und der damit assoziierten morphologischen und physiologischen Adaptationsmechanismen", Dissertation Universität Kiel

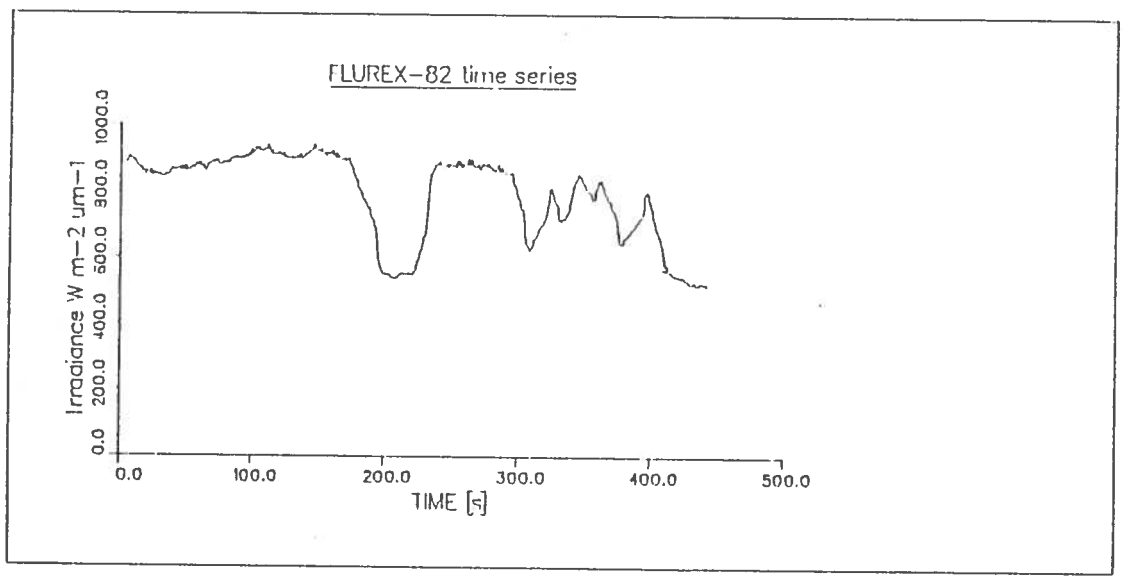

Fig.1 Time series of the downwelling irradiance at 445 nm

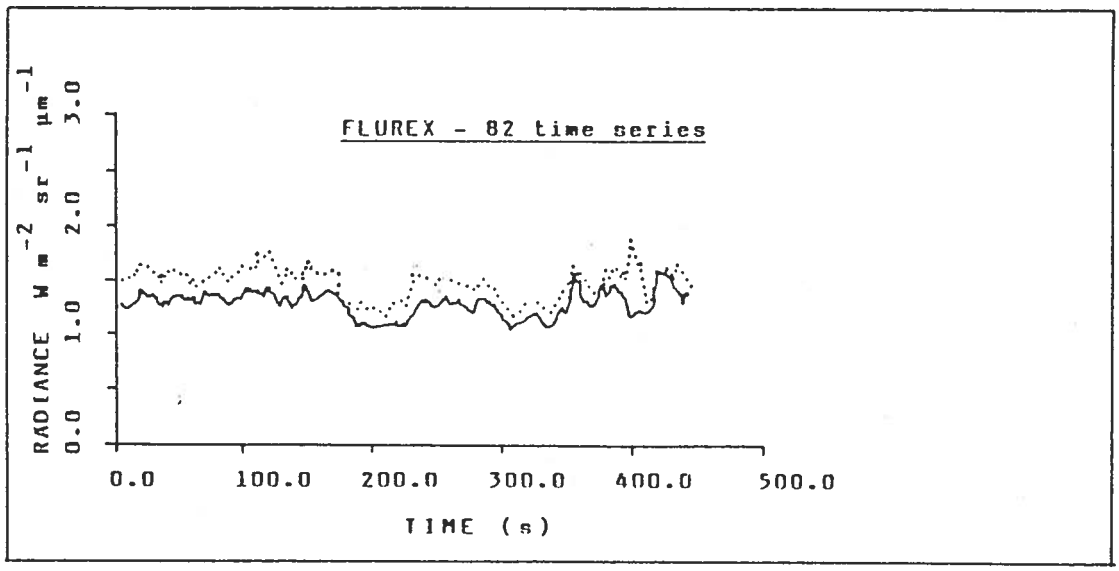

Fig.2 Time series of the water radiance at 645 nm and 685 nm measured 3 m above the surface
... L(645) ___ L(685)

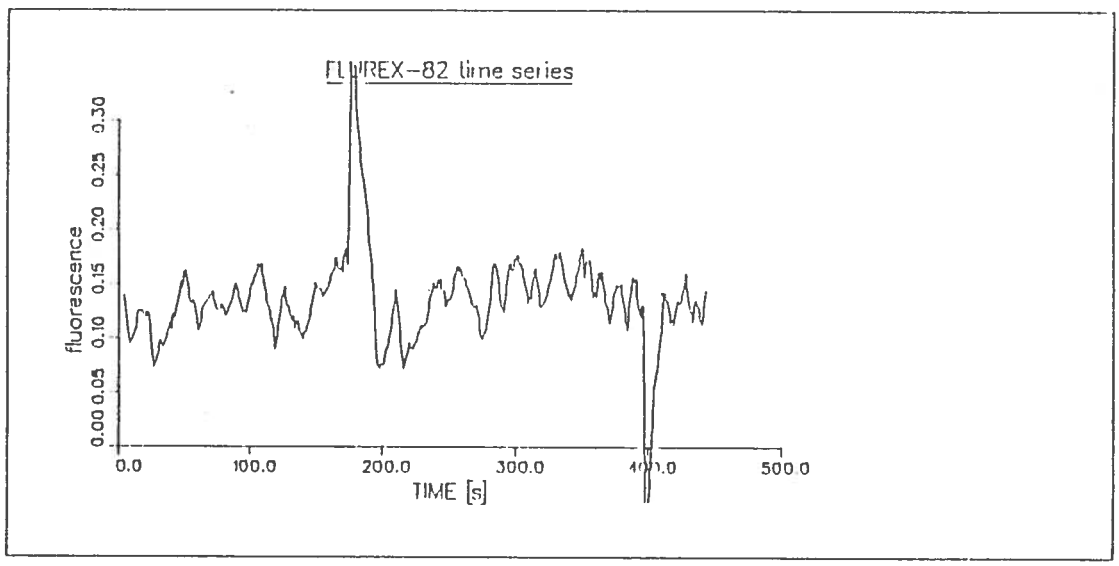

Fig.3 Time series of the fluorescence calculated as: L(685)/L(base) - 1

'86 Cospar Proceedings

THE ROLE OF PASSIVE OCEAN SPECTRAL FLUORESCENCE MEASUREMENTS IN SATELLITE DETERMINATIONS OF MARINE PRIMARY PRODUCTION

B.J. Topliss* and T.C. Platt**

*Atlantic Oceanographic Laboratory, **Marine Ecology Laboratory,
Department of Fisheries and Oceans, Bedford Institute of Oceanography,
P.O. Box 1006, Dartmouth, Nova Scotia, Canada B2Y 4A2

ABSTRACT

The detection of spectral fluorescence is a rapidly-growing tool for marine biologists interested in both phytoplankton biomass and species composition. The presence of solar stimulated fluorescence at 685 nm (associated with chlorophyll a) has been detected in data sets collected from areas as diverse as the high Arctic and the Caribbean Sea. Interpretation and modelling of passive fluorescence signals in terms of optical efficiencies is dependent on accurate estimates of specific absorption coefficients. This in turn requires an optical modelling of the associated water mass in a similar manner to that used in interpretation of remote sensing signals (such as from the CZCS - Coastal Zone Colour Scanner, or the planned OCI - Ocean Colour Imager). A potential relationship between passive chlorophyll fluorescence efficiency and photosynthetic efficiency of chlorophyll a is outlined for the field data and the relevance of such a relationship to future remote sensing signals such as from the FLI (Fluorescence Line Imager) is discussed.

INTRODUCTION

Most work in remote sensing of water colour is orientated towards producing pigment maps. However, the signal received by the CZCS (Coastal Zone Colour Scanner, /1/) is a function of the optical absorption and scattering caused not only by marine phytoplankton but also by other substances. The FLI (Fluorescence Line Imager /2/, is an alternative surface chlorophyll mapping device. In addition to being programmable for CZCS characteristics, it can also measure the electro-magnetic output of the biological photosystem in the form of chlorophyll fluorescence. If primary production could be estimated directly by electro-magnetic means, information collected at sea would be more directly comparable with contemporary optical remote sensing techniques. Photosynthesis is presently estimated either by measuring the assimilation of carbon /3/ or the evolution of oxygen /4/. Recently it has been demonstrated /5,6/ that the fluorescence emission of chlorophyll pigments at 685 nm can be detected throughout the water column in the upward irradiance in the ocean. The spectral absorption characteristics of phytoplankton can also be measured at sea /7,8/. The use of fluorescence emission, together with pigment absorption, is examined in this text for its potential to estimate biological productivity. Investigation of other fluorescence features is commented on and finally the possible implications of using passive fluorescence as a remote sensing tool are discussed.

FIELD MEASUREMENTS

Theory has attributed the existence of high apparent surface reflectance at the chlorophyll a emission wavelength to either fluorescence /9,10/ or to anomalous dispersion /11/. In situ optical data illustrating the passive fluorescence feature have, however, been relatively few. The optical measurements discussed in this text have all been made with a Techtum quantum irradiance meter capable of scanning from 400 to 750 nm. Chlorophyll fluorescence measurements presented in detail here were taken on a series of CSS Hudson Cruises throughout the Canadian Eastern Arctic (August/Sept. 1983) and on the Grand Banks off Newfoundland (April 1984). The spectral upward irradiance signal is only a few percent of the downward signal, such that at wavelengths greater than 600 nm the background upward light field below 10 m is very weak (approximately 0.06% of surface light for 650 nm at 20 m). This makes it easy to distinguish the enhanced 680 nm feature from any fluctuations in background caused by changes in surface intensity and sea state. The fluorescence feature has an approximate gaussian shape with a half-band width, after correction for the gaussian response of the instrument, of 24 nm $\pm$ 3 nm. The peak wavelength is 681 nm $\pm$ 6 nm and the peak height decays almost exponentially with depth. The absolute level of passive fluorescence has been shown /6/ to depend on the intensity of the incident radiation, the penetration depth of the excitation wavelength and the quantity of chlorophyll-like pigments throughout the water column. The above characteristics allow us to associate the enhanced feature with the fluorescence properties of chlorophyll a. This fluorescence feature has now also been observed on additional cruises of the CSS Hudson in

the Caribbean Sea and eastern U.S. seaboard (1984) and in the Gulf of Maine and open Atlantic waters (1985). The chlorophyll pigment range for which the feature has been detected (with the Techtum instrument) is from 0.08 to 30.0 mg chl *a* m^{-3}.

FLUORESCENCE AND PHOTOSYNTHESIS

Early theory /12/ suggested an inverse relationship between photosynthesis and fluorescence. The efficiency of photosynthesis was measured by carbon-14 experiments /13/ performed on samples taken at discrete depths on the Arctic (1983) and Grand Banks (1984) cruises. In the parameterization of the photosynthesis - light curves /13/ the initial slope, α, of the photosynthesis-light curve has been related to the quantum yield of photosynthesis and hence as an index of photosynthetic efficiency. Passive fluorescence efficiency has been calculated for an exact 1-D solution /10/ and 2-D solutions /11/. Simplified field calculations have also been presented /6,14/. In these field models, fluorescence efficiency, $\eta(z)$ is defined as the probability that the absorption of a photon at the excitation, λ_x, will produce a photon at an emission λ_m, at depth z. The fluorescence signal $F(\lambda_m, z)$ is quantified only at the maximum emission wavelength. Fluorescence efficiency can then be related to the measured fluorescence signal via the relationship /14/:

$$F(\lambda_m,z) = \frac{\eta(z)}{2} \frac{H(\lambda_x,z)\,(K_T(\lambda_x) - K_w(\lambda_x))}{(K_T(\lambda_x) + K_T(\lambda_m))} \qquad (1)$$

where: $H(\lambda_x,z)$ is the quantum irradiance (photons $m^{-2}s^{-1}$) incident at depth z on an optically thin layer of photoplankton pigments of concentration C (mg chla m^{-3}): K_T is the total attenuation coefficient at any wavelength and $K_w(\lambda_x)$ is the attenuation coefficient due to pure water.

For a medium in which chlorophyll pigments are the only absorbing material other than water, the total attenuation coefficient K_T at any wavelength can be partitioned so that:

$$K_T(\lambda) = K_C(\lambda)C + K_w(\lambda) \qquad (2)$$

where: $K_C(\lambda)$ is the specific attenuation coefficient for chlorophyll pigments. Partitioning is only strictly valid for inherent optical properties such as absorption /15/ but where the ratio of absorption to scattering is high the technique provides useful working models /8/. Use of a broad band estimate for attenuation $K_T(w,z)$ provides a first approximation for spectral variations in phytoplankton absorption /14/. Spectral attenuation data from the High Arctic and Grand Banks was consistent with a relationship,

$$K_C(441)C = 0.041 + 0.0186\,C \quad \text{and } r = 0.93 \qquad (3)$$

This is similar to the relationship /16/ found for productive waters off the west coast of Africa (coefficients 0.058 and 0.018 respectively). For the Arctic and Grand Banks data, figure 1 shows the relationship between photosynthetic efficiency, α, and fluorescence efficiency, η, to be approximately inverse. Since this is expected from first principles /12/, such a plot, even with large errors, appears extremely promising. Photosynthetic efficiency was examined for potential strong covariance with environmental variables such as temperature and percentage light level. As no strong covariance was found the hypothesis that the $\alpha - \eta$ relationship is purely an indirect statistical one is diminished. Most of the stations used had light values below the 10% light level, where photosynthesis could be considered to be light limited. Pigment concentrations were between 1 and 15 mg m^{-3} which together with the relationship given in equation (3) are characteristics of non-oligotrophic waters.

AUXILLARY PIGMENTS

Other pigments besides chlorophyll *a* are known to fluoresce. In particular, cyanobacteria (very small sized cells) carry the accessary pigment, phycoerythrin, whose fluorometric characteristics are fluorescence emission between 570 and 595 nm accompanied by weak fluorescence of chlorophyll *a* /17/. Whereas there are several species that fluoresce in the far 500 nm's, *Synechococcus* (emitting at approximately 585 nm) is currently considered to be the most abundant marine cyanobacterium /18/. Measuring the in-situ fluorescence of phycoerythrin has not been easy. Fluorescence signals /17/ appear to be extremely small even in surface waters where cyanobacteria is most abundant. Some explanations for the very poor detection /17/ have been offered, these include: relative fluorescent fluxes for phycoerythrin between 3 to 10 times less than that for chlorophyll; low cellular concentration of phycoerythrin in natural populations; fluorescence yields less than 1/2 that of chlorophyll; narrow excitation spectrum, approximately 30 nm as opposed to 100 nm for

chlorophyll; and higher background irradiance at 590 nm. In deep waters of the Caribbean, Open Atlantic and Gulf of Maine cruises additional signals were observed in the upward irradiance spectrum. The feature illustrated in Fig. 2 appeared only at the bottom of the photic zone and hence at low light levels. This was initially assumed to be due to the very high levels of background irradiance higher up in the water column.

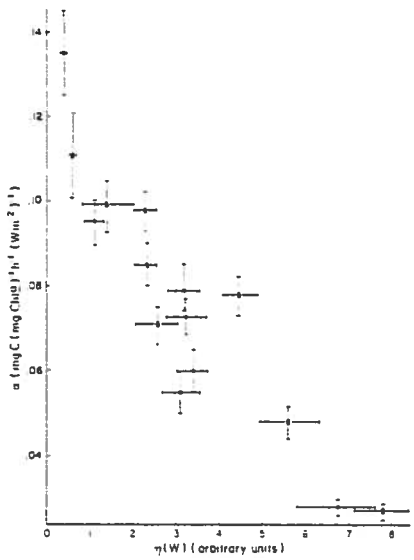

Fig. 1 Plot of photosynthetic efficiency, α, versus fluorescence efficiency η(w) using total energy. Error bars are one standard error. After /14/.

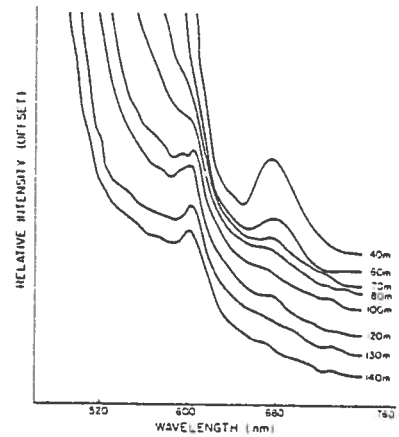

Fig. 2 Long wave length upward irradiance at station in the Caribbean Sea.

The features occurred close to 600 ± 10 nm with a half-band width (approximately 18 nm) close to that of the instrument's filter band-width (instrumentation error as a source of this feature was eliminated). Phycoerythrin was measured by flow cytometer techniques on the Caribbean cruise and was found to be abundant higher up in the water column (R. Olson personnel communication). Only very small or insignificant quantities were detected at the bottom or below the photic zone. All the occurrences of the feature illustrated in Figure 2 were characterized by becoming visible only when the chlorophyll a fluorescence signal was rapidly diminishing or was too weak to detect. The wavelength of emission detected was longer than might be expected from the cyanobacteria group. However, no comparative field data on auxillary pigments were available at these locations, so these features require further study. In particular, future optical-pigment studies might examine the occurrence of pigments at the bottom of the photic zone in conjunction with possible nitrogen transfer from deeper waters /19/.

DISCUSSION

Passive fluorescence efficiency calculated with a simple 1-D field model has given an inverse relationship with photosynthetic efficiency consistent with early theory. Theoretical considerations have also been outlined /20/ which indicate that photosynthetic efficiency can be used as a primary production index on a large scale. Together these provide the possibility of estimating marine primary productivity over the large spatial areas covered by remote sensing devices. However, chlorophyll a is not the only biological pigment to fluoresce and hence channel optical energy through the photosystem. The presence of accessory pigments will influence the use of chlorophyll a as an estimate of biomass and hence any indirect (statistical) estimate of productivity. For example, in open ocean areas cyanobacteria may account for up to half of primary production /21/ and are identified by the presence of pigments other than chlorophyll a. A fuller understanding of the channelling of optical energy by phytoplankton and photosynthetic bacteria requires utilizing full spectral information in both laboratory and remote sensing applications. Fluorescence from accessory pigments may become detectable via high-sensitivity or high-energy electro-magnetic/remote sensing multi-spectral techniques, but as yet such work is in its infancy and auxillary fluorescence signals observed in this study have not yet been firmly identified. A parallel study of active or stimulated fluorescence yield for the Arctic, Labrador and Sargasso Seas gave no coherent relationship with any of the P-I parameters /14/. Potential differences between active and passive fluorescence may become important for those remote sensing techniques that compare active (laser) and passive sensors for mapping biological pigments. The use of an optical estimate of the total

energy absorbed (inclusive of chlorophyll content) has the advantage of automatically accommodating any changes in the specific chloropnyll attenuation coefficient between species. Any optical method must, however, also accommodate different water masses. These water type problems are a major limitation on current bio-optical modelling techniques particularly as applied to remote sensing studies for ecological interpretation.

CONCLUSIONS

This study indicates that if bio-optical modelling can be successfully extended to all water types for ship and satellites alike, then not only biomass but productivity estimates may be directly obtainable. All the space-technology components for such methods are already available but the scientific components still require careful or further examination.

ACKNOWLEDGEMENTS

Thanks go to Drs. Miller, Olson, Li, Harrison, Horne and Lewis. Thanks for technical support go to B. Irwin and B. Hartling. Appreciation is expressed to the officers and crew of the CSS Hudson for their cooperation and patience. Thanks to Drs. Booth and Kiefer for providing information on phycoerythrin and chlorophyll fluorescence.

REFERENCES

1. Hovis, W.A., D.K. Clark, F. Anderson, R.W. Austin, W.H. Wilson, E.T. Baker, D. Ball, M.R. Gordon, J.L. Mueller, S.Z. El-Sayed, B. Sturn, R.C. Wrigley and C.S. Yentsch. Science 210, 60 (1980)

2. Gower J.F.R., G.A. Borstad and D. Tuax In: Proceedings of the 9th Canadian Symposium on Remote Sensing, pp. 145 (1985)

3. Steeman, Nielson, E. Journal du Conseil. Conseil Permanent International pour L'Exploration de la Mer 18, 117 (1952)

4. Strickland J.D.H. Fisheries Research Board of Canada Bulletin, 122,172 (1960)

5. Kishino M., S. Sugihara and N. Okami La Mer 22, 220 (1984)

6. Topliss, B.J. Oceanologica Acta 8, 263 (1985)

7. Morel A. and L. Prieur Limnology and Oceanography 22, 709 (1977)

8. Smith, R.C. and K.S. Baker Limnology and Oceanography 23, 260 (1978)

9. Gordon, H.R. Appl. Opt. 18, 8, 1161 (1979)

10. Kattawar, G.W. and J.C. Vastano Appl. Opt. 21, 14, 2489 (1982)

11. Gordon, H.R. J. Opt. Soc. Am. 64, 6, 773 (1974)

12. Butler W.L. In: Current topics in bioenergetics Vol. 1, D.R. Sanadi ed. Academic Press, New York. pp 49 (1966)

13. Platt, T. and A.D. Jassby Journal of Phycology 12, 421 (1976)

14. Topliss, B.J. and T. Platt Deep Sea Research 33, 849 (1986)

15. Morel A. and A. Bricaud Deep-Sea Research 28, 1375 (1981)

16. Prieur L. and S. Sathyendranath Limnology and Oceanography 26, 671 (1981)

17. Booth, C.R. and D.A. Kiefer NASA Final Report SBIR Phase I-84-1: 18-15-1315 (1985)

18. Waterbury, J.B., S.W. Watson, R.R.W. Guillard and L.E. Band, Nature, London, 277, 293 (1979)

19. Fogg, G.E. Proc. R. Soc. London, Series B, 228, 1 (1986)

20. Platt, T. Deep-Sea Research 33, 149 (1986)

21. Li, W.K.W., D.V. Subba Roa, W.G. Harrison, J.C. Smith, J.J. Cullen, B. Irwin, and T. Platt. Science 219, 292 (1983)

Talk Outline: **Trevor Platt**

Estimation of Primary Production by Remote Sensing

Remote sensors collect information per unit surface area of the ocean. Primary production per unit area depends, to the first order, on incident radiation and chloroplyll content of the water column. A simple model yields the result that the relevant photosynthesis characteristic is the initial slope of the photosynthesis-light curve. This parameter can be measured by routine radioactive tracer incubation measurements at sea. The model assumes (1) that photosynthesis is linear in available light (only true at low light, but the bias can be corrected as a function of a dimensionless property of the photosynthesis-light curve); (2) that the vertical distribution of phyloplankton pigments is uniform (detailed consequences of this assumption still to be calculated). This simple model proves to describe field data on water column photosynthesis very well.

Photosynthesis and fluorescence are complementary processes with respect to the photons absorbed. Thus for a given photon flux absorbed, fluorescence is likely to be low when relative photosynthesis is high, and vice versa. One might therefore expect an inverse correlation between relative fluorescence and relative photosynthesis. Using as an index of relative photosynthesis the initial slope of the photosynthesis-light curve (referred to above), we have indeed found such an inverse correlation with the normalised amplitude of the chlorophyll emission at 685 nm (detected in the submarine light field).

These observations lay the basis for a possible avenue to estimation of primary production from remote sensing. There are, however, several complications (wavelength dependence, photoadaptation and so on) to be addressed along the way.

ON THE USE OF THE SOLAR-STIMULATED FLUORESCENCE SIGNAL FROM CHLOROPHYLL A FOR AIRBORNE AND SATELLITE MAPPING OF PHYTOPLANKTON

J.F.R. Gower* and G.A. Borstad**

*Institute of Ocean Sciences, P.O. Box 6000, Sidney, B.C., V8L 4B2, Canada **Borstad Associates Ltd, #100, 9865 West Saanich Rd, Sidney, B.C., V8L 3S1, Canada

ABSTRACT

Since our early measurements of the solar-stimulated fluorescence signal from chlorophyll a in airborne, water color surveys along the British Columbia coast, we have applied the technique in a number of areas, including the waters of the Canadian arctic and Europe, and further evaluated its potential and problems. The results show that mapping using the fluorescence signal has definite operational advantages, and can enhance the accuracy of airborne chlorophyll surveys made using the more conventional broad-band green/blue signals. Also, measurement of the fluorescence may allow better estimation of primary productivity rates.

To produce similar data over large areas, observations of chlorophyll fluorescence from high altitudes or from space, are required. This sets stringent demands on design of a suitable sensor. This paper will discuss the implications of the various airborne and in-water results, and show examples of the data recently acquired from the "Fluorescence Line Imager", an imaging spectrometer designed specifically for this type of chlorophyll mapping from high altitudes.

INTRODUCTION

In 1974 the Institute of Ocean Sciences (IOS) took delivery of a custom designed silicon diode array, multichannel spectrometer, (the "IOS spectrometer") which digitally records the intensities of light dispersed onto the 256 elements of a Reticon photodiode array. This was incorporated into a airborne observing package, designed to view the water surface through a polarizer at the Brewster angle, so as to reduce surface reflected light and make observations possible when flying under cloud. The instrument is calibrated between flights with a white card in sunlight, and produces spectra of reflectance factors (L_u^+/E_d^+), which should equal the irradiance reflectance multiplied by a constant factor of about 0.6.

In the first test observations in April 1975 /1/, a small increase in reflectance was observed, centered at a wavelength of 685 nm and with a width of about 25 nm, easily resolved by our spectrometer resolution of 14 nm. The amplitude of the peak showed a good correlation with the near surface chlorophyll concentration. On the basis of this proportionality, and the peak's position and width, it was ascribed to fluorescence of chlorophyll a stimulated by ambient (sun and sky) light. The signal was reported at about the same time in under-water measurements /2/.

It had earlier been suggested that a combination of chlorophyll absorption at 670 nm, with reflectance and water absorption at longer wavelengths could explain such a peak. However accumulated evidence now supports the fluorescence interpretation.

Figure 1 shows two reflectance spectra taken 3 minutes apart with the IOS spectrometer, from a ship in the Baltic. Most of the change is in the height of the increase at 685nm. This type of variation is consistent with the fluorescence interpretation and seems to indicate a change in fluorescence efficiency. Accurate measurement of such a difference spectrum also gives a precise position and width of the line.

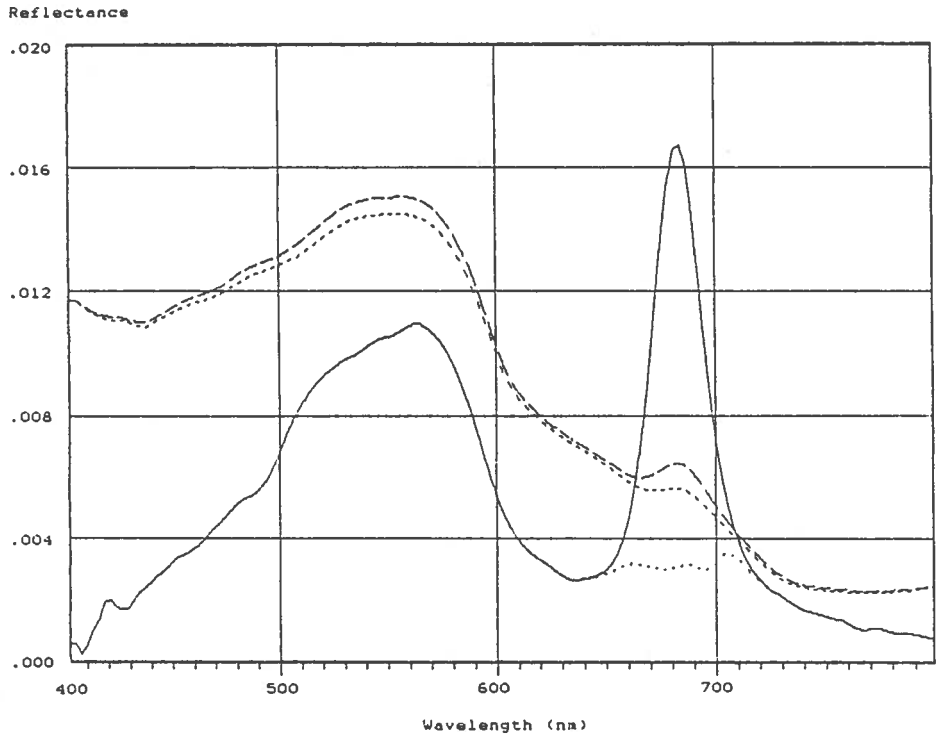

Fig. 1. A reflectance increase (solid curve, at 20 times scale) observed from the deck of a ship, between spectra (dashed lines) taken at two locations roughly 300 m apart. The dotted line is the residual after subtracting a Gaussian line shape centered at 683.5 nm and 24 nm wide at half height.

OBSERVATIONS OF NATURALLY STIMULATED CHLOROPHYLL FLUORESCENCE

Observations of this fluorescence can be applied to remote sensing surveys of near surface phytoplankton. Such surveys are usually based on radiance or reflectance measurements at blue and green wavelengths, to monitor the effects of chlorophyll absorption and associated backscatter in phytoplankton. Surveys based on passive fluorescence can take advantage of the relatively narrow bandwidth of the fluorescence line and its position at the red end of the spectrum, where atmospheric radiance is low.

Disadvantages would be expected from the relatively low signal available, and the varying fluorescence efficiency of different phytoplankton species in different physiological states. Nonetheless, initial experience in relatively large scale surveys have been undertaken with the IOS spectrometer, for example in the eastern Canadian arctic in August 1979 [3], and have given successful results.

The fluorescence and green to blue ratio methods of chlorophyll mapping can be compared by analyzing observed or modeled spectra using characteristic vector, or factor analysis. This derives the (relatively few) additive component spectra that contribute significantly to the total variance over different spectral ranges [4,5,6]. The corresponding chlorophyll measurements can then be fitted by combinations of these components, with the goodness of the fit indicating the value of the spectral range for chlorophyll sensing. In two studies, [5,6], observed and model data for coastal water were found to indicate a better fit using fluorescence data.

Since the fluorescence signal has a linear response to chlorophyll (except where high concentrations of absorbing material are present), and gives a specific narrow spectral signature, it could be expected to give improved measurements in coastal or "case 2" waters where concentrations are high (.5 $mg.m^{-3}$ and above), and other suspended or dissolved material can influence the optical water properties, especially at shorter wavelengths.

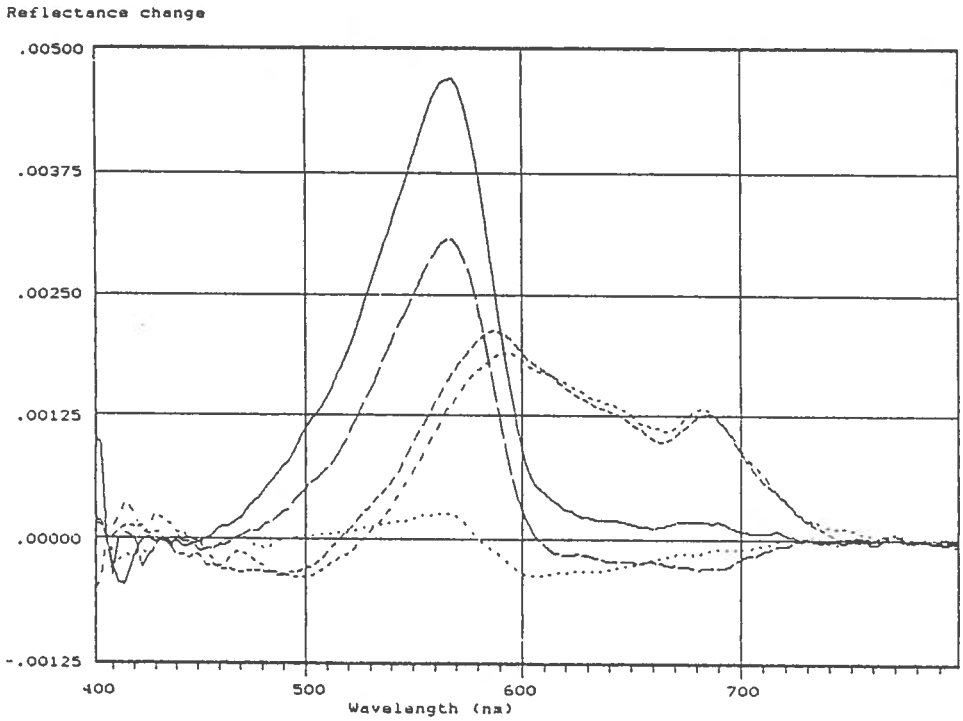

Fig. 2. The spectral form of the reflectance increase for water 5 meters (solid line), 7 meters (long dashes), and 11 meters deep (dots), and at two points where the fluorescence signal was observed to increase (medium dashes).

For lower chlorophyll concentrations in less complicated, "case 1", off-shore water, the green to blue ratio, with its sensitivity for concentrations down to .02 mg.m^{-3}, should give improved results.

A further advantage of the fluorescence technique was observed in airborne observations in the Baltic, where variations in apparent water reflectance were caused by a contribution from the sea bottom, or from near-bottom re-suspended material.

Increases in spectral reflectance observed in a region with shallow water and patches of high chlorophyll, relative to nearby relatively clear, deep water, are shown in figure 2. The increases evidently fall into two types: those due to bottom reflectance, between 500 and 600 nm where the diffuse attenuation coefficient of the water is minimum, but giving no change in fluorescence signal, and those due to near-surface phytoplankton showing a broader peak, with fluorescence emission at 685 nm.

In these shallow waters the increase between 500 and 600 nm causes a corresponding rise in the green to blue ratio. The fluorescence signal was relatively unaffected, because of the limited depth penetration of the fluorescent emission.

VARIATIONS IN APPARENT FLUORESCENCE EFFICIENCY

Apparent variations in fluorescence efficiency (output per unit chlorophyll) occur when comparing the slopes of the plots of fluorescence versus measured near-surface chlorophyll for a variety of surveys undertaken with the IOS spectrometer system for which sufficient comparison data is available. Figure 3 shows the slopes of the best fit lines on a linear scale, over the indicated chlorophyll ranges on 9 different occasions from 1975 to 1982, all but one (i) in western Canada coastal waters.

The lines in figure 3 represent close correlations (r^2 0.8 to 0.9), both for areas of order 100 Km on a single day, and, at a single point, during a day and for periods of up to 10 days.

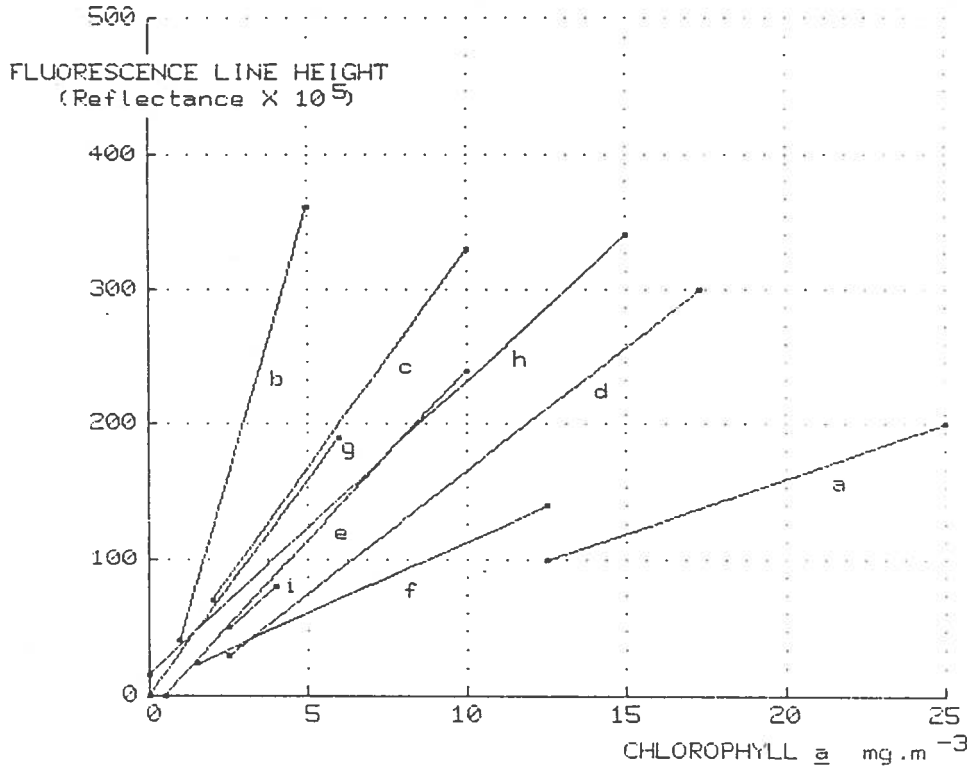

Fig. 3. Mean relations between fluorescence and chlorophyll concentration observed on 9 occasions.

It can be seen in figure 3 that with the exception of (a), (b) and (f), the lines have slopes in the range 17 X 10^{-5} to 33 X 10^{-5} of reflectance increase per mg.m^{-3} chlorophyll a. Results from the Canadian arctic /3/ also suggest a mean relation with a slope of about 20 X 10^{-5} in these units. It would be tempting to ascribe the slopes of lines (a) and (b), derived from the first observations in 1975 and 1976 respectively, to poor calibration of the early measurements. However all sequences of spectra show roughly the same range of water reflectances.

In summary figure 3 shows a mean fluorescence output proportional to chlorophyll a, equal to 24 X 10^{-5} of reflectance per mg.m-3 of chlorophyll a, and with an rms variation by a factor of 1.8 on either side of this value. If cases (a) and (b) are excluded then the rms variation is by a factor of 1.3.

Variations in fluorescence efficiency over at least a 4:1 range are observed from fluorometer results (e.g./7/). However, these observations make use of stimulating light that differs in intensity and spectrum from natural illumination. They also represent a range of depths, light intensities and of sample treatments, so they may not be directly comparable to the variations shown here.

THE FLI INSTRUMENT FOR FLUORESCENCE IMAGING

Successful work on fluorescence measurements has spurred the development of an imaging spectrometer capable of mapping the spatial distribution of fluorescence emission from sea water. The instrument is named the Fluorescence Line Imager (FLI) /8/. It was designed as an airborne prototype for a satellite instrument, with the same spatial resolution as the CZCS or its airborne equivalents (about 2000 pixels over a 70 degree swath, equivalent to 1 Km resolution from orbit), and covering the spectral range 430 to 805 nm, with 2.5 nm resolution.

The FLI can operate in two modes. In imaging mode it acts as a push-broom scanner with about 1900 pixels per line, and with band spectral properties (positions and widths) under computer control in steps of 1.3 nm. In spectral mode it acts as 40 spectrometers providing low spatial resolution imagery in 288 bands.

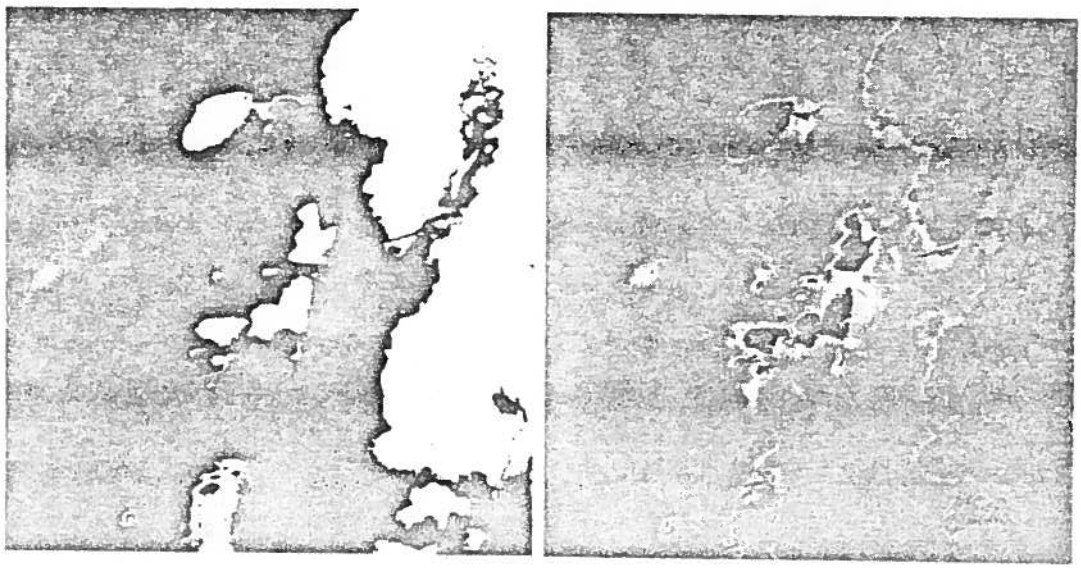

Fig. 4. FLI output in imaging mode. Left: A coastal region of eastern Canada imaged in a band from 500 to 580 nm, chosen to maximize water penetration in this geographic area. Right: A difference image designed to maximized bottom reflectance changes.

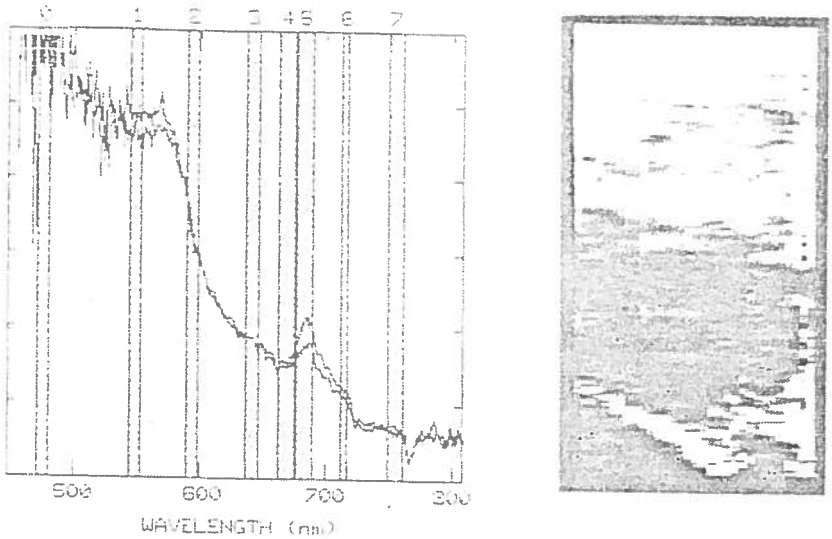

Fig. 5. FLI output in spectral mode.
(a. left) Radiance spectra observed with the FLI imaging spectrometer in a region of changing chlorophyll, and one of the spectral band configurations (shaded columns) designed to avoid oxygen and water vapor absorption features, and to detect fluorescence and shorter wavelength effects from sea water.
(b. right) A low resolution (spectral mode) image showing the distribution of chlorophyll fluorescence around the C.S.S. Hudson off the Canadian east coast in July 1985. The ship and its wake appear on the bottom of the image.

Figure 4 shows images from the FLI in imaging mode. Although no high resolution images of chlorophyll fluorescence distribution have yet been produced with the FLI, its band selection capabilities have already been found useful in a number of other studies, here, the mapping of benthic algae.

In spectral mode, changes in fluorescence have been successfully mapped. Figure 5(a) shows water radiance spectra, indicating a change in the line height at 685 nm. The shaded bands selected for high resolution imaging show that this mode would have mapped this change. Unfortunately, no such data has yet been processed. However, figure 5(b) shows how the spectral mode data can be used to produce a low spatial resolution image of the fluorescent emission. Spectra in figure 5(a) were selected from the upper and lower halves of figure 5(b).

The instrument has been flown in a number of exercises. Over water it is being applied for many purposes in addition to fluorescence imaging, such as coastal water bathymetry, and aquatic vegetation surveys. It also finds many applications over land, particularly in mapping leaf chlorophyll reflectance changes in response to plant stress.

CONCLUSIONS

Mapping of the naturally stimulated fluorescence from chlorophyll a is a useful remote sensing technique, both alone and as an adjunct to measurements of absorption and scattering effects, using the green to blue ratio, especially in coastal waters. Recent developments in two dimensional array image sensors make feasible the sensitivity and spectral resolution required of a satellite sensor capable of providing both types of data.

An important goal of satellite water color mapping is the measurement of primary productivity. This is known to vary with the fluorescence efficiency of the phytoplankton /9/, suggesting an important application of this type of optical remote sensing.

REFERENCES

1. Neville, R.A., and J.F.R Gower, 1977, "Passive remote sensing of phytoplankton via chlorophyll a fluorescence", J. Geophys. Res. 82, 3487-3493.

2. Morel, A. and L. Prieur, 1977, "Analysis of variations in ocean color", Limnol. Oceanog., 22, 709-722.

3. Borstad, G A., and J.F.R. Gower, 1984, "Phytoplankton chlorophyll distribution in the eastern Canadian Arctic", Arctic, 37, 224-235

4. Doerffer, R., 1981, "Factor analysis in ocean color interpretation", in Oceanography from Space, J.F.R. Gower, (Ed), Plenum, New York, pp339-345.

5. Gower, J.F.R., S. Lin and G.A. Borstad, 1984, "The information content of different spectral ranges for remote chlorophyll estimation in coastal waters", Int. J. Remote Sensing, 5, 349-364.

6. Fischer, J., R. Doerffer and H. Grassl, 1986, "Factor analysis of multispectral radiances over coastal and open ocean water based on radiative transfer calculations", Applied Optics, 25, 448-456

7. Kiefer, D.A., 1973, "Fluorescence properties of natural phytoplankton populations", Marine Biology, 22, 263-269.

8. Borstad, G.A., H.R. Edel, J.F.R. Gower, and A.B. Hollinger, 1985, "Analysis of test and flight data from the Fluorescence Line Imager", Canadian Special Publication of Fisheries and Aquatic Sciences, 83, 38pp.

9. Topliss, B.J. and T. Platt, 1986, "Passive fluorescence and photosynthesis in the ocean: implications for remote sensing", Deep Sea Research, 33, 849-864.

Joint Canadian / German Workshop on High Spectral Resolution
Imaging for Land and Ocean Remote Sensing

Ottawa, 14 - 17 October 1986

AIRBORNE REMOTE SENSING OF CHLOROPHYLL FLUORESCENCE IN THE NORTH SEA AND BALTIC SEA

V. Amann *
R. Doerffer **
J.F.R. Gower ***
H.H. Kim ****
H. van der Piepen *

* Institut für Optoelektronik, DFVLR, Oberpfaffenhofen, FRG
** Institut für Physik, GKSS, Geesthacht, FRG
*** Institute for Ocean Science, DFO, Sidney, B.C., Canada
**** Goddard Space Flight Center, Greenbelt, MD 20771, U.S.A.

CONTENTS

List of Illustrations iv

List of Tables v

1. Introduction 1

2. Fladenground Experiment (FLEX) 2

2.1 General 2
2.2 Data processing 3
2.3 Data analysis 4
2.3.1 Chlorophyll concentrations derived from color ratios 4
2.3.2 Chlorophyll concentrations derived from fluorescence 5
2.3.3 Factor analysis 6
2.3.4 Temporal development of the bloom 9

3. Ocean Color Scanner Experiment German Bight (OCEG) 12

3.1 Introduction 12
3.2 Spectral signature analysis 12
3.3 Comparison of fluorescence and absorption data 18
3.4 Mapping of fluorescence 21

4. Fluorescence Experiment (FLUREX) 23

4.1 Introduction 23
4.2 Environmental conditions 24
4.3 Analysis of IOSS data 25
4.3.1 Data processing 25
4.3.2 Results 25
4.4 Analysis of SCR data 28
4.4.1 Data processing 29
4.4.2 Influence of the flight altitude 29
4.4.3 Correlation of airborne data with sea truth . 30
4.4.4 Temporal and spatial variability 33

5. Conclusions 37

6. Literature 39

7. Acronyms 42

8. Instrument specifications 44

8.1.1 Eighteen Channel Radiometer (GKSS) 44
8.1.2 Ocean Color Scanner (NASA) 44
8.1.3 IOS Spectrometer (DFO) 44
8.1.4 Six Channel Radiometer (DFVLR) 46

1. INTRODUCTION

The phenomena associated with the natural (sun-stimulated) fluorescence of chlorophyll-a in water have been investigated under a variety of environmental conditions in several experiments involving shipborne, airborne and platform-based observation techniques. In this study relevant data from the North Sea and the Baltic Sea have been analyzed in an attempt to answer the following questions:

- Is it possible to detect a meaningful fluorescence signal by means of special airborne radiometers and scanners?
- How does the fluorescence signal change with increasing aircraft altitude?
- How does the fluorescence signal change with different illumination conditions?
- How does the fluorescence signal change with the pigment concentration?
- What is the correlation between the color ratios and the fluorescence signal?
- Is it possible to map the near-surface chlorophyll concentration by means of the fluorescence in different types of water?

In order to answer these questions, data from the
- Fladenground Experiment (FLEX)
- Ocean Color Scanner Experiment German Bight (OCEG)
- Fluorescence Experiment (FLUREX)

were used, especially aircraft measurements and biochemical measurements from ships and platforms (ground truth) in an attempt to prove the applicability of the fluorescence method. The observation techniques, the specific environmental conditions, the data processing and the results of the data analysis are discussed in the following sections.

2. FLADENGROUND EXPERIMENT (FLEX)

2.1 General

Within the context of an international experiment in 1976, the spring plankton bloom in the northern section of the North Sea was investigated by means of combined aircraft and ship measurements [Amann and Doerffer, 1983]
The *general* objective of the experiment was to monitor and to analyse the physical, chemical and biochemical processes which determine the temporal development of the spring plankton bloom. For this purpose it was necessary to map the area of interest, a square with 100 km lenghth as shown in Figure 1, every few days in regard to SST and chlorophyll concentrations by means of an aircraft. (For instrument specifications refer to section 9.)

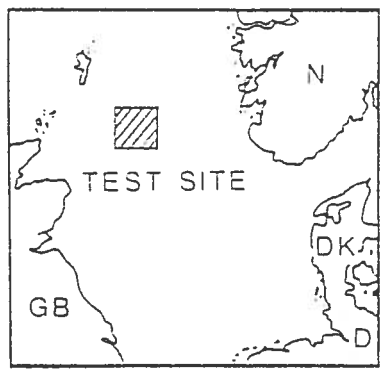

Figure 1. Test area in the North Sea during FLEX 76.

The more *specific* tasks in regard to fluorescence in this experiment were the detectibilty of the relevant signal from aircraft through a bloom cycle, the comparison with color ratio measurements and the correlation with sea truth in case I water [Gordon and Morel, 1983].

2.2 Data processing

The signal measured by the aircraft, the upwelling radiance $L(\lambda)_u$ consists essentially of the radiance backscattered by the water body, $L(\lambda)_W$, the radiance reflected at the water surface, $L(\lambda)_S$ and the radiance scattered by air molecules and aerosols, $L(\lambda)_R + L(\lambda)_A$. For the evaluation of the airborne radiometer data by means of the blue/green color ratio, the complex processes can be reduced to the following relationship:

$$L(\lambda)_u = L(\lambda)_W + L(\lambda)_S + L(\lambda)_R + L(\lambda)_A.$$

The first step in the evaluation of the radiometer data thus consists of the computation or estimate of $L(\lambda)_S$ and $L(\lambda)_R + L(\lambda)_A$.

For the correction of the surface reflection, the spectral radiance of the sky had to be determined. In case of a clear sky, the off-zenith fraction of the sky radiance (corresponding to the tilt of the instrument by 20 $^{\circ}$ away from the sun) was estimated from the relevant literature and, under the assumption of 2 % reflectivity, subtracted from $L(\lambda)$. In case of an overcast sky, a fraction of the downwelling irradiance as measured at the top of the aircraft was used directly as an input for the 2 % reflectivity.

So as to correct for the backscattering of the atmosphere, overflights at different altitudes above the same ship position. were performed. From these vertical profiles the values of $L(\lambda)_R$ and $L(\lambda)_A$ were determined through an extrapolation to zero altitude. The derived corrections were applied to the entire test area under the assumption of a homogeneous atmosphere.

Data for the evaluation of the fluorescence were not radiometrically corrected because it was assumed, that the contribution of the atmosphere is negligable in the red part of the spectrum at this altitude.

2.3 Data analysis

2.3.1 Chlorophyll concentrations derived from color ratios

The chlorophyll concentration was calculated from the color shift of the radiance values $L(\lambda)_W$.
However, so as to compensate for the changing illumination conditions, the water-leaving reflectance $R(\lambda)_W$ was calculated by referring the upwelling radiance to the downwelling irradiance $E(\lambda)$ as described above. Then the color shift was derived from the ratio L_{560}/L_{445} and calibrated in terms of an absolute concentration by means of water samples collected by the ship. The relationship between the chlorophyll concentration and the green/blue ratio is shown in Figure 2.

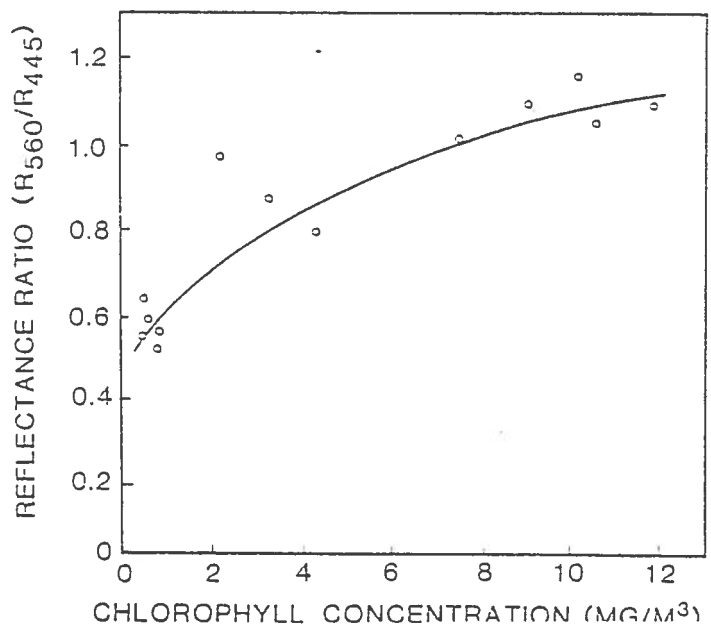

Figure 2. Comparison of the blue/green ratio with the in-situ chlorophyll concentration.

2.3.2 Chlorophyll concentrations derived from fluorescence

Alternatively the natural fluorescence at 685 nm was used so as to determine the chlorophyll concentration. For this purpose the relative fluorescence signal was calculated from the relationship

$$\text{Fluorescence Signal (FS)} = L_{W(685)} - (L_{W(645)} + L_{W(724)})/2 \ .$$

(Compare also the similar processing of IOS Spectrometer data in section 4.3.1) The linear relationship between the fluorescence and the chlorophyll concentration in 2 m water depth is shown in Figure 3.

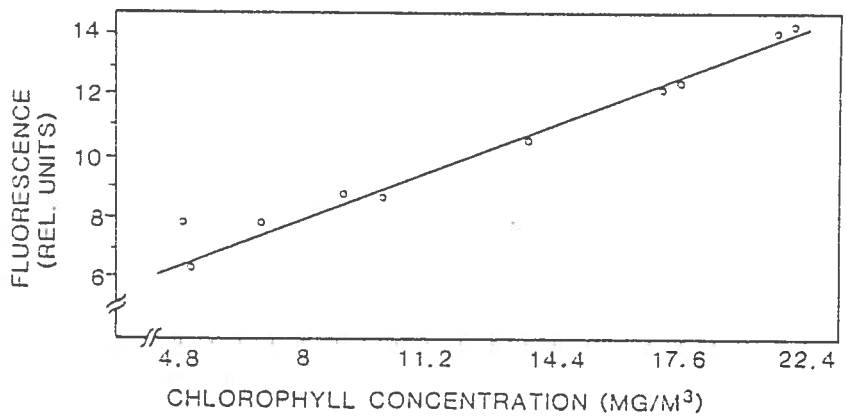

Figure 3. Comparison of the fluorescence with the in-situ chlorophyll concentration. (Correlation coefficient $r = 0{,}98$, $\alpha \leq 1\ \%$).

For this analysis, data along a 90 km profile were compared. (Water samples along the profile were collected by the British R/V Cirolana, while the fluorescence measurements were performed with the 18 channel radiometer, ECR (GKSS) from a flight altitude of 600 m.) By means of the above-mentioned calibration, a chlorophyll distribution map was finally calculated by interpolating between individual flight tracks (Figure 4 on page 6).

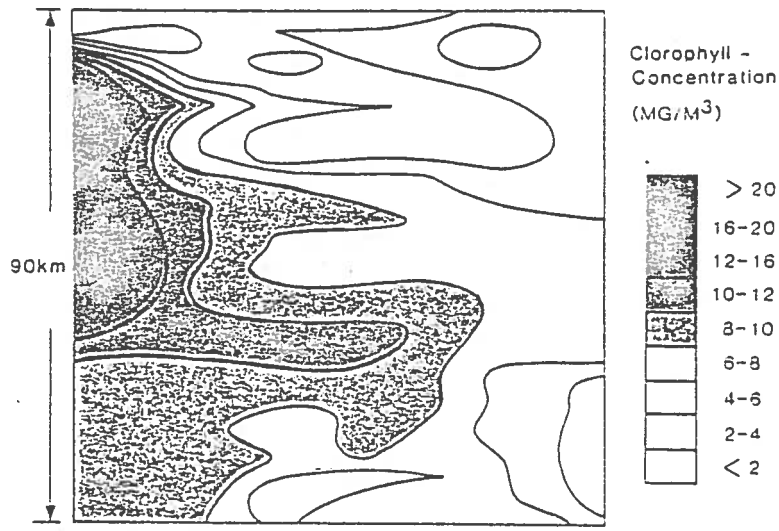

Figure 4. Chlorophyll distribution map within the FLEX box derived from airborne fluorescence measurements (5 May 1976).

2.3.3 Factor analysis

The type of factor analysis used here is described in Uberla 1971, Comrey 1973 and Cooley and Lohnes 1971.
The first step in extracting the useful information from the spectra with m spectral channels is the eigenvalue analysis [Mueller, 1973]. Figure 5 on page 7 shows the eigenvalues of 16 principal components from a 30 km profile in the FLEX area. It can clearly be seen that two components can be separated while all others represent noise. An additional low-pass filtering of the data enhances this separation.
Figure 6 on page 7 shows the two extracted factors after orthogonal rotation [Kaiser, 1958] and their correlation (factor loadings) with 16 spectral channels. The dominating factor 1 shows 2 maxima: a negative correlation in the blue part of the spectrum around 470 nm and a positive correlation at 685 nm, corresponding to the fluorescence peak of chlorophyll-a.
Due to these properties, this factor may be interpreted as phytoplankton. Factor 2 shows an increasing positive correlation towards the red part of the spectrum which may be due

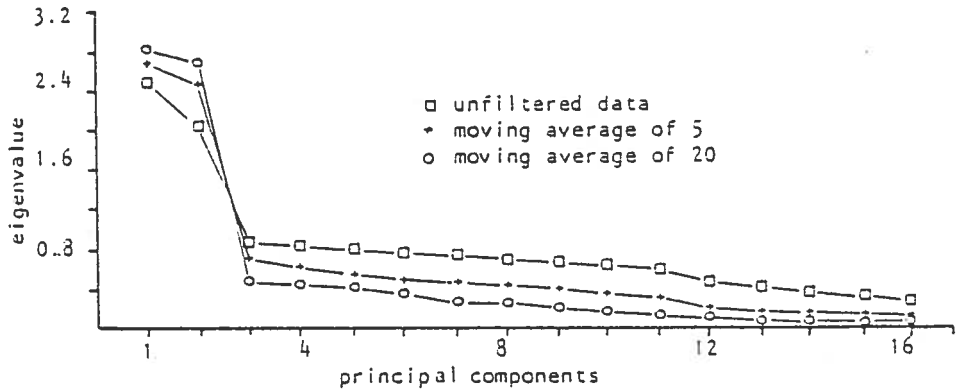

Figure 5. Eigenvalues of the principal components in order of their variance.

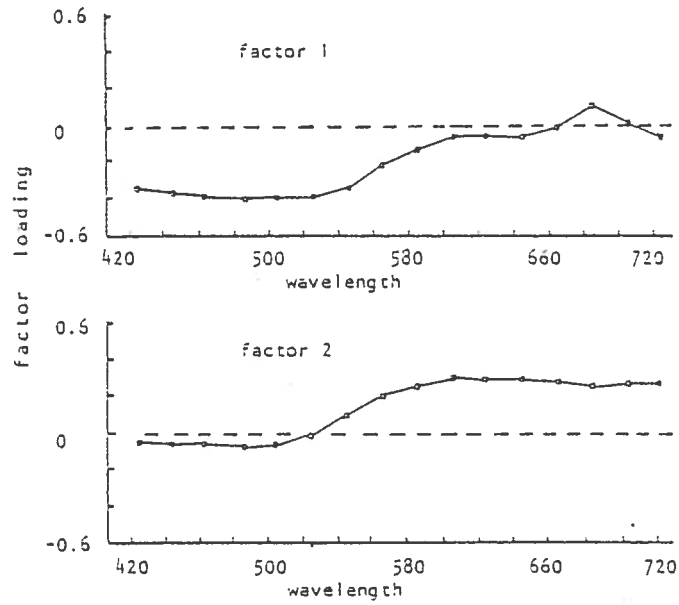

Figure 6. Correlation between the 2 factors and the spectral channels.

to the scattering particles in the water. Therefore this factor can be interpreted as suspended matter.
The values of the factors (factor scores) calculated for each single spectrum along the flight profile are shown in Figure 7 on page 8 (graph a) and Figure 8 on page 9 (graph a). The shape of the two profiles shows that the two factors are independent.

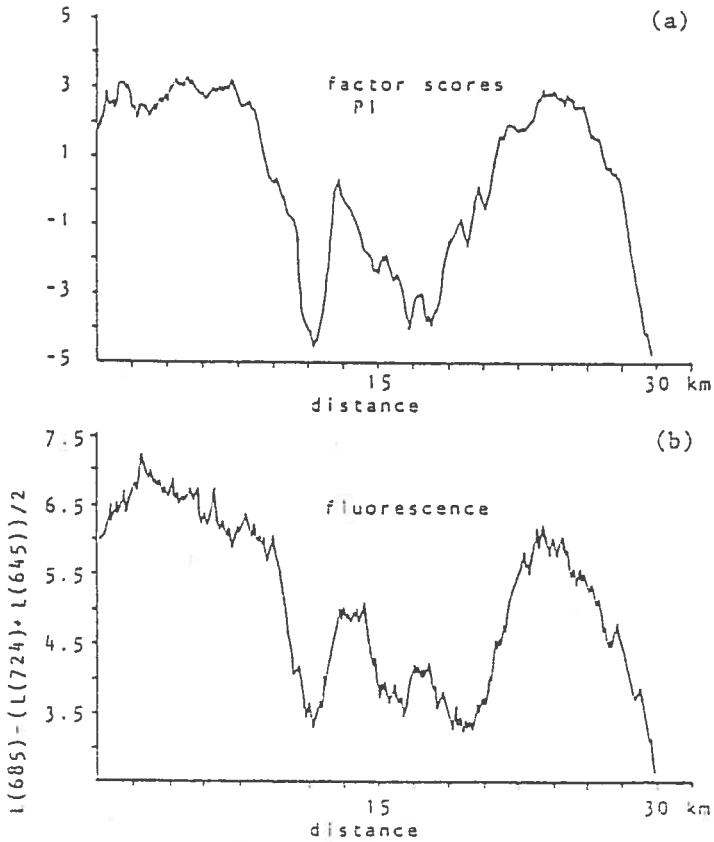

Figure 7. Comparison of the factor values with the fluorescence algorithm.

Finally the factor scores profile of factor 1 was compared with the same profile evaluated by using the fluorescence signal obtained in the way as described before (Figure 7 on page 8 graph b). Similarily the factor scores profile of factor 2 was compared with the blue/green ratio (Figure 8 on page 9, graph b).

These results show that the information content of the spectra as derived by the factor analysis co-varies very well with the fluorescence signal as derived by the FLH analysis.

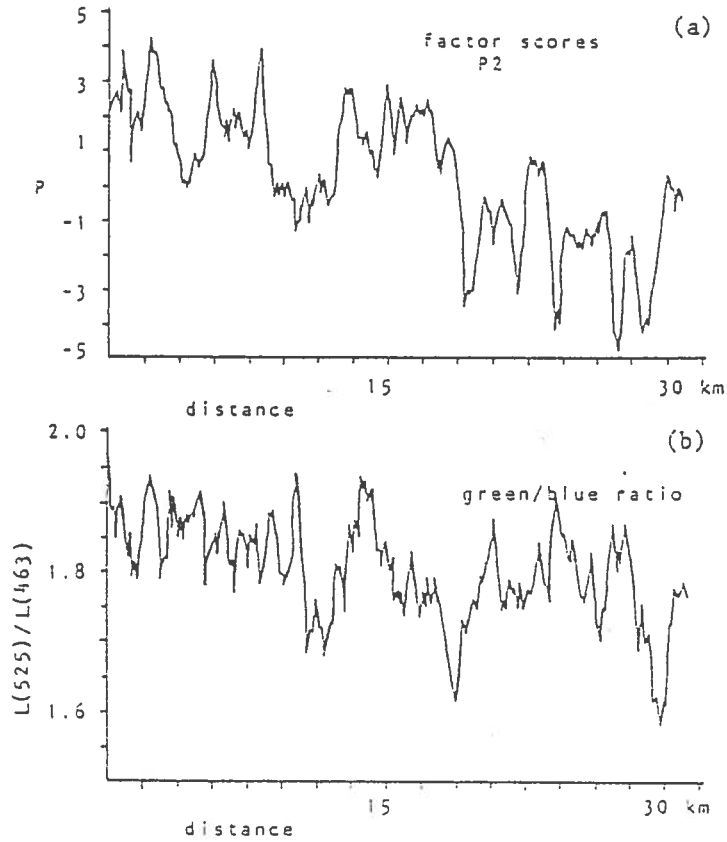

Figure 8. Comparison of the values of factor 2 with the green/blue ratio.

2.3.4 Temporal development of the bloom

The temporal development of the plankton bloom was monitored by means of both, the green/blue ratio and the sea surface temperature. Figure 9 on page 11 indicates the development through the different phases in a comparison between airborne and shipborne measurements. The upper part of Figure 9 shows the temporal development of the sea surface temperature (solid lines=shipborne measurements, dots=airborne measurements) and the formation and final shift of the thermocline. (The vertical bars indicate the range of the SST in the test area.)
The lower part of Figure 9 shows the corresponding development of the plankton bloom during the same period (solid line = shipborne measurements, dots = airborne measurements). The

vertical bars indicate the range of the chlorophyll concentration in the test area.
It can be seen that the airborne measurememnts of the color ratio above the central ship position correlate very well with the shipborne measurements. The overall chlorophyll distribution along the flight profiles shows a strong variability during the growing phase of the bloom (end of April).
This experiment also pinpoints the importance of airborne monitoring so as to extrapolate from ship measurements into a larger area but also to verify single ship measurements in cases of a strong patchiness. Thus it is possible to obtain a synoptic view from a test site which cannot be obtained by ship measurements alone especially in cases of a strong spatial and temporal variability.

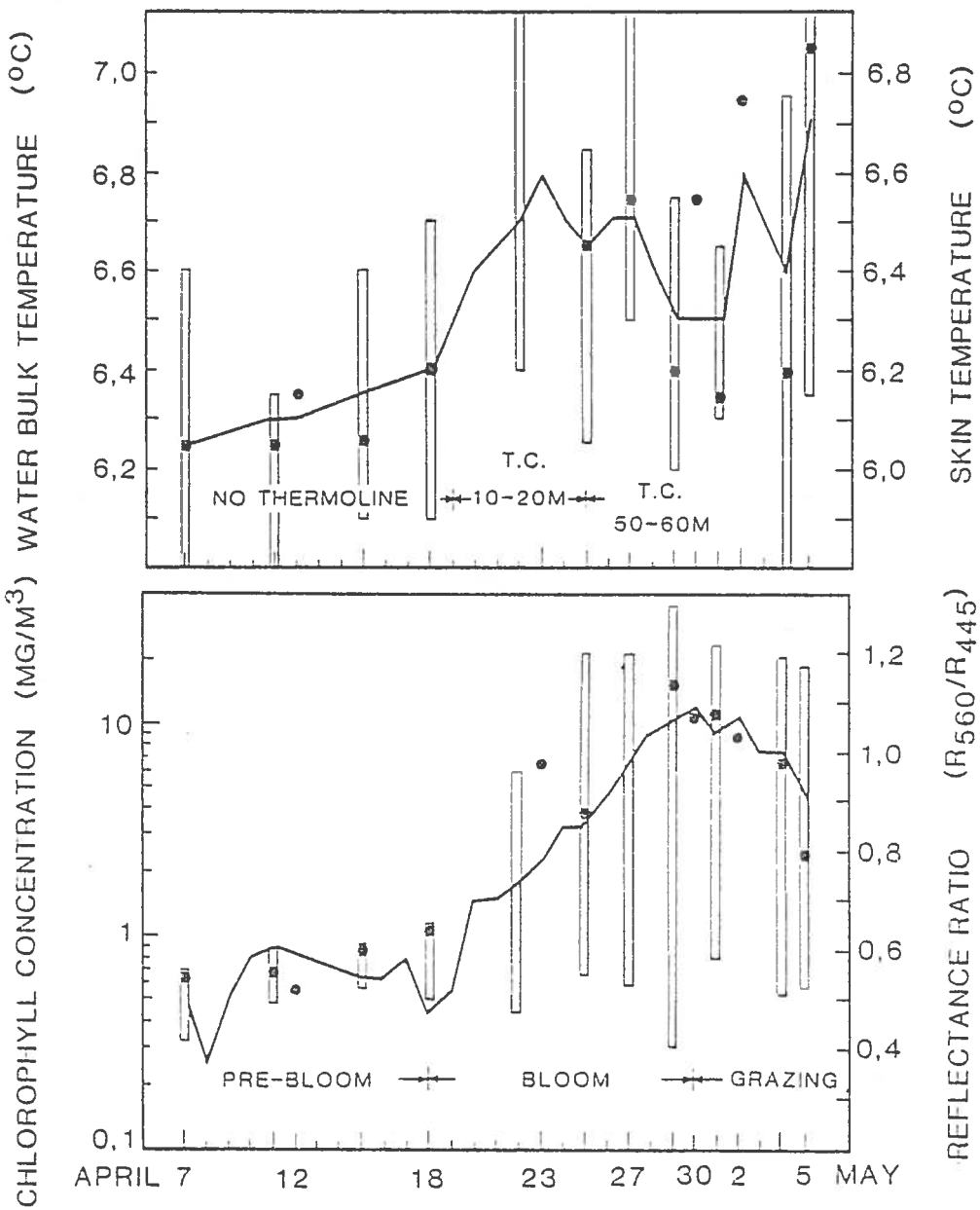

Figure 9. Temporal development of the plankton bloom during a period of two weeks. The upper part shows the development of the sea surface temperature (SST), while the lower part shows the corresponding development of the plankton in terms of chlorophyll concentration. (Solid lines correspond to ship measurements, while dots indicate the corresponding airborne measurements. The vertical bars indicate the range in the test area.)

3. OCEAN COLOR SCANNER EXPERIMENT GERMAN BIGHT (OCEG)

3.1 Introduction

As part of the scientific cooperation with NASA in conjunction with the OSTA-I/OCE mission, the Ocean Color Scanner (OCS) on loan from NASA Goddard Space Flight Center was flown together with other instruments above the Elbe estuary during the summer 1981 (OCEG). The flight tracks and the position of the R/V Monitor (B in flight track 7 in Figure 10 on page 13), which was anchored in the middle of the river near Cuxhaven.
While the more *general* objective of this experiment was the preparation for the underflight of the OSTA-I mission, [van der Piepen et al, 1983], the *specific* objectives in regard to the chlorophyll fluorescence were to investigate the latter effect in extreme turbid waters (case II) containing large amounts of yellow substance and suspended matter, to study the atmospheric effects from different flight altitudes, and finally to map the fluorescence signal from a high altitude [Kim et al, 1985].

3.2 Spectral signature analysis

The upwelling spectra in the OCS channels (for instrument specifications refer to section 9) collected at different altitudes were converted into albedos by referring the data to the downwelling flux calculated by means of a radiative transfer model, called Dave Code [Kim et al, 1985]. (The ship measurements were referred to the downwelling flux by means of a grey card.) The results for the altitudes of 30 m and 3.600 m respectively together with a spectrum collected simultaneously from the ship are shown in Figure 11 on page 14.
The agreement between the 30 m aircraft and the ship data is good, considering that the two radiometers were not cross-calibrated. The atmospheric effects due to the Rayleigh scattering in the blue region are clearly visible in the data taken at 3600 m altitude.
The fluorescence peaks at 685 nm are visible in all cases. even though the ship data shows a slight shift towards 700 nm. Such

an effect has often been observed when a high local concentration of chlorophyll or phaeo-pigments is found in water containing large amounts of suspended matter. This causes the absorption at 670 nm to broaden, shifting the apparent fluorescence peak to the red. This subtle structural shift is not detected in the aircraft data because the OCS has comparatively wide bandwidths.

Further demonstration of the atmospheric effects on pertinent 492 nm and 682 nm spectral channels is given in Figure 12 on page 15. The upwelling radiance measurements taken at a number of different altitudes along with a theoretical point at 20,000 m are plotted to give a vertical profile.

Interestingly, the reflectance of the 492 nm radiation increases steadily with altitude, as the effects of molecular Rayleigh scattering begin to accumulate. However, the reflectance of the 682 nm channel displays somewhat different pat-

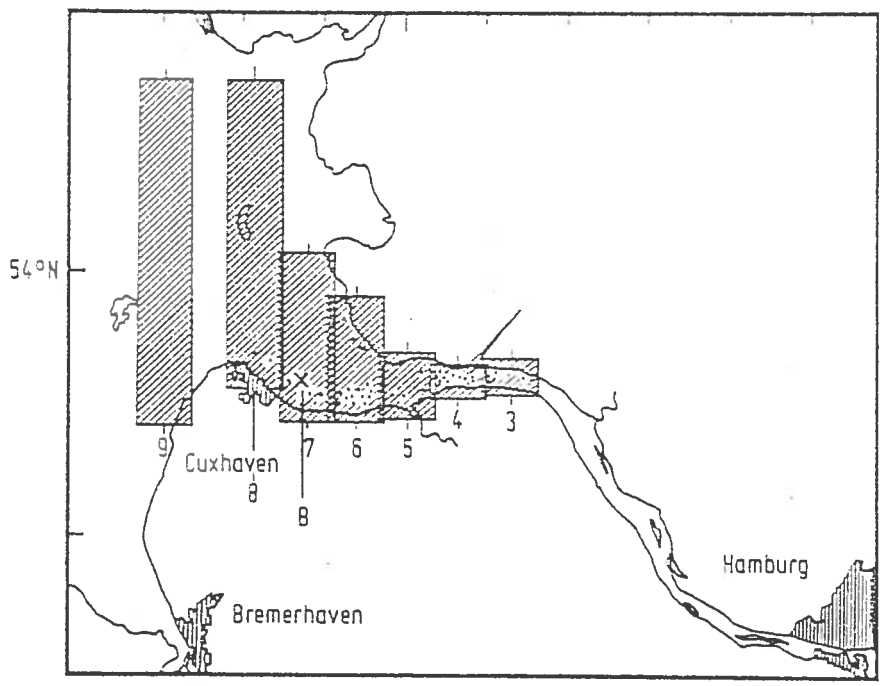

Figure 10. Map of the Elbe river and its estuary showing the aircraft coverage on 13 August 1981. At point B upwelling spectra were collected from different altitudes. (The solid dots indicate the approximate location of 30 pixels from which upwelling spectral signatures were analyzed.)

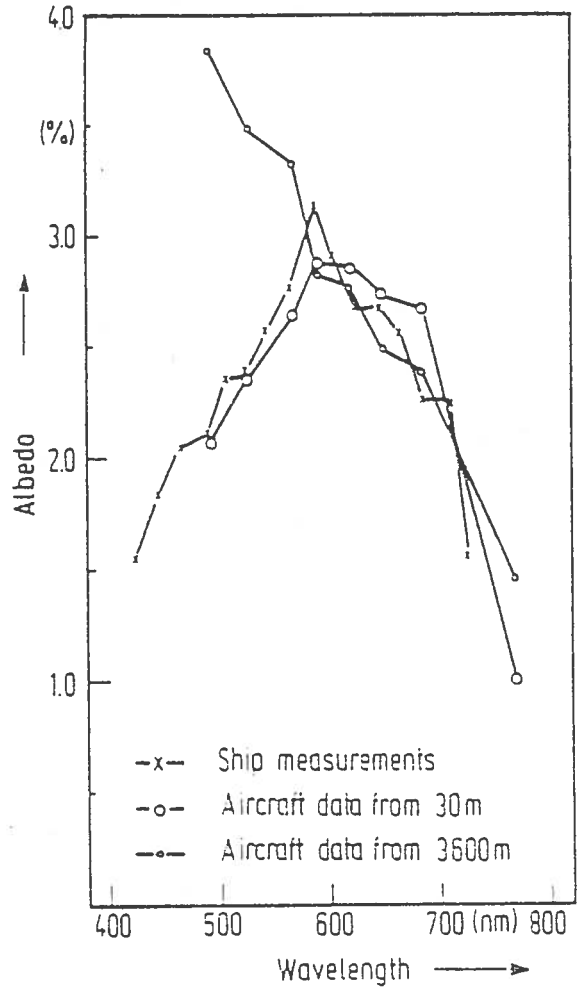

Figure 11. Upwelling radiance spectra taken from 30 m and 3.600 m altitude and by an 18 channel ship-borne radiometer.

terns. Although the surface albedo at 682 nm is actually larger than at 492 nm (2.75% vs 2,05%), a small decline is detected until it reaches the height of 2.000 m. This phenomenon is probably caused by the fact, that the water-leaving radiance is being attenuated at a faster rate, due to the combined absorptional effects of the atmospheric gases and aerosols in the lower troposphere, than the increase in the atmopsheric radiances. Since the total radiance is a sum of the two components, a minimum will be formed as the atmospheric radiance gradually begins to compensate for the transmission loss of the upward radiation.

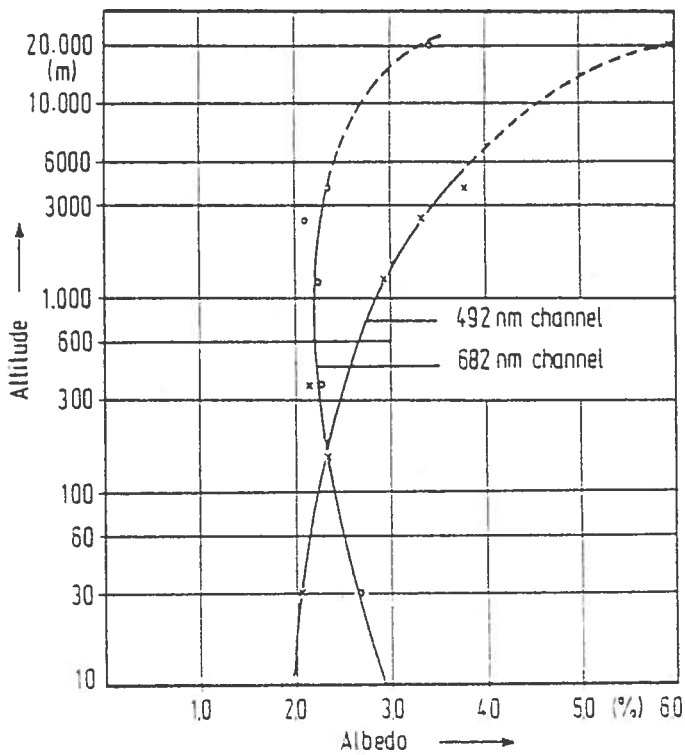

Figure 12. Vertical profiles of upwelling radiances at 492 nm and 682 nm (extrapolated by means of a model to 20.000 m).

Table 1 on page 16 gives a breakdown of the upwelling radiance of the 685 nm radiation at the top of the atmosphere. The computational results are based on an atmopsheric radiance model known as the Dave Scaler Code [Dave, 1972]. According to this model, a sea surface albedo change from 0 to 3.0 % will cause the albedo being perceived by a satellite to increase from 1.95 % to 3.43 %. This is equivalent to a transmission loss of 50 % as the water-leaving radiation at 685 nm reaches the top of the atmosphere.

For further image processing, a proven atmospheric-effect-removal algorithm was used [Viollier et al, 1980]. The method applies an inversion procedure, which transforms the raw radi-

Ground reflectivity (%):	Reflectivity at 80 km (%):
0	1.95
3.0	3.43

Table 1. Estimated upwelling intensities at the top of the atmosphere at 685 nm (solar zenith angle = 45°, scanner look angle = nadir, τ_{Mie} = 0.2).

ance data into ocean albedo using a series of single-scattering radiative transfer equations. In essence, the algorithm calculates molecular Rayleigh and ozone contributions , which are subtracted from the total radiance. The effects of aerosol Mie scattering in the atmosphere are estimated by the use of the near-infrared channel at 772 nm, where the water is black. The extrapolation to the other channels was performed by using an Angstrom coefficient of n = 0.8, which describes the wavelengths dependence of aerosol scattering.

Figure 13 on page 17 illustrates resultant water-leaving spectra taken from a pair of high and low chlorophyll window sites. The drawing also shows how the two different chlorophyll-analysis methods are being applied. The absorption method utilizes the reflectance ratio of the blue and green channels, and the steepness of the slope is used as an indication of the relative richness of the chlorophyll pigments in the water. (Note that the spectral channel at 492 nm was used, because it is less susceptible to the presence of yellow substance than a channel centred around the chlorophyll-a maximum.)
In case of the fluorescence the algorithm also requires three channels, a fluorescence channel near 685 nm and two adjacent channels at both, longer and shorter wavelengths. The longer wavelength channel is used for the removal of the aerosol effects, while the short-wavelength channel is used to remove water signals of non-fluorescent origin.
The algorithm implemented to retrieve the fluorescence requires the initial removal of the atmospheric effects. Corrected

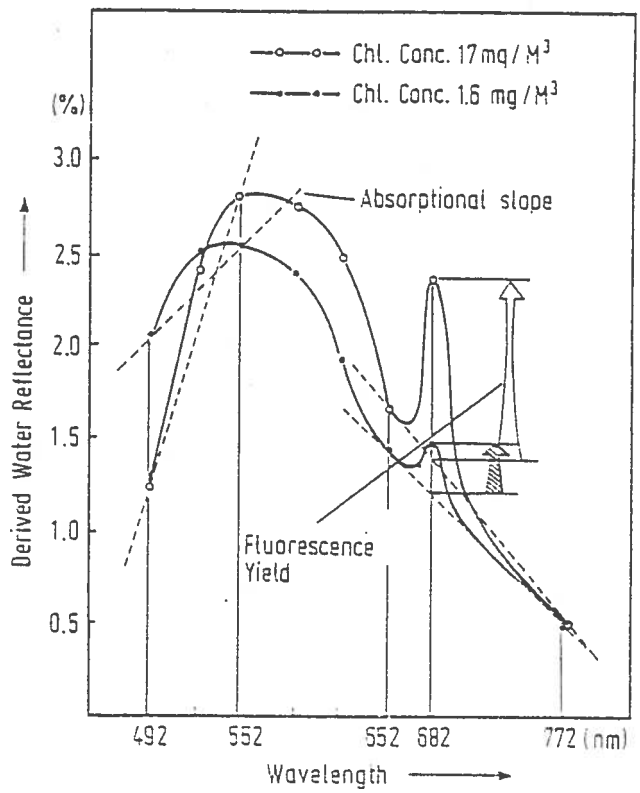

Figure 13. Derived water-leaving spectra (reflectance) for a pair of high and low clorophyll window sites.

water-leaving reflectances at 682 and 652 nm, $R_{(w)682}$ and $R_{(w)652}$ are obtained from

$$R_{(w)682} = R_{(t)682} - (\lambda_{682}/\lambda_{772})^{-n} \times R_{(c)772} \quad \ldots\ldots\ldots \quad (1)$$

$$R_{(w)652} = R_{(t)652} - (\lambda_{652}/\lambda_{772})^{-n} \times R_{(c)772} \quad \ldots\ldots\ldots \quad (2)$$

where $R_{(t)}$ denotes the reflectance obtained before any correction procedures, and $R_{(c)}$ refers to the reflectance obtained after the molecular Rayleigh and the ozone effect corrections. It is to be noted that molecular Rayleigh effects in the long-wavelength visible and near-infrared regions are negligibly small, and for practical purposes can be ignored. Then instead of $R_{(c)772}$, $R_{(t)772}$ can be used in equations 1 and 2.

The next step is to remove non-fluorescent water background by the use of the adjacent short-wavelength channel at 652 nm:

$$R_{(F)682} = R_{(w)682} - (\nu_{682}-\nu_{772}/\nu_{652} - \nu_{772}) \times R_{(w)652} \quad .. \quad (3)$$

$R_{(F)682}$ refers to the fluorescence reflectance for the 682 nm channel and the ν denotes the wave number in $1/\lambda$ (wavelength). By substituting equations 1 and 2 into 3, the fluorescence algorithm can be given as

$$R_{(F)682} = R_{(t)682} - a \times R_{(t)652} - b \times R_{(t)772} \quad ..... \quad (4)$$

where a and b are a pair of experiment specific constants obtained by entering appropriate atmospheric parameters and computations.
Equation 4 is convenient because, in order to retrieve the fluorescence intensity of the 682 nm channel, it is not necessary to go through the elaborate process of computing the atmospheric effects pixel by pixel as in the case of the absorption method. Instead, a simple subtraction process with two preset constants is all that is required.

3.3 Comparison of fluorescence and absorption data

The rapid changes of the river relative to the position of the R/V Monitor made it difficult to correlate all aircraft data directly with the ship measurements of the chlorophyll concentrations. The rapid fluctuation of chlorophyll readings during the 3 h span while the R/V Monitor was anchored at point B (Figure 10 on page 13) is evident from Table 2 on page 19.
As an alternative, the fluorescence signal (here called fluorescence yield, FY) derived from the data were compared with those chlorophyll concentrations obtained from the same data set via the absorption method. A set of 30 window sites were randomly selected along the deep ship channel (Figure 10 on page 13) whenever high and low fluorescence contrasts were found. Each window data point consists of an averaged radiance value taken from 9 contiguous pixels. In Figure 14 on page 20 derived

Time: GMT	Chl.-a: mg/m^3	Phaeo: mg/m^3	Seston: mg/m^3	K(abs): 1/m	Transm: %
12:50	4	12	7.3	1.0	85.3
14:53	6	16	7.1	1.4	80.4
15:44	7	6	5.5	1.0	83.6
16:11	2	20	7.6	1.3	79.9

Table 2. Ship measurements of water parameters in the Elbe at point B (13 Aug. 81).

chlorophyll concentrations from the absorption method are plotted against the derived fluorescence yields.
The ordinate chlorophyll values are derived from

$$\text{Chlorophyll Conc.}(mg/m^3) = 1.5 \times (R_{492} / R_{552})^{-3} \quad \ldots (5)$$

The coefficients 1.5 and 3.0 are empirical parameters that have been taken from the results of previous OCS flight experiments which used 472/552 channels. Other investigators have quoted different empirical parameters for CZCS 520/550 nm channel ratios [Clark, 1981, Smith and Wilson, 1981, Gordon et al, 1983]. However, the 492 nm channel is situated closer to 472 nm than to 520 nm and so the values from the previous OCS experiment were used. A regression line which best fits the 30 window radiance data has turned out to be exponential in the form:

$$\text{Chlorophyll Conc.}(mg/m^3) = 0.36 \times \exp.(2.8 \times FY) \quad \ldots (6)$$

with a correlation coefficient $r = 0.74$ ($\alpha \leq 0.1$ %).
As discussed earlier, various factors influence the 685 nm fluorescence. For instance the ship data indicate that the Elbe river water contains a high concentration of phaeo-pigments (see Table 2), which show a similar absorption and emission spectrum as chlorophyll-a. It is known that these are strongly correlated with suspended matter. Thus the comparatively good

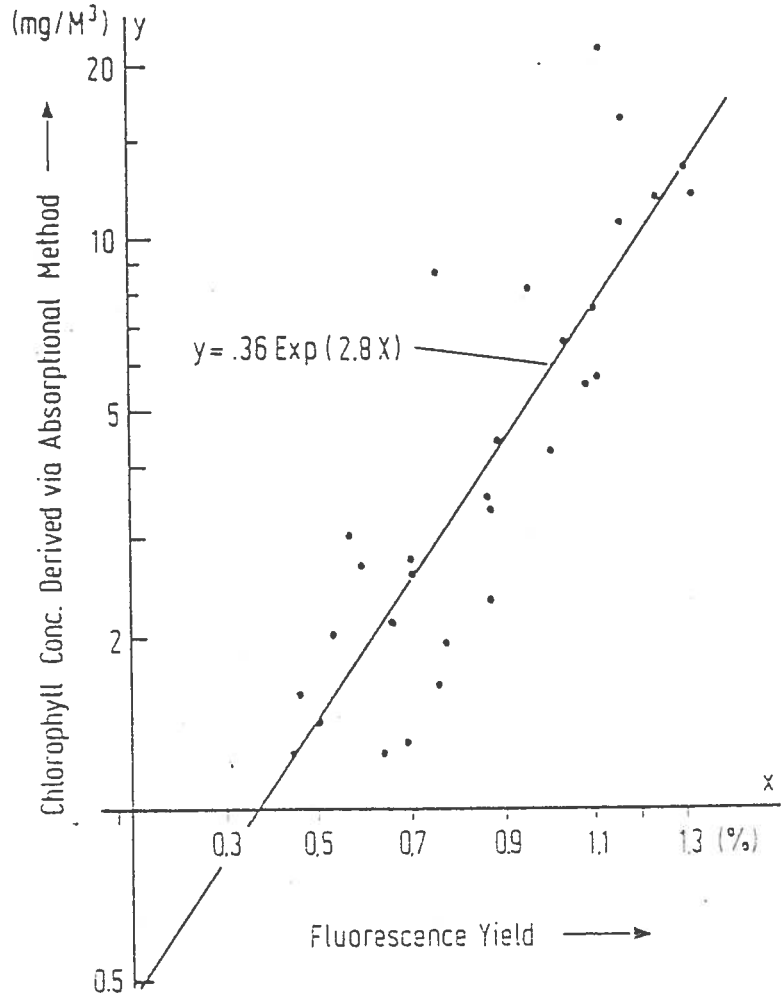

Figure 14. Regression of chlorophyll concentrations (derived from the blue/green ratio) versus 682 nm fluorescence yields for 30 pixels selected along the deep ship channel.
The ordinate chlorophyll values are derived from Chlorophyll Conc. $(mg/m^3) = 1.5(R_{492}/R_{552})^{-3.0}$.
(The coefficients 1.5 and 3.0 are empirical values that have been taken from the results of previous investigations with the same instrument.)

correlation of the fluorescence signal with the chlorophyll quantity derived from the blue/green ratio (Figure 14) is probably caused by this effect and may not be representative for other types of case II waters. The chlorophyll quantity given in equation 6 should therefore be considered as a first order approximation, and is quoted merely to demonstrate that

under these particular environmental conditions a correlation exists between the sun-stimulated fluorescence and the pigment/seston quantity in the water.

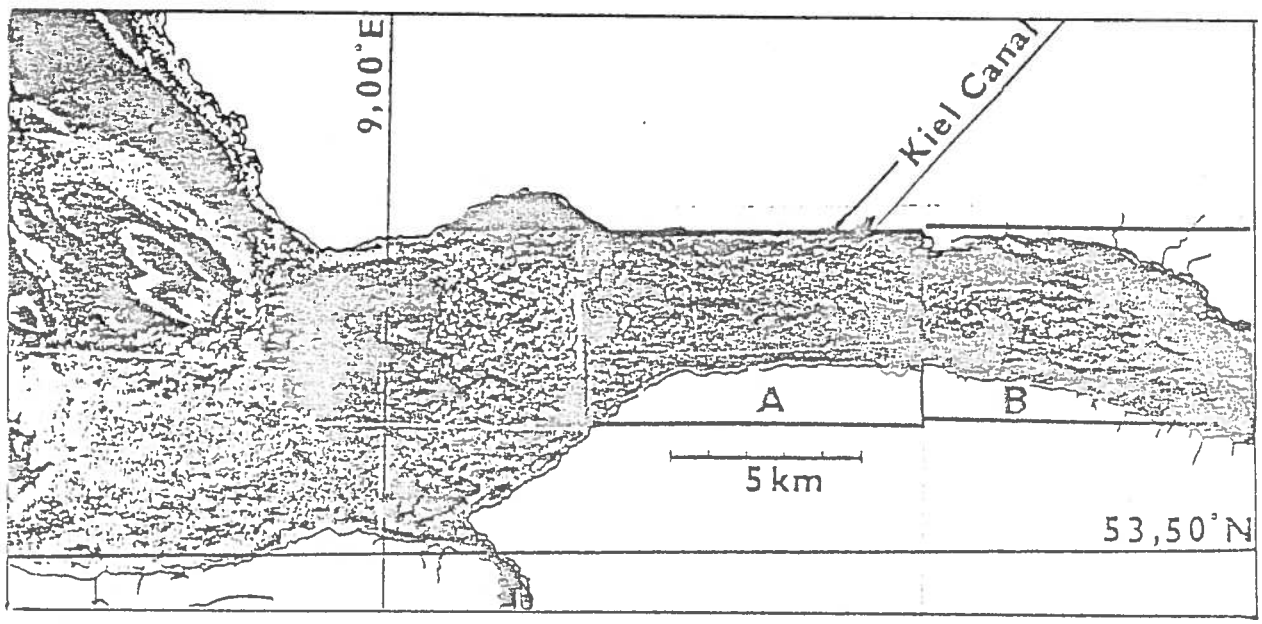

Figure 15. Fluorescence imagery of the Elbe estuary derived from OCS data. (The green hue corresponds to a high, the yellow hue to a medium, the blue hue to a low fluorescence signal.)

3.4 Mapping of fluorescence

Figure 15 shows a fluorescence image of the lower Elbe River and its estuary in false color derived from OCS data. It is composed of 4 flight segments (compare tracks 3 to 6 in Figure 10 on page 13) and has been geometrically corrected for a mercator projection. (Areas characterized by a low fluorescence signal are shaded blue, areas of medium fluorescence are shaded yellow, areas of high fluorescence are shaded in green.)

The fact that the 4 flight sections do not match fully radiometrically is caused by the different overflight times. This indicates the rapid changes in this estuary due to the tidal effects.

Section B in Figure 15 shows some ship wakes which are accentuated, possibly because the ship's motion churns up fresh plankton from the sublayer to the surface. According to Kiefer, 1973 the fluorescence signal varies in part due to an inhibition in the fluorescence of cells exposed to intense sunlight. The freshly upwelled deep-layer phytoplankton does not show such fatigue, thereby providing a marked contrast. A signal increase of as much as 30 counts (from 100 to 130) was detected in the 682 nm channel. This is shown in Figure 16, where the actual counts of the 682 and 655 nm channels of a transecting line are plotted. This increase is equivalent to a radiance increase of 0.07 mW/cm^2usr.

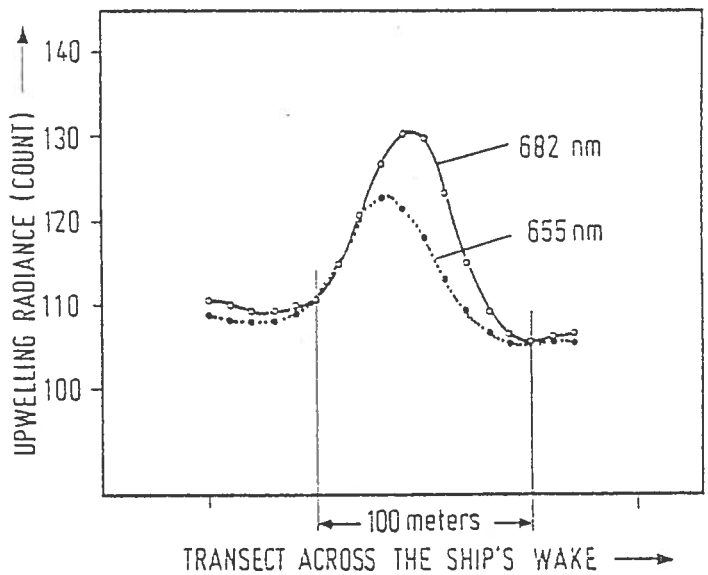

Figure 16. Radiance counts of 655 nm and 682 nm channels across one of the ship wakes of section B in Figure 15 on page 21.

4. FLUORESCENCE EXPERIMENT (FLUREX)

4.1 Introduction

Within the context of FLUREX 82, the Six Channel Radiometer (SCR) of DFVLR and the IOS Spectrometer [Walker et al, 1975] were flown together with other instruments (OCR) above specific positions (R/V Alkor, FPN) within the FLUREX test sites (Figure 17 and Figure 18 on page 24).

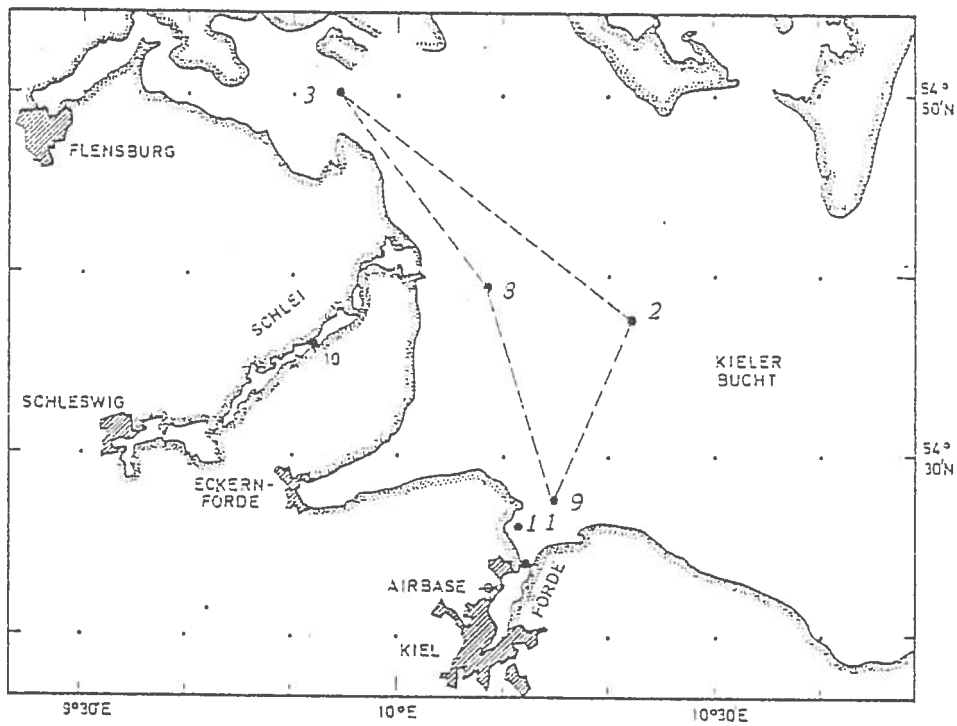

Figure 17. Positions of R/V Alkor in the Kiel Bight during FLUREX.

While the *general* objectives of this experiment were investigations concerning the fluorescence effect, the more *specific* objectives were to study this effect under extremely high chlorophyll concentrations (river Schlei) and again to monitor the relevant signals under these environmental conditions from different flight altitudes. Results from the airborne obser-

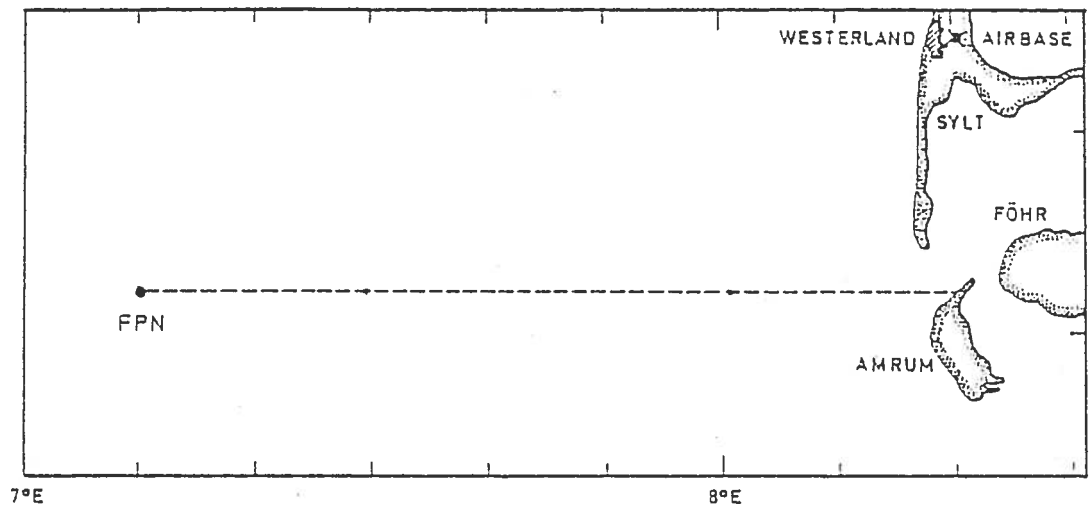

Figure 18. Position of the FPN and flight tracks in the German Bight during FLUREX.

vations and their correlation with the ground truth are discussed in the following sections.

4.2 Environmental conditions

In spite of the success of the experiment in general, the data collection by means of SCR and IOSS was somewhat influenced by the limited range of pigment concentrations both, in the Baltic Sea and in the North Sea. With the exception of the area in and near the river Schlei (Baltic Sea), the concentrations were low at the FPN (North Sea) and low to medium in the Kiel Bight (Baltic Sea).
Typical near-surface chlorophyll values, measured in-situ during the operation of the IOSS on the DO 28 were:

- o in the Kiel Bight: 2.3 - 4.0 mg/m^3
- o in the river Schlei: 39.6 - 56.5 mg/m^3
- o at the FPN: 0.43 - 1.0 mg/m^3.

Typical (near-surface) chlorophyll values measured in-situ during the operation of the IOSS on board of the R/V ALKOR were:

- o in Kiel Bight and river Schwertine: 2.4 - 10.3 mg/m^3
- o in and near river Schlei: 4.3 - 58.6 mg/m^3.

The results of the data analysis are thus restricted to these particular environmental conditions.

4.3 Analysis of IOSS data

4.3.1 Data processing

By referring the upwelling radiance to the downwelling irradiance, IOSS data is expressed in terms of reflectances. From this data the fluorescence line height (FLH) is calculated as the excess reflectance x 10^6 at 684 nm above a linear baseline connecting reflectances at 651 nm and 716 nm. In case of the exceptionally high chlorophyll values as found in the river Schlei, the reflectance of the next channel (at 702 nm) was used instead. (Compare also with the "fluorescence signal" in section 2.3.2 where, however, radiances have been used instead of reflectances.)

4.3.2 Results

In a first step, a linear regression analysis in the form

$$y = a + b \times x$$

was performed between the IOSS-derived fluorescence line height values (FLH) from both, ship overflights (at 500 feet altitude) and ship-based measurements (all together 31 data points) versus the available near-surface (0.5 m) chlorophyll values (from R/V ALKOR and the FPN). The result is shown in Figure 19 on page 26.
As mentioned, the data point clusters correspond essentially to the conditions at the FPN ($\leq$ 1 mg/m^3), in the Kiel Bight (medium values up to 10.3 mg/m^3) and the river Schlei (high values).

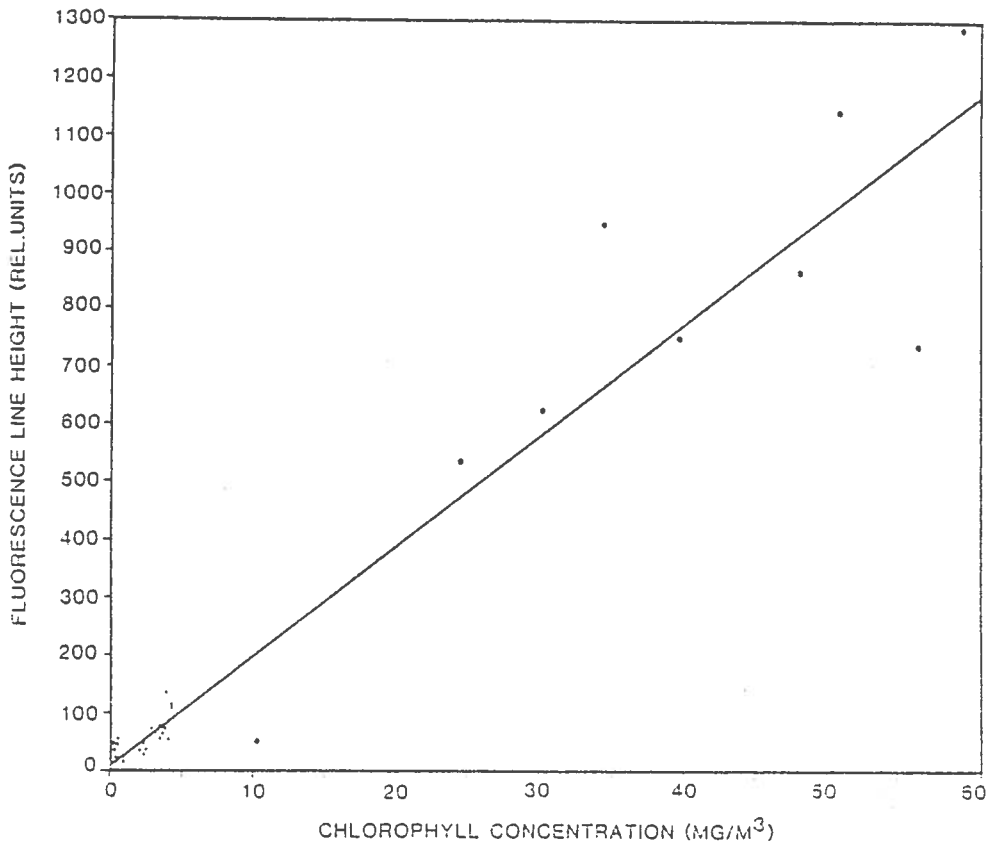

Figure 19. Linear regression between IOSS-derived FLH (airborne and shipborne) versus ground truth (R/V ALKOR and FPN). The correlation coefficient is r = 0.96 ($\alpha \leq 0.1$ %).

The relationship between the FLH (in rel. units) and the chlorophyll concentration (in mg/m^3) can be described by the expression

$$FLH = 10.7 + 19.3 \times Chlor.Conc.$$

with a correlation coefficient r =0.96 ($\alpha \leq 0.1$ %). A similar relationship

$$FLH = 4.99 + 19.5 \times Chlor.Conc.$$

with a correlation coefficient r = 0.96 ($\alpha \leq 0.1$ %) is found, if the data points from the FPN (values ≤ 1 mg/m^3) are omitted

and thus only data from the Baltic Sea is used (Figure 20 on page 27, A).

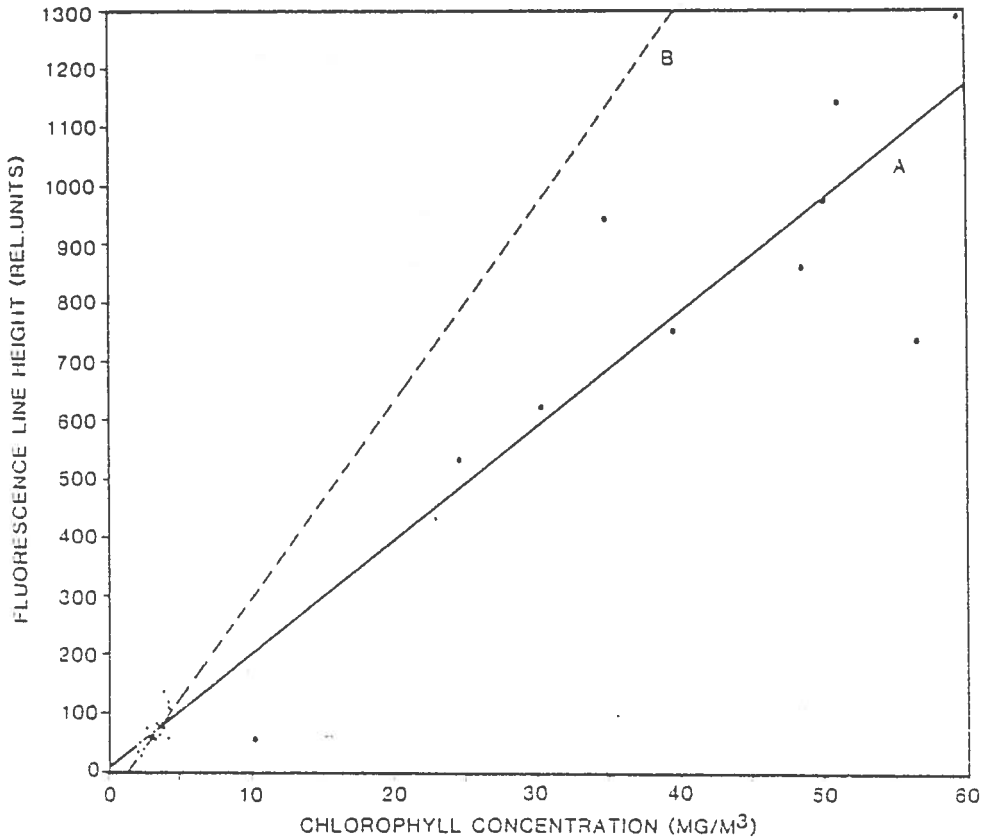

Figure 20. Linear regression between IOSS-derived FLH versus ground truth (R/V ALKOR only).
A = values between 2.3 and 58.6 mg/m^3
(r= 0.96, $\alpha \leq 0.1\%$)
B = values between 2.3 and 4.30 mg/m^3
(r =0.78, $\alpha \leq 0.1\%$)

The clustering of data points affects the slope of the regression line and subsequently the sensitivity of the method. If only medium concentration values (2.3 - 4.3 mg/m^3) in Figure 19 on page 26, B are used for the correlation (15 data points), a much steeper slope is derived as expressed by the relationship

$$FLH = -45.2 + 34.0 \times Chlor.Conc.$$

The reason for this effect is probably the re-absorption of the fluorescence signal at very high concentrations and the resulting quenching and shift of the fluorescence peak (compare also Figure 11 on page 14). Furthermore, the fluorescence cross section at lower concentrations may be comparatively larger than at higher concentrations. This latter effect, however, is not yet verified.

The correlation coefficient is higher, $r = 0.98$ ($\alpha \leq 0.1$ %) if only shipborne FLH data are correlated with the in-situ measurements of near-surface chlorophyll from the R/V ALKOR in the Kiel Bight and in the river Schlei (14 data points). The reason for this is probably the patchiness, which introduces an error into the correlation of airborne with shipborne data.

A smaller number of airborne IOSS data were compared with in-situ measurements (R/V ALKOR) at different depth. The derived correlation coefficients are:

at 0.5 m:	$r = 0.97$, $\alpha \leq 0.1$ %	(10 data points)
at 2.0 m:	$r = 0.99$, $\alpha \leq 0.1$ %	(7 data points
at 5.0 m:	$r = 0.66$, $\alpha \leq 8$ %	(6 data points).

These results indicate that representative fluorescence signals are only derived from the upper few meters of the water column. A stratification and the corresponding increase of the chlorophyll concentration at larger depth can not be assessed by the fluorescence method.

4.4 Analysis of SCR data

Both, mapping flights, overflights at different altitudes were undertaken above the FPN and above various positions of R/V Alkor in the Kiel Bight (Figure 17 on page 23, Figure 18 on page 24).

4.4.1 Data processing

SCR data were calibrated against a calibration standard and radiance values calculated for each channel above selected positions or along individual flight tracks. (For SCR specifications refer to section 9.1.4.)
FLH was calculated as the difference of upwelling radiance at 682 nm and a linear baseline between 649 and 749 nm. (Compare also section 4.3.1.) Alternatively the normalized fluorescence line height (NFLH) was calculated by dividing the FLH by the value of the above-mentioned baseline at 682 nm.

4.4.2 Influence of the flight altitude

Flight 14 on 25 April 82 above R/V Alkor (position 2 in the Kiel Bight) was selected so as to demonstrate the (almost) linear increase of upwelling radiance values with increasing altitude till approx. 1500 m, while above that the increase slows down (Figure 21 on page 30). As expected, the increase at shorter wavelengths is faster than that at longer wavelengths (Rayleigh- and aerosol scattering). SCR channel 682 nm does not show any exceptional response in this plot. Figure 22 on page 31 shows the same data but altitude and wavelength inverted. It indicates clearly the fluorescence peak not only at 150 m but also at higher altitudes. FLH does not show a strong dependance on the altitude since both, fluorescence and baseline wavelengths appearently respond in a similar way to the atmospheric effects on the measaured signal. This can be seen more accurately in Figure 23 on page 32 which shows the variability of FLH within the close environment of R/V Alkor at different altitudes together with their mean and standard deviation.
Again, the dependance on altitude is minor. The small *horizontal* variation indicates that the FLH values derived are significant.

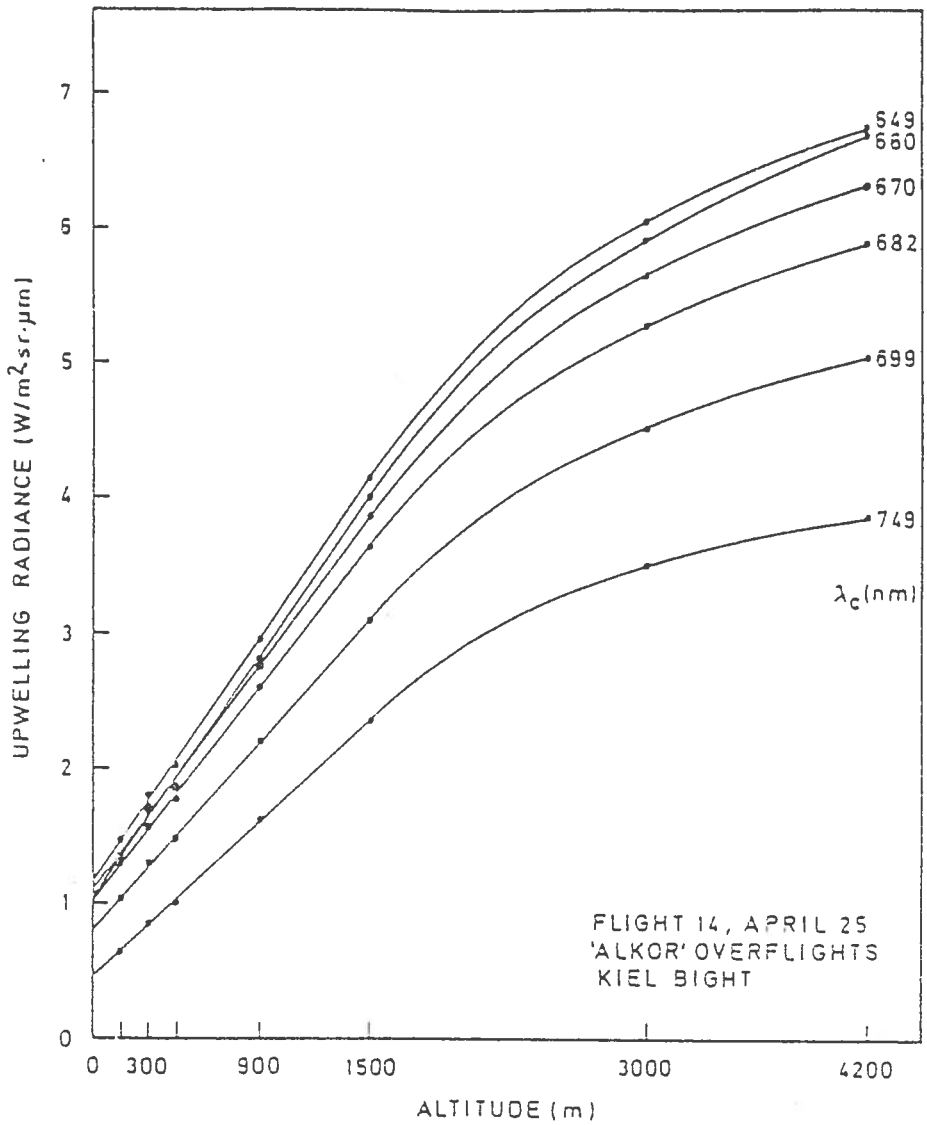

Figure 21. Upwelling radiances (at SCR wavelengths) versus flight altitude (flight 14 on 25 April 82 above R/V Alkor at position 2 in the Kiel Bight).

4.4.3 Correlation of airborne data with sea truth

A linear regression was performed between SCR-derived FLH data from all flights (150 m altitude) above the North Sea and the Kiel Bight (without data from the river Schlei) versus ground truth (R/V Alkor and FPN).. The result is shown in Figure 24 on page 33. Based on 16 data points, the relationship can be expressed by

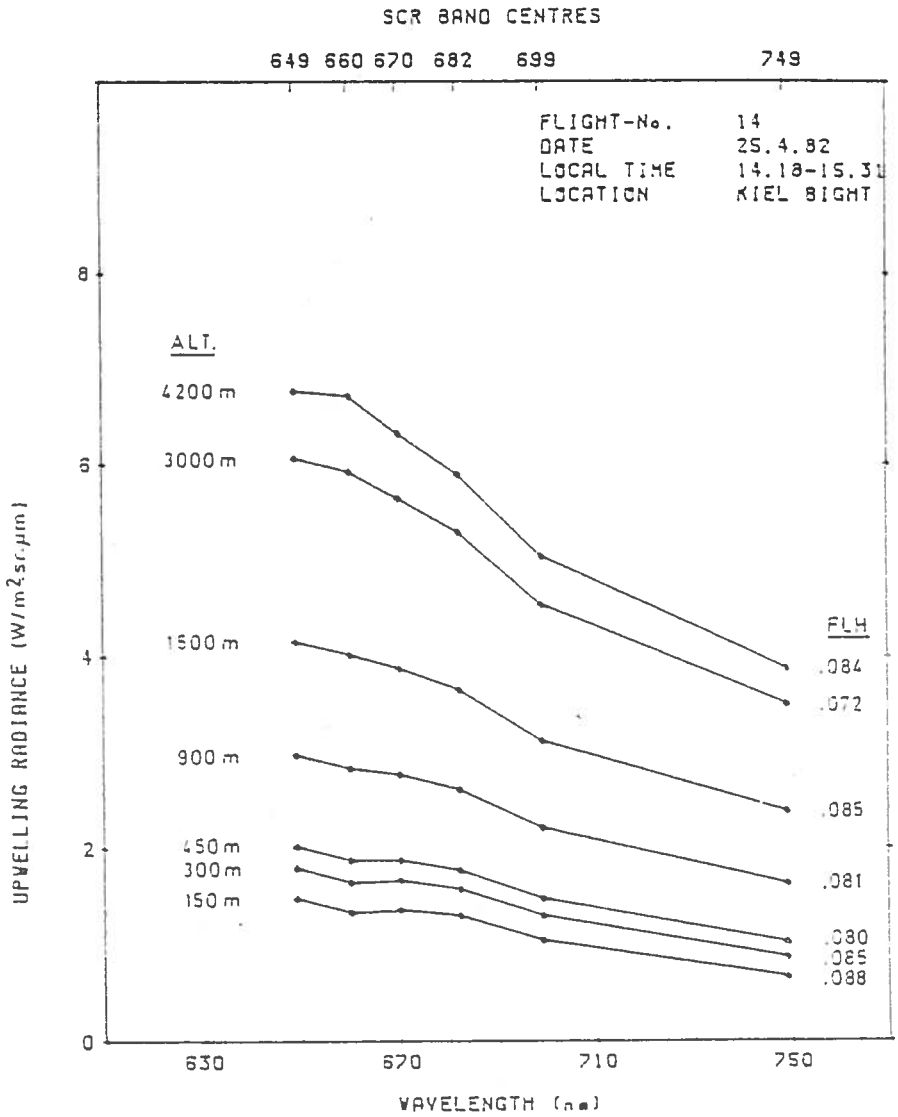

Figure 22. Upwelling radiances versus SCR wavelengths at different altitudes (flight 14 on 25 April 82 above R/V Alkor at position 2 in the Kiel Bight).

FLH = 0.026 + 0.03 × Chlor. Conc.

The correlation coefficient is r = 0.80.
Based on the same data points, however, correlated with the NFLH instead (Figure 25 on page 34), improves the correlation to r = 0.91. The reason seems to be again the high correlation of

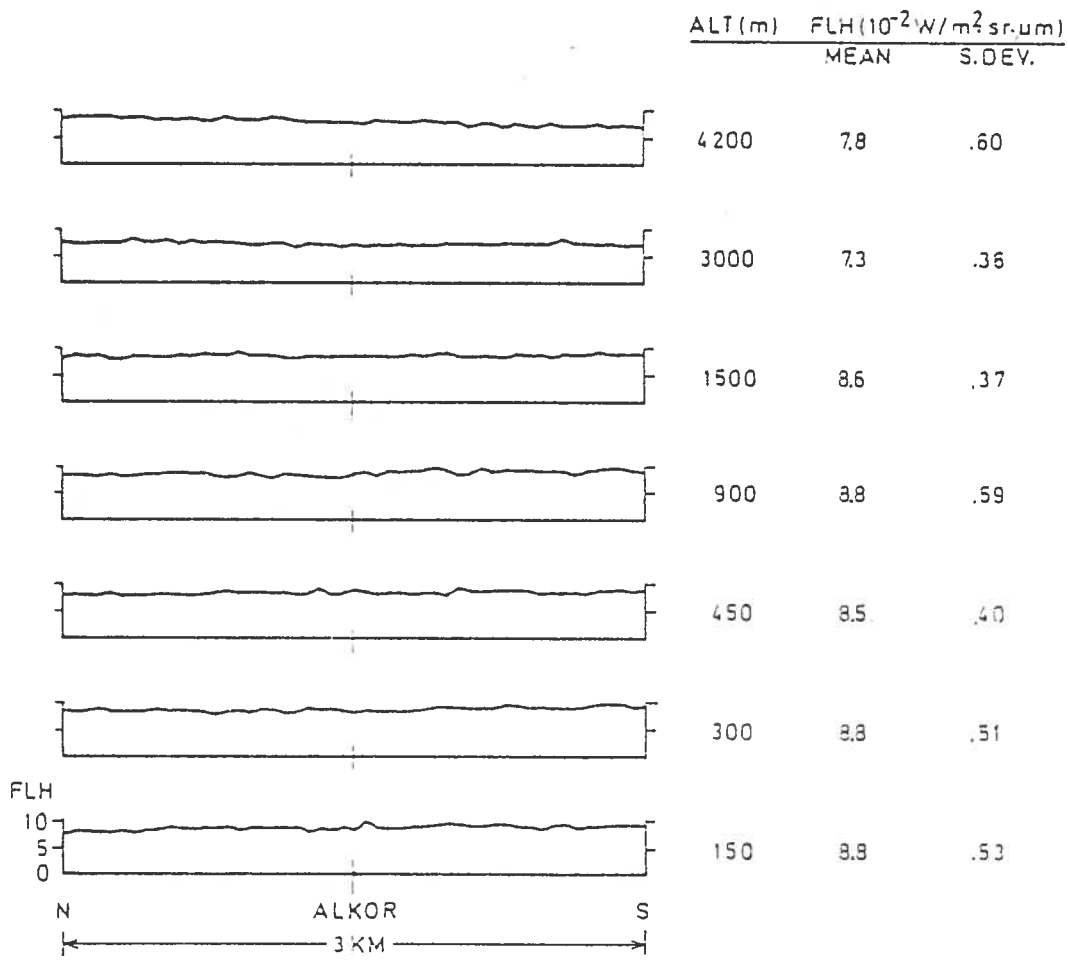

Figure 23. FLH along the flight path near R/V Alkor at different altitudes (flight 14 on 25 April 82 above R/V Alkor at position 2 in the Kiel Bight).

the baseline with the downwelling irradiance. Thus the NFLH (in terms of upwelling radiance) is almost identical with the FLH derived from IOSS reflectance values as indicated in section 4.3.

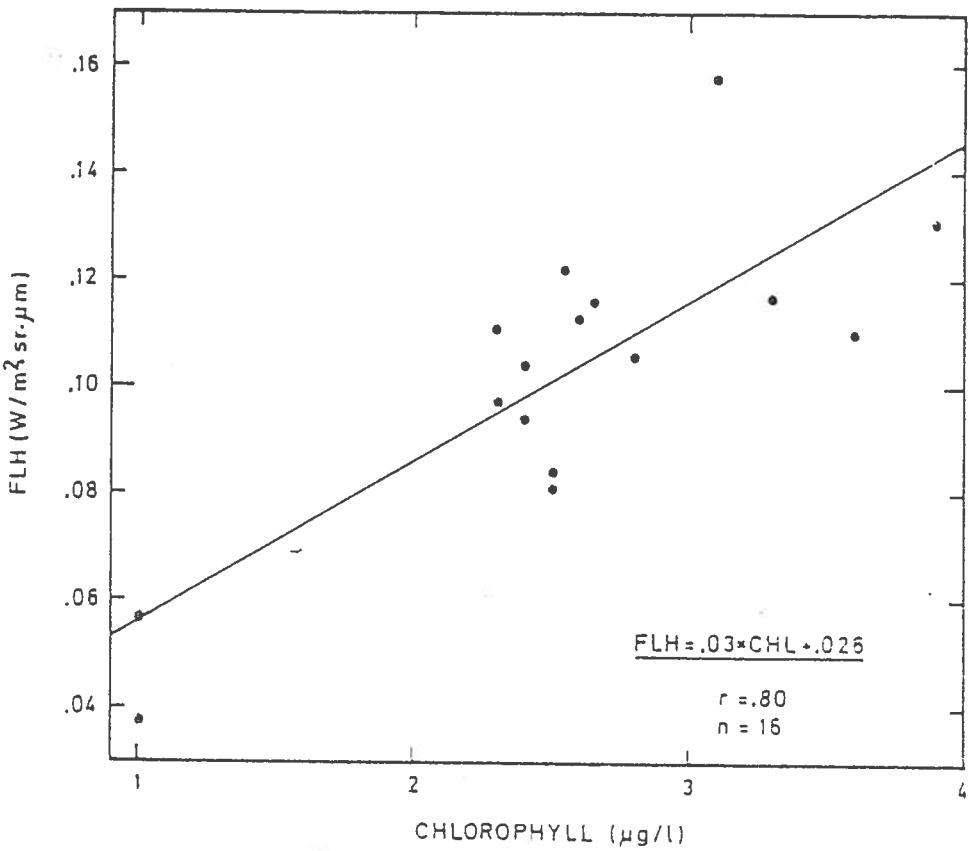

Figure 24. Linear regression between SCR-derived FLH versus ground truth. The correlation coefficient is r = 0.80.

4.4.4 Temporal and spatial variability

The temporal variability of the NFLH (as representation of the chlorophyll concentration) is shown in Figure 26 on page 35 for the flights 15 to 19 on 27 April 82 above the environment of R/V Alkor at position 11 in the Kiel Bight. Flights were performed at different altitudes and different directions across a distance of 1.6 km each.
Since the base line increases with height, only a low altitude-dependance is observed. While the NFLH varies according to the flight direction in each case, the value above the anchored R/V Alkor (A in Figure 26 on page 35) follows the temporal change of the in-situ measured chlorophyll concen-

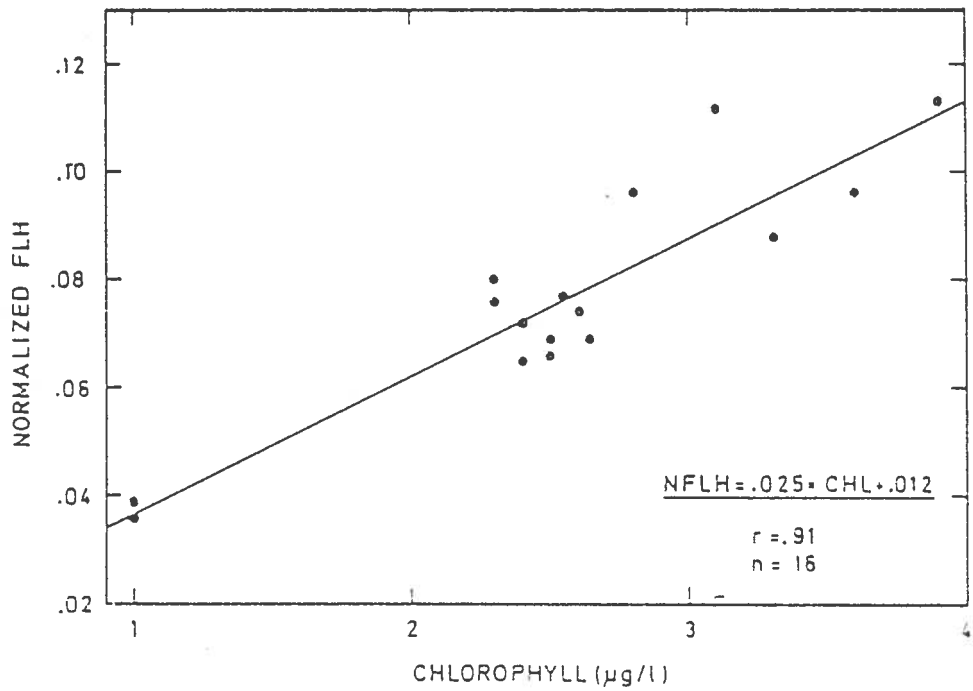

Figure 25. Linear regression between SCR-derived NFLH versus ground truth. The correlation coefficient is r = 0.91.

tration during the day (i.e., high during the morning, decrease around noon, increase during the afternoon).

Large scale variations of chlorophyll (in terms of NFLH) along the flight path are shown in Figure 27 on page 36 and Figure 28 on page 37 for two consecutive flights with a time laps of a few hours on 27 April 82. (NFLH has been calibrated with the ground truth derived from Figure 25.)
Generally speaking the derived chlorophyll concentrations in the near-shore areas are comparatively high while the values towards the east are almost by a factor of 2 lower. This corresponds very well to the generall chlorphyll pattern as was measured directly by the R/V Alkor. Small scale structures are reproducible from one flight to the next.

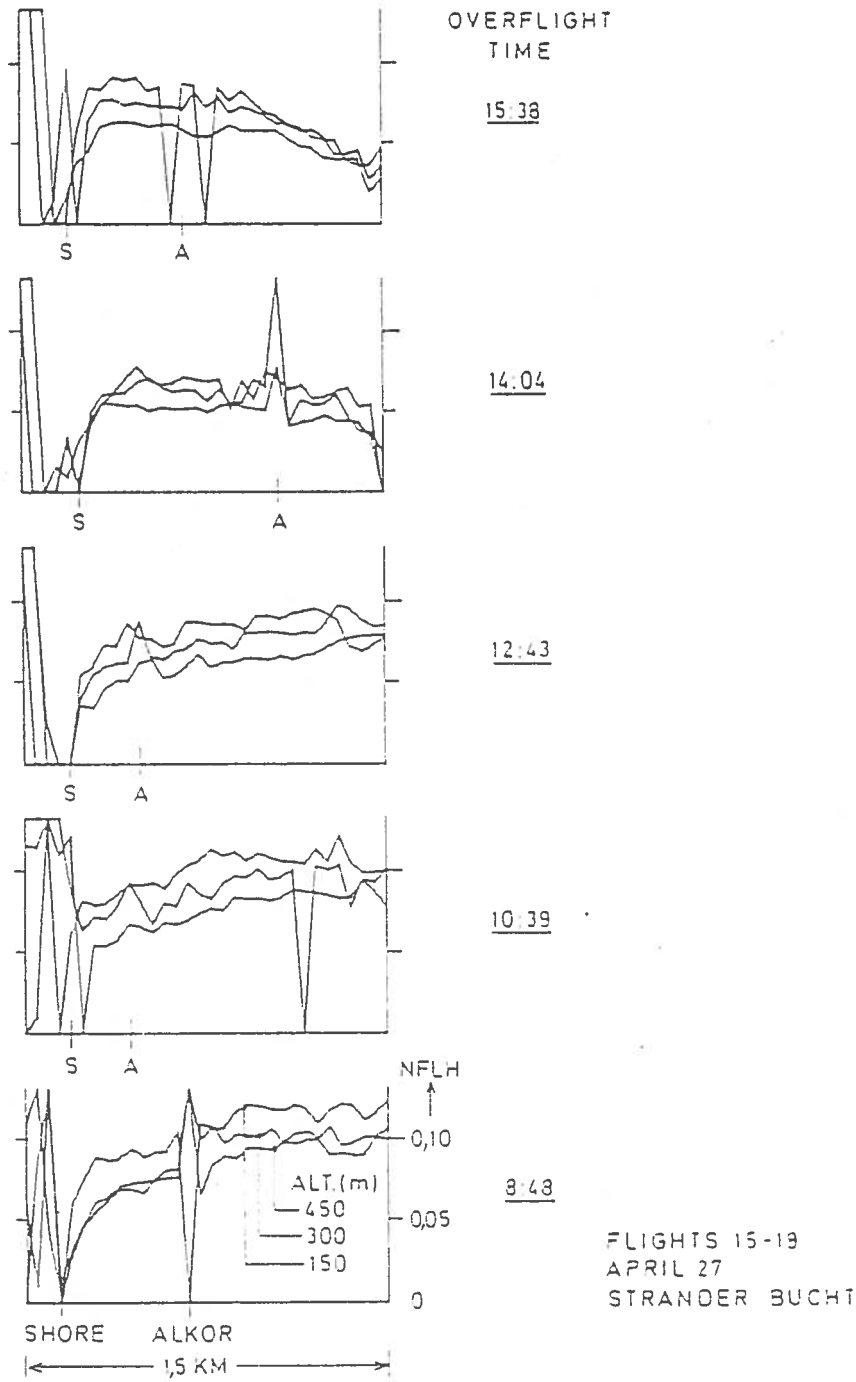

Figure 26. Temporal variability of NFLH along the flight path near R/V Alkor at different altitudes (Flights 15 to 19 on 27 April 82 above position 11 in the Kiel Bight). S refers to shore crossing, A refers to R/V Alkor crossing.

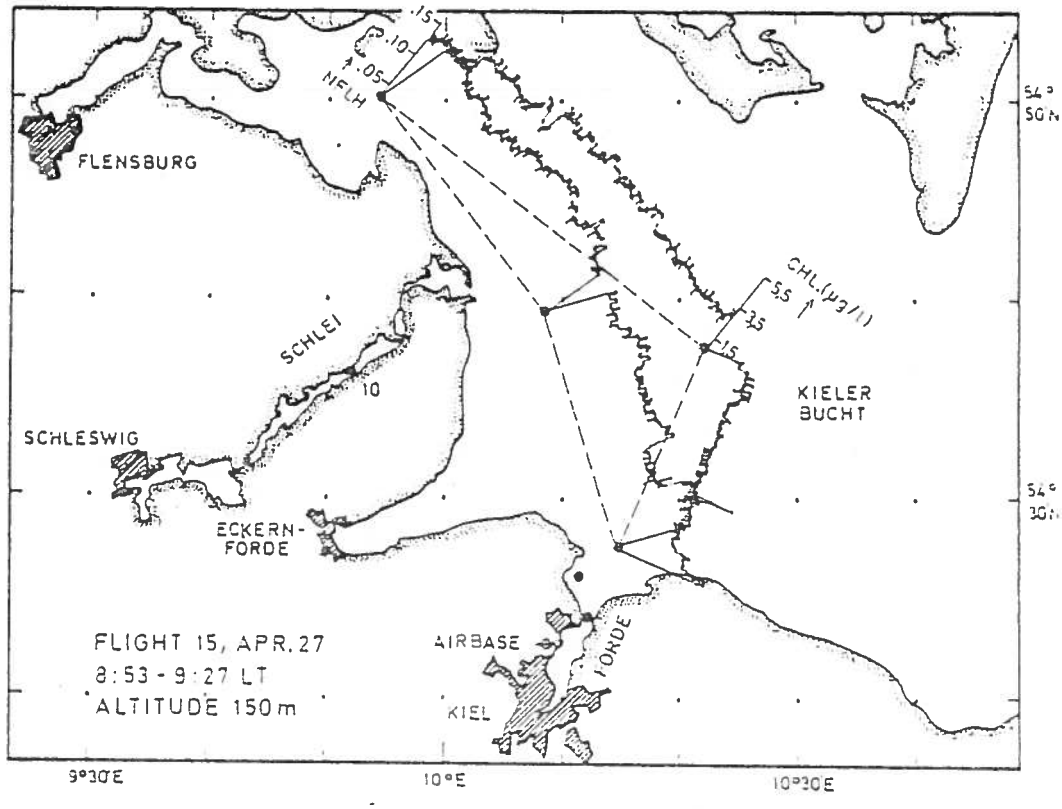

Figure 27. Large scale variation of chlorophyll along the flight path derived from NFLH with a calibration against ground truth from Figure 25 (flight 15 on 27 April 82 in the Kiel Bight).

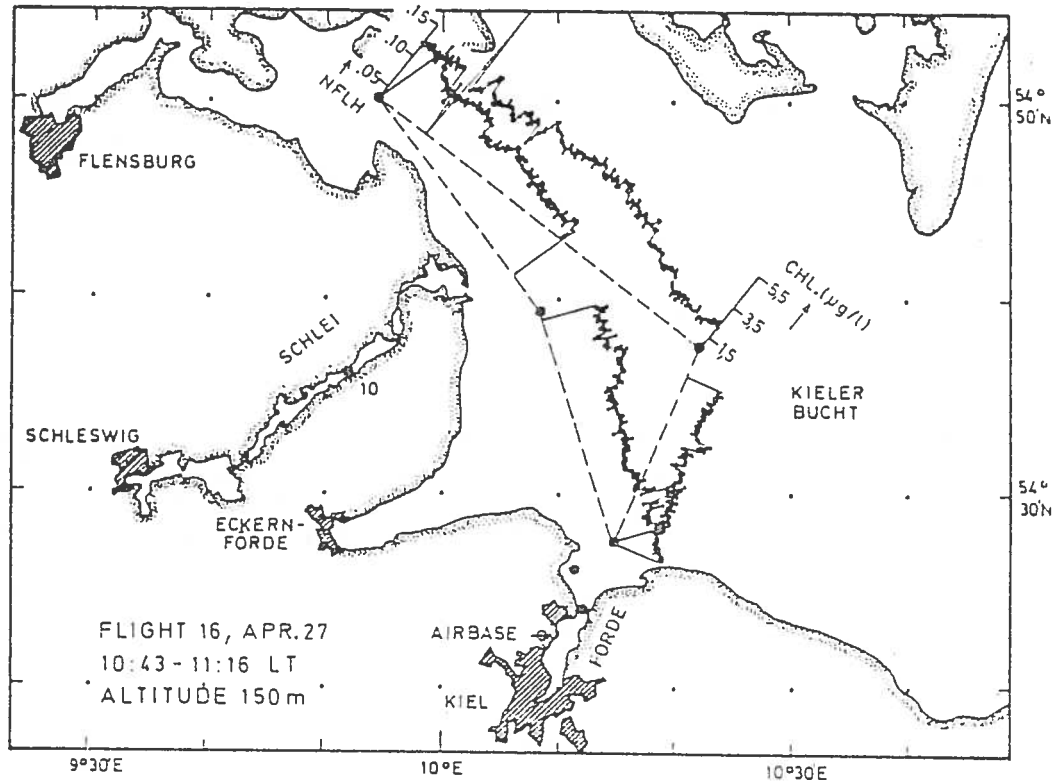

Figure 28. Large scale variation of chlorophyll along the flight path derived from NFLH with a calibration against ground truth from Figure 25 (flight 16 on 27 April 82 in the Kiel Bight).

5. CONCLUSIONS

The possibility of using the natural (sun-stimulated) fluorescence of chlorophyll-a at 685 nm for the remote assessment of near-surface pigments in coastal waters has been investigated during the course of several experiments in the North Sea and the Baltic Sea using different (imaging and non-imaging) sensors under a variety of environmental conditions.
Although the data analysis presented here does not necesseraly permit conclusions in regard to specific effects (like e.g.,

influence of the illumination, influence of stratification, influence of plankton species etc.), it shows clearly that natural fluorescence (expressed by FLH or NFLH) can be applied in general to the mapping of near-surface chlorophyll from aircraft in the concentration range above approximately 2 mg/m^3 in different types of water ranging from comparatively clear North Sea water (case I), through river water containing very high pigment concentrations as can be found in the river Schlei (case I), to extreme turbid water (case II) with large amounts of yellow substance and suspended matter as can be found in the Elbe estuary.
Furthermore, the measurements from aircraft flights at different altitudes indicate that the fluorescence signal can still be detected with sufficient accuracy from high altitudes.

6. LITERATURE

Amann, V. and R. Doerffer, 1983:
Aerial survey of the temporal and spatial distribution of phytoplankton during FLEX 76.
North Sea Dynamics (Eds. Sündermann/Lenz) Springer Verlag pp.517-529.

Borstad, G.A. and J.F.R. Gower, 1984:
Phytoplankton chlorophyll distribution in the Eastern Canadian Arctic.
Arctic 37 (3), pp.224-233.

Clark, D.K., 1981:
Phytoplankton pigment algorithms for Nimbus-7 CZCS.
Oceanography from Space (Ed. J.F.R. Gower) Plenum Press New York, Mar. Sci. 13, pp.227-238.

Comrey, A.L., 1973:
A first course in factor analysis.
Academy Press.

Cooley, W.W. and P.R. Lohnes, 1971:
Multivariate data analysis.
Wiley and Sons, New York.

Dave, J.V., 1972:
Development of programmes for computing characteristics of ultraviolet radiation.
NASA Contract Report NAS-5-21680, IBM Palo Alto.

Gordon, H.R. et al, 1983:
Phytoplankton pigment concentrations in the Middle Atlantic Bight: Comparison of ship determinations and CZCS estimates.
Appl. Opt.22 pp.20-36.

Gordon, H.R. and A. Morel, 1983:
Remote assessment of ocean color for interpretation of satellite visible imagery.
Lecture notes on coastal and estuarine studies 4 (Springer).

Gower, J.F.R., S. Lin and G.A. Borstad, 1984:
The information content of different optical spectral ranges for remote chlorophyll estimation in coastal waters.
Int. J. Remote Sensing 5 (2), pp. 349-363.

Kaiser, H.F., 1958:
The varimax criterion for analytic rotation in factor analysis.
Psychometrika 23.

Kiefer, D., 1973:
Fluorescence properties of natural phytoplankton populations.
Marine Biology 22(3), 263-269.

Kim, H.H. et al, 1981:
Ocean chlorophyll studies from a U-2 aircraft platform.
JGR 85, pp.3982-3990.

Kim, H., H. van der Piepen, V. Amann and R. Doerffer, 1985:
An evaluation of 685 nm fluorescence imagery of coastal waters.
ESA Journal 9(1), 17-27.

Lin, S., G.A. Borstad and F.F.R. Gower, 1984:
Remote sensing of chlorophyll in the red spectral region.
Remote Sensing of Shelf Sea Hydrodynamics (ed. by J.C.J. Nihoul).
Elsevier Science Publishers B.V. Amsterdam, pp. 317-336.

Morel, A. and L. Prieur, 1977:
Analysis of variations in the ocean color.
Limnol. Oceanogr. 22, 709-722.

Mueller, J.L., 1973:
The influence of phyto plankton on ocean color spectra.
Ph.D. Thesis, Oregon State University, Corvallis, Oregon.

Smith, R.C. and W.H. Wilson, 1981:
Ship and satellite bio-optical research in California Bight.
Oceanography from Space (Ed. J.F.R. Gower) Plenum Press New York,
Mar. Sci. 13, pp.281-294.

Uberla, K., 1971:
Faktorenanalyse.
Springer Verlag, Berlin.

van der Piepen, H., H.H. Kim, W.D. Hart, V. Amann, H. Helbig,
A.F.G. Fiuza, M. Viollier and R. Doerffer, 1983:
The ocean color experiment (OCE) on the second orbital flight test
of the Space Shuttle (OSTA-I).
IEEE Trans. Geoscience and Rem. Sens. GE-21 (3), 350-357.

Viollier, M., D. Tanre and P.Y. Deschanps, 1980:
An algorithm for remote sensing of water color from space.
Boundary Layer Met. 18, pp.247-267.

Walker, G.A.H., V.L. Buchholz, D. Camp, B. Isherwood
and J.F.R. Gower, 1975
A silicon diode array spectrometer for ocean colour monitoring.
Canadian Journal of Rem. Sensing 1, 26-30.

7. ACRONYMS

CZCS .... Coastal Zone Color Scanner
ECR ..... Eighteen Channel Radiometer
IOSS .... Institute of Ocean Sciences Spectrometer
FLEX .... Fladengrund Experiment
FLUREX .. Fluorescence Experiment
FLH ..... Fluorescence Line Height
FLI ..... Fluorescence Line Imager
FPN ..... Forschungsplattform Nordsee
NFLH .... Normalized Fluorescence Line Height
OCE ..... Ocean Color Experiment
OCEG .... Ocean Color Scanner Experiment, German Bight
OCR ..... Ocean Color Radiometer
OCS ..... Ocean Color Scanner
SCR ..... Six Channel Radiometer
SST ..... Sea Surface Temperature

APPENDIX

8. INSTRUMENT SPECIFICATIONS

8.1.1 Eighteen Channel Radiometer (GKSS)

In context with the experiments FLEX, OCEG and FLUREX, the Eighteen Channel Radiometer (ECR) was mounted on the aircraft (FLEX) or alternatively on R/V Monitor (OCEG) and R/V Alkor (FLUREX) to measure upwelling radiance spectra in coarse steps. The ECR specifications are listed in Table 3.

FOV	1^{o}
IFOV	non applic.
Quantization	8 bit
Number of channels	18
Spectral range ...	420 - 720 nm (equal steps,), 895 nm
Half widths:	9 - 12 nm each

Table 3. ECR specifications during FLEX and OCEG.

8.1.2 Ocean Color Scanner (NASA)

In context with the experiment OCEG, NASA's OCS was mounted on the DFVLR DO 28 and flown during August 1981 over the Elbe river and estuary for mapping flights (altitude 3.600 m) and for ship overflights (R/V "Monitor") at different altitudes. The OCS specifications are listed in Table 4 on page 45.

8.1.3 IOS Spectrometer (DFO)

In context with the experiment FLUREX, the IOSS was mounted on the DFVLR DO 28 (pointing forward under the Brewster angle) and flown during April 1982 above test sites in the Kiel Bight and the German Bight. In addition the IOSS was also mounted on the

FOV		90^{o}
IFOV		2.6 mrad
Quantization		10 bit
Spectral bands:		
	Centre wavelengths:	Halfwidth:
	464 nm	20 nm
	492 nm	20 nm
	524 nm	20 nm
	552 nm	20 nm
	587 nm	20 nm
	618 nm	20 nm
	655 nm	20 nm
	682 nm	20 nm
	772 nm	100 nm

Table 4. OCS specifications during OCEG 1981.

R/V Alkor during the same period and operated in the Kiel Bight. The IOSS specifications are listed in Table 5 on page 45.

FOV	0.7^{o} x 0.2^{o}
IFO	not applic.
Quantization	12 bit
Spectral range	400 to 800 nm
Number of channels	256
Halfwidth of channels	14 nm
Tilt (forward or backward)	53^{o}
Response time	0.1 sec (min.), 2 sec (typical)

Table 5. IOSS specifications during FLUREX 1982.

8.1.4 Six Channel Radiometer (DFVLR)

In context with the experiment FLUREX, DFVLR's SCR was mounted in a nadir looking mode on the the DFVLR DO 28 and flown in a large variety of flight patterns (mapping flights, different altitude flights, multi-temporal flights) during April 1982 above the German Bight and the Kiel Bight. The SCR specifications are listed in Table 6.

FOV	5^{o}
IFOV	not appl.
Quantization	12 bit
S/N ratio	2000 : 1
Spectral bands:	
Centre wavelengths:	Halfwidths:
649 nm	11 nm
660 nm	11 nm
670 nm	12 nm
682 nm	10 nm
699 nm	12 nm
749 nm	14 nm

Table 6. SCR specifications during FLUREX 1982.

Sun Stimulated Chlorophyll Fluorescence within a Daily Cycle

R. Doerffer and J. Fischer

GKSS Forschungszentrum Geesthacht

CONTENT

1. Introduction
2. Data base
2.1 Field experiment
2.2 Model calculation
3. Results
3.1 General data
3.2 Radiance data
3.3 Derivation of irradiance and skylight reflectance parameters from radiance measurement
3.4 Test of algorithms
4. Discussion and conclusions
Acknowledgements
References

1. Introduction

The usefulness of natural sun stimulated fluorescence of chlorophyll for remote sensing of phytoplankton has been demonstrated by a number of investigations /1,2,3,4/.

One of the main problems concerns the variability of the specific fluorescence efficiency as a function of the physiological state of the organisms as well as of environmental factors as illumination. From investigations using in-situ fluorometers with artificial light source it is known that a changing irradiance - due to water depth or daylight changes - can have a strong effect on the fluorescence stimulated by the artificial light source /5,6,7,8/. However, the influence of these quantities to sunlight stimulated chlorophyll fluorescence has not been investigated.

This paper will answer the following three questions by combining results of a field experiment and model calculations:

1. What is the efficiency of the conversion of light absorbed by phytoplankton into light emitted by fluorescence?

2. Does the efficiency vary as a function of irradiance due to the sun elevations within one day?

3. Which algorithm can be used to calculate the fluorescence from radiance spectra of the water surface accounting for changing irradiance?

2. Data Base

2.1. Field Experiment

The field experiment - to investigate the daily cycle of the natural fluorescence efficieny of phytoplankton - was part of the Fluorescence Remote Sensing Experiment FLUREX. It was carried out in the Kiel Bight (Baltic Sea) on 27 April 1982 from the research vessel ALKOR of the Institute für of Meereskunde, Kiel.

The ship was anchored from 8:20 to 17:20 h in a calm bay, where advection of water masses was expected to be low.

The following parameters were recorded:

Water leaving radiance and downwelling irradiance were measured using a filter wheel spectrometer (EO-SUAREZ) with 16 interference filters in the spectral range 420 - 720 nm and 1 filter at 895 nm (half bandwidth 10 - 12 nm). The instrument was mounted at the ships bow to avoid shading and reflection of the ships body. The observation angle was about 20° off nadir with a sun azimuth angle of 160° - 200° to minimize sun and skylight specular reflectance.

Chlorophyll concentrations were measured from acetone extracts of water samples using the UNESCO method for calculating the concentration. The data were interpolated in time using the record of a continuous flow TURNER fluorometer.

Additional parameters used for this investigation were the global irradiance, measured on deck, and the suspended matter dry weight from water samples.

The spectrometer samples at a rate of 2 spectra per second. To enhance the signal/noise ratio about 50 spectra were integrated to form one sample after passing a procedure which skips all spectra below or above the standard deviation of the set. During this experiment 21 samples, distributed over the observation day, were used together with corresponding chlorophyll concentration data to investigate the problem.

2.2 Model Calculation

To analyze different factors influencing the radiance spectra some aspects of the experiments were also

simulated with the GKSS Radiative Transfer Model. This model /9,10/ simulates multiple scattering in water and atmosphere, all sun- and observation-angles and a rough sea surface for a prescribed wind speed.

For the requested task the following situation was assumed:

atmosphere:	cloudless, visibility > 20 km
sun elevation:	variable, as for the field experiment
sea surface:	calm, wind speed 1.5 m/s
yellow substance:	constant, a_y(380nm) = 1.5 m-1
suspended matter:	2mg/l constant
chlorophyll:	variable, as for the field experiment
stratification:	neglected

Multispectral radiances including fluorescence were calculated according to optical properties of water, yellow substance and suspended matter and the absorption spectrum of phytoplankton /11,12,13,14/ ,taking into account a scalar irradiance of phytoplankton and a constant fluorescence efficieny of 0.3 % of the absorbed radiation. The fluorescence peak is centered around 685 nm with a Gaussian distribution according to /15/.

The wavelengths used for the calculation were slightly different from those of the radiance measurements:

Model: L(640) L(670) L(685) L(711)

The radiances L were calculated for just above the sea surface including skylight specular reflectance.

3. Results

3.1 General Data

The general data describing the situation of the day are:

observation time: 8:20 h - 17:20 h Mean European Summer Time
weather: cloudless, calm, visibility > 10 km
zenith distance of sun: 70 - 40 deg
global irradiance: 350 - 815 W m^{-2}

During the observation period the irradiance was changing by a factor of 1 : 2.3 . The chlorophyll concentration (Fig.1) varied from 2.5 to 4 mg m^{-3} with a minimum at noon and thus an opposite trend compared to irradiance (fig.2).

3.2 Radiance data

All measured radiance spectra are summarized in fig.3. The following characteristics are obvious:

The maximum radiance at a wavelength of 550 nm and the steep decrease to the blue part of the spectrum indicate high yellow substance concentration, which is typical for water of the Baltic sea. Radiance spectra for low and high sun elevation (Fig.4) both contain the expected maximum assigned to chlorophyll fluorescence with a low value for the noon sample and a high value for the sample with low sun elevation.

For the extraction of the fluorescence signal the radiances at 645, 665, 685 and 724 nm were analyzed according to the scheme in fig.5. L(645) and L(724) were used to calculate a linear baseline for L(685), with

$$base = (L(645) + L(724))/2$$

For the model data the radiances at 640 and 711 nm were used with

$$base = (L(711)*(685-640) + L(640)*(711-685)) / (711-640)$$

From L(665) also an estimate of the chlorophyll absorption centered at 670 nm can be derived, as used in one of the algorithms. The radiance at 685 nm above the baseline - the fluorescence line height - was assumed to be caused by chlorophyll fluorescence only. Values for the fluorescence line height were found in the range of 0.10 to 0.16 $W\ m^{-2}\ sr^{-1}\ \mu m^{-1}$.

3.3 Derivation of irradiance and skylight reflectance parameters from radiance measurement

According to the main goal of the experiment - to test whether the fluorescence efficiency is independent of the sun elevation - it is necessary to find an algorithm, which allows to normalize the fluorescence signal with a measure of the downwelling irradiance. It was intended to extract this information directly from the radiance measurement, e.g.from the baseline radiance.

The baseline radiance as measured above the sea surface contains specular reflected skylight as well as subsurface radiance. Both are related to the downwelling irradiance.

Two approaches using the baseline as an irradiance measure are possible:

1. The baseline radiance is dominated by the specular reflected skylight; without further manipulation

one uses in this case the close relation between the near nadir sky radiance and the downwelling irradiance.

2. One can try to eliminate the reflected skylight from the baseline radiance and use then the remaining baseline radiance as a measure of irradiance. In this case the reflectance of the water body - the subsurface radiance - is dominant.

In our experiment the radiometer was pointed 20° off nadir to meet the minimum in skylight reflectance. The remaining reflected skylight around 685 nm is very low compared to the blue-green spectral range (fig.6).

An estimate of the relation between the baseline radiance and the downwelling irradiance can be derived from the time series of these two parameters (fig.2, fig.7). To confirm the indicated correlated trend we have compared the corresponding parameters from the model data base. Fig.8 shows the relation between the baseline radiance and the reflected skylight radiance, which was calculated from the nadir skylight radiance with a specular reflectivity of 0.02. Zenith distances of 35, 50.7, 66.5, and 82.2° and constant concentrations of water constituents have been considered. A significant linear correlation between both parameters is obvious.

The same procedure using the model was carried out to compare downwelling irradiance Ed with the baseline radiance L : For zenith distances from 35 to 82.2° the correlation is not linear.

A prerequisite to use either the baseline radiance for a normalisation of the fluorescence line height or the radiance at 724 nm for skylight correction of the baseline is a constant ratio of the radiances at 645 and 724 nm.

The field data confirm this prerequisite: the ratio L(724/L(645) is nearly constant for the period 9h to 16h (fig.10). Thus for that period of the day, which is suitable for passive remote sensing, the baseline radiance or the radiance at 724 nm may be used for correction procedures as discussed above.

On these premises we have tested different algorithms using field and model data as described in the next chapter.

3.4 Test of algorithms

At first the classic green blue algorithm in form of the ratio L(545)/L(445 was related to the chlorophyll concentration (fig.11). The unsignificant negativ correlation derives mainly from the problem of the

specular reflected skylight, which cannot be corrected with the procedure described above due to the high skylight in the blue-green spectral range. The time series of this parameter as well as that of the ratio (L(545)/Ed(545)) / (L(445)/Ed(445)) is given in fig.12. For the period 10h to 16h it reflects the course of the chlorophyll concentration. But for low sun elevations, where the skylight becomes dominant under clear sky conditions, the green/blue ratio parameter do not longer apply.

The simplest fluorescence parameter, which has to be tested, is the radiance at 685 nm above the baseline (the fluorescence line height):

$$L_u(685) - base$$

Assuming a constant fluorescence efficiency one has to expect that this parameter must depend - beside on concentration - on the amount of light available for the algae (the irradiance). Fig.13 shows the relation as a function of the chlorophyll concentration. Because the high concentrations were found in the morning and evening one can conclude that the downwelling irradiance is responsible for the negative and low correlation coefficient.

The next step was to try to normalize the fluorescence line height by the baseline radiance under the assumption that the baseline is a measure for the downwelling irradiance (s.3.3) and therefore also a measure for the amount of light available for the fluorescence process:

$$Fluorescence = (L(685) - base)/base$$

This algorithm calculates the fluorescence line height as fraction of the baseline radiance. The time series of this parameter (fig.14) does agree with the temporal chlorophyll distribution of that day.

This fluorescence parameter is highly correlated with the chlorophyll concentration reaching a correlation coefficient of 0.97 (Fig.15) and giving a regression line of

$$fluor. = -0.0303 + 0.0667 * Chl.Conc.\ [mg\ m^{-3}].$$

The same algorithm was also applied to the model data, which were calculated for the same concentrations of chlorophyll and suspended matter, sun elevation, visiblity and sea surface roughness as the field data; for Gelbstoff a mean value for this area was assumed. The result is presented also in fig.15. The regression line does agree with that of the field data.

To check whether this relation is independent of the

irradiance the model calculation was carried out also for a constant sun zenith distance of 50.7° (fig.16). The slope of this regression line is much flatter:

$$\text{fluor.} = 0.0824 + 0.0307 * \text{Chl.Conc. [mg m}^{-3}\text{]}$$

We assume that the difference between both slopes must be related to the influence of the skylight reflectance, which is - as mentioned - not linear correlated with the downwelling irradiance.

To eliminate or reduce the influence of the specular reflected skylight we have used the radiance at 724 nm for the correction of the specular reflected skylight. To a first approximation water is dark at this wavelength and the wavelength dependence is small in the range 645 to 724 nm .

Under these assumptions we have substracted L(724) from L(685),L(665) and L(645) and - after this manipulation - used the algorithm as described above again.

For the field data (fig.17) we get

$$\text{fluor.} = -0.110 + 0.144 * \text{chlor. conc. [mg m}^{-3}\text{]}$$

and for the model data (fig.18) we get

$$\text{fluor.} = 0.371 + 0.132 * \text{chlor. conc. [mg m}^{-3}\text{]}$$

Nearly identical slopes indicate that the above correction procedure for specular reflected skylight allows an elevation independent calculation of the fluorescence line height.The difference in the bias term must be related to the different wavelengths used for the baseline calculation.

Another possible algorithm is to calculate the difference between the radiances at 665 nm - which is influenced by the absorption of chlorophyll - and 685 nm:

$$\text{fluor.} = (L(685) - L(665))/\text{base}$$

For field data a slightly better correlation coefficient of 0.98 is found if compared to the algorithm using the difference between the baseline radiance and L(685). Also the agreement between the time series of this parameter and the chlorophyll concentration is improved (fig.19).

4. Discussion and conclusions

The first obvious result is the high linear correlation between fluorescence line height and chlorophyll density

even for a narrow range of 2.5-4.0 mg m-3 chlorophyll. It demonstrates that the fluorescence derived from radiances measured above the sea surface allows to resolve concentrations in the same order as conventional methods using water samples.

The assessment of the algorithms is complicated due to the correlation between sun elevation and chlorophyll concentration during the observations. Since the absolute fluorescence line height is a function of irradiance, it was necessary to find an algorithm independent of sun elevation within that period of the day, where passive remote sensing is possible.

A normalization by the baseline radiance shows in fact a high correlation between fluorescence and chlorophyll density for our field data, but this may also be due to the correlation between chlorophyll concentration and sun elevation. We have to assume that the relation between specular reflected skylight and irradiance is the main reason for this effect.

The model data have shown that the relation between specular reflected skylight and downwelling irradiance is not linear. That means that the use of the baseline as a measure of the downwelling irradiance is depending on the zenith distance of the sun. It is therefore necessary to eliminate the specular reflected skylight. Because of the fact that at 724 nm the water is nearly black, it is possible to use this channel to estimate the skylight reflectance and subtract the radiance from the other channels used for the fluorescence calculations.

The field data have shown that after this procedure one gets a regression slope which is the same as the slope from model data for a constant sun zenith distance. This procedure seems to be appropiate for chlorophyll determination under conditions of changing sun zenith angles.

For constant illumination, as it is the case for the evaluation of data from sun synchronous satellites, the simple fluorescence line height algorithm without normalization is the optimum procedure. In this case the specular reflected light is automatically eliminated by the difference procedure itself. It was demonstrated that the spectral ratio of the two baseline channels is constant during mean to high sun elevations, which is a prerequisite for this procedure.

Finally the question has to be answered whether the fluorescence efficiency is constant at least for the period of the day where passive remote sensing can be carried out. The high significant linear relation between chlorophyll concentration and fluorescence derived from the field data as well as from the model data and its good agreement (fig.15) confirm that the

efficiency is constant. The good agreement between field and model data also confirms the fluorescence efficiency of 0.3 % for this day. Because this value was found also for other areas, as the North Sea, and by other authors with different methods /8/, it must be assumed, that 0.3% is a typical value.

Another estimate, which can be derived from the experiment, is the fluorescence energy per concentration unit normalized by the downwelling irradiance at 685 nm.

This estimate is derived from the slope of the regression, the irradiance at 685 nm and the height of the baseline. The slope indicates the fluorescence energy per 1 mg m^{-3} chlorophyll in terms of the fraction of the baseline height. .

For the 12h station of the field experiment this value was calculated according to the following scheme using the algorithm with skylight correction:

slope:
0.144061, i.e the fluorescence line is 14.4% above the baseline per 1 mg m^{-3} chlorophyll

baseline radiance:
0.575 W m^{-2} sr^{-1} μm^{-1}

downwelling irradiance Ed(685):
1054 W m^{-2} sr^{-1} μm^{-1}

nominal reflectance of baseline (baseline radiance * π / Ed) : 0.171%

fluorescence albedo:
0.0247 % per 1 mg m^{-3} chlorophyll, without skylight correction this fluorescence albedo is 0.0214%.

Acknowledgements

We thank Dr.R.Boje, Institut für Meereskunde Kiel, for chlorophyll and suspended matter data of the water samples and Prof.Dr.H.Graßl and Dipl.Met. P.Schlüssel for the global irradiance data.

References

1. R.A. Neville and J.F.R. Gower, Passive Remote Sensing of Phytoplankton via Chlorophyll *a* Fluorescence , J. Geophys. Res. 82, 3487 (1977)

2. J.F.R. Gower and G.A. Borstad, Use of the In Vivo Fluorescence Line at 685 nm for Remote Sensing Surveys of Surface Chlorophyll a, in Oceanography from Space, J.F.R. Gower, Ed.(Plenum, New York,

1981), pp. 329-338.

3. R. Doerffer, Factor Analysis in Ocean Colour Interpretation,in Oceanography from Space, J.F.R. Gower, Ed.(Plenum, New York, 1981), pp. 339-345.

4. V. Amann and R. Doerffer, Aerial Survey of the Temporal Distribution of Phytoplankton During FLEX'76, in North Sea Dynamics, Sündermann and Lenz, Ed.(Springer-Verlag Berlin Heidelberg), pp. 517-529 (1983).

5. D.A. Kiefer, Chlorophyll *a* Fluorescence in Marine Centric Diatoms: Responses of Chloroplasts to Light and Nutrient Stress, Mar. Biol., pp. 23, 39-46 (1973)

6. M.R.Abbott, P.J. Richerson and T.M. Powell, In situ Response of Phytoplankton Fluorescence to Rapid Variations in Light, Limnol. Oceanogr., 27(2), pp. 218-225 (1982)

7. B.J. Topliss, Optical Measurements in the Sargasso Sea: Solar Stimulated Chlorophyll Fluorescence, Oceanol. Acta, 8(3), pp. 263-270 (1985)

8. K.P. Günther, Die Abhängigkeit der In Vivo Chlorophyll *a* Fluoreszenz marinen Phytoplanktons von der Globalstrahlung, Dissertation Fachbereich Physik der Universität Oldenburg, FRG (1984)

9. J. Fischer and H. Grassl, Radiative Transfer in an Atmosphere-Ocean System: An Azimuthally Dependent Matrix- Operator Approach, Appl. Opt. 23, 1032 (1984)

10. J. Fischer, R. Doerffer, H. Grassl, Factor Analysis of Multispectral Radiances over Coastal and Open Ocean Water based on Radiative Transfer Calculations, App. Optics, 25(3), 448 (1986)

11. L. Prieur and S. Sathyendranath, An Optical Classification of Coastal and Oceanic Waters Based on the Specific Absorption Curves of Phytoplankton Pigments, Dissolved Organic Matter, and Other Particulate Materials, Limnol. Oceanogr. 26, 671 (1981).

12. A. Morel, Optical Properties of Pure Water and Pure Sea Water; in: N.G. Jerlev and E. Steemann-Nielsen (Ed.), Academic Press, 317 (1974).

13. R. Doerffer, Untersuchungen über die Verteilung oberflächennaher Substanzen im Elbe-Ästuar mit Hilfe von Fernmeßverfahren, Archiv f. Hydrobiologie 43, 119 (1979).

14. N.K. Hojerslev, On the Origin of Yellow Substance in Marine Environment, in: Workshop on Eurasep OCS Experiment (1979), pp.13-28.

15. H.R. Gordon, Diffuse Reflectance of the Ocean: The Theory of its Augmentation by Chlorophyll a Fluorescence at 685 nm, Appl. Opt. 18, 1161 (1979).

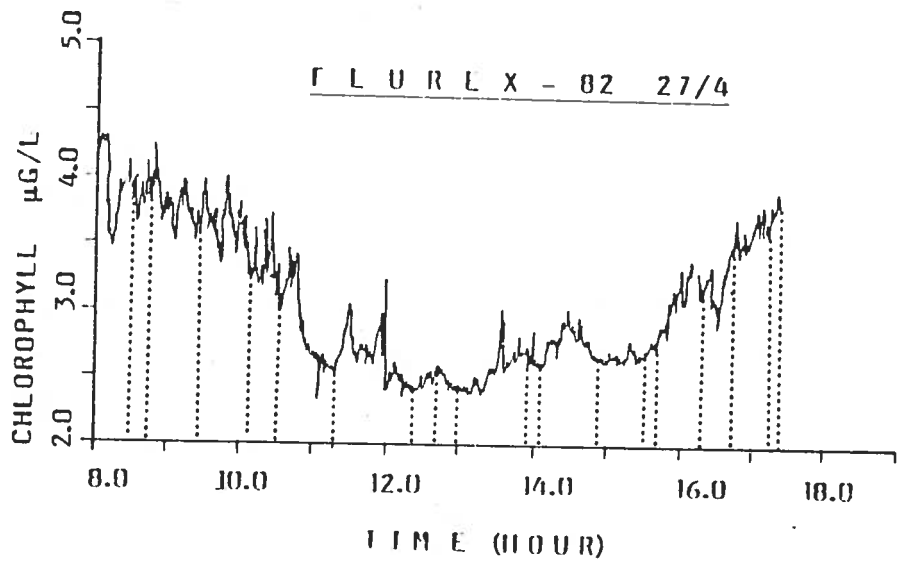

Fig.1 The concentration of chlorophyll at the station Strander Bucht
dotted lines indicate radiance measurements

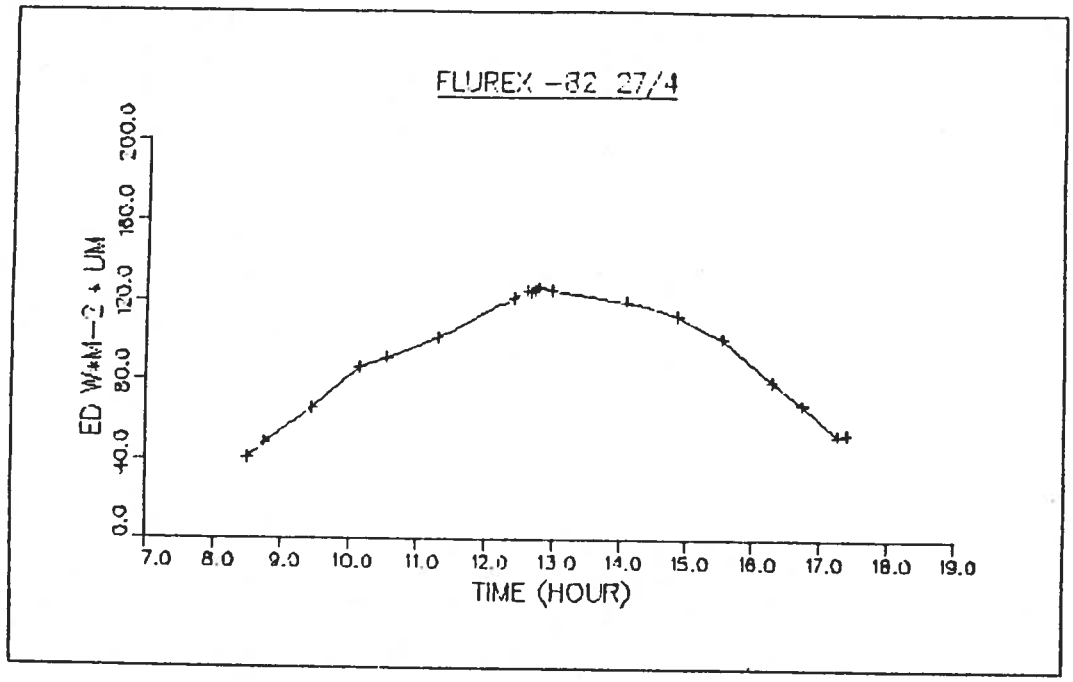

Fig.2 Time series of the downwelling irradiance at 545 nm

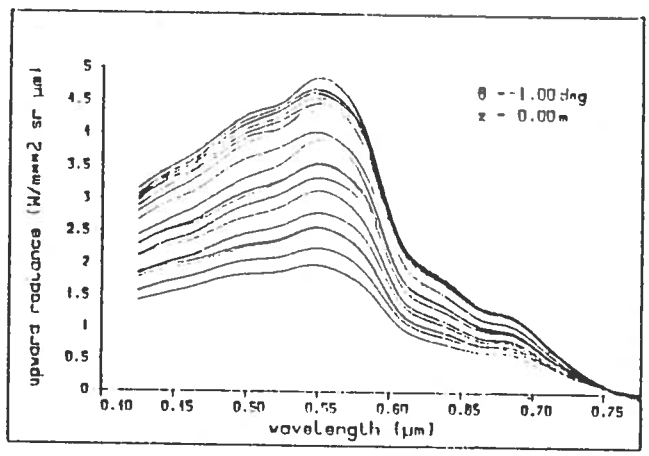

Fig.3 Radiance spectra of station Strander Bucht

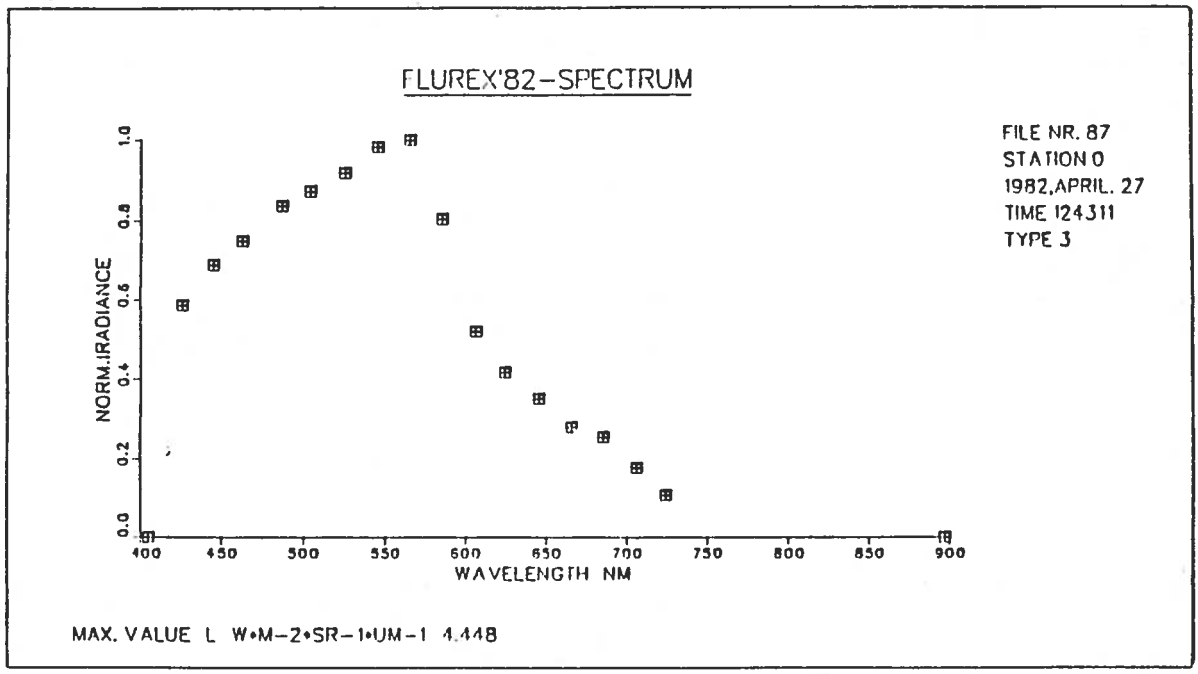

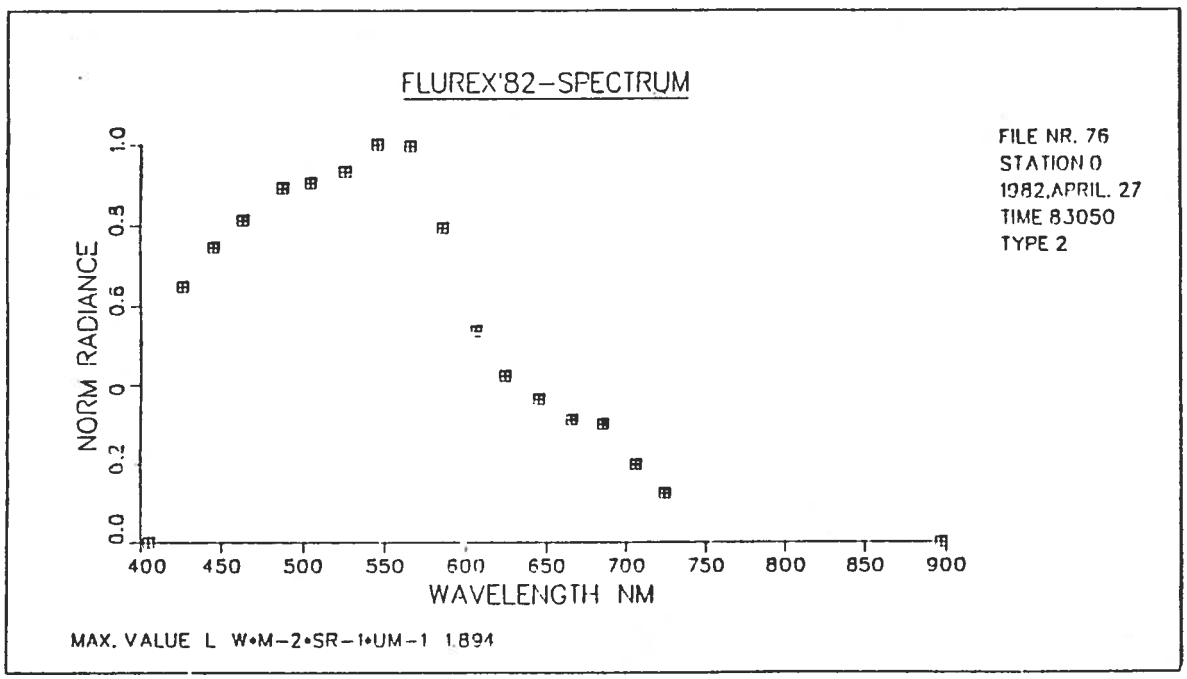

Fig.4: a) Radiance spectra at high sun elevation (50°) chlorophyll concentration 2.6 mg/m^{-3}

b) at low sun elevation (24°), chlorophyll concentration 3.9 mg/m^{-3}

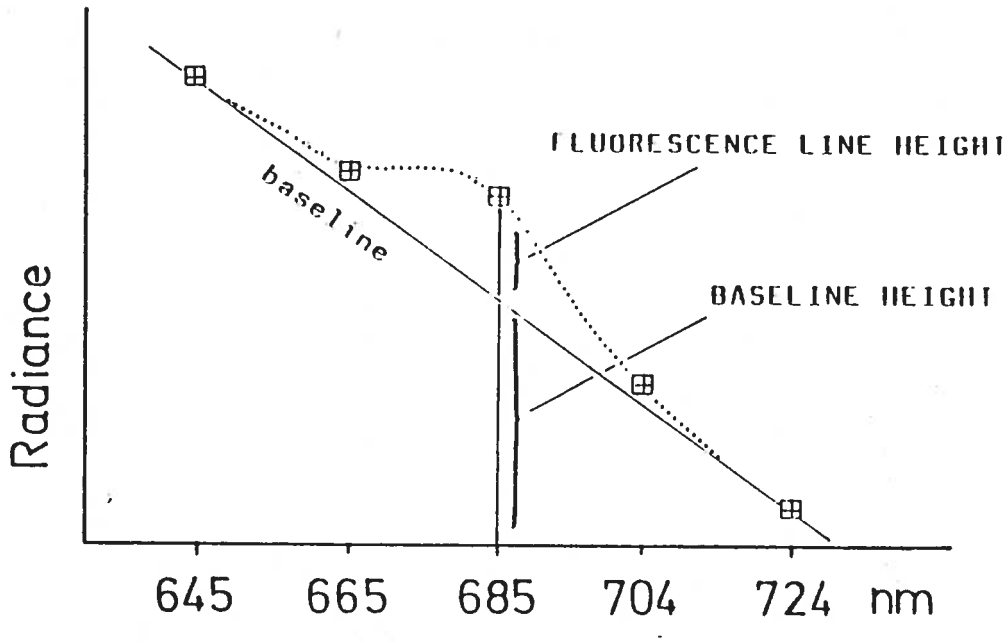

Fig.5 Scheme of parameters in fluorescence algorithms

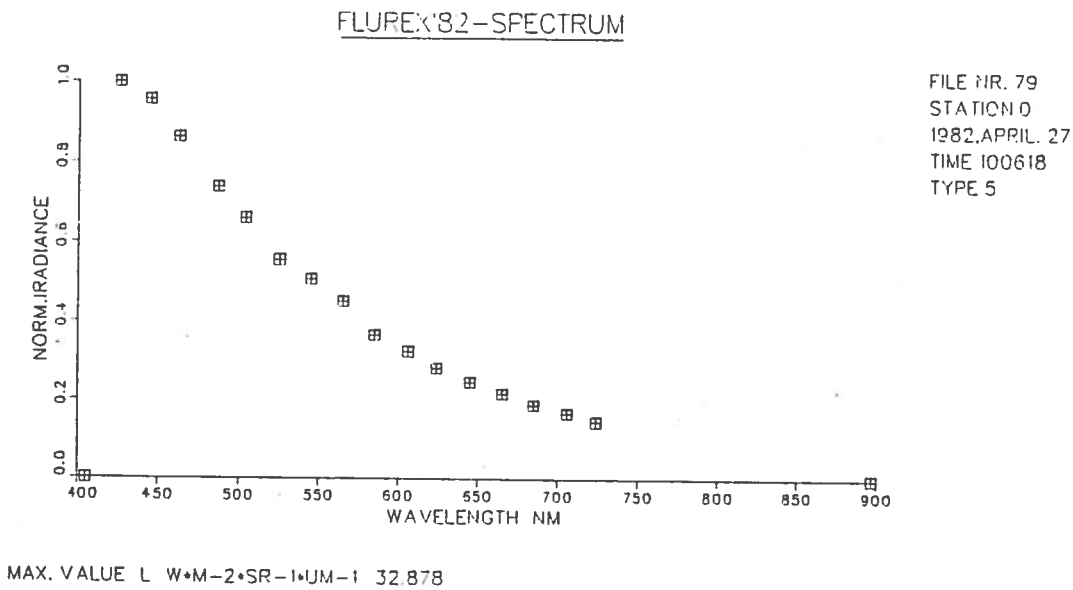

Fig.6 Skylight radiance spectrum

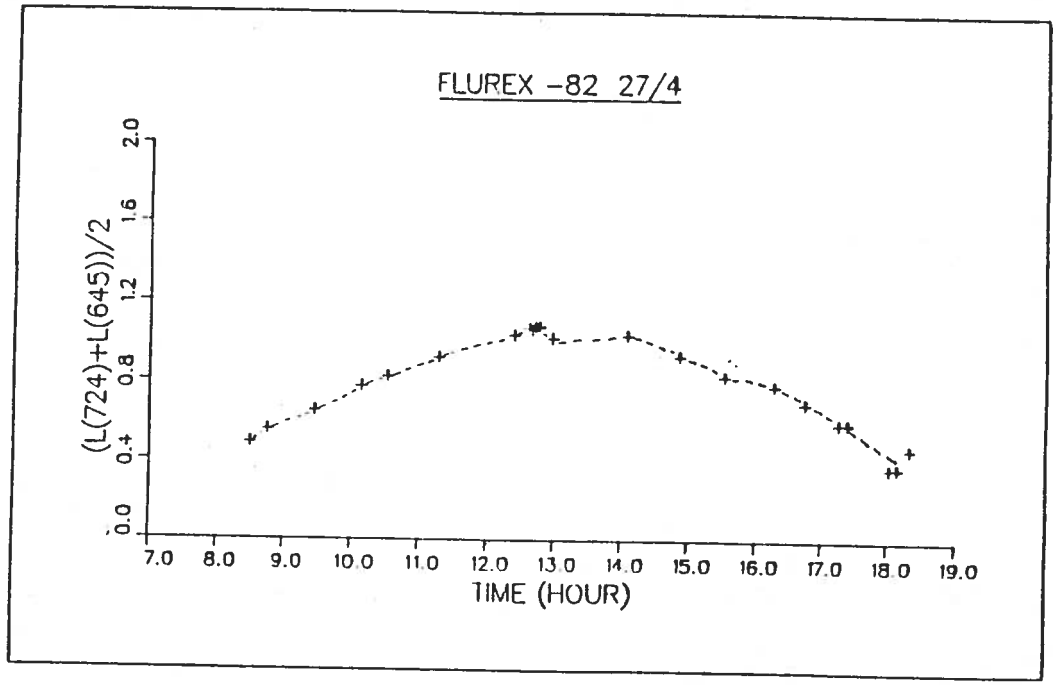

Fig.7 Time series of the radiance baseline at 685 nm

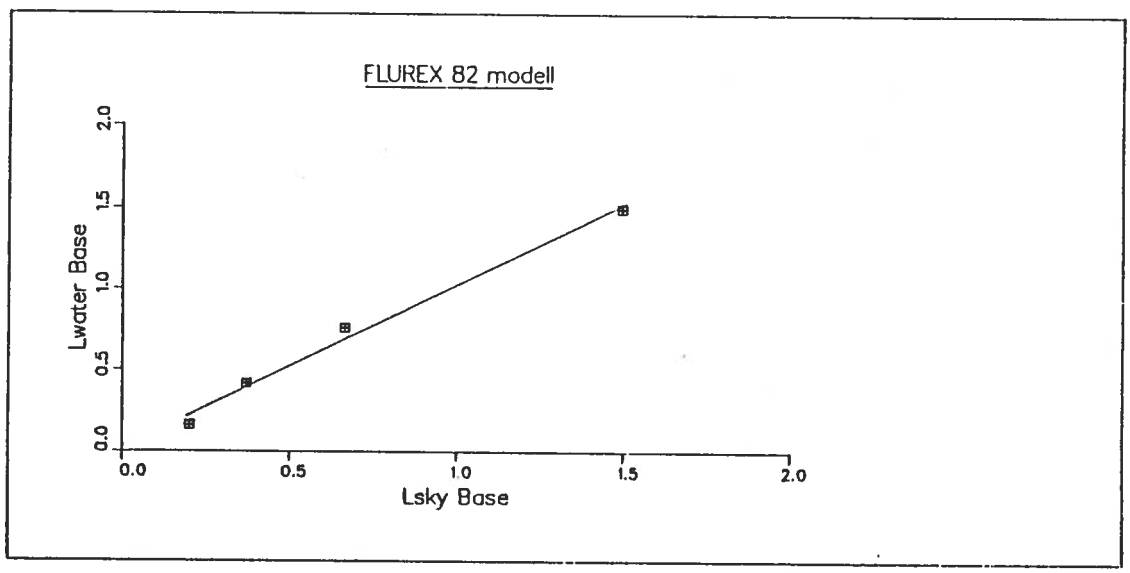

Fig.8 Relation between the specular reflected sky radiance (calculated according to the baseline algorithm) and the fluorescence baseline for zenith angles of 35-82°. Scales are in W m^{-2} sr^{-1} um^{-1}.

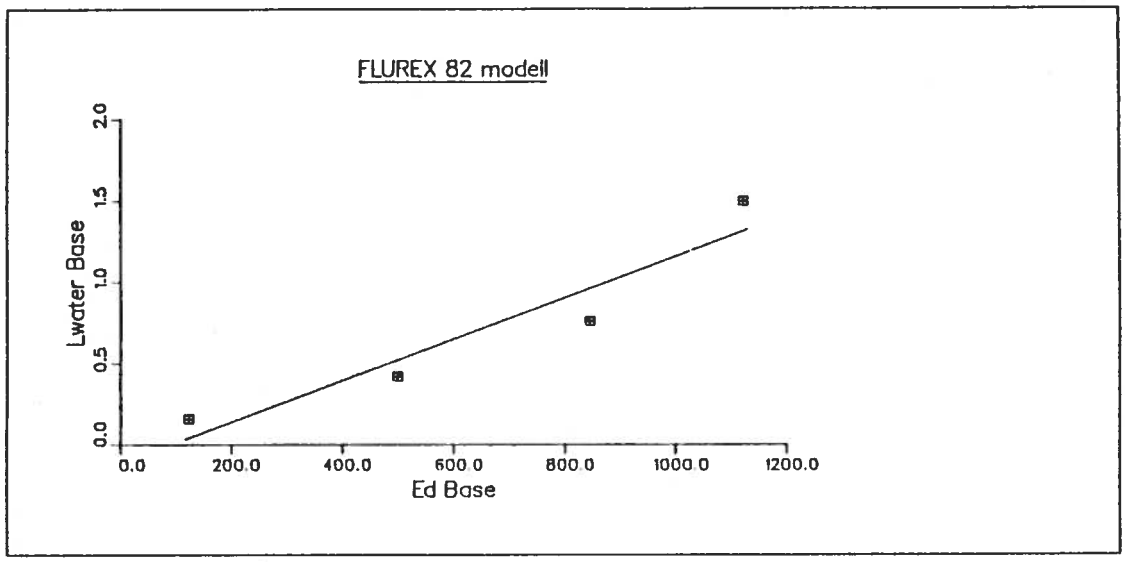

Fig.9 Relation between the downwelling irradiance [W m^{-2} um^{-1}], calculated according to the baseline algorithm, and the fluorescence baseline [W m^{-2} sr^{-1} um^{-1}] for zenith angles of 35-82°

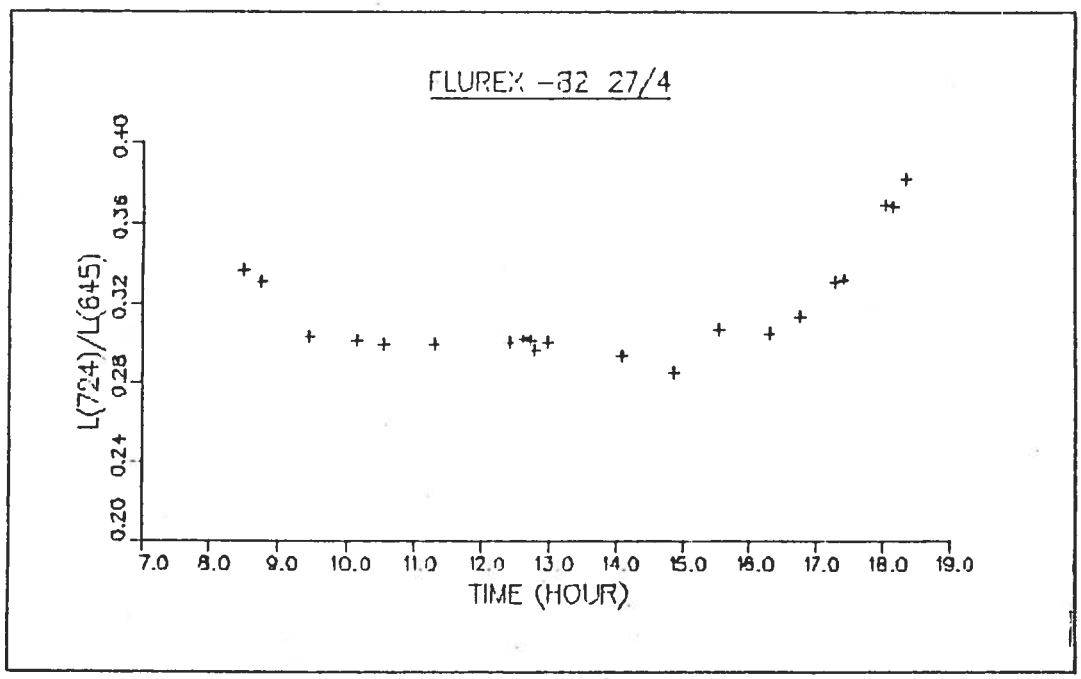

Fig.10 Time series of the radiance ratio L(645)/L(724)

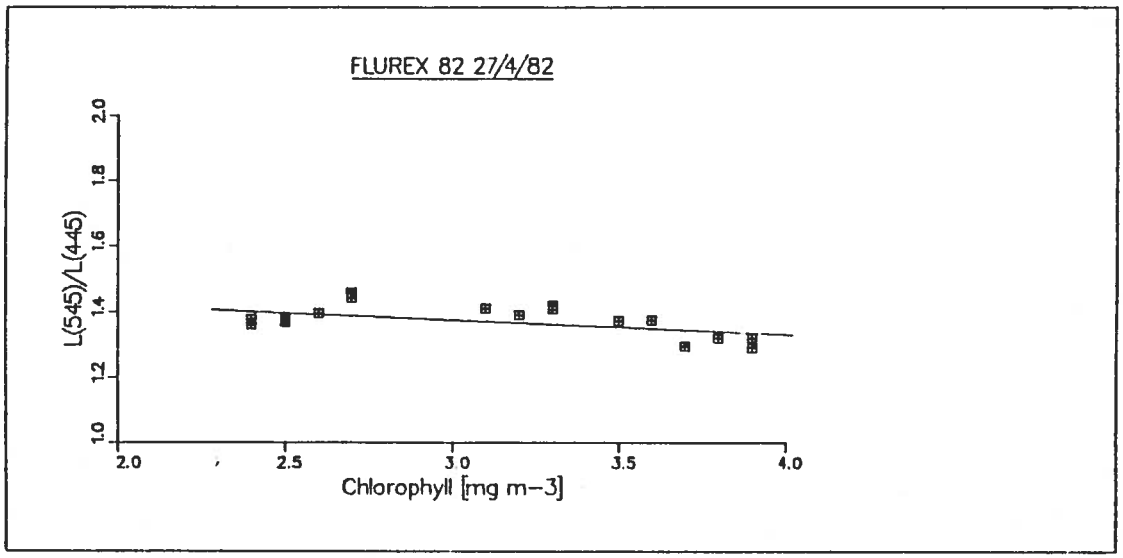

Fig.11 Relation between the chlorophyll concentration and radiance ratio L(545)/L445). Correlation coefficient is -0.55 for n=21.

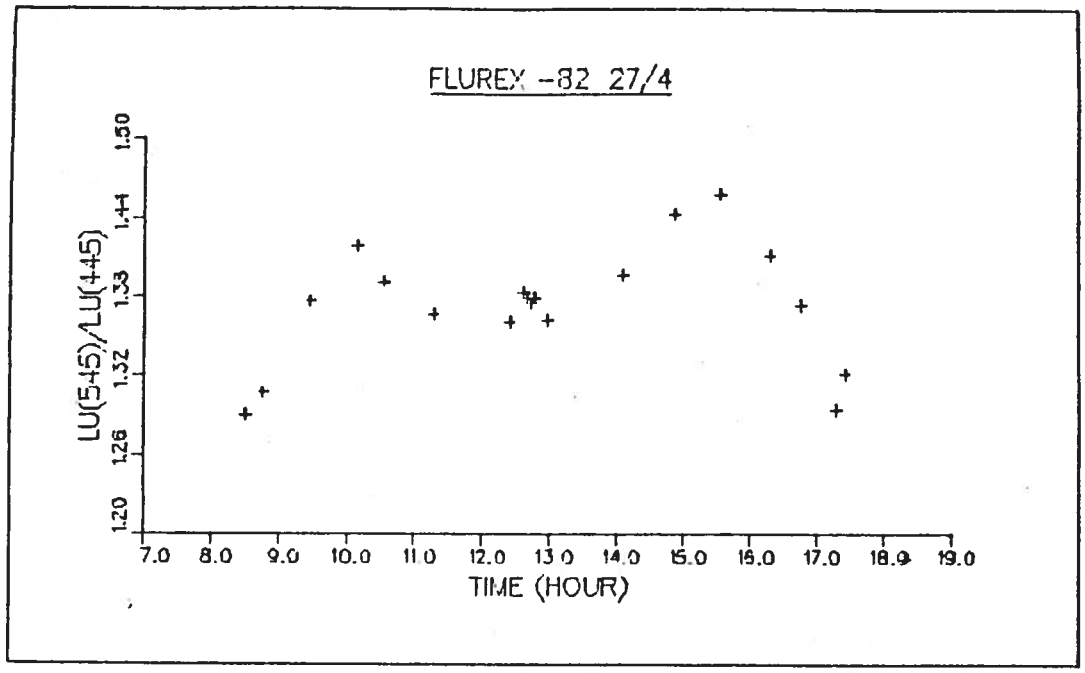

Time series of radiance color ratio

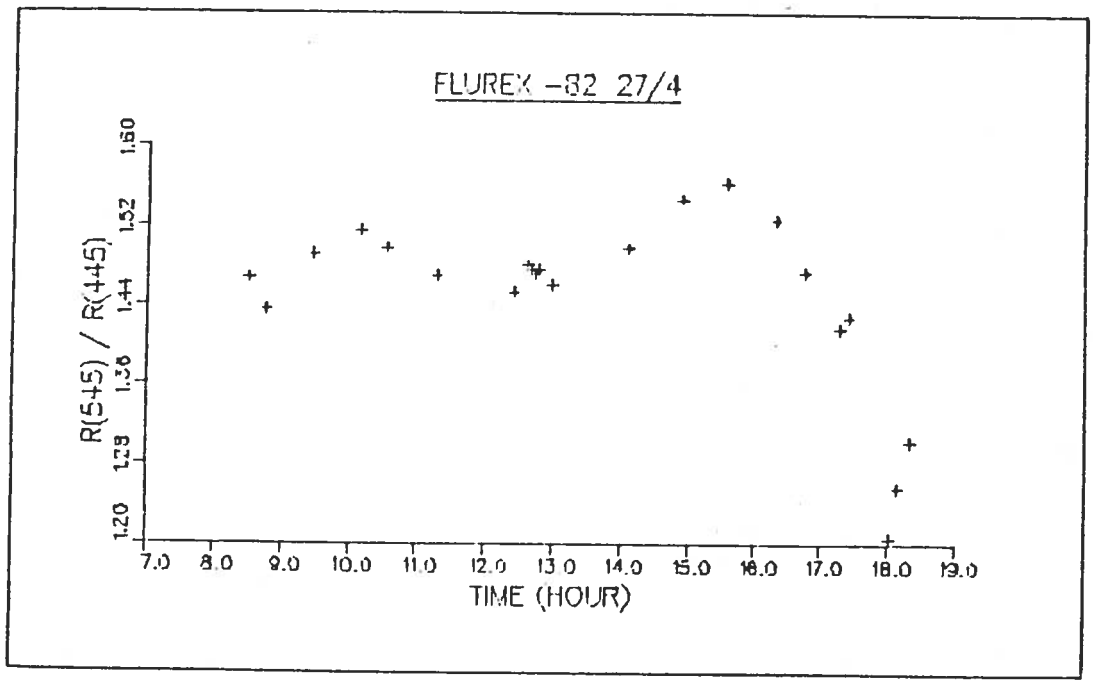

Time series of reflectance color ratio

Fig.12 Time series of the radiance ratio L(545)/L(445) (a) and the corresponding reflectivity ratio (b)

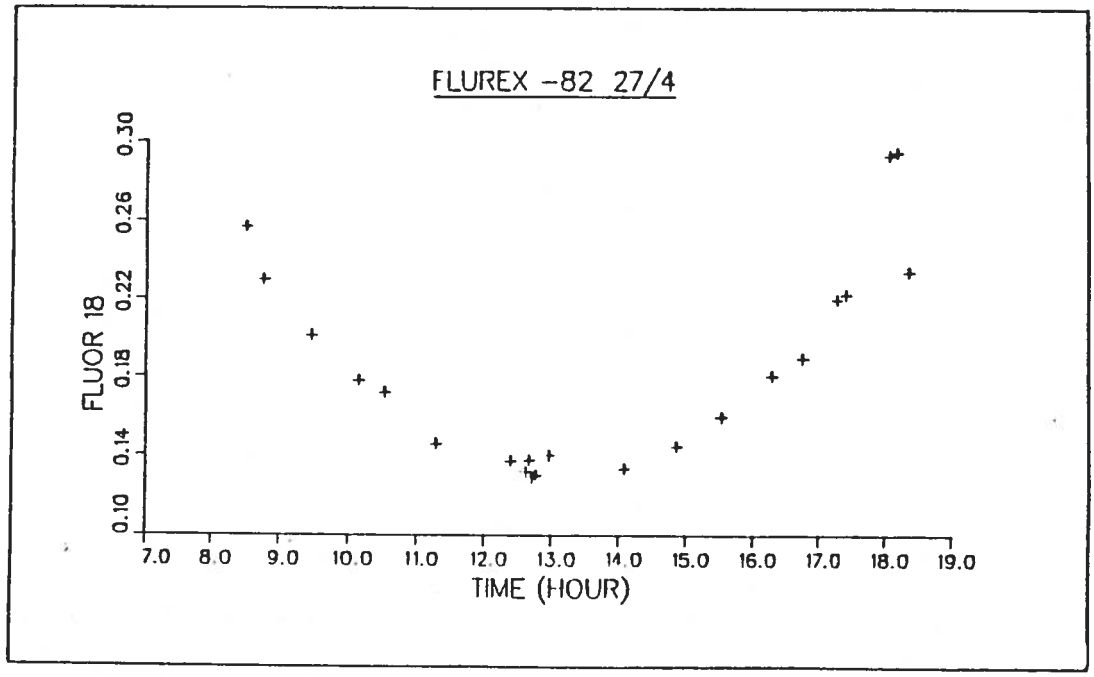

Fig.13 Time series of the baseline normalized fluorescence

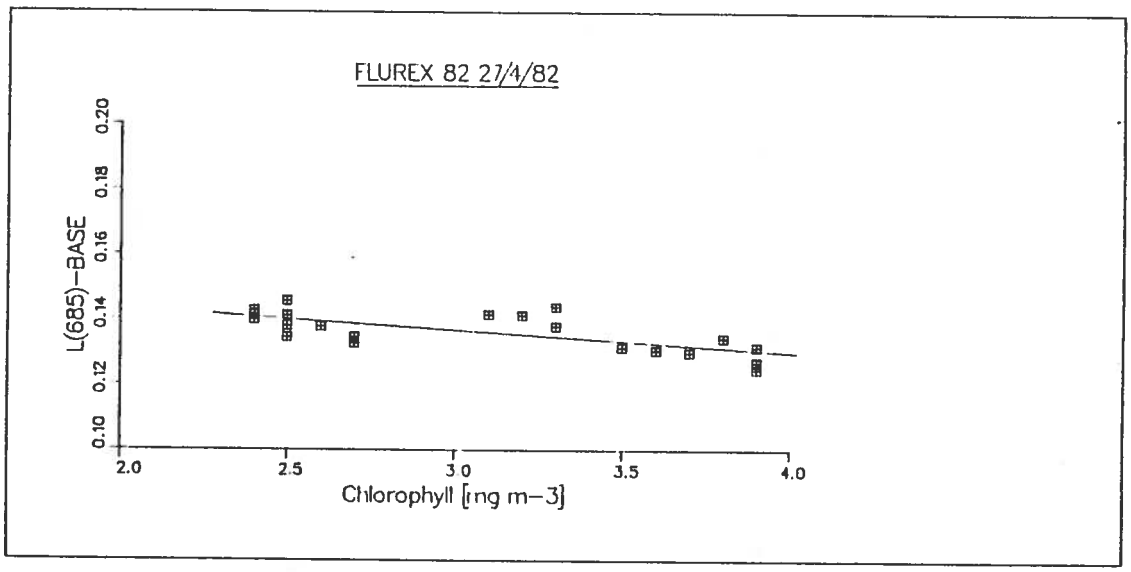

Fig.14 Relation between the chlorophyll concentration and the fluorescence line height [W m^{-2} sr^{-1} um^{-1}] for 21 samples, correlation coefficient is -0.67

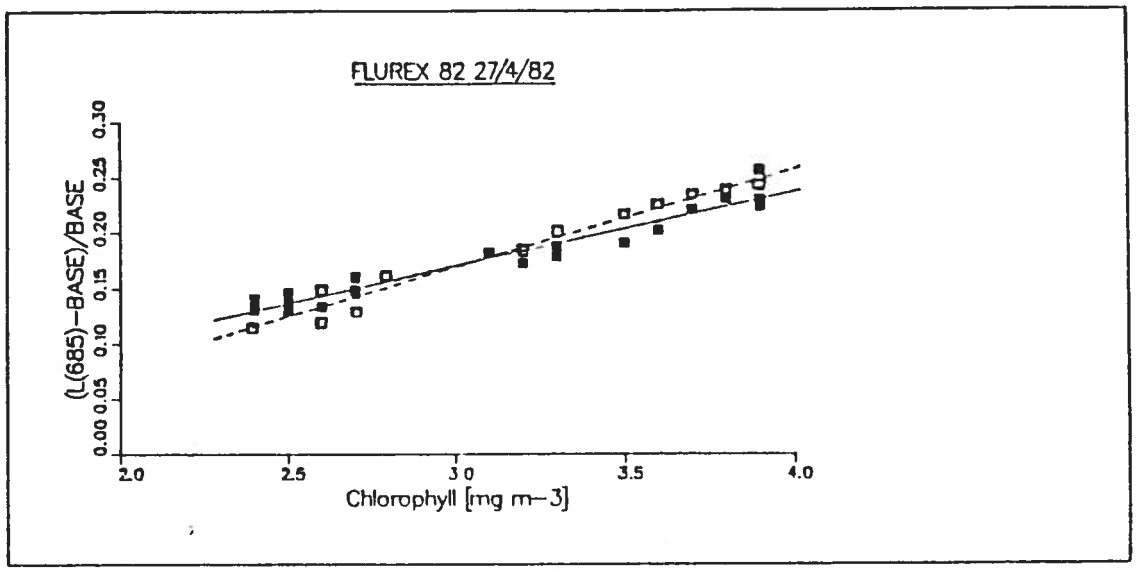

Fig.15 Relation between the chlorophyll concentration and the baseline normalized fluorescence, open squares: model calculation, filled squares: FLUREX data

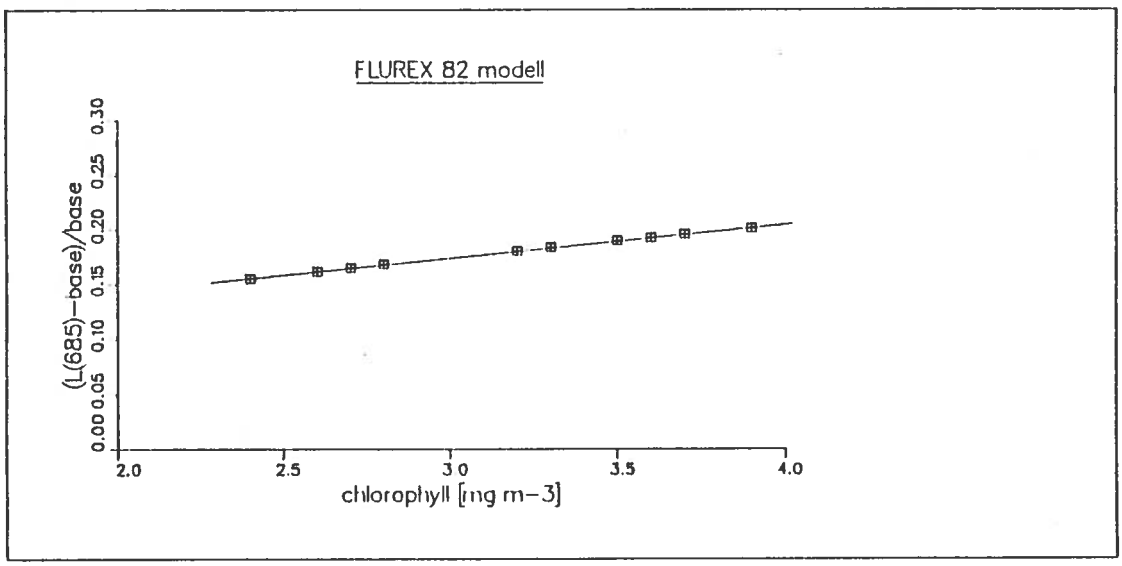

Fig.16 Relation between the chlorophyll concentration and the baseline normalized fluorescence for a zenith distance = 50.7°

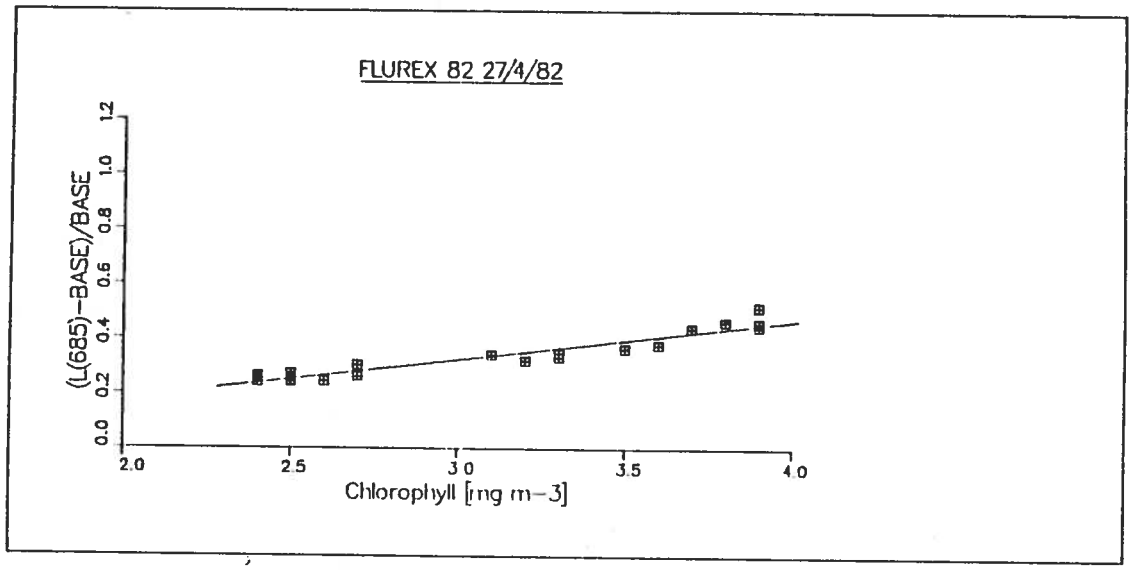

Fig.17 Relation between the chlorophyll concentration and the baseline normalized fluorescence after correction of the specular reflected sky light

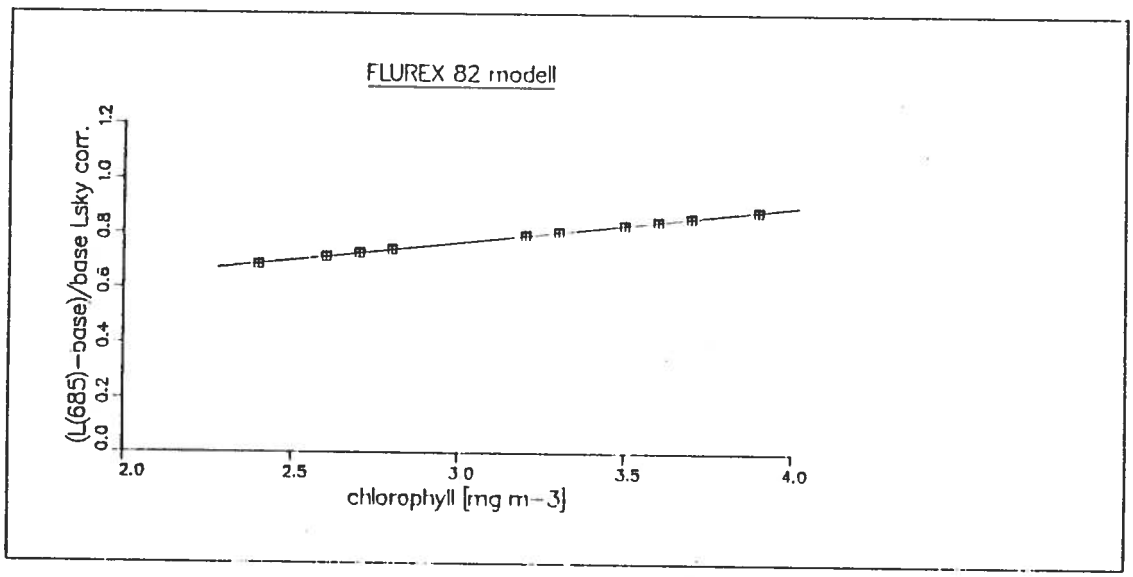

Fig.18 Relation between the chlorophyll concentration and the baseline normalized fluorescence after correction of the specular reflected sky light for a zenith distance of 50.7° ,model data

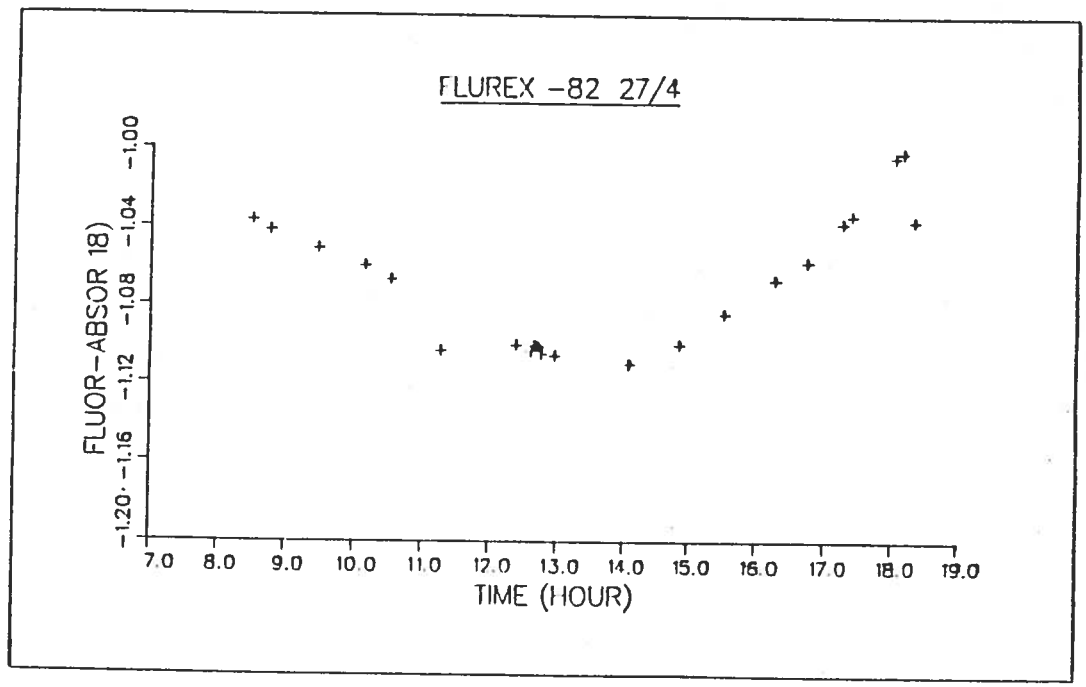

Fig.19 Time series of the fluorescence calculated as the baseline normalized difference between L(685) and L(665)

WORKSHOP ON HIGH SPECTRAL RESOLUTION IMAGING
FOR LAND AND OCEAN REMOTE SENSING
Ottawa, 14-17 October, 1986

Distribution of Gelbstoff in coastal waters and its investigation with laser remote sensing

G. Budéus[1], D. Diebel-Langohr[2], F. Dörre[2],
T. Hengstermann[2], G. Krause[1],
R. Reuter[2], P. Schlittenhardt[3]

[1] Institute for Polar and Marine Research, Bremerhaven, FRG
[2] University of Oldenburg, Oldenburg, FRG
[3] Joint Research Centre, Ispra, Italy

ABSTRACT The fluorescence lidar operated from aircraft allows a nearly synoptic investigation of extended areas of the sea which is particularly important if hydrographic conditions are changing rapidly in time, e.g. due to tides. Among the substances that are detectable with lidar, Gelbstoff (dissolved organic matter) gives rise to very dominant fluorescence signals. Due to its good stability this material can be used as a natural tracer for transport and mixing studies, and for the identification of characteristic water masses and frontal systems. Results obtained in the German Bight and in the Adriatic Sea are reported.

The use of satellites for the delineation of chlorophyll a distributions from water colour measurements at blue/green wavelengths has led to remarkable results over the open ocean where water colour is governed by phytoplankton pigments alone. Problems arise for the interpretation of radiometer data obtained over coastal waters where other substances optically compete with these pigments. The recent development of solar-induced chl a fluorescence as a further and spectrally independent parameter opens a new chance for quantitative investigations of coastal areas where, in addition to chl a, the observed radiance spectrum is strongly influenced by suspended minerals and Gelbstoff.

The further development and verification of this method necessitates an evaluation of new algorithms for data interpretation and sensor calibration which have to be verified on the basis of ground truth measurements, in particular of chl a, Gelbstoff, and light attenuation data.

A method complementary to shipboard ground truth investigations makes use of airborne fluorescence lidars. With these instruments a nearly synoptic survey of extended areas of the sea can be achieved. As an example, mapping of the hydrographic situation present in the German Bight requires a measuring time of 2 hours which is essentially shorter than the tidal period. The ability of a specific and continuous detection of those substances or water column parameters which are investigated with satelliteborne radiometers means that this remote sensor is a candidate for an efficient collection of ground truth data.

Basically the fluorescence lidar consists of a high power laser emitting at near UV or visible wavelengths, and of a gated signal receiver for the detection of laser-induced radiation from the upper water layers. Pulsed laser systems and gated signal detectors are throughout utilized in order to discriminate daylight background from the laser-induced water column return.

In clear case II waters the lower limit of sensitivity is at about the same level as with laboratory instrumentation. However, accuracy is reduced through the air/sea interface transmission: waves give rise to an apparent signal noise of about 10 - 20 % which hampers the resolution of structures at very small scales. Moreover, absolute calibration of airborne fluorosensor signals is a difficult task and has not been achieved so far; signal calibration is generally done on the basis of *in situ* data.

The laser fluorosensor was used as an airborne sensor for the first time by Kim (1973) for algae detection. Since that time a number of working groups have developed and operated such systems for the purpose of hydrographic studies, see, for example, Bristow et al. (1981, 1985), Diebel-Langohr et al. (1985, 1986a-b), Hoge et al. (1982, 1983, 1986), Houghton et al. (1983) and O'Neil et al. (1980).

The following hydrographic parameters can be evaluated:

- spectral light turbidity from the analysis of water Raman scattering (Bristow et al., 1981; Hoge and Swift, 1983),

- Gelbstoff (Bristow and Nielsen, 1981; Hoge and Swift, 1982; Diebel-Langohr et al., 1985, 1986a) and

- Chlorophyll (Kim, 1973; Browell, 1977; Hoge and Swift, 1983) from their specific fluorescence.

The effect of multiple scattering on the detected signal has been theoretically investigated by Gordon (1982), Poole and Esaias (1982) and Schmitz-Peiffer (1986). Spectral light turbidity derived from water Raman scatter intensity takes on some intermediate values between the beam attenuation coefficient c and the diffuse attenuation coefficient K. The actual value depends on the turbidity itself, on the elastic scattering properties of the hydrosol and on the footprint diameter R of the detector telescope field of view (R having a typical value of one meter). Multiple scattering is negligible with $R*c < 1$, and becomes dominant with $R*c > 5$; then, measured attenuation coefficients approach c and K, respectively.

The potential of fluorosensors having time resolving lidar capabilities has been successfully demonstrated. These systems make use of nanosecond laser pulses and of a fast signal detection. Delineation of depth profiles of hydrographic parameters, particularly of water turbidity, has been achieved down to water depths of about 5 attenuation lengths with a resolution in the order of one meter (Hoge and Swift, 1983; Diebel-Langohr et al, 1985, 1986b). Moreover, the possibility of evaluating quantitative attenuation coefficients without the need of an absolute calibration of the instrument has been demonstrated (Diebel-Langohr et al., 1986b).

Algorithms for signal interpretation

The laser-induced scattering or fluorescence signal dP received from a depth interval dz at depth z can be written for arbitrary emission and detection wavelengths as (Browell, 1977)

$$dP = A\,\sigma\,\{\exp(-\tau)/(z+mH)^2\}\,dz \qquad (1)$$

with $z = 0$ at the water surface and z positive downwards, τ representing the effective optical depth

$$\tau = \int_0^z c(z')\,dz' \quad ,$$

with $c = c_{ex}(z,\lambda_{ex}) + c_{em}(z,\lambda_{em})$ sum of light attenuation coefficients at the excitation and the emission wavelengths,

and where

$\sigma = \sigma(z,\lambda_{ex},\lambda_{em})$ quantum efficiency of fluorescence or water Raman scatter,
H aircraft flight height (positive),
m refractive index of water,
A summarizes instrumental factors as the laser power and detector efficiency and others, signal losses in the atmosphere, and the influence of the rough water surface on the beam propagation.

The general solution of the lidar equation (1) for a homogeneous water layer (c = const, σ = const) between depths z_1 and z_2 in a water column with arbitrary stratification is found by integration (Diebel-Langohr et al., 1986a):

$$P_{z1 \to z2} = A \exp\left(-\int_0^{z1} c\, dz\right) \sigma/c$$

$$* \{1/(z_1+mH)^2 - \exp(-c(z_2-z_1))/(z_2+mH)^2\} , \quad (2)$$

whereby the approximation $c >> (z + mH)^{-1}$ is utilized which holds in all practical cases (H ≥ 100 m). This form allows a calculation of the response of water layers which are stratified within the penetration depth of the fluorosensor, and the investigation of other layered structures as e.g. thin films of pollutants on the sea surface.

The total signal received in the depth averaging mode of a laser fluorosensor (i.e. not regarding a depth-resolving lidar capability) is then obtained by the summation of all contributions (2) between $z_1 = 0$ and $z_2 >> 1/c$. Assuming an optically deep and homogeneous water column, the direct integration of the lidar equation (1) yields (Browell, 1977):

$$P = [A/(mH)^2] * [\sigma/c]$$

When measuring water Raman scattering R - which mostly necessitates subtraction of fluorescence background - the corresponding scatter efficiency σ_R can be assumed to be a constant in a first approximation, and the signal intensity reflects the inverse sum of light attenuation coefficients at the laser excitation and the water Raman scatter wavelength:

$$R \sim 1/c = 1/(c_{ex} + c_R) \quad (3)$$

Gelbstoff or chlorophyll fluorescence signals F read:

$$F \sim \sigma_F / c = \sigma_F / (c_{ex} + c_F) \qquad (4)$$

with σ_F the fluorescence efficiency, c_F the fluorescent matter attenuation coefficient.

Normalization of a fluorescence signal to water Raman scattering yields then:

$$F/R = \sigma_F (c_{ex} + c_R)/(c_{ex} + c_F) \qquad (5)$$

The expression (5) is applicable for a delineation of the fluorescent matter concentration which is assumed to be proportional to the fluorescence efficiency σ_F, provided the ratio of attenuation coefficients $(c_{ex} + c_R)/(c_{ex} + c_F)$ shows only moderate changes (Bristow et al., 1981; Hoge and Swift, 1982; Diebel-Langohr et al., 1986a). This implies a careful choice of excitation and detection wavelengths: to avoid errors due to differential absorption, their spectral position should be set as close as possible.

Absorption and fluorescence of Gelbstoff

The potential of remote measurements of Gelbstoff depends on the optical properties of this material. Both absorption and fluorescence determine the laser fluorosensor signal according to the algorithms given above. On the other hand, radiometer data are governed by the absorption characteristic; a possible relevance of sunlight-induced fluorescence for the radiometer signal has not been investigated so far.

Gelbstoff absorption is dominating at blue/green wavelengths where the absorption coefficient can be approximated by an exponential function (Nyquist, 1979; Bricaud et al., 1981). Beam attenuation spectra of filtered water samples of the German Bight , Fig. 1, demonstrate this clearly. The diffuse attenuation coefficient of clear water (Smith and Baker, 1981) is given in the same figure for comparison. The weak absorption bands of Gelbstoff generally found at red wavelengths play only a minor role for the optical characteristic of seawater in this spectral range.

Fluorescence emission of Gelbstoff results in a broad spectral band covering the whole visible beyond the excitation line (Nyquist, 1979; Bristow and Nielsen, 1981).

With excitation at wavelengths in the near UV the spectrum shows a maximum at about 430 nm: Fig. 2.

Small but significant variabilities of the absorption and fluorescence signature are observed depending on the area under investigation. These findings confirm that absorbing and fluorescent compounds of Gelbstoff are not identical. For the same reason a regression analysis of absorption and fluorescence data generally leads to low correlation coefficients in the order of 0.5 - 0.8 (Reuter et al., 1986).

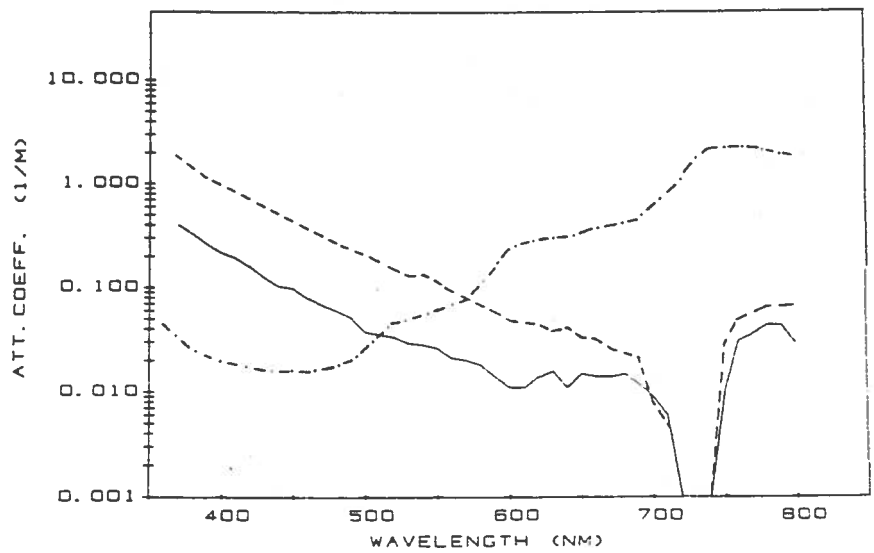

Fig. 1: Spectra of the Gelbstoff attenuation coefficient of samples taken in the German Bight (full line: research platform 'Nordsee', open sea; dashed line: 8°25'E 54°15'N, coastal area), and of the diffuse attenuation coefficient of pure water (dotted line) according to Smith and Baker (1981).

These findings are also supported by investigations of the long term stability of optical parameters of Gelbstoff. It turns out that the temporal variation of absorption and fluorescence is ruled by different time constants under both illuminated and dark storage conditions (Diebel-Langohr et al., 1986c).

Airborne fluorosensor measurements of Gelbstoff

To show examples of data obtained with the airborne fluorosensor method, results of the oceanographic experiments

* ADRIA'84, which was performed in the north-west Adriatic Sea in August 1984, aiming at an investigation of the hydrographic processes present in this area in the summer period (Schlittenhardt, 1986), and

* 'Fronten 2', which was carried out in the German Bight in October 1985 as part of an interdisciplinary research programme on water masses and frontal systems in that area (Krause et al., 1986).

are presented.

The fluorescence lidar utilizied in these campaigns was the Oceanographic Lidar System (OLS) developed at the University of Oldenburg. The instrument is a profiling sensor operated at 200 m flight height which has been designed for near UV (308 nm), blue (450 nm) and green (533 nm) laser excitation and for a sensitive time-resolved signal detection at a few emission wavelengths characteristic of the water column parameters under investigation (Fig. 2). A detailed

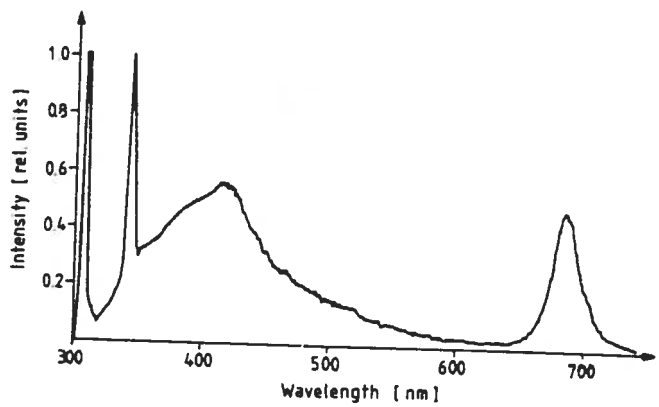

Fig. 2: Emission spectrum of a water sample taken from the German Bight. Excitation wavelength is 308 nm. Water Raman scatter is observed at 344 nm. Gelbstoff and chl a fluorescence show maxima at 430 and 685 nm, respectively.

description of the system has been reported elsewhere (Diebel-Langohr et al., 1985, 1986a).

From the time-resolved lidar data depth-averaged fluorescence and water Raman scatter signals of the surface layer were computed off line by numerical integration according to Equ. (4) and (3). From these data,

the UV attenuation coefficient	$c(308)+c(344) \sim 1/R(344)$	
the blue/green attenuation coefficient	$c(450)+c(533) \sim 1/R(533)$	
the Gelbstoff concentration	$F(380)/R(344)$	ADRIA'84
	$F(366)/R(344)$	'Fronten 2'
and the chl a concentration	$F(685)/R(533)$	

are derived in relative units according to Equ. (3) and (5).

Four ships were involved in the ADRIA'84 campaign to cover different areas of the northern Adriatic with measurements of CTD, seston and dissolved material, and of various optical parameters; a comprehensive presentation of results is given in a joint data catalogue (Schlittenhardt, 1986). In the experiment 'Fronten 2' ground truth CTD and optical measurements were done on board R/V Victor Hensen.

* Adriatic Sea

The northern part of the Adriatic Sea is the shallowest area of the Mediterranean. Large river run-off, extended lagoon systems having considerable exchange of water with the open sea, and the increase in surface temperture during summer result in strong gradients of the hydrographic parameters.

This is displayed in the results of a flight with the Oceanographic Lidar System on August 30, 1984 , Fig. 3. The Po river plume with a pronounced patchiness of the measured data, and the existence of different water masses having a relatively homogeneous composition, are clearly recognized.

Water Raman scatter normalized fluorescence intensities $F(380)/R(344)$ range between 3 and 10 in front of the Po delta, and 0.3 in the clear water area in the southern part of the off-shore flight track on 13°00' E. At these locations the Gelbstoff attenation coefficient $c_Y(450)$ is estimated to be 0.2 and 0.01 m^{-1}, respectively.

The data derived from the lidar measurements are strongly - but not linearly - correlated between themselves, and with *in situ* findings. Mean values of airborne and ground truth data taken from selected positions indicated in Fig. 4 are given in Table 1.

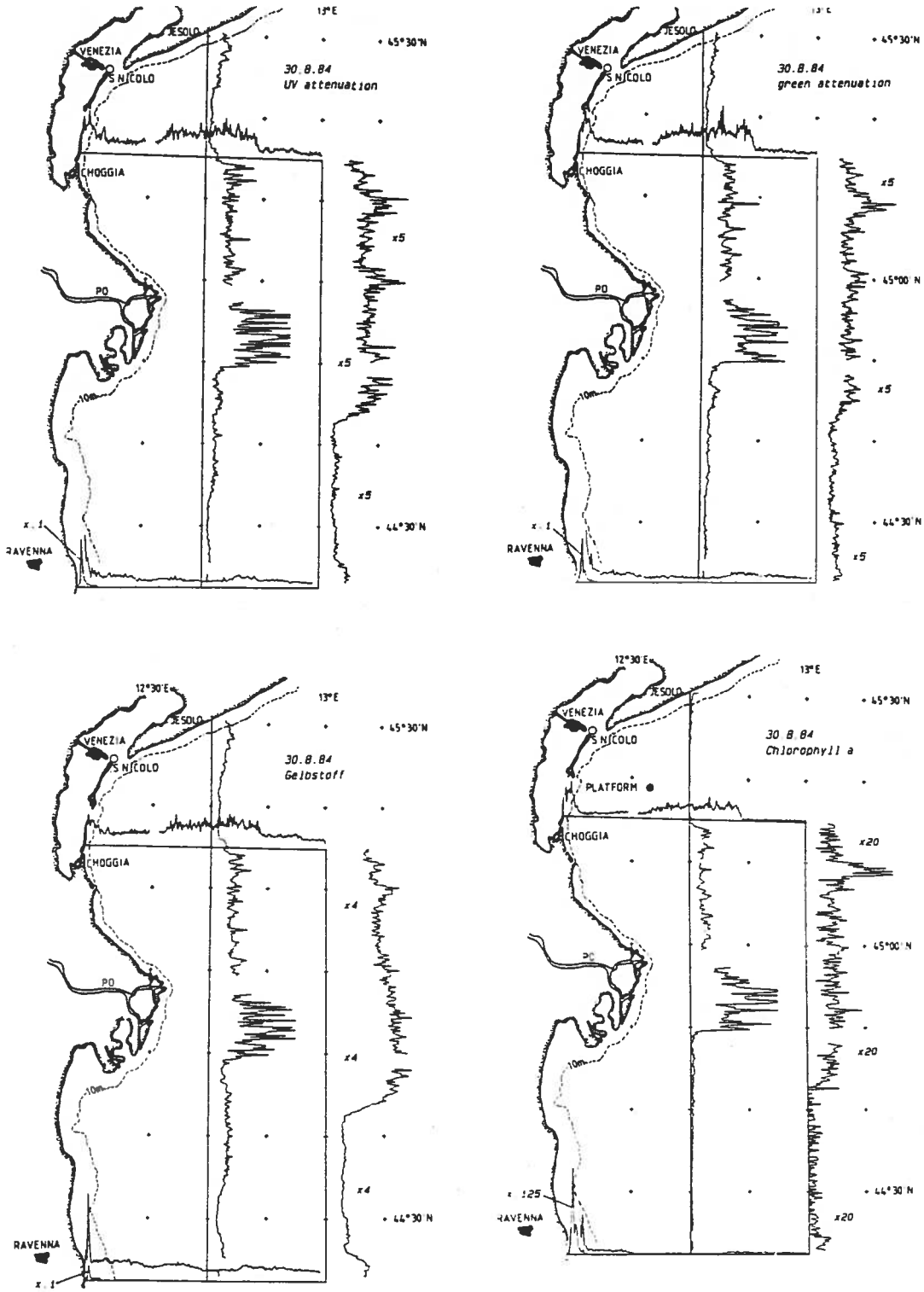

Fig. 3: Distribution of the UV and blue/green attenuation coefficient, and the Gelbstoff and chlorophyll a concentration in the northern Adriatic Sea with lidar on August 30, 1984. Flight tracks (straight lines) are used as baseline for the given data. Scaling of the profiles is identical except for the track on 13°00'E and the area near Ravenna.

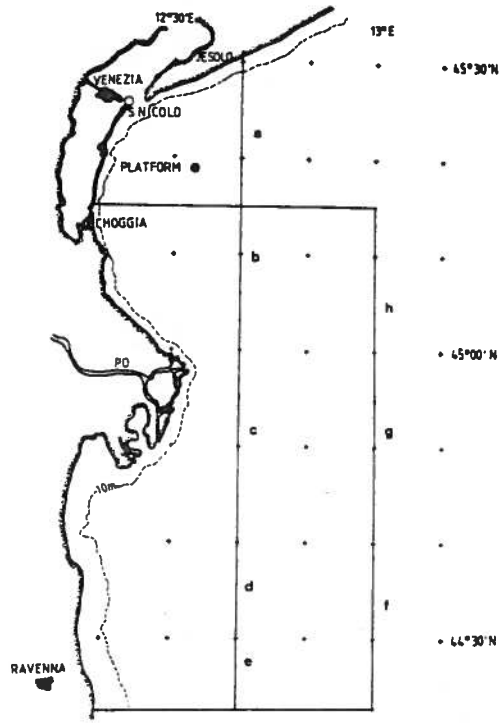

Fig. 4: Position of selected data along the flight track chosen for Table 1.

	lidar				-ground truth-	
flight track	UV att [relat. units]	blue/green att	Gelb-stoff [Raman norm.	chl a fluor.]	Gelb-stoff [r.U.]	chl a [µg/l]
a	.74	2.14	.61	.08	48.2	.28
b	3.29	12.08	1.76	4.40	89.0	1.04
c	9.29	25.12	4.61	16.17	126.6	8.23
d	1.38	3.75	1.33	.46	70.3	.82
e	.78	2.87	.85	.30	70.1	.64
f	.31	1.41	.29	.07	24.4	.13
g	1.11	3.00	1.23	.40	54.3	.53
h	1.04	3.19	.89	.04	50.5	.44

Table 1: Mean valueas of airborne lidar and of ground truth data of selected positions shown in Fig. 4

The high covariance of Gelbstoff and chlorophyll present in the northern Adriatic is a consequence of the Po river discharge which is the dominating source of Gelbstoff and nutrients when compared to other freshwater input and advective transport of open sea water. In addition to the river plume in front of the Po delta, an extended mixed water mass with enhanced Gelbstoff concentrations is found with very stable hydrographic conditions over the 3 days period of investigation.

* German Bight

The distribution of Gelbstoff obtained during the experiment 'Fronten 2' on October 4, 1985 with the Oceanographic Lidar System is given in Fig. 5. Isolines correspond to F(366)/R(344) with 308 nm excitation.

Airborne Gelbstoff data were compared with salinity measured in the surface layer at identical ship and aircraft positions, whereby the difference of the sampling time of data chosen for this purpose did not exceed one hour. Correlation of these parameters is high, Fig. 6, as it is typically found in the German Bight. The distribution of Gelbstoff in this area is largely dominated by river discharge and reflects well the hydrographic situation in this area, particularly the mixing of river water and the formation of haline fronts (see, for example, Krause et al, 1986).

On the basis of the high correlation of Gelbstoff and salinity, and because of the observed stability of the hydrographic parameters over the period of measurements (3 - 5 October), an identification of characteristic water masses was performed using the airborne lidar and the shipboard data: Fig. 7 and Table 2.

The distribution of water surface salinity derived from shipboard CTD measurements in the period of investigation is shown in Fig. 8. For this presentation, a conversion of geographical positions to coordinates fixed with the moving water mass has been done to avoid errors due to tides.

To further describe the hydrographic situation, airborne and shipboard results obtained on longitude 54°15'N are shown in Figs. 9-10. In addition to Gelbstoff data, profiles of UV and blue/green light attenuation coefficients and of water Raman normalized chlorophyll a fluorescence are given for comparison in Fig. 9. Fig. 10 displays isolines of salinity in the water column along the same section. The formation of water types 1 2 and 5 (Table 2), separated by transition areas about 3 kilometers wide can be cearly seen.

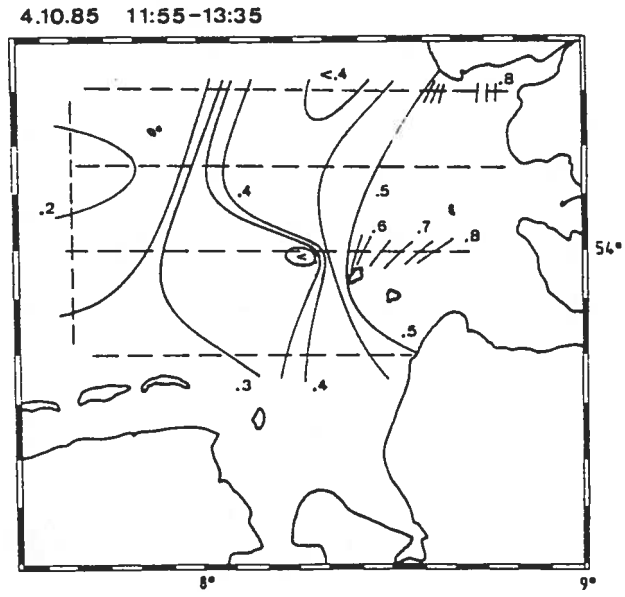

Fig. 5: Distribution of water Raman normalized Gelbstoff fluorescence obtained with lidar on October 4, 1985, in the German Bight. Isolines correspond to F(366)/R(344). Dashed lines represent flight tracks.

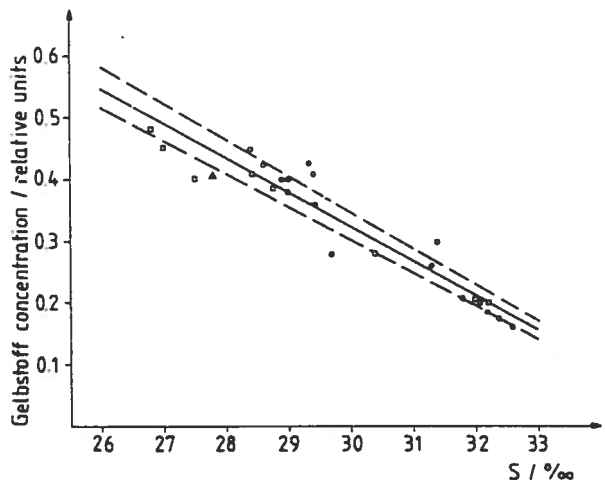

Fig. 6: Plot of water Raman normalized Gelbstoff fluorescence versus salinity in the surface layer. Full line corresponds to linear regression with r = -0.96. Dashed lines mark the width of the signal fluctuation of airborne data.

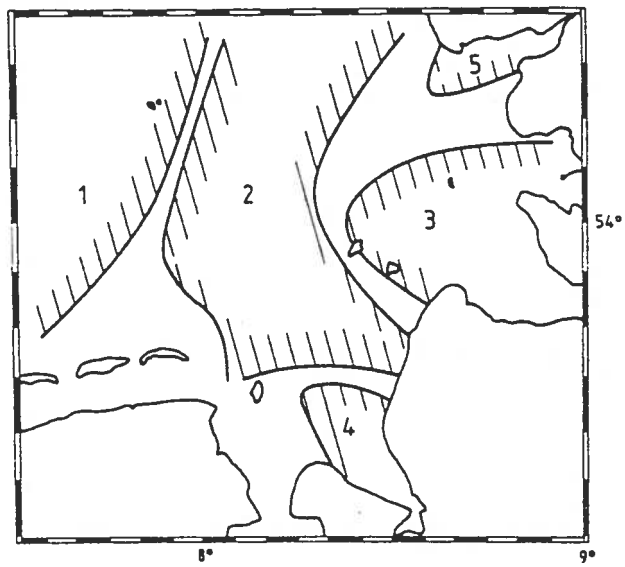

Fig. 7: Characteristic water masses derived from airborne Gelbstoff fluorescence and shipboard salinity data.

water mass	Gelbstoff F(366)/R(344)	salinity [‰]
1	< .25	> 3.1
2	.3 ... .45	2.8 ... 3.0
3	> .6	< 2.7
4	> .6	< 2.7
5	> .6	< 2.7

Table 2: Characteristic water masses shown in Fig. 7 and corresponding Gelbstoff and salinity values.

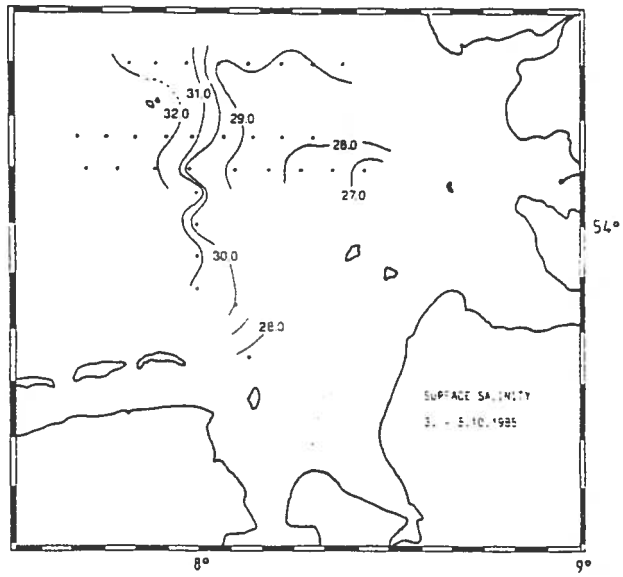

Fig. 8: Distribution of surface salinity obtained from shipboard CTD measurements on October 3 - 5.

A close correlation of Gelbstoff and chlorophyll data cannot be found in the airborne profiles of this experiment. Phytoplankton growth is obviously not strongly related to physical hydrographic parameters, if we consider Gelbstoff to be inversely proportional to salinity according to Fig. 6.

Conclusions

The development of the airborne laser fluorosensor method during the past decade has reached a level which allows an application of this sensor for various tasks in oceanography. These cover investigations of dynamic processes, primary production, pollution monitoring and of other subjects.

For the purpose of optical satellite data ground truth collection, the oceanographic laser fluorosensor is of advantage for several reasons:

* the sensor allows a sensitive and specific detection of light attenuation and of chlorophyll, Gelbstoff and

suspended minerals by use of fluorescence and Raman spectroscopy. Lower limit of sensitivity for Gelbstoff and chlorophyll measurements is close to that of laboratory instrumentation.

* besides atmospheric contributions these parameters completely determine the radiance spectrum measured by the satellite;

* it is particularly the sensitive detection of Gelbstoff which allows an investigation of the characteristic hydroraphic processes since Gelbstoff concentrations are cloasey related to salinity data

* a good coverage of extended areas of the sea is easily achieved.

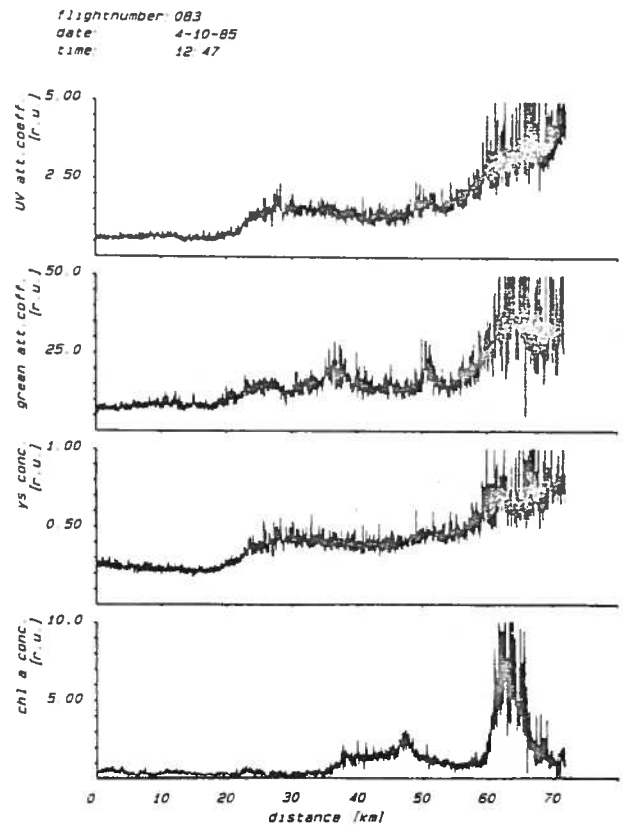

Fig. 9: airborne lidar profiles obtained on longitude 54o14'N on October 4. UV and blue/green attenuation, and concentrations of Gelbstoff and chlorophyll are given.

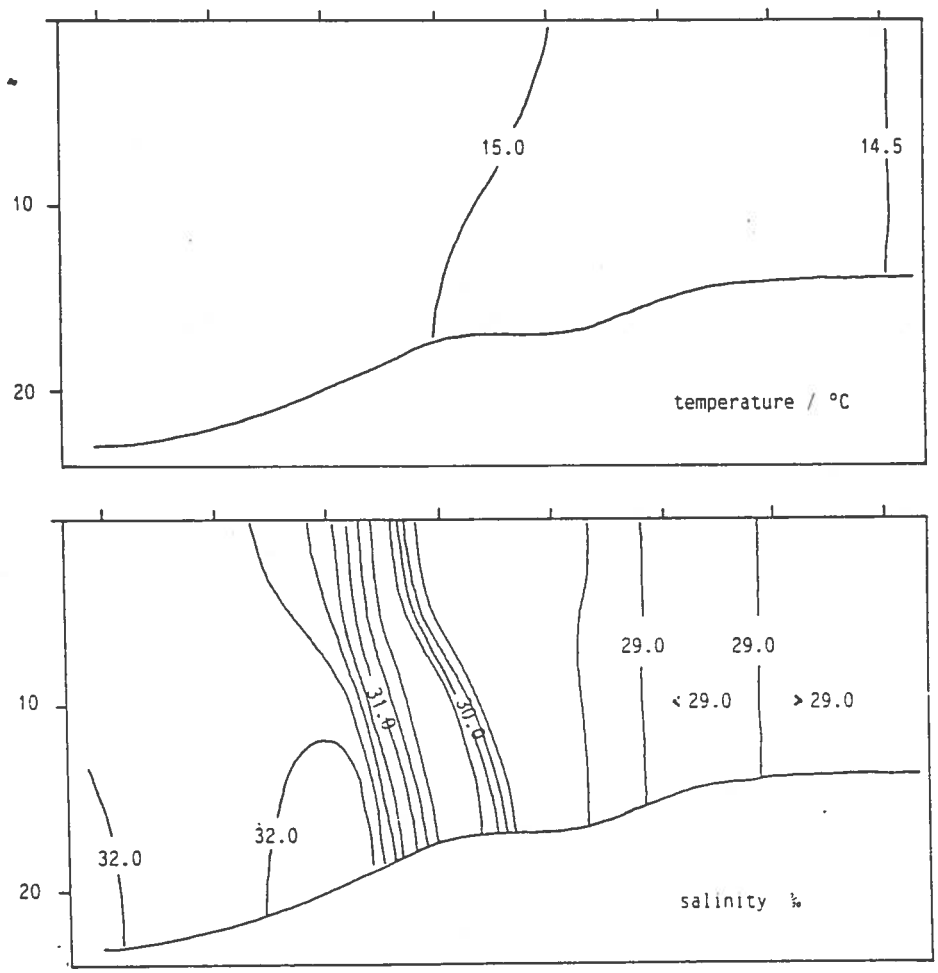

Fig. 10: East-west section on 54°15'N from 8°25'E to 7°50'E, October 4, 1985. Ship stations are marked.

Limitations arise from the fact that attenuation data can be derived in absolute units only with limited accuracy, if shipboard ground truth is not available. However, fluorescence data are given with high accuracy due to the normalization to water Raman scatter.

Other problems are due to the fluorometric method of investigation. Particularly fluorescent compounds of Gelbstoff are not identical with the absorbing fraction. This can lead to erroneous results when estimating Gelbstoff absorption coefficients from fluorescence data. Further investigations of the chemical and optical properties of Gelbstoff are necessary to better understand the relations between absorbing and fluorescent dissolved matter.

Acknowledgements

Development of the Oceanographic Lidar System is financed by a grant from the Bundesministerium für Forschung und Technologie, Bonn; research on water masses and frontal systems in the German Bight by a grant from the Deutsche Forschungsgemeinschaft, Bonn.

References

Amann, V., Reuter, R. and Schlittenhardt, P. 1986. ADRIA'84: airborne investigations of Gelbstoff by optical radiometry and fluorescence lidar. ESA/EARSeL Symposium on 'Europe from Space'. Symp. Proc., Lyngby, 25-29 June 1986, 4 pp.

Bricaud, A., Morel, A., and Prieur, L. 1981. Absorption by dissolved organic matter (yellow substance) in the UV and visible domains. Limnol. Oceanogr., 26: 43-53.

Bristow, M. and Nielsen, D. 1981. Remote monitoring of organic carbon in surface waters. U.S. Environmental Protection Agency, Las Vegas, Nevada, Proj. Rept. EPA-600/4-81-001, Feb. 1981, 83 pp.

Bristow, M., Nielsen, D., Bundy, D. and Furtek, R. 1981. Use of water Raman emission to correct airborne laser fluorosensor data for effects of water optical attenuation. Appl. Opt., 20: 2889 - 2905.

Bristow, M.P.F., Bundy, D.H., Edmonds, C.M., Ponto, P.E., Frey, B.E. and Small, L.F. 1985. Airborne laser fluorosensor survey of the Columbia and Snake rivers: simultaneous measurements of chlorophyll, dissolved organics and optical attenuation. Int. J. Remote Sensing, 6: 1707 - 1734.

Browell, E.V. 1977. Analysis of laserfluorosensor systems for remote algae detection and quantification. NASA Technical Note TN D-8447, NASA Langley Research Center, Hampton, June 1977, 39 pp.

Diebel-Langohr, D., Hengstermann, T. and Reuter, R. 1985. Laser remote sensing of the marine environment: recent results obtained with the Oceanographic Lidar System. In Spectral Signatures of Objects in Remote Sensing. 3rd International Colloquium, pp. 267 - 272. ESA SP - 247, Dec. 1985, 580 pp.

Diebel-Langohr, D., Hengstermann, T. and Reuter, R. 1986a. Identification of hydrographic fronts by airborne lidar measurements of Gelbstoff distributions. In Marine Interfaces Ecohydrodynamics, pp. 569 - 590. Ed. by J.C.J. Nihoul. Elsevier, Amsterdam, 1986, 670 pp.

Diebel-Langohr, D., Hengstermann, T. and Reuter, R. 1986b. Water depth resolved determination of hydrographic parameters from airborne lidar measurements. In Marine Interfaces Ecohydrodynamics, pp. 591 - 602. Ed. by J.C.J. Nihoul. Elsevier, Amsterdam, 1986, 670 pp.

Diebel-Langohr, D., Doerffer, R., Reuter, R., Dörre, F. and Hengstermann, T. 1986c. The influence of Gelbstoff on remote sensing of seawater constituents from space. 6. Long term stability of Gelbstoff concerning its optical properties. ESA Contract No. RFQ 3-5060/84/NL/MD, Aug. 1986, 24 pp., in press.

Gordon, H.R. 1982. Interpretation of airborne oceanic lidar: effects of multiple scattering. Appl. Opt., 21: 2996 - 3001.

Hoge, F.E. and Swift, R.N. 1982. Delineation of estuarine fronts in the German Bight using airborne laser-induced water Raman backscatter and fluorescence of water column constituents. Int. J. Remote Sensing, 3: 475 - 495.

Hoge, F.E. and Swift, R.N. 1983. Airborne detection of oceanic turbidity cell structure using depth-resolved laser-induced water Raman backscatter. Appl. Opt., 22: 3778 - 3786.

Hoge, F.E., Berry, R.E. and Swift, R.N. 1986a. Active-passive airborne ocean color measurement. 1: Instrumentation. Appl. Opt., 25: 39-47.

Hoge, F.E., Swift, R.N. and Yungel, J.K. 1986b. Active-passive airborne ocean color measurement. 2: Applications. Appl. Opt., 25: 48-57.

Houghton, W.M., Exton, R.J. and Gregory, R.W. 1983. Field investigation of techniques for remote laser sensing of oceanographic parameters. Rem. Sens. Env., 13: 17 - 32.

Kim, H.H. 1973. New algae mapping technique by the use of an airborne laser fluorosensor. Appl. Opt., 12: 454 - 462.

Krause, G., Budeus, G., Gerdes, D., Schaumann, K. and Hesse, K. 1986. Frontal systems in the German Bight and their physical and biological effects. In Marine Interfaces Ecohydrodynamics, pp. 119 - 140. Ed. by J.C.J. Nihoul. Elsevier, Amsterdam, 1986, 670 pp.

Leonard, D.A., Caputo, B. and Hoge, F.E. 1979. Remote sensing of subsurface water temperature by Raman scattering. Appl. Opt., 18: 1732 - 1745.

O'Neil, R.A., Buja-Bijunas, L. and Rayner, D.M. 1980. Field performance of a laser fluorosensor for the detection of oil spills. Appl. Opt., 19: 863 - 870.

Nyquist, G. 1979. Investigation of some optical properties of seawater with special reference to lignin sulfonates and humic substances. PhD Thesis, Göteborgs Universitet, 200 pp.

Poole, L.R. and Esaias, W.E. 1982. Water Raman normalization of airborne laser fluorosensor measurements: a computer model study. Appl. Opt., 21: 3756 - 3761.

Reuter, R., Diebel-Langohr, D., Doerffer, R., Dörre, F., Haardt, H. and Hengstermann, T. 1986. The influence of Gelbstoff on remote sensing of seawater constituents from space. 3. Optical properties of Gelbstoff. ESA Contract No. RFQ 3-5060/84/NL/MD, Aug. 1986, 58 pp., in press.

Schlittenhardt, P. 1986 (Ed.). ADRIA 84 Data Catalogue. Commission of the European Communities, Joint Research Centre ISPRA, S.A. I.05.E2.85.23, May 1986.

Schmitz-Peiffer, A. 1986. Fernerkundung ozeanischer Schwebstoffe mit flugzeuggetragenen Lasern und Satellitenradiometern. PhD Thesis, Universität Kiel, 135 pp.

Smith, R.C. and Baker, K.S. 1981. Optical properties of the clearest natural waters (200-800 nm). Appl. Opt., 20: 177 - 184.

AIRBORNE FLUORESCENCE MAPPING: APPLICATIONS AND POTENTIAL

Gary Borstad, Borstad Associates Ltd.

The Fluorescence Line Imager arose from experience with an non-imaging spectrometer built for DFO by UBC astronomers in 1974. The IOS spectrometer uses a 256 channel Reticon linear array sensor and dispersive optics to produce spectra with a 12nm resolution. Reflectance ratios (L_u/E_d) of the sea (FIG. 1.) show a fluorescence peak at 685 nm.

WATER COLOUR SURVEY APPLICATIONS

For oceanographic surveys, water colour indices are calculated from each spectrum (at integration times of .1 to 1 sec) and plotted as strip charts (FIG. 2). Sea surface temperature is also measured with an infra-red radiometer. The technique allows rapid surveys of large and remote locations. In this plot of a track across the mouth of Lancaster Sound, the FLH and G/B ratio vary together (FIG. 5) and opposite to thermal changes.

FIG. 3. illustrates the results of three days of flying in the Eastern Canadian Arctic in August 1979 (Borstad and Gower, 1984). Surface phytoplankton chlorophyll was highest in patches associated with eddying along the edge of the Baffin Current which flows southward along the west side of Baffin Bay.

In situ vertical profiles of chlorophyll were made from a ship at about the same time as the airborne survey. These showed that the top 35m of the Baffin Current and further offshore, which had surface temperatures of >0°C were nearly homogeneous. The integrated pigment content (0-35m) was 40-75X that at the surface (FIG. 4). Strong subsurface chlorophyll maxima present under the cold melt waters near the coast would lead to large under-estimates of the pigment present using surface measures alone, but the combination of ship and aircraft data permitted quantitative 3D mapping.

In another Arctic survey in the Canadian Beaufort Sea in late August 1983 (Borstad, 1984) phytoplankton, sediment content and temperature were mapped to provide information concerning the environment of the bowhead whale, an endangered baleen (FIG. 6). Late summer upwelling along the Yukon coast west of 137°W resulted in increased fluorescence there. A large congregation of bowheads near King Point appeared to be associated with the upwelling. The largest numbers of this group were in colder, less turbid water near the coast (FIGS 7 and 8). Several studies arising from this one have since shown the animals congregate along the edge of the river plume and in these shallow coastal upwellings where their zooplankton food is more abundant.

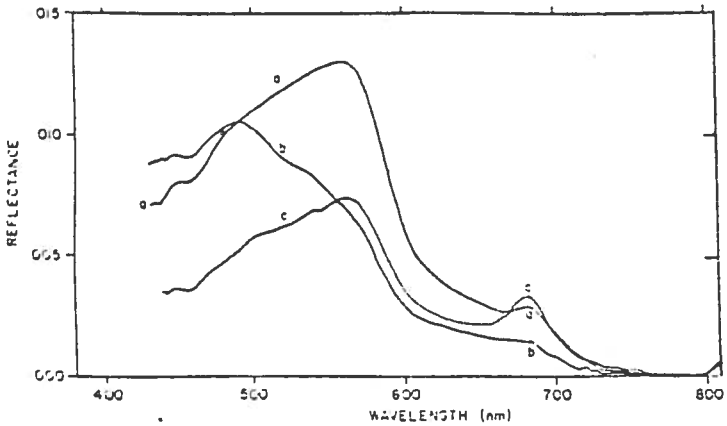

OBSERVED AIRBORNE WATER COLOUR VARIATIONS
ACROSS THE EASTERN ENTRANCE OF LANCASTER SOUND
CFOX ARCTIC, AUGUST 26, 1979

(1)

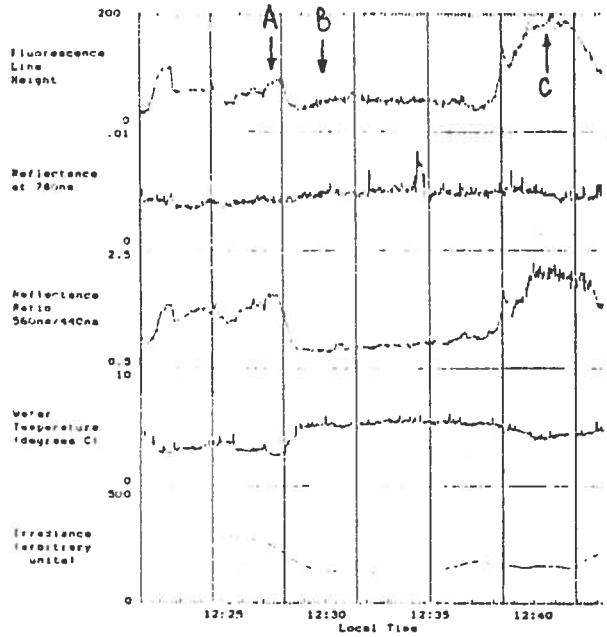

Data extracted from airborne spectral measurements over the eastern entrance of Lancaster Sound, August 26 1979, showing the correlation between fluorescence and ratio indicators of phytoplankton pigments, and a negative correlation with water temperature.

(2)

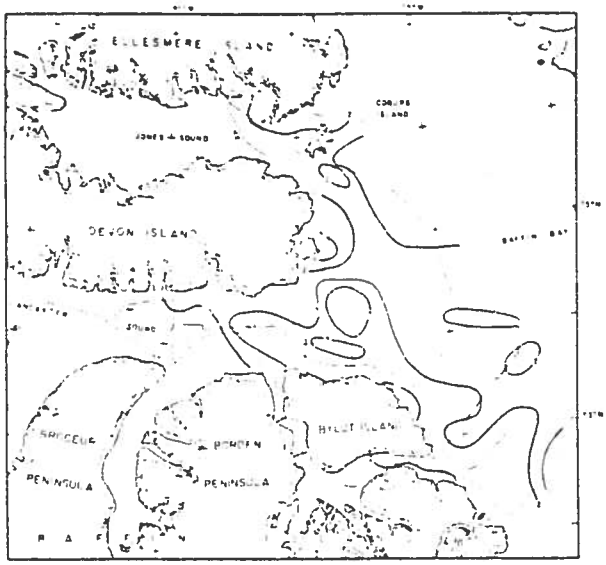

(3)

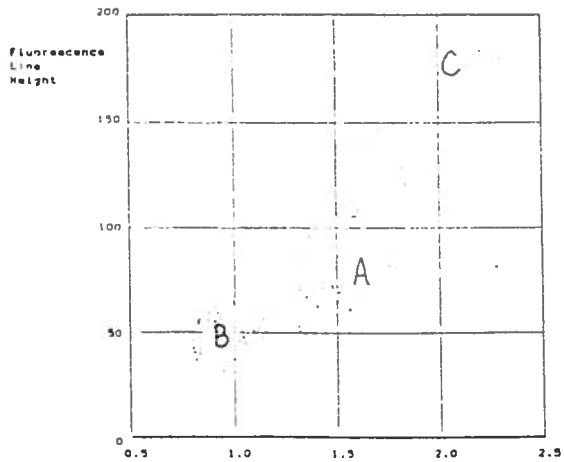

Scatter plot showing the correlation between fluorescence line height and reflectance ratio for the data in 2.

(5)

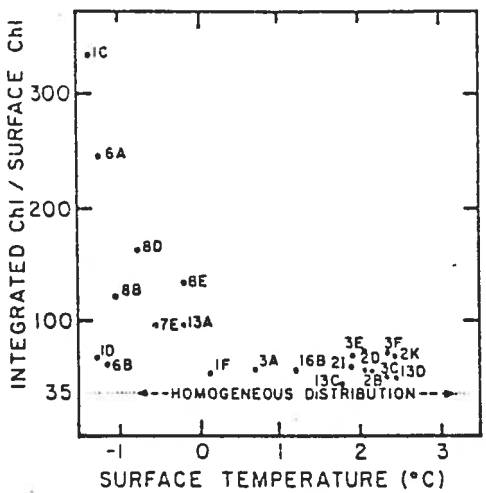

(4)

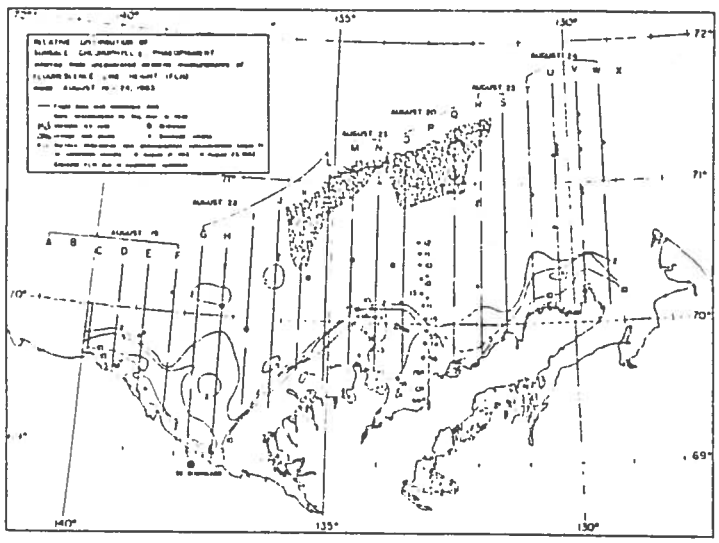

6

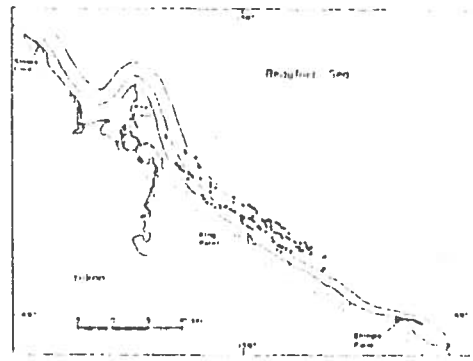

7

Distribution of bowhead whales observed by McLaren and Davis (1984) along the Yukon coast in the vicinity of King Point. Dotted lines indicate survey transects; symbols represent locations of individual animals sighted.

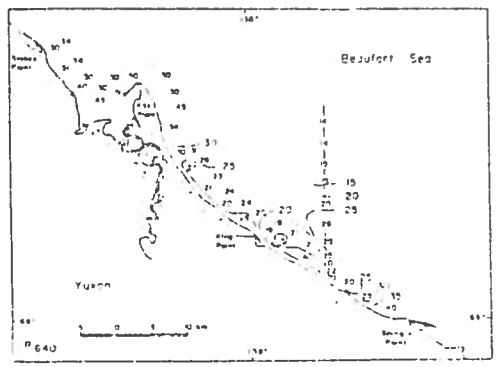

8

Variations of red reflectance in the vicinity of King Point 22 August 1983. Values plotted are R643 × 1000 (i.e. 25 = 0.025). Waters having R643 greater than about 0.015 are visibly turbid to the eye.

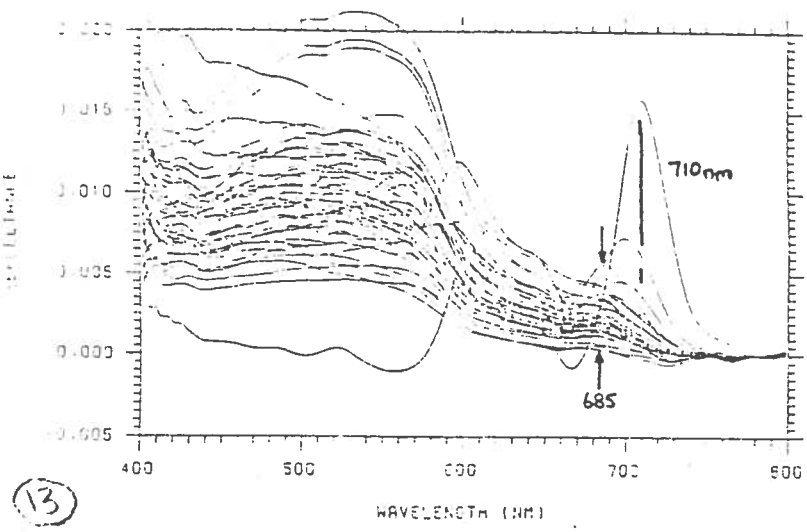

13

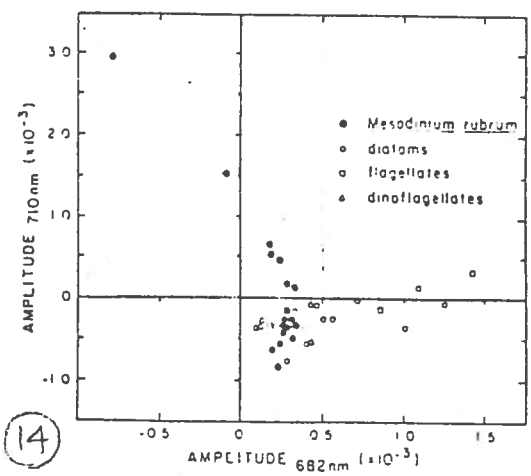

14

EXAMPLES OF AQUATIC APPLICATIONS OF THE FLI

Gary Borstad, Borstad Associates Ltd

The design driver for the FLI was the requirement to image water spectral reflectance changes resulting from varying phytoplankton concentrations in the near surface layers of the sea, specifically the narrow chlorophyll emission peak at 685 nm.

1. * Radiance sensors have to avoid solar and absorption lines.
   * Oxygen line at 686.8nm overlaps with chlorophyll fluorescence peak, but it has a sharp lower edge.
   * FLI spectral bands can be placed to avoid absorption, even in the 'dirty window' near 720nm.
   * A 'Reflectance' spectum can be fabricated which shows the fluorescence line.

2. * Spectra from a family of lakes with increasing chlorophyll concentration show increasing 685nm emission peak.
   * Yamaska Reservoir (37 mg Chl/m^{-3}) shows a shifted emission peak, the resultant wavelength of which is a fucntion of Chl absorption and fluorescence as well as atmospheric Oxygen absorption. This spectrum also shows evidence of chlorophyll b absorption at 640nm.

3. * Comparison of FLI measured fluorescence (FLH) with <u>in situ</u> chlorophyll in 8 lakes in southern Quebec, and at 5 oceanic stations off Cape Hatteras, Virginia shows good agreement.

4 5 and 6. * Comparison of two measures of FLH with fluorescence measured with the NASA Airborne Oceanographic Laser (AOL) along a line south east of Cape Hatteras shows very close agreement. More overlap between ship based chlorophyll measurement and the AOL also showed excellant correlation. Both FLH calculations were from 3 points. FLH_1 used a base line on either side of the 684nm peak (figure 5). FLH_2 used a base line extrapolated to 684nm from lower wavelengths.

7. *A spectral image of Chlorophyll fluorescence in the vicinity of CSS Hudson (seen under way in the lower part of the image) south west of Yarmouth, Nova Scotia in July 1986. Highest concentrations are seen in a patch near the top of the image.

8. *Spectra from two locations (single pixels) in the spectral image in Figure 7, showing a change in fluorescence.

9. *Most of the colour changes visible in lower Chesapeake Bay in December 1984 were a result of suspended inorganic solids. A simple measure of upwelling signal at 750nm correlates well with <u>in situ</u> measurements of Total Suspended Solids. Spatial imagery shows complicated patterns of TSS off the mouth of the Bay (see Borstad et al, 1985).

(7)

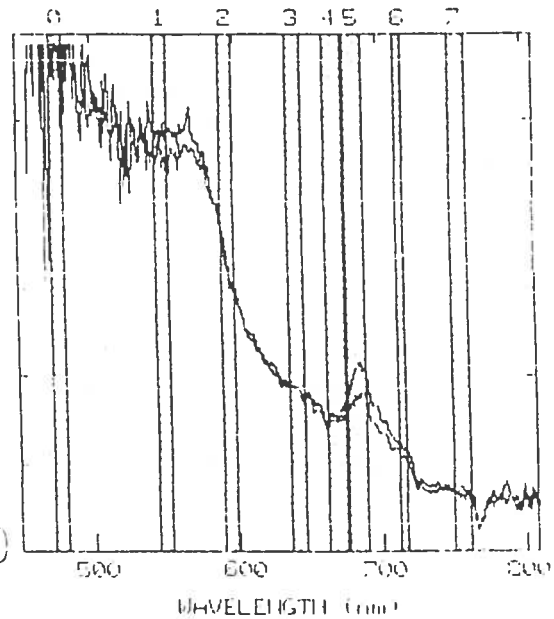
0
1
2
3
4
5
6
7
500
600
700
800
WAVELENGTH (nm)

(8)

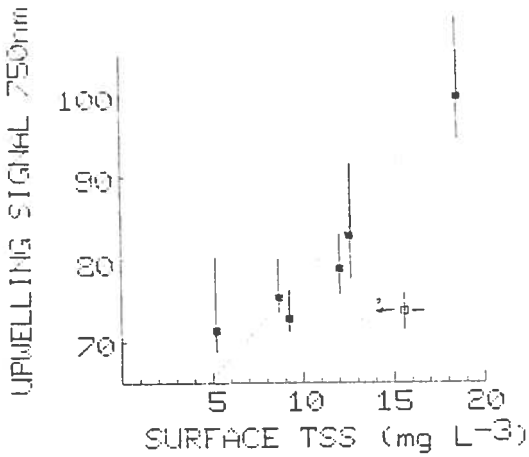
UPWELLING SIGNAL 750nm
100
90
80
70
5
10
15
20
SURFACE TSS (mg L⁻³)

(9)

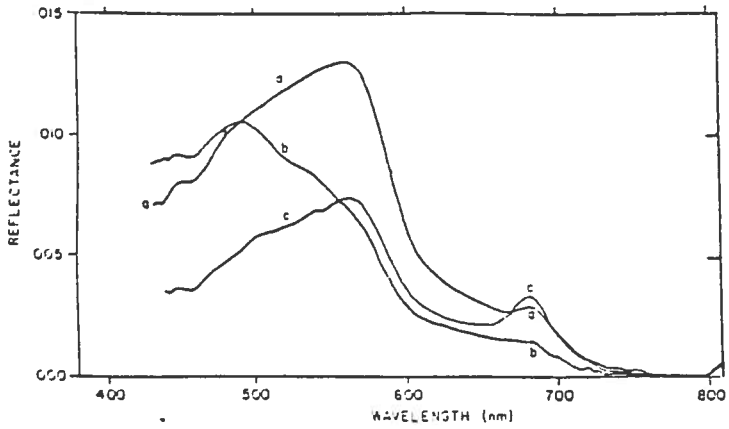

OBSERVED AIRBORNE WATER COLOUR VARIATIONS
ACROSS THE EASTERN ENTRANCE OF LANCASTER SOUND
CFOX ARCTIC, AUGUST 26, 1979

(1)

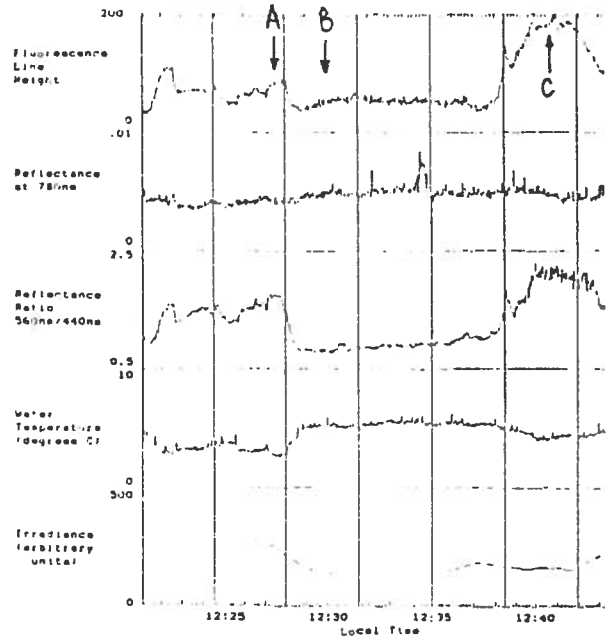

(2)

Data extracted from airborne spectral measurements over the eastern entrance of Lancaster Sound, August 26 1979, showing the correlation between fluorescence and ratio indicators of phytoplankton pigments, and a negative correlation with water temperature.

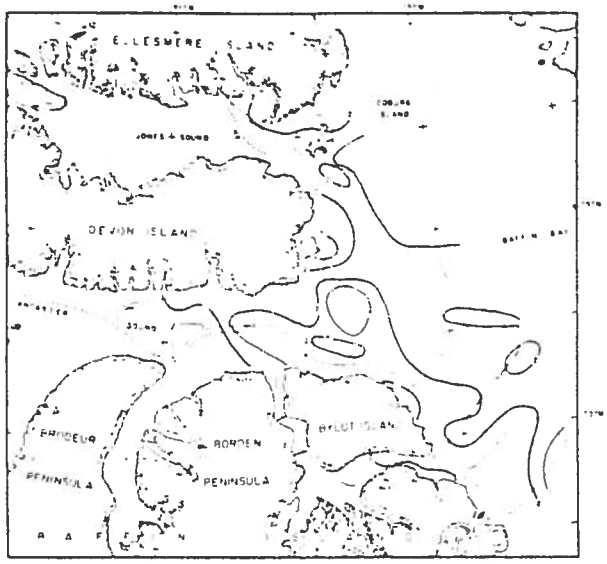

(3)

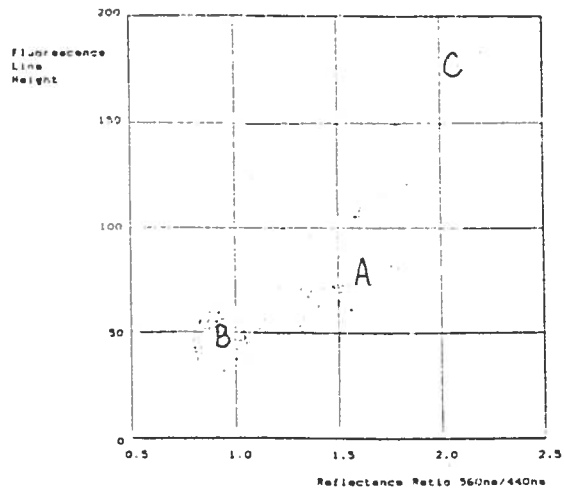

(5)

Scatter plot showing the correlation between fluorescence line height and reflectance ratio for the data in 2

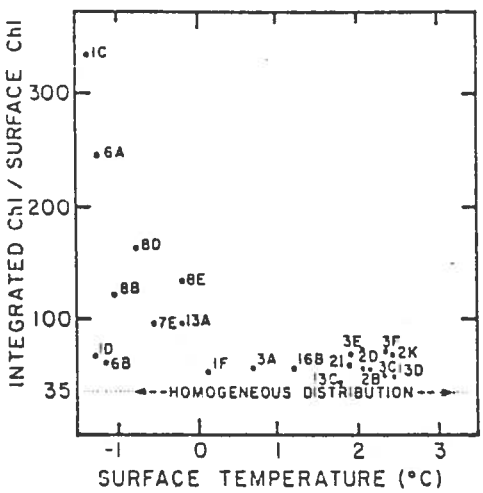

(4)

FLI WORKSHOP ON HIGH SPECTRAL RESOLUTION IMAGING
FOR LAND AND OCEAN REMOTE SENSING
OTTAWA OCTOBER 14-17, 1986

ANALYSIS OF FLI VEGETATION REFLECTANCE RED EDGE DATA

J.R. Miller, M. Boyer, E.W. Hare, M. Belanger, York University

J. Wu, on leave Shandong University, CHINA

and A.B. Hollinger and D.R. Sturgeon, Moniteq Ltd.

During the summers of 1985 and 1986 the FLI has been used to collect airborne data from forests in Canada, the United States and central Europe over sites that were selected on the basis of suspected localized vegetation stress due to possible excess metal uptake or reported regional forest decline due to suspected acid deposition damage. The vegetation red reflectance edge, which occurs in the 650 to 800 nm spectral region, has received increased attention during the past several years as a potential indicator of vegetation stress; previous laboratory and field measurements have shown shifts in the red edge of up to 10 nm in response to stress due to uptake of heavy metals. Preliminary analysis of FLI spectral mode data show the potential of this sensor to detect small spectral changes. It is expected that the FLI has an important role to play in evaluating the effects of canopy morphology and mixed species on the potential of mapping vegetation stress using remote sensing.

York University is currently undertaking a joint field and airborne research programme into the potential to remotely map changes in the red reflectance edge. An inverted-Gaussian model has been introduced to describe the vegetation red edge. This model (Miller et al., 1985: Hare et al., 1984) represents the vegetation reflectance as:

$$R(\lambda) = R_s - (R_s - R_o)e^{\frac{-(\lambda-\lambda_o)^2}{2\sigma^2}}$$

R_s is the shoulder reflectance,

R_o is the reflectance minimum corresponding to the chlorophyll absorption maximum at about 685 nm,

λ_o is the wavelength of the reflectance minimum,

σ is the Gaussian model deviation parameter and,

$\lambda_p = \sigma + \lambda_o$ is the edge inflection wavelength considered the "position" of the red edge.

Analysis of Fluorescence Line Imager Data of Different Forest Types

Donald G. Leckie
Petawawa National Forestry Institute
Canadian Forestry Service
Chalk River, Ontario
K0J 1J0

There is a large need for remote sensing systems capable of providing information on forest type and condition. Of particular interest to the forest manager are species discrimination and assessment of insect, disease and other forest damage. The Fluorescence Line Imager (FLI) offers unique capabilities appropriate for these applications and a study was initiated to investigate the technology. The capabilities of the technology for determining spectral details of different forest types and changes in forest condition are examined and the variability of spectra of forest types is quantified.

FLI data in the spectral mode was acquired October 3, 1985 over two test strips on the Petawawa National Forestry Institute research forest. Flying altitude was 350 m giving a spatial resolution of 2 m across track and 12 m along track. The forest of the test strips includes plantations of coniferous species of ages from 5 to 60 years and natural stands of deciduous, coniferous and mixed woods. Deciduous trees were near the peak of fall colouration.

Data was analyzed at the Institute of Ocean Sciences, Sidney, B.C. with the assistance of G.A. Borstad Associates Ltd. Several methods of display of spectral information were examined. An effective display was plotting a sequence of each spectra on a three dimensional plot with one axis as wavelength, another as intensity and a third as pixel number along a given camera band. A good indication of forest type and variability in spectra of forest type is given. Despite limitations in the spatial resolution and geometric characteristics of the spectral data image, the imaging is sufficient to determine areas of different forest types. Selected spectral bands were used to display an image of data acquired in the spectral mode.

Areas of similar tree species, age and density were defined on the images and the mean spectra for each area calculated. The standard deviation at each spectral wavelength was also determined. Mean spectra obtained from pixels within the same camera bands were compared. The spectral detail of fall colouration of deciduous stands is clearly evident. There is a large variability in the radiance spectra both between sites and within sites of similar forest types.

The role and applications of FLI spectral mode data in forestry is as yet unclear. However, it is clear that the technology can provide useful information regarding the spectral characteristics of forest features which can be used to increase the effectiveness of forestry applications of linear array imagers such as the FLI in spatial mode.

637 26

Bathymetric analysis of geometrically corrected imagery data collected using a two dimensional imager

N.T. O'Neill, A.R. Kalinauskas, J.D. Dunlop, A.B. Hollinger

MONITEQ Ltd.
630 Rivermede Road, Concord, Ontario, Canada L4K 2H7

H. Edel

Fisheries & Oceans Canada, 200 Kent Street, 12th Floor, Ottawa, Ontario, Canada K1A 0E6

M. Casey

Canadian Hydrographic Service
Fisheries & Oceans Canada, 615 Booth Street, Ottawa, Ontario, Canada K1A 0E6

J. Gibson

Canada Centre for Remote Sensing
Energy, Mines & Resources Canada, 2464 Sheffield Road, Ottawa, Ontario, Canada K1A 0Y7

Abstract

In August of 1985 a programmable multispectral imager (FLI for Fluorescence Line Imager) was flown along with a Inertial Navigation System over the Red Bay region of Lake Huron. The objective of the mission was to collect digital imagery which could be processed into an accurate geometrically correct bathymetric map. The results of the geometric correction processing were found to be accurate to the output pixel level (5 x 5 meters). Sampled profiles of the geometrically corrected image showed systematic shallow bias errors of less than 1.6 meters for depths less than 6 meters and 0.6 meters for depth less than 4 meters.

Introduction

Airborne optical imagery for purposes of passive bathymetry in shallow waters is a promising hydrographic technology which provides 100% surface coverage and which exploits the speed and flexibility of airborne remote sensing. The high sampling density and broad swath coverage achieved by current pushbroom scanning systems are strong agruments for the utilization of this technology as an alternative or supplement to traditional methodologies of operational hydrography.

To date the acceptance of passive bathymetry as a hydrographic tool has not been widespread due principally to comparatively small depth penetration, uncertainty in absolute accuracy, and to the difficulty of converting airborne images to map quality data bases.

We present in this report the results of an airborne imaging experiment whose goal was the production of an accurate, geometrically correct bathymetric map. The scope of the experiment included the field measurement/acquisition of the airborne imagery, inertial navigation system data, radiometric, geometric, and atmospheric corrections as a precursor to the application of the bathymetry algorithms. The techniques and instrumentation employed to perform the tasks are described and results of intermediate processing steps are presented along with an analysis of the bathymetric output products.

Field experiment and equipment

On August 4, 1985 a programmable multispectral imager (FLI for Fluorescence Line Imager) was flown over the Red Bay area of Lake Huron in a Falcon aircraft belonging to the Canada Centre for Remote Sensing (CCRS). Data was logged on high density tapes and later transcribed to computer compatible tapes on the AIR system belonging to CCRS. An inertial navigation system (Litton Systems LTN-51) was also flown in the Falcon and its output recorded on dedicated CCTs. Ground truth consisted of solar extinction and ground reflectance measurements made using a programmable multispectral radiometer. The geocoded soundings of the Canadian Hydrographic Service (CHS) were acquired for the purposes of calibrating and validating the bathymetry processing steps. Survey photographs which could be triangulated from known geocoded points to selected scene points were provided by Terra Surveys Inc.

The Red Bay area is a test sounding area for CHS and as such provided a density of soundings commensurate with the high resolution sampling capability of the FLI. In addition the bathymetric parameters of the general area were fairly well understood since numerous

Published in the Proceedings of the Society of
Photo-Optical Instrumentation Engineers, 1986

field trips have been carried out in the past to perform in-situ water quality and bottom type measurements[1].

The FLI is a programmable imagery spectrometer which uses a set of two dimensional CCD array sensors for gathering electronic imagery from an airborne platform[2]. It employs multiple optical trains collectively covering a wide swath in a pushbroom mode. Each CCD samples the image at 385 spatial locations with a 0.7 milliradian field of view and at 288 spectral columns covering the spectral region from 430 to 800 nm. Data is digitized to 12 bits and summed to give 8 pre-programmed 16 bit spectral bands. The bathymetry spectral bands which were chosen are shown in Table 1.

Table 1. FLI Bandset for Bathymetry

FLI Band #	Wavelength Interval (nm)
0	450 - 475
1	515 - 525
2	545 - 555
3	525 - 545
4	570 - 580
5	600 - 625
6	660 - 680
7	740 - 758

For the Red Bay experiment 4 of 5 CCD cameras were utilized to give a total swath of 1540 pixels or approximately 56°. At the nominal flying height of 12000 feet (3660 m), velocity of 170 knots (315 km/hr), and line sampling time of 90 msec the swath width was approximately 4 kilometers and the pixel size 2.6 meters cross track and 7.9 meters along track.

Figure 1 shows a coarse scale map of the area flown and the flight line swath. At the time of the overflight (approximately 1400 EST) sky conditions were clear and wind conditions calm. To minimize sunglint problems the FLI module housing the 5 CCD cameras were tilted forward by 15°.

Geometric corrections processing

The end product of the geometric correction processing is a map product whose line pixel geometry is related by a simple linear transformation to the Universal Transverse Mercator (UTM) coordinates (easting and northing). In this form the radiometric data and derived quantitites (such as depth and bottom classification) can be compared on a pixel by pixel basis to other geocoded data bases.

The navigational data must be corrected for linear drifts and offsets which are inherent errors in inertial systems. This correction (flight path rectification) is accomplished by extracting the associated errors through the use of absolute positions of ground control points (GCPs) and applying these corrections to all navigational data samples[3]. The GCP acquisition was performed by first locating common ground features in the FLI imagery (displayed on an RGB image display system) and georeferenced photographs supplied by Terra Surveys Inc. The absolute accuracy of the latter points was estimated at better than 60 cm and hence was considerably better than the positional resolution which could be expected from the FLI imagery (7.8 meters by 2.6 meters footprint size). A total of 12 points were collected although in principle a minimum number of 4 GCPs would suffice for the purposes of implementing the flight path rectification algorithm. Attitude and positional data derived from the output of the Inertial Navigation System (Litton Systems LTN-51) at sampling frequencies of 10 and 50 msec respectively were interpolated to the nominal sampling times associated with the FLI imager lines for the Red Bay flight (90 msec integration time).

The flight path rectification algorithm is based on the assumption that the systematic errors in the position and attitude data can be represented by a low order polynomial in time. Given the known (absolute) positions of ground control points, the nominal position of the aircraft, the sensor geometry relative to the aircraft, and the image plane position of the ground control points a regression inversion is performed to yield the coefficients which define the low order polynomial. The polynomial is then applied line by line on the navigation sensor independent file to yield a corrected output file. This process is repeated in a recursive fashion until the estimated error is smaller than a predefined value.

The success of the flight path rectification algorithm was measured in terms of the residual differences between the GCP positions calculated from the corrected navigation file and the true GCP positions acquired from the survey photographs. Before the

corrections were applied to easting and northing positions were characterized by residual offsets of approximately 1140 and 700 meters respectively (at the 1st GCP) and residual drifts of approximately 36 meters/min and 41 meters/min respectively. After the 2nd iteration of the flight path rectification these residuals had been reduced to an rms level of 1.8 and 3.7 meters respectively. In terms of the final output pixels of 5 x 5 meters this result represents sub pixel accuracy.

To provide digital imagery which can be compared on a pixel by pixel basis to information from other data sets, the raw imagery must be resampled to a georeferenced output grid. The output grid was selected to have its line pixel geometry aligned with the UTM easting and northing axis and was characterized by pixel sizes of 5 x 5 meters.

A simple linear transformation between output image line pixel positions and the UTM grid was then computed. As a check of this transformation the first 2 ground control points were selected (by cursor positioning) from the output image and their line pixel coordinates measured. The residuals for the two points were computed and found to be of the order of one output pixel. Considering that the cursor location of the GCPs could well have been 1 output pixel off (5 meters) this result represents the best accuracy achievable.

A resampling window of 5 x 5 input pixels was utilized in a quadrature sum which approximated the convolution of the input image with a sinc function centered at the point of interest (assuming a band limited Fourier spectra). To avoid frequency ringing due to the finite width of the resampling window, a cosine shaped damping function was applied to the resampling window. The resulting image was free of any pixel dropouts or visual anomalies which could be related to the resampling algorithm.

Water depth processing

The geometrically corrected imagery was then analyzed in a preprocessing interactive session, which was followed by production processing in a batch mode. The purpose of the preprocessing session was to extract the atmospheric and water optical parameters needed to analyze the FLI imager data for bathymetry. Preprocessing was also used to verify that the intermediate results and water depths were physically realistic as well as consistent throughout the scene.

An estimation of the upwelling path radiance at the sensor altitude is the first step of preprocessing. The magnitude of the path radiance is estimated from the longer red channel (750 nm) signal over deep water in the scene (greater than 4 meters in depth) and the spectral dependency of the scattering optical depth derived from ground radiometric measurements (this may also be predicted from meteorological conditions).

Path radiance is calculated by using Gordon's[4] expression only with slight modifications. The changes are due to the difference in sensor altitude (from satellite to 12000 feet) and a different red band wavelength (from 670 nm to 750 nm). Once calculated, path radiance is subtracted from the total signal associated with each pixel.

The remaining signal is converted from radiance to reflectance given the total downwelling flux above the water surface. Finally the component of reflectance due to surface reflection is subtracted to yield the signal caused by scattering from the water volume (R_V) compounded with reflection from the water bottom (A).

The simple two stream radiative transfer model is applied to produce the basic bathymetry equation:

(1) $$R_V = R_\infty + (A - R_\infty) \text{ EXP } (- 2KD)$$

where R_∞ is the volume reflectance for very deep water, K is the diffuse attenuation coefficient (1/m), and D is depth (m).

The diffuse attenuation coefficient (K) is the optical quality coefficient that describes in a first order sense, the radiative transfer mechanisms which influence the spectral radiative output of natural waters. K is calculated over deeper water pixels (preferably greater than 5 m) by predicting the magnitude of the coefficient from radiance ratios[5].

Once K is predicted the chlorophyll-a concentration is calculated using Clark's[6] expression. The K values for different wavelengths are derived using Smith and Baker's[7] relationship.

When very deep water pixels (greater than 15 m) are not available in the scene, as in the Red Bay imagery, the R_∞ is derived from shallower depths (greater than 4 m) by using a

variation of Austin and Petzold's[5] radiance relationships. Only one wavelength (670 nm)[1] is used by running a polynomial fitting routine to derive the full R_∞ spectra[8]. As a method of comparison, true water depths are used along with the two stream bathymetry equation and the other water parameters explained above, to calculate R_∞ over all visible wavelengths.

It was assumed that water optical parameters do not vary greatly through one scene. Therefore, the optical parameters were extrapolated to the remainder of the image.

The final parameter required for passive bathymetry is the spectral reflectance of the underlying bottom surface. This spectral data is derived from ground truth spectra (or from near shore pixels in the imagery). A maximum of three bottom types are used in bathymetry processing. The three bottom albedos found in the Red Bay area are: (i) sand, (ii) rock, gravel, sand, silt, and (iii) mud and vegetation.

Location of the bottom types through the image is determined by a clustering analysis of two dimensional scatterplots of the imagery.

Camera 2 was excluded from the final bathymetry processing because it's iris was stopped down for over land data collection. However, when camera 2 was included, bottom type classifications showed large undefined areas. This was caused by the different intensity values between FLI cameras.

Having determined all critical auxiliary parameters a depth dependent surface reflectance algorithm is utilized to produce a spectrally dependent reflectance look up table whose free parameters are bottom type and depth. During the processing stage the spectral signal levels from each pixel are utilized to (a) classify the bottom according to criteria established during the preprocessing classification session and (b) to compute the spectral reflectance for comparison with the stored look up table. Thus the depth at the pixel of interest is taken to be the depth of the spectral reflectance curve from the look up table which most closely duplicates the shape and magnitude of the computed pixel reflectance.

Table 2 shows the spectra for (i) path radiance, (ii) volume reflectance (R_∞), (iii) diffuse attenuation coefficient, and (iv) three bottom type albedos. The path radiance spectra has a monotomic decrease with wavelength as expected. Only a small fraction of the path radiance is part of the reflected signal, so that radiometric errors are small, while larger radiometric error in the blue has minimal influence because the blue volume reflectances are insensitive to depth.

The R_∞ spectra derived in the preprocessing sessions indicate a fairly light load of suspended solids which is representative of Bruce Peninsula waters[1]. Chlorophyll-a being the major absorber of the visible light field in water affects the diffuse attenuation coefficient as mentioned above. Therefore, as the chlorophyll-a concentration changes so do the R_∞ and K spectral shapes[9].

The assumption of limited variation of water optical parameters within one scene applies most favorably to open waters. However when islands and inlets are part of the scene, the natural water currents do not allow for maximum mixing. Therefore, the R_∞ used in the scene was to be representative of the average over the image area. This was also true of the K spectra derived in preprocessing.

The bottom type albedos were acquired from ground truth reflectance measurements using a barium sulfate plate standard (Lambertian diffuser). Bottom types were measured near shore having an air water interface. Therefore the bottom spectra were corrected to below surface data[10].

Table 2. Preprocessing Derived Optical Spectra

Wavelength (nm)	460	520	550	575	610	670	750
Path Radiance	1.214	0.787	0.648	0.594	0.511	0.384	0.310
Volume Reflectance (R_∞)	5.0	8.2	9.3	8.85	4.5	2.0	
Diffuse Attenuation Coefficient	0.288	0.213	0.20	0.239	0.542	0.658	
Bottom Albedo							
Sand	9.15	12.85	15.8	19.0	19.7	18.6	
Rock/Gravel/Sand/Silt	8.05	11.15	13.73	16.3	17.0	16.93	
Mud/Vegetation	3.45	4.2	5.0	5.45	5.8	6.1	

Comparison of computed depth and soundings

Figures 2 and 3 show a comparison of computed and sounded depths along two separate Northing transects. The rms residual errors relative to the sounded depths are presented below in Table 3 as a function of camera number (camera #5 corresponding to the leftmost region of Figures 2 and 3). An inspection of these residuals along with Figures 2 and 3 reveals an evident correlation with camera numbers and depth.

The camera 5 residuals are felt to be due to a real increase in the optical clarity of the water. Since the present bathymetry algorithms do not allow for spatial variation in the predicted value of the diffuse attenuation coefficient, depth biases related to the real variation of this parameter will occur. In the camera 5 results the increased signal level due to a real decrease in the diffuse attenuation coefficient yields estimates of depth which must be shallow biased if the assumed value of the diffuse attenuation coefficient is overestimated.

In general such errors of estimate will be more severe in deeper water where the effects of particulate scattering dominate bottom reflectance information and the resultant reflectance becomes progressively less sensitive to changes in depth. This is particularly true for the apparent calibration offsets in the bathymetric computations at the larger depths and is borne out by the larger rms residuals in the (deeper) Figure 3 plots.

Table 3. RMS Errors for Computed Depths (meters)

	Camera 5	Camera 4	Camera 3
Figure 2	1.6	1.1	0.6
Figure 3	1.2	1.5	0.4

The camera 3 results are less than 0.6 meters for both transects. Given that the resolution of the reflectance look up table from which depths were extracted was 0.5 meters the rms residuals of this camera are commensurate with the best achievable accuracy. It should be noted however that the superior results achieved for camera 3 are partly attributable to the shallower depths in this region (less than approximately 4 meters).

Summary and conclusion

For sampled imagery profiles of geometrically corrected line scanner data, bathymetric processing yielded measured residuals ranging from less than 1.6 meters for generally deeper water (< 6 meters) to 0.3 meters for shallower water (< 4.2 meters). The greater part of the residual magnitudes were caused by CCD problems found in camera 4, and the spatial variations in water quality parameters, over the swath of the Red Bay scene.

The scanner nonuniformities of CCD sensors are presently being corrected. Therefore, it is expected that the depth computations should reduce the residual range.

Acknowledgments

The authors would like to thank CCRS for its support through the use of field equipment and the AIR II system (presently being developed at MONITEQ Ltd.). We are also grateful to Fisheries and Oceans Canada for financial support of this project.

References

1. Miller, J.R., Dick, K.J., Kalinauskas, A.R., "Water Depth Mapping by Passive Remote Sensing", Final Technical Report - PRAI Project #P-8105. 1984.
2. Hollinger, A.B., "Airborne Programmable Imaging Spectrometer for Shallow Water Digital Mapping", U.S. Army Corps of Engineers Surveying Conference, Jacksonville, Florida. 1985.
3. Gibson, J.R., "A Block Adjustment System Using External Navigation Data", Ph.D. Thesis, University of New Brunswick. 1984.
4. Gordon, H.R., Clark, D.K., "Atmospheric Effects in the Remote Sensing of Phytoplankton Pigments", Boundary-Layer Meteorology (18). 1980.
5. Austin, R.W., Petzold, T.J., "The Determination of the Diffuse Attenuation Coefficient of Sea Water Using the Coastal Zone Color Scanner", "Oceanography from Space", (edited by Gower, J.), Plenum Press, New York. 1981.
6. Clark, D.K., "Phytoplankton Pigment Algorithms for the NIMBUS-7 CZCS", "Oceanography from Space", (edited by Gower, J.), Plenum Press, New York. 1981.
7. Smith, R.C., Baker, K.S., "Optical Classification of Natural Waters", SCRIPPS Institution of Oceanography, SIO Ref. 77-4. 1977.
8. MONITEQ Ltd., "Enhancement of Water Quality Software Final Report", CA910-3-0059/

610. 1985.
9. Morel, A., "In-Water and Remote Measurements of Ocean Color", Boundary-Layer Meteorology, (18). 1980.
10. Lyzenga, D.R., "Reflectance of a Flat Ocean in the Limit of Zero Water Depth", Applied Optics, (16). 1977.

Figure 1. Red Bay Map and Flight Line

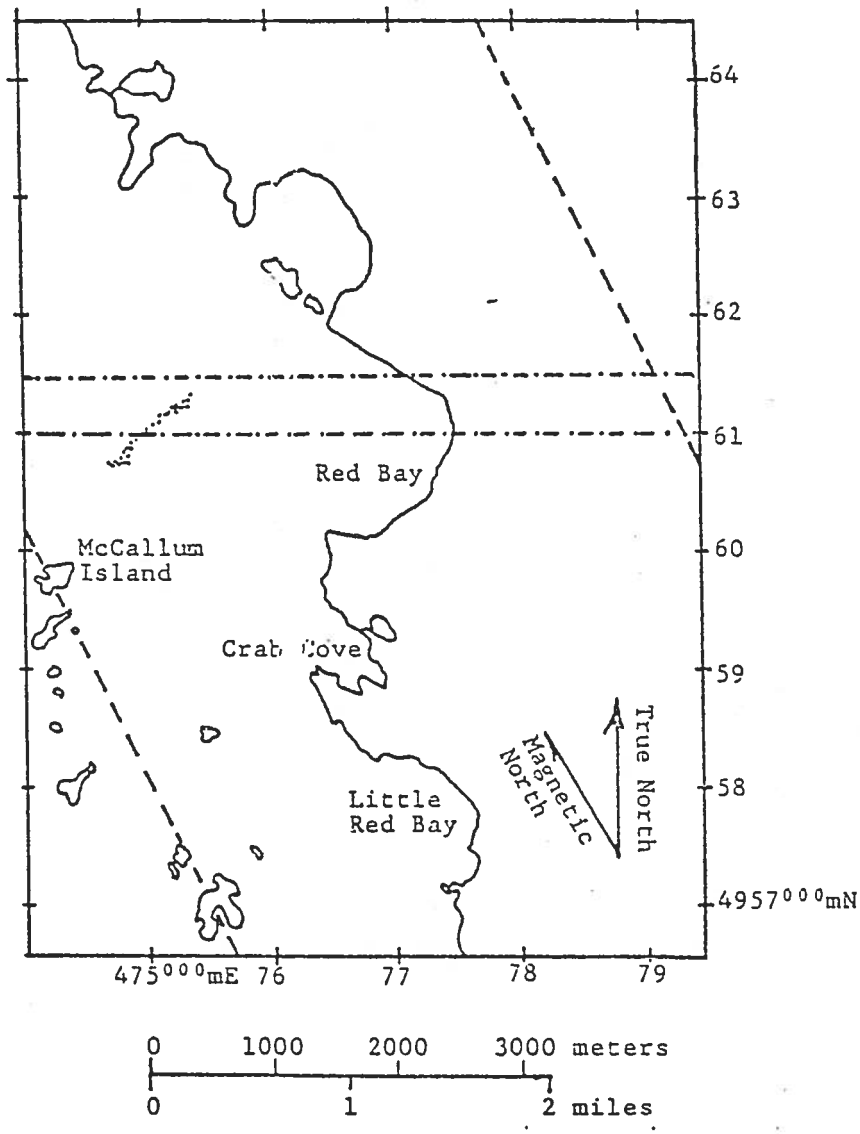

Figure 3. Depth Line Profile along UTM 4,961,000 North

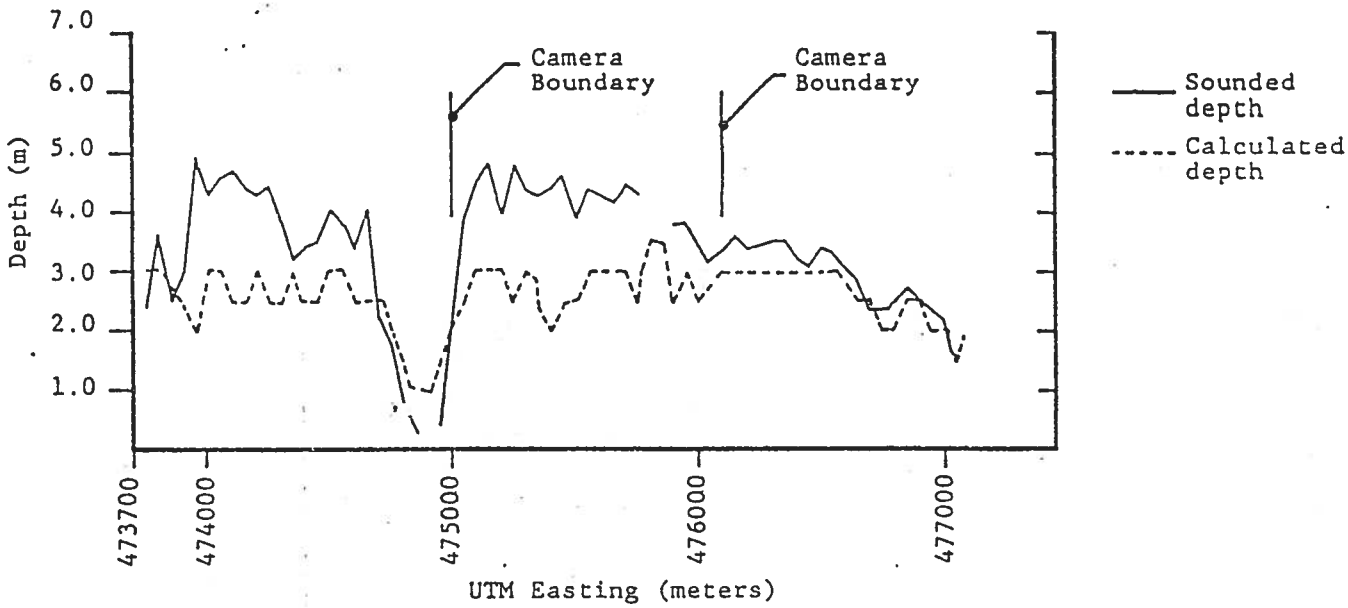

Figure 2. Depth Line Profile along UTM 4,961,500 North

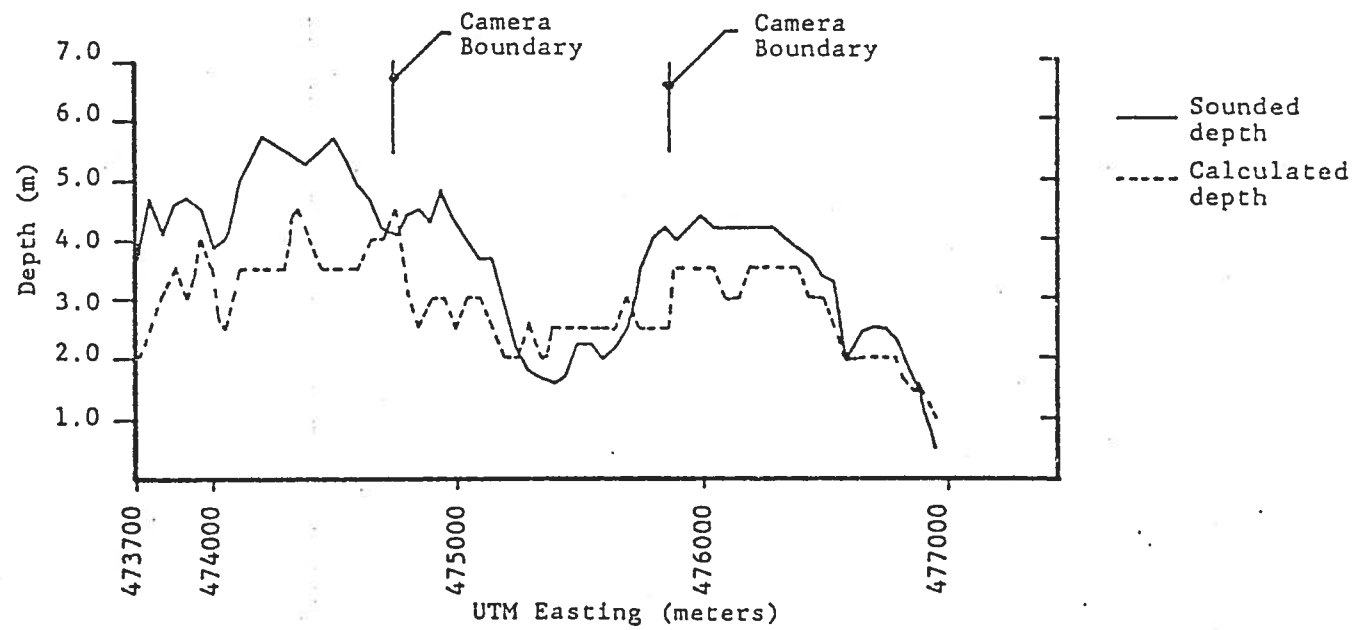

THEMATIC CARTOGRAPHY OF SUBMERGED MARINE PLANTS USING THE FLUORESCENCE LINE IMAGER

Marie Catherine Mouchot

Canada Centre for Remote Sensing

Ottawa, Ontario

Glyn Sharp

Invertebrates and Marine Plants Division

Fisheries Research Branch

Halifax Fisheries Research Laboratory

Department of Fisheries and Oceans

Scotia-Fundy Region

Halifax, Nova Scotia

Elizabeth Lambert

Department of Geography

University of Montreal

Montreal, Quebec

1. INTRODUCTION

Laminaria (kelp) are brown marine algae with long slender stalks and a broad flattened blade attached to the substrate by fibrous holdfasts. They occur in a wide variety of marine environments from the lower intertidal to depths exceding 20 m. Exploitation of Laminaria species exceed 250,000 t wet weight annually in the northern hemisphere (Anon, 1981).

In southwestern Nova Scotia (map 1) kelp resources were assessed between 1948 and 1949, MacFarlane (1952). Advances in ground survey and aerial photography techniques combined with impending utilization of resources lead to a reassessment of resources in 1979 (Sharp et al. 1981; Sharp and Carter 1986). The limited depth penetration by normal color aerial photography (4.0 m) necessitated extensive groundtruthing. Remote sensing techniques have the potential to allow greater depth penetration and higher resolution of resources than conventional photography. However, due to the very weak luminances emanating from a body of water a sensor such as a thematic mapper, developed to pick up the much stronger luninances of terrestrial targets, is not of great interest. Therefore, we tested a new sensor the fluorescence line imager (FLI) developed by Fisheries and Oceans Canada (Gower 1982).

The discrimination of a submerged target, ie. the determination of its intrinsic parameters, is made difficult by the multitude of causes generating variations to the signal returned to the sensor. These variables are:

- bottom reflectance;
- extinction coefficient depth;
- sea state;
- path radiance.

The establishment of thematic cartography for submerged marine plants requires isolatation of causes for signal variation due to the modification of bottom characteristics. Unfortunately the most significant modifications of marine plants reflectance appear at wavelengths of minimum light transmission.

The extinction coefficient as a function of wavelength varies with the water mass (Fig. 1). If we designate the coefficient by K, the transmittance inside a water mass is defined by (-X.K.Z). Where Z designates depth and X is a function of the path followed. At 700 nm, the value of K reaches 0.7 (1/m). L(0) is the luminance descending immediately below the surface, therefore, the luminance at depth Z will be L(Z) as follows:

$$L(Z) \approx L(0) \exp(-0.7.Z) \qquad 1\text{-}1$$

At a depth of 3 m, only 10% of the initial radiance will have been transmitted (Fig. 2).

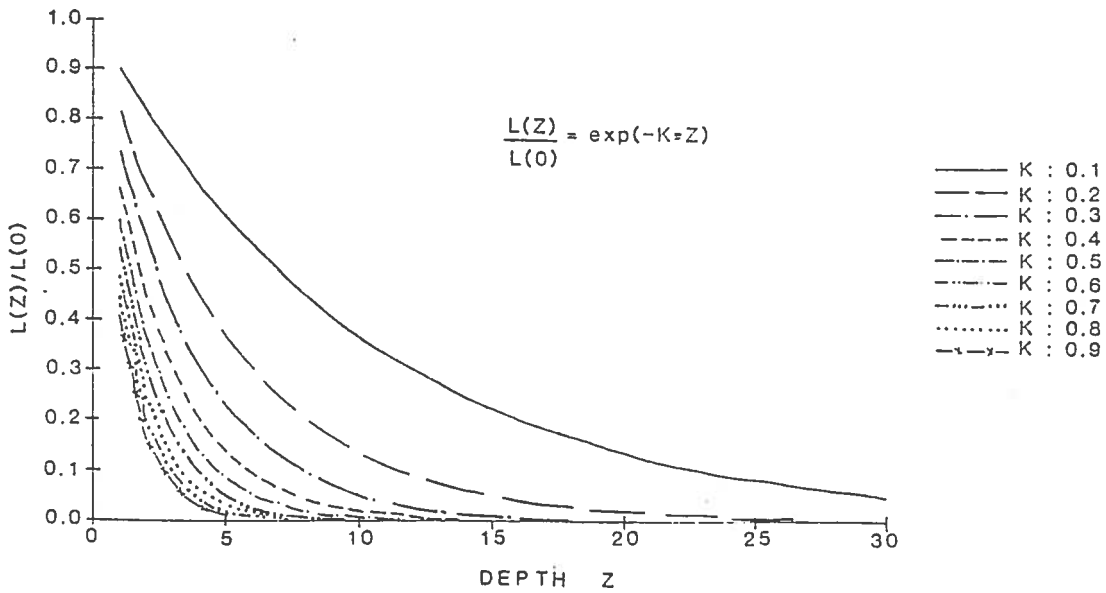

Figure 1: Curves of transmittance as a function of depth.

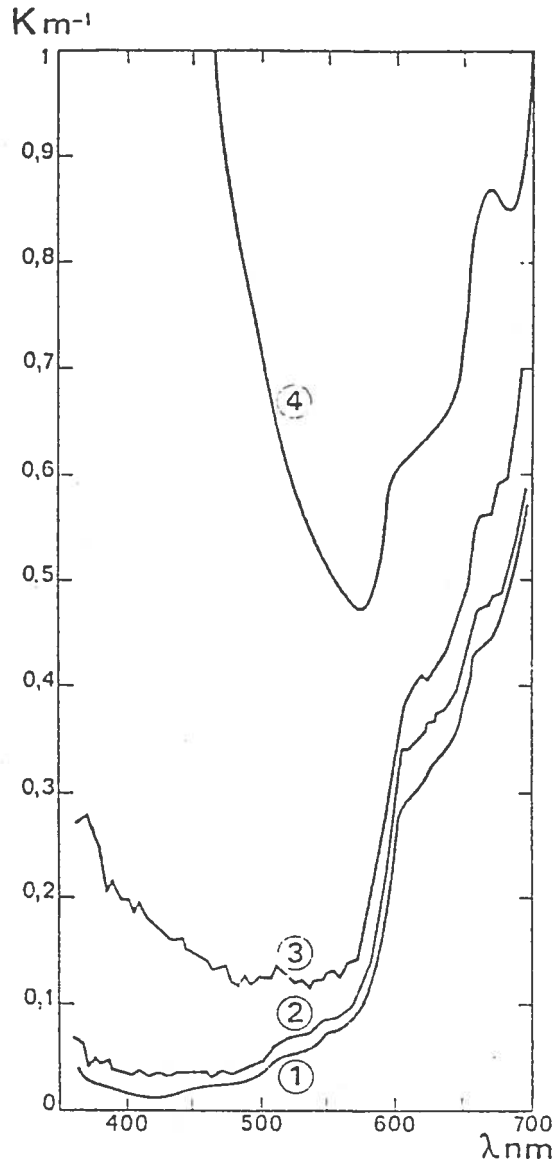

Figure 2. The variation of extinction coefficients with wavelength relative to the spectral density of the descending illumination.

Curve 1: Crater Lake (Oregon U.S.A.) at 10 m depth.

Curve 2: Gulf Stream (25°45'N, 79°30'W), mean value between 0 and 25 m depth.

Curve 3: Gulf of California (25°51'N, 111°2'W) at 8.5 m depth.

Curve 4: San Vicente Lake (California) mean value between 0 and 10 m depth.

Adpated from A. Ivanoff, 1975.

2. THE STUDY AREA

The study area was situated at the southwestern tip of Nova Scotia, extending 30 km north-south and 15 km east-west (map 1). The area included a group of islands in shallow waters (less than 15 m) with high benthic productivity. Two Laminaria species (kelp) are predominant in the subtidal Laminaria longicruris and Laminaria digitata, others Alaria esculenta and Saccorhiza dermatodea are common in the shallow subtidal (Fig. 3). Agarum cribosum occurs in depths below 5 m. The main understory species are short (10 cm) bushy red algae Chondrus crispus and Phyllophora spp. At the edge of the subtidal ~ 0 m Chondrus may predominate but will thereafter, be intermixed with canopy Laminaria species (Fig. 3). Zostera marina phanerogram (eel grass) occurs from 0 to 3 m in areas of mud and sand.

The field data was collected by the Marine Plants Division, Department of Fisheries and Oceans Canada, in Halifax, N.S. (Sharp, et al. 1981; Sharp and Carter 1986).

Our data base was thematic cartography of marine plants obtained by aerial photography and SCUBA diving in 1979. The information was supplemented, at the time of the fly over by real time data: sonar bathymetry, underwater radiance, water samples (for sediment content analysis) and by dives along the flight path where changes in the distribution of marine plants could have taken place.

Analysis of groundtruthing data found the extinction coefficient varied little over the study zone. As a result it was defined as a constant, like the atmospheric transmittance and the surface reflection coefficient.

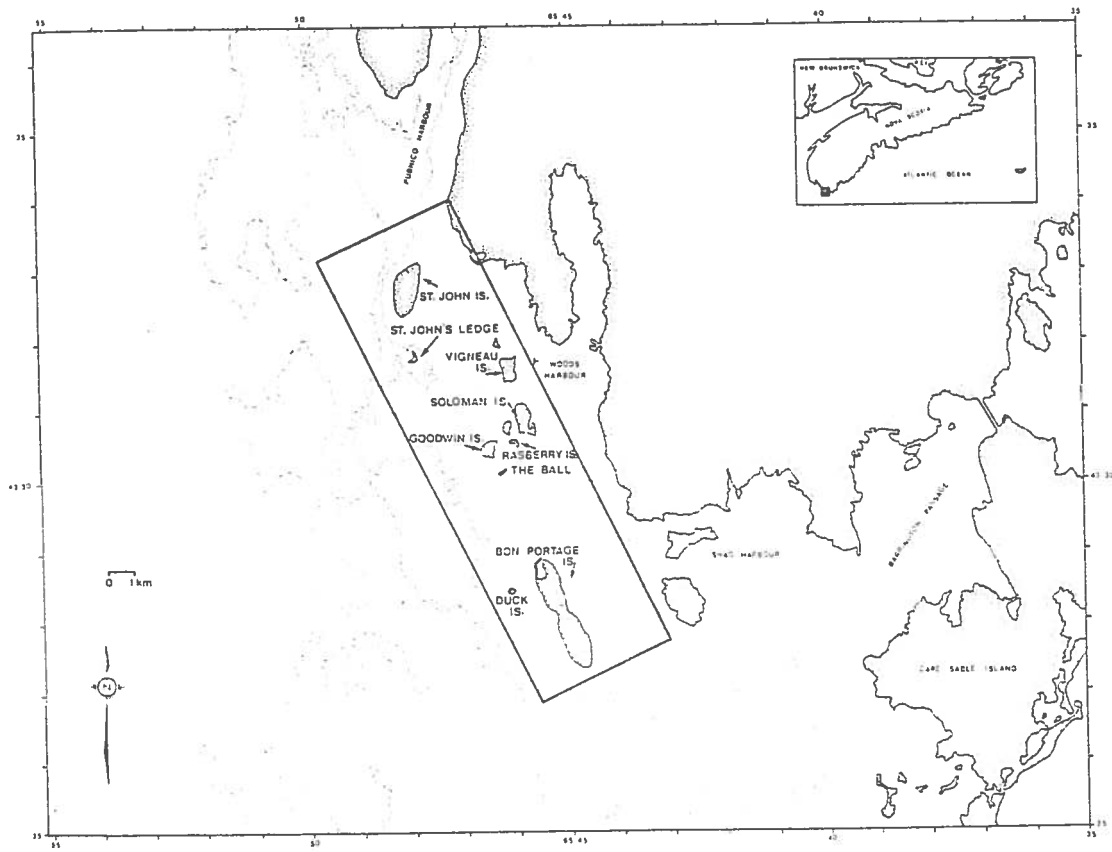

Map 1. The study area

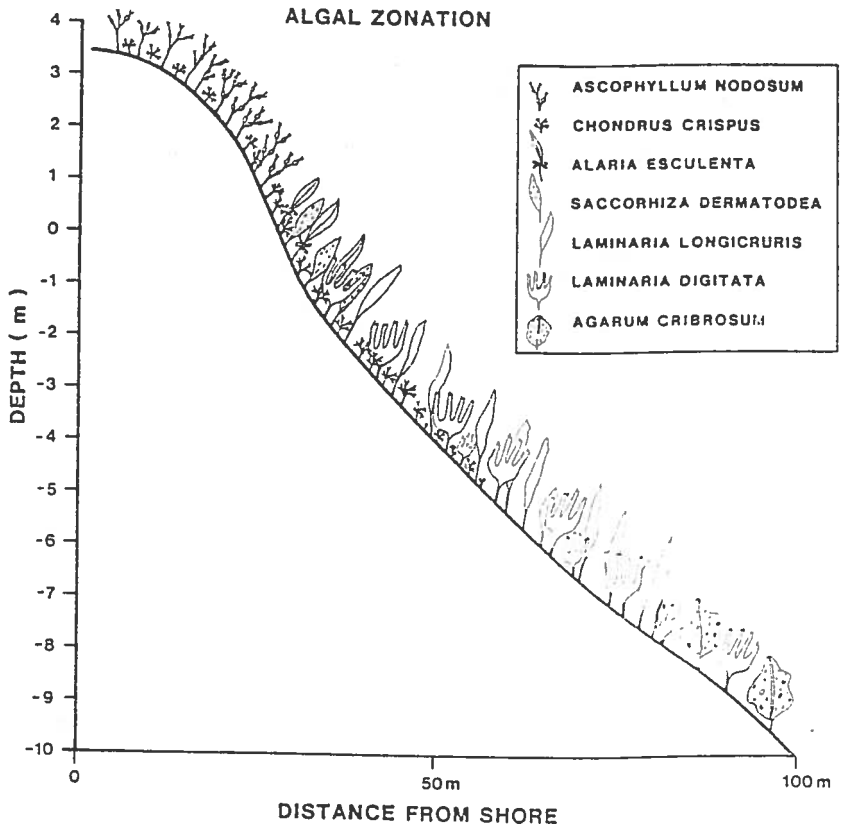

Figure 3. The zonation of major seaweeds in southwestern Nova Scotia relative to tidal level.

3. THE DATA IMAGES

The FLI uses 5 CCD (Charge Coupled Device) frame transfer arrays with two dimensional arrays of light sensitive silicon diodes. Each array contains in the long dimension 385 elements and, in the second dimension, 288 elements covering 430 to 800 nm at spectral intervals of 1.4 nm (Borstad et al, 1986). The desired spectral intervals were obtained by selecting the corresponding diodes in a range from 430 to 800 nm (Table 1).

Table 1. Experimental wavelengths and corresponding diode selection

Channel No.	Wavelength in nm	No. of diodes
1	430 - 460	0 - 22
2	500 - 530	53 - 76
3	550 - 580	91 - 114
4	600 - 630	129 - 152
5	640 - 670	160 - 183
6	690 - 720	199 - 222
7	740 - 770	237 - 261
8	780 - 800	268 - 284

The intrinsic restriction of each camera ($\sim 14°$) field made it possible to avoid the strong differences of luminance appearing between the center and the edges of the image. A faulty adjustment of the different camera gain allowed us to keep only two cameras (number 2 and 3) for analysis purposes; giving a ground cover of 770 pixels. Channel 1 was not utilized due to a high noise level. Therefore, the analysis was completed from seven spectral channels and two cameras.

The dimensions of the pixel, calculated from the acquisition parameters (Table 2) is 6 m in the perpendicular direction of the flight line and 27 m in the direction of the flight line. The later value, was higher than expected, due to weak scanning frequency specified at the time of the flight. (To obtain a square pixel of 6 m, we would have needed a scanning frequency of 37 Hz).

Table 2. Acquisition parameters for FLI data southwestern Nova Scotia.

Date/hour	Altitude (m)	Speed (m/s)	Heading (Deg)	Scanning (Hz)
27-07-85 12:25 (low tide height = 0.9m)	8,536	227	161	8.3

Wheather conditions during the flight were clear skies and a sea state 2.

An echo phenomenon caused by an internal reflection at the camera's optical system level was present on the image. The configuration of the ground target, i.e. an island of high reflectance at one end of the camera and the ocean, of low reflectance at the other end created this phenomenon. The intensity of echo I, is defined as the ratio of the radiance (L) of a deep water target in the echo zone over the radiance of a deep water target outside the echo zone. This ratio increased with wavelength from 1.06 in channel 2 to 1.50 in channel 8. It means an exponential increase which may be described by $I=0.65e^{\lambda}$, with λ in μm. Diagrams 1 to 3 show the intensity of the phenomena in camera 3 along a line going from St. John Island to Bon Portage Island (the radiance intensity carried by the y axis is encoded in digital count). Photography no. 1 displays the phenomena occuring in channel 7 between St. John Island and Goodwin Island. The echo zones were excluded from the subsequent analysis.

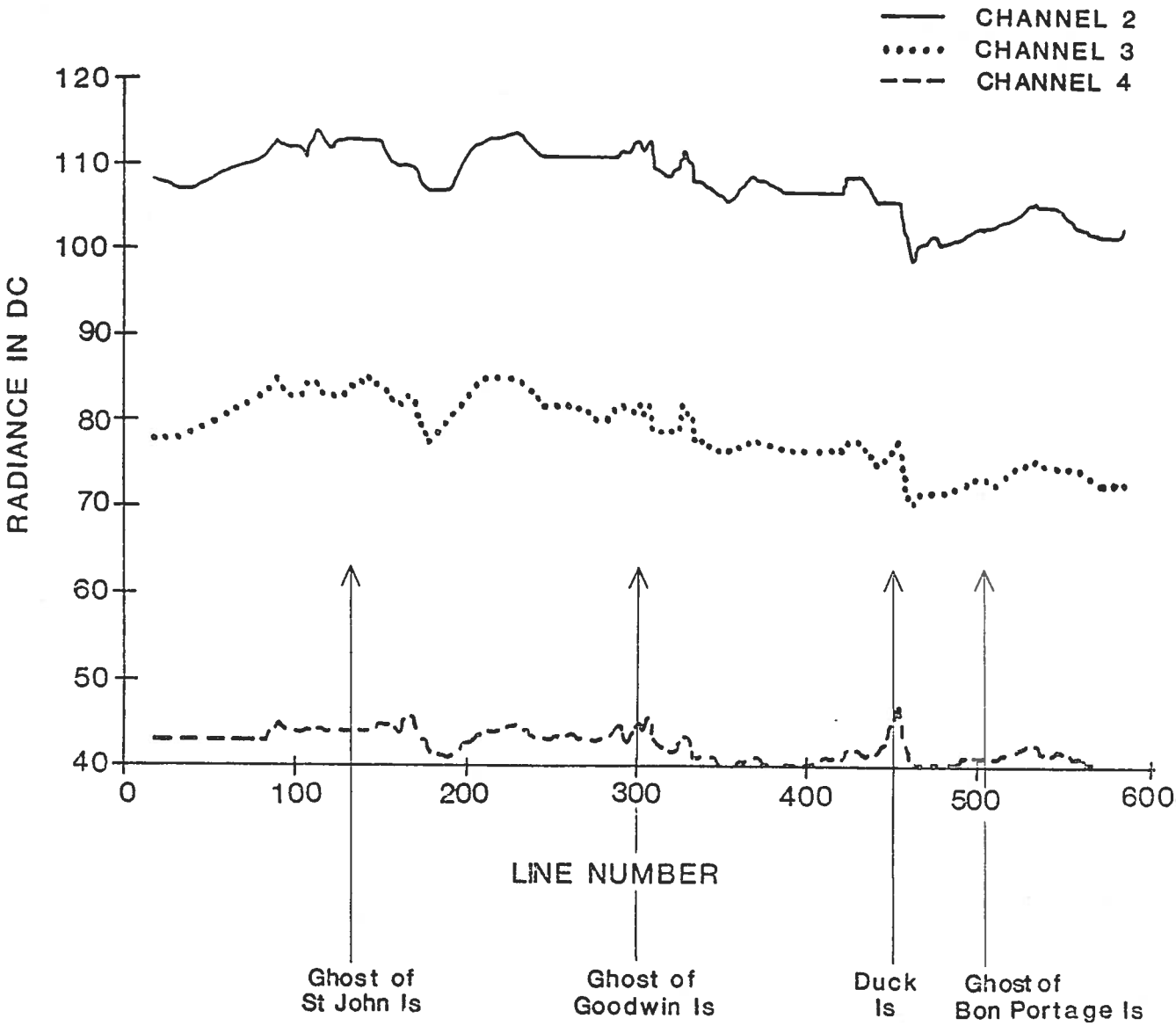

Diagram 1.The ghosting effect:channels 2,3,4

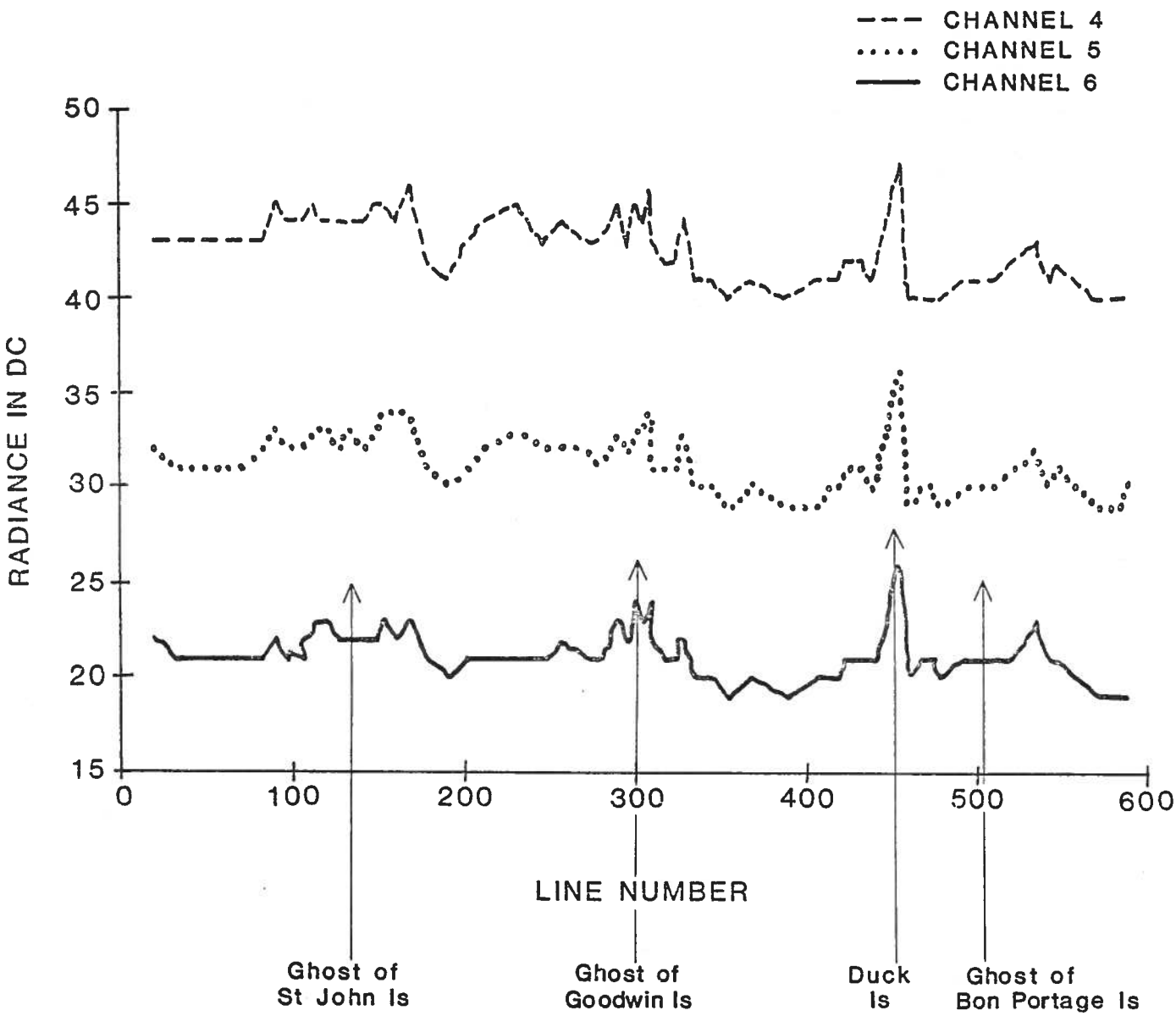

Diagram 2.The ghosting effect:channel 4,5,6

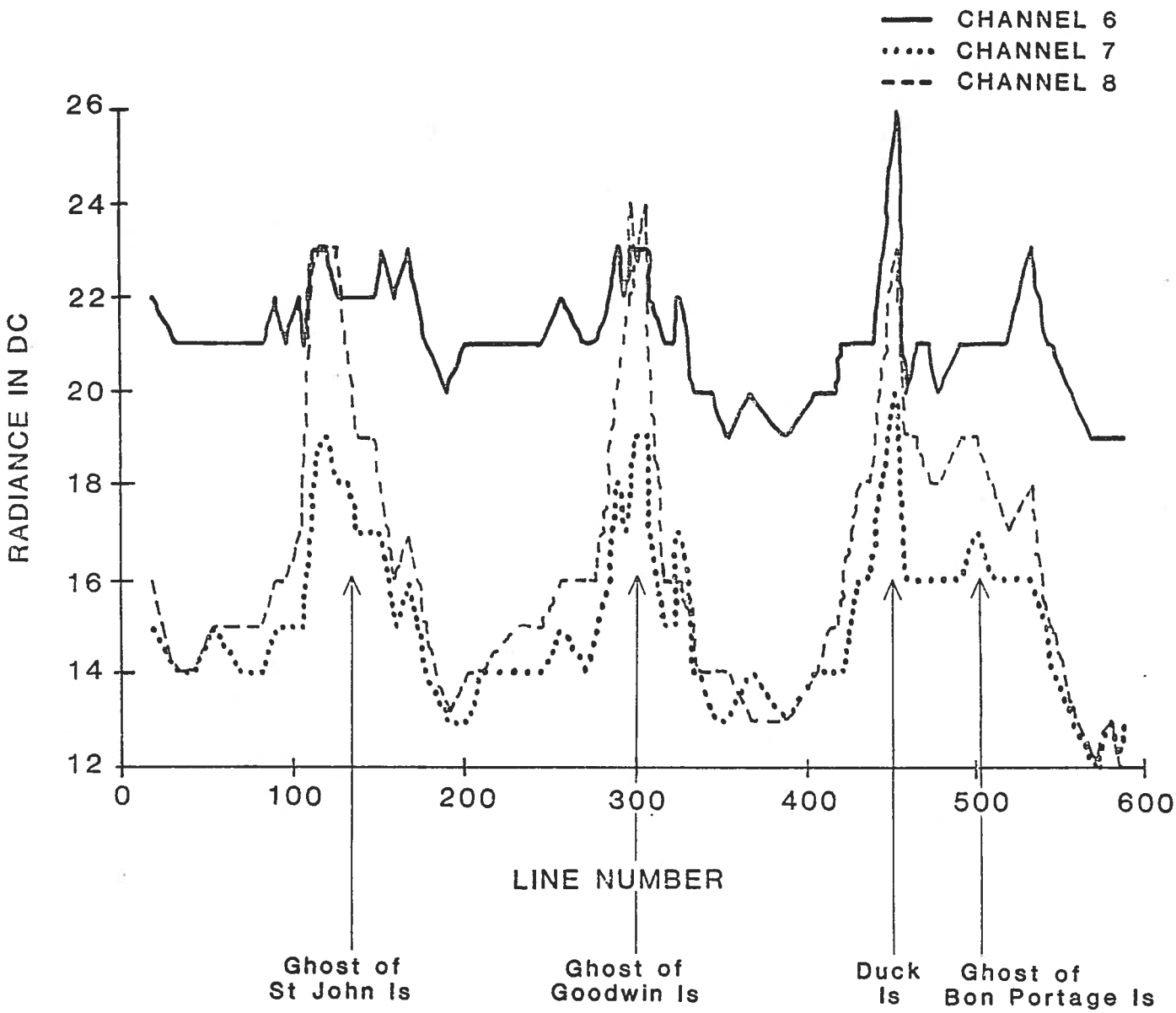

Diagram 3.The ghosting effect:channels 6,7,8

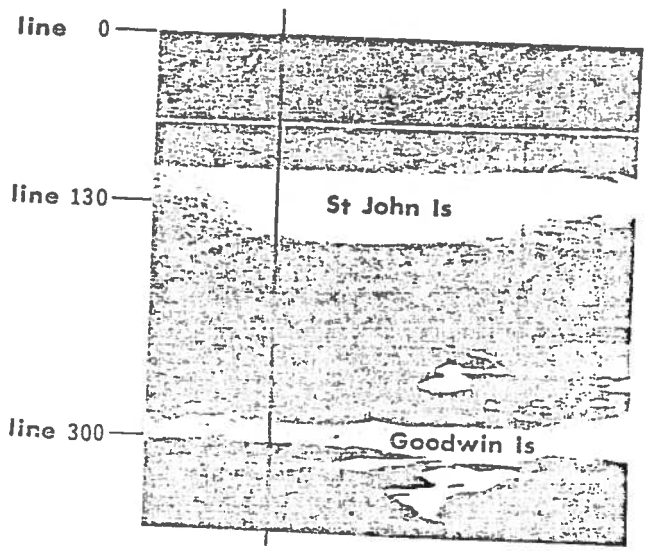

Photography 1: the ghosting effect in channel 7

4. METHODOLOGY

Two methods were evaluated to discriminate between the effect of depth and the effect of reflectance from the bottom. The first, (Lyzenga 1978, 1979, 1981) uses the band ratios and should allow without knowledge of the local bathymetry isolation of targets with the same reflectance. In this study none of the band ratios considered allowed discrimination with enough confidence between different bottom reflectances.

As a result we developed a second method. The data from the local bathymetric map was numerized and superimposed to the remote sensing image, providing a known depth for each point. In keeping the basic equation (Lyzenga, 1978):

$$L_i = L_{pi} + \propto R_i \exp(-X_i \cdot K_i \cdot Z) \qquad 3\text{-}1$$

where L_i denotes the radiance received at the sensor emenating from the target considered, L_{pi}, the radiance observed above deep water, R_i, the bottom reflectance and $\propto$ a parameter taking into account solar illumination, surface reflection and atmospheric transmittance.

We then chose a target of known reflectance at two distinct depths: Z_1 and Z_2:

$$L_1 = L_{pi} + \propto R_i \exp(-X_i \cdot K_i \cdot Z_1) \qquad 3\text{-}2$$

$$L_2 = L_{pi} + \propto R_i \exp(-X_i \cdot K_i \cdot Z_2)$$

$$\frac{L_1 - L_{pi}}{L_2 - L_{pi}} = \exp[-X_i \cdot K_i (Z_1 - Z_2)] \qquad 3\text{-}3$$

$$(-X \cdot K)_i = \frac{\ln \frac{L_1 - L_{pi}}{L_2 - L_{pi}}}{\Delta Z}$$

Once the coefficients $(-X \cdot K)_i$ were determined in each of the spectral bands, we corrected the original image by applying:

$$\propto R_i = \frac{L_i - L_{pi}}{\exp\,(-X_i \cdot K_i \cdot Z_{mean})}$$

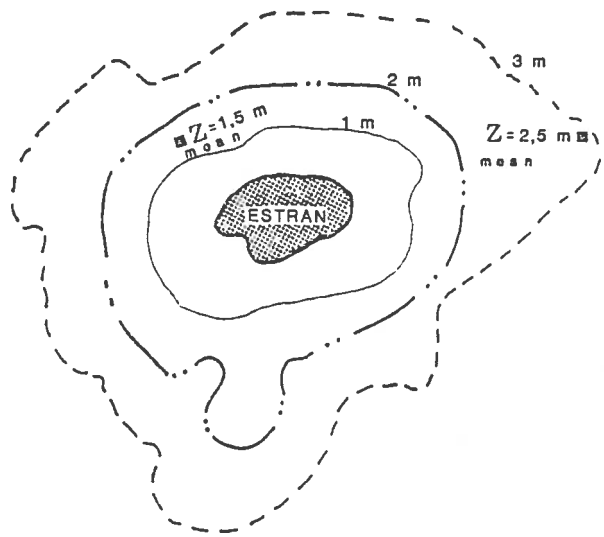

Figure 4. Definition of mean depth applied for the correction of depth effect.

5. ANALYSIS AND RESULTS

The problem of depth effect correction is not as simple as the model lead us to believe. The theory applies well to the species type Chondrus or Zostera and to the non-poplulated substrates, but it is different for Laminaria. Kelp, having a large vertical structure, will cause the return signal to be issued for a same zone from many depths. In addition, their length is not a direct function of depth which makes the correction of the effect of depth according to local bathymetry problematic (Fig. 5 a & b).

The presence of currents in the study zone tend to flatten the kelp against the substrate, increasing the phenomena's complexity and the difficulty of modeling corrections.

We introduced through this depth correction, an over correction of the reflectance of the deeper zone kelp of the deeper zone. In the shallower zones there are mixed populations of Chondrus and - kelp or Chondrus and - Zostera, the correction was wrong, because the reflected signal came from the upper part of the plant and is not at the same depth for the different species. An important error was probably introduced in the definition of equation 3-1.

L_i is defined by: (Austin, 1974).

$$L_i = \alpha R_i \cdot \exp(-X_i \cdot K_i \cdot Z_i) + \beta Rw_i) \qquad 4\text{-}1$$

Where R_{wi} represents the ratio of ascending light to descending light at wavelength i.

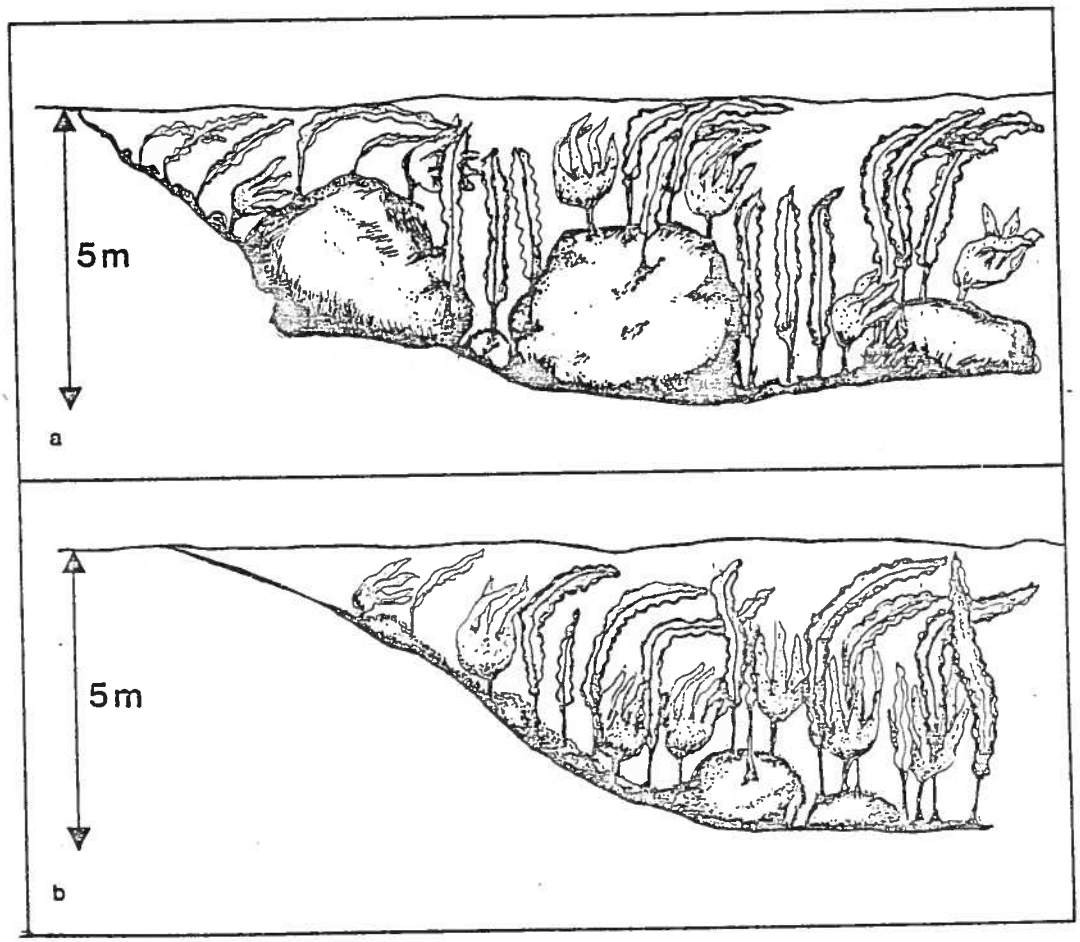

Fig.5. The depth effect

To obtain equation 3-1 we suppose that in deep water $L_i = L_{pi} = \beta RW_i$; the value RW_i is supposed to be independent from depth. However, it was observed (Ivanoff, 1961) that in shallow waters, the accumulation of particles near the bottom could bring about an increase in the ratio RW.

Equation (3-1) should therefore read:

$$L_i = L_{pi} + \alpha R_i \exp(-X \cdot K \cdot Z) + \varepsilon_z \qquad 4\text{-}2$$

The error introduced in the calculation of $(X \cdot K_i)$ will then be of the order of:

$$\varepsilon = \frac{S_1}{L_1 - Lp_i} - \frac{S_2}{L_2 - Lp} \qquad 4\text{-}3$$

where the indices 1 and 2 denote depths Z_1 and Z_2. The shallower the water, the more we will underestimate the value of $(X \cdot Z)$. Particularly above non populated substrates (sand), the reflectance will be under evaluated.

The bathymetric map due to its limits of resolution does not always show single anomalies (shoals) often populated by species other than those normally defined at the depth marked on the map.

We had to conclude that in the case of remote sensing of a mixed marine plants population (plants with a predominant vertical morphology and plants with a predominant horizontal morphology) associated with non populated substrates, it was better not to resort to depth correction.

The data was analyzed directly by principal components analysis of the seven spectral bands, after masking, by threshold in band 8 (near-infrared), the emerged zone.

By principal component analysis the maximum contrasts were extrac·ed out of each of the seven original channels, to assemble them into a reduced number of images. These contrasts, expressed by the variances, are accentuated according to the targets, such as sand, subtidal algae and the intertidal plant species. The zones of sand were the easiest to discriminate on the original images, while there was little differences between the levels of gray representing the intertidal and the submerged plants (Fig. 6). To accentuate the contrasts of the plant population zones we defined three training sites in three different populations. The first site was situated in a Laminaria population (-2 to -15 m). The second site included an intertidal algae population, mainly composed of Chondrus (+1.0 - -3 m). The third site, also in shallow waters (+.3- -5 m), was a Zostera marina population. All the populations mentioned above were submerged at the time of the flight.

Four components were then produced using the covariance matrices:

"Laminaria" site, with 7 spectral bands;

"Chondrus" site, with 7 spectral bands;

"Chondrus" site, with 5 spectral bands;

"Zostera" site, with 7 spectral bands.

Sixteen images were finally generated, amongst which five were kept to form a color composite where the contrasts between the different targets proved to be best defined.

Examination of the eigenvectors demonstrates the degree of the variance of the original images in these five new components (Table 3).

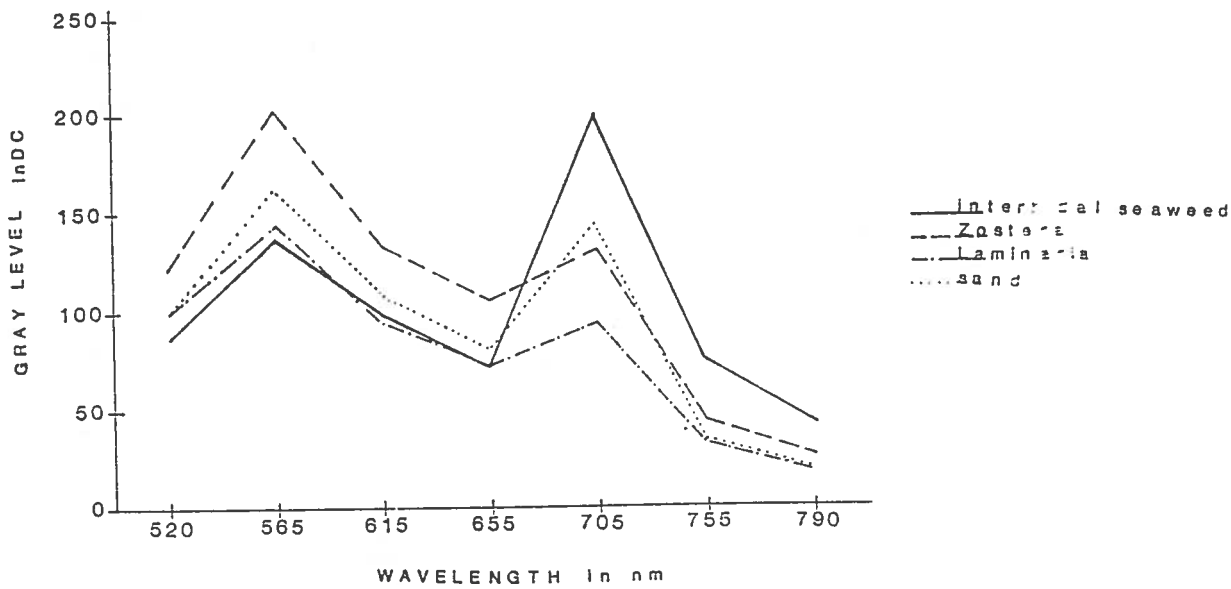

Fig 6. Radiances in DC of different kinds of seaweed.

Table 3. Eigenvectors of the principal components combined to form the final image for the target species.

Description of the training site						
Channel	Laminaria fourth	Chondrus second	Component FLI Channel	Chondrus third	Zostera second	Zostera third
2	-8.83	3.76	2	0.83	1.50	11.93
3	-16.53	0.11	3	-	2.15	-0.76
4	23.49	-1.09	4	1.76	1.22	-7.86
5	17.85	0.55	5	-	0.78	1.29
6	-11.77	-0.94	6	0.82	-1.23	0.15
7	0	1.62	7	-0.89	0.11	-0.82
8	0.11	-0.96	8	-0.58	0.09	-0.47

The image created from the Laminaria training site contains a highlighting of the algae population submerged in deep waters. This information comes mainly from channel 4 (615 nm) and 5 (655 nm). Channels 7 and 8 (755 and 790 nm) made no contribution to the formation of this component. The component created from the "Chondrus" site, with the seven spectral bands, contains information coming mainly from channel 2 (520 nm), while the use of only five bands created a component where the weight of channel 4 is the most important. Thus, information was obtained on the submerged intertidal algae at two levels. In the first case, the shallow depth populations are highlighted and in the second case, the mixed populations of Chondrus crispus and Laminaria (transition zone). The components created with the training site "Chondrus", emphasize the variance

of channel 7 and 8, revealing the plant biomass floating near the surface of the water. The populations of Zostera marina are shown by accentuating the contrasts of channel 3 (565 nm), for the second component and those of channel 2, for the third component. The variance in channel 7 and 8 is very weakly represented in these two components; similar to kelp, this type of plant is totally submerged.

The five components were associated to form a color composite according to 3 axis; red, green and blue (Table 4). Photography no. 2.

Table 4. Representation of the principal components in the final image.

Axis	Color	Principal components	Site
1	red	fourth	Laminaria
2	green	third and second	Chondrus and Zostera
3	blue	second and third	Chondrus and Zostera

We obtained for each group of plants defined (Laminaria, Chondrus, Zostera and mixed population) an estimate of the areas populated (Table 5). Numerized bathymetry was used to calculate the area of species distribution by 1 m depth ones.

Table 5. The coverage by depth of the different species determined from the FLI image of the study area.

Depth (m)	Laminaria	Chondrus	Area (ha) Mixed populations	Zostera	Total
0-1	66.89	3.66	50.85	52.42	174
1-2	105.93	0.46	14.56	4.41	125
2-3	112.42	0			
3-4	228.74	0	16.75	0.40	246
4-5	59.53	0	2.84	0.10	62
5-7	51.16	0	2.84	0	54
7-9	34.45	0	2.22	0	37
9-11	26.37	0	0	0	26
11	0	0	0	0	0
Total	685	4	95	58	842

Dark green = Laminaria
Pink = Laminaria-Chondrus
Red = Chondrus

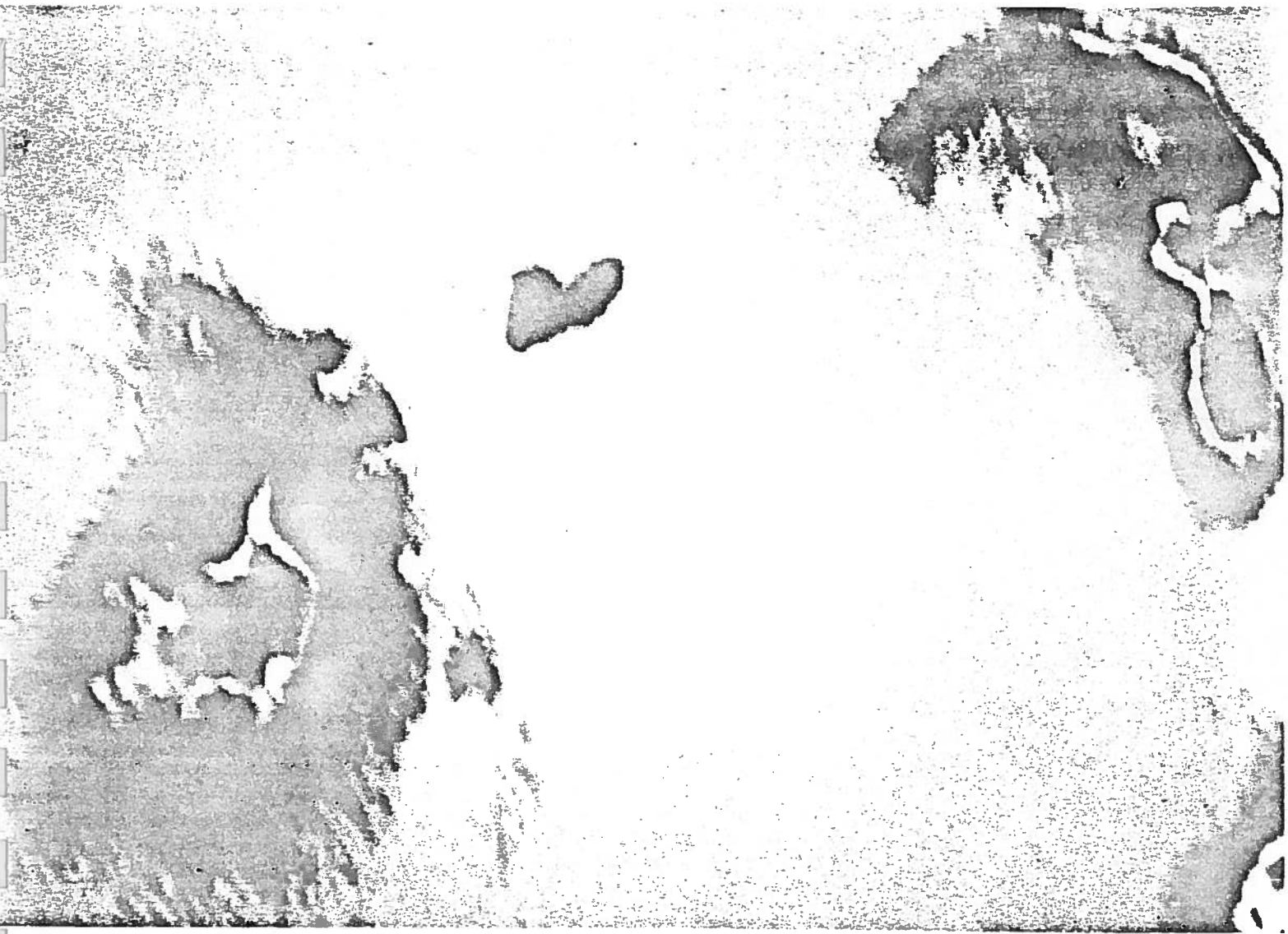

Photography 2. Color composite : area of St. John Ledge

Analysis by manual methods of 1:10:000 Kodak Aero color 23 x 23 cm format diapositives defined 363 ha of *Laminaria* in the study area (Sharp and Carter, 1986). Groundtruthing by divers added 214 ha to the total area. However, FLI analysis defined 322 ha more *Laminaria* beds than color photography (Table 6).

Table 6. A comparison of remote sensing and direct survey methods used to locate *Laminaria* resources.

	SURVEY METHOD				
Location	Color photo Kelp ha	Groundtruthing+ Kelp ha	Total	FLI Kelp ha	Mixed
St. John Is.	20	21	41	30	5
Bon Portage Is.	113	100	213	290	19
Duck Is.	16	23	39	41	6
St. John Ledge	36	40	76	62	9
Subarea totals	185	184	369	423	39
Survey area	363	214	577	685	

+additional area detected

The conservation assumptions made for the areas between groundtruth transects partially explains the earlier underestimate of kelp cover. The peak biomass density occurs between 1 and 5 m depth (Sharp et al. 1981). The zone maximum occurence identified by FLI was similar, 65% of kelp cover was located between 1 and 4 m (Table 5). Mixed populations of kelp and *Chondrus* had a maximum coverage in the 0-1 m depth zone. Since the emerged zone was eliminated from the analysis an unknown fraction of the area identified as *Chondrus* - *Laminaria* mix in 1981 would be eliminated in FLI analysis.

St John Island's subtidal areas ranged from extensive shallows 2 m on its eastern shores to a steeply sloping (20 m) wave exposed western shore.

FLI analysis identified 52% more cover than color photography (Table 6). Groundtruthing located an additional 21 ha primarily in depths below 5 m (Sharp and Carter, 1986).

Bon Portage Island was the largest land mass and longest shore line in the survey area (map 1). The wave exposed western shore had a shallow slope to a depth of 10 m over 1 km from shore. The eastern wave sheltered shores made a transition from boulder substrate to sand within 200 m of shore and 4 m depth. FLI analysis detected a wider distribution with depth versus distribution in the total survey area. The water penetration conditions were ideal on the eastern side of Bon Portage Island; calm clear waters with contrasting substrate types allowed color photography to accurately describe this area. However, less ideal conditions on the western side were more suitable to FLI. Use of FLI added 71.0 ha of kelp principally in depths 5 m (Table 6).

Duck Island on the western side of Bon Portage Island had very close agreement between groundtruthing and FLI analysis (Table 6). The small confines of Duck Island allowed more accurate use of color photography and groundtruthing.

St. John Ledge is an area with a small intertidal area and extensive shoals (5 m). Groundtruthing defined a kelp area exceeding that located color photography (Table 6). Similar to Duck Island the groundtruthing to area ratio was high.

FLI determination of the maximum limits of kelp distribution was in close agreement with groundtruth results (Table 7). Except in a few cases (e.g. Bon Portage east) these limits exceeded those defined by aerial photography. Comparison of mixed species distriubution was difficult since

Table 7. A comparison of FLI analysis of kelp and mixed species limits with groundtruth 1:10,000 color photography data from southwestern Nova Scotia.

Location	Transect number	Target	FLI		Groundtruth		Air Photo	
			Outer limit m	Depth m	Outer limit m	Depth m	Outer limit	Depth m
St. John Ledge	42	mixed	~200	3	140	3		
		kelp	500	7	700	9	400	5
St. John Ledge	44	mixed	100	1	45	1		
		kelp	600	10	600	10	500	8
St. John Ledge	41	mixed	100	1.5	140	1.5		
		kelp	400	10	400	10	250	2
St. John Ledge	43	mixed	100	1	100	1		
		Kelp	300	6	300	6	300	6
St. John Ledge	19	mixed	200	1	140	1		
		kelp	400	10	400	10	250	4
St. John Is.	15	mixed	50	2	20	2		
		kelp	100	5	250	10	100	5
	22		200	6	220	6	100	4
Bon Portage Is.		mixed	50	1	40	1	150	4
West	39	kelp	1000	10	600	8	150	
East	5	mix	50	1	35	1		
			2000	4	220	4	200	4

the presence of an understory did not relate directly to the designation mixed. Groundtruthing could not define a 50/50 cover as the determination was based upon an abundance index for Chondrus and density for Laminaria. The mixed zone was frequently narrow (100 m) and the resolution of FLI was a factor. However, the correspondence between these two measures was within a factor of 2 (Table 7). No comparison was made for the mixed zone between FLI and air photos since for analysis we eliminated the emerged zone included in aerial photography.

Three areas resulted from FLI analysis had anomalies or an indeterminate target. Special groundtruthing was completed in these areas to identify the targets.

Zostera/Laminaria mix over a sand substrate grading to exclusively Zostera gave a specific signature. A similar mix of Zostera and Laminaria occurred between Goodwin and Raspberry Island.

Bon Portage Island North East tip had two areas of which proved to be sand/rock bottom with filamentous alga Chorda filum in patches.

FLI identifed the population up to a depth of -11 m. The presence of populations at greater depth is uncommon. North of St. John Island, we found kelp below 11 m, that was not recorded up by the FLI. In the Coastal waters of the North Atlantic, a depth of 10 to 11 m represents the threshold limit of detection of marine plants for the FLI.

Nevertheless, if the sensor seems to be capable of detecting marine plants at 10 m, it does not mean that it can pick up a signal coming from that depth. Indeed, the species populating these depths are of strong vertical structures and it is, in the majority of cases, the upper part of the plant that is at the origin of the signal received by the sensor.

7. CONCLUSION

FLI is a method of resource assessment providing depth penetration beyond the limits of maximum Laminaria coverage. To obtain equivalent resolution conventional air photography must be supplemented by costly ground surveys (Sharp, et al. 1981). The combination of bathemetric and FLI data permits correlation of coverage with depth; which is one of the most important factors determining resource utilization.

The setbacks experienced when we tried to correct for the effect of depth have emphasized the need for a cautious approach when using remote sensing bathymetric studies (Jain et.al. 1983 and 1982).

Notwithstanding the defects of quality of the sensor, that were already mentioned, first-rate results were obtained regarding the distribution of the submerged marine plants. The performance of the FLI images, in this field is, by far, superior to those of other methods used for the same purposes, whether aerial photograph or satellite images.

ACKNOWLEDGEMENTS

The authors thank Dr. J. Gower, Department of Fisheries and Oceans, Pacific for asccess to the FLI and critical review. G. Borstad for providing the FLI data. D. Tremblay for technical asistance, T. Alföldi and B. Neville for support and helpful critique. The pilot and crew of the CCRS Falcon for data acquisition.

REFERENCES

Austin, R.W., 1984. The Remote Sensing of Spectral Radiance from Below the Ocean Surface. Optical Aspects of Oceanography, pp. 317-343.

Borstad, G.A. et al., 1985. Analysis of Test and Flight Data from the Fluorescence Line Imager. Canadian Special Publication of Fisheries and Aquatic Sciences 83, Department of Fisheries and Oceans, Ottawa.

Gower, J.F.R., 1982. The "Fluorescence Line Imager" Program for Improved Mapping of Sea Surface Chlorophyll from Space. NAFO Science Coun. Studies, Volume 4, pp. 61-62.

Ivanoff, A., 1961. Quelques résultats concernant les propriétés diffusantes des eaux de mer, Union Geod. Géophys. Intern., Monographie, 10, pp. 45-51.

Ivanoff, A, 1975. Introduction à l'océanographie T.2. Propriétés physiques et chimiques des eaux de mer. éd. Vuibert.

Jain, S.C. et al., 1982. Passive Bathymetric Measurements of Inland Waters with an Airborne Multispectral Sanner. Proceedings of the International Symposium on Remote Sensing of Environment, January, Le Caire, Egypte, Vol. II, pp. 947-951.

Jain, S.C., H.H. Zwick et R.A. Neville, 1981. Passive Bathymetry with Airborne Multispectral Scanner, 7th Canadian Symposium on Remote Sensing, Manitoba, pp. 513-519.

Jerlov, N.G., 1968. Optical Oceanography, Elsevier Publishing Company.

Lyzenga, D.R., 1978. Passive Remote Sensing Techniques for Mapping Water Depth and Bottom Features, Applied Optics, Vol. 17, 3, pp. 379-383.

Lyzenga, D.R., 1981. Remote Sensing of Bottom Reflectance and Water Attenuation, Parameters in Shallow Water Using Aircraft and LANDSAT Data, International Journal of Remote Sensing, Vol. 2, pp. 71-82.

Lyzenga, D.R., 1979. Shallow-water Reflectance Modeling with Applications to Remote Sensing of the Ocean Floor, 13th International Symposium on Remote Sensing of Enfironment, pp. 583-602.

Sharp, G., J. Carter, D. Roddick and G. Carmichael, 1981. The utilization of color aerial photograph and groundtruthing to assess subtidal kelp (Laminaria) resources in Nova Scotia, Canada. Tech. Papers ASP-ACSM meeting San Francisco. pp. 57-67.

Sharp, G and J. Carter, 1986. Biomass and population structure of kelp (Laminaria spp) in southwestern Nova Scotia, Can. Man. Rep. Fish & Aqua. Sci. in press.

Anom, 1981. Pilot survey of the world seaweed industry and trade. International Trade Centre UNCTAD/GATT Geneva 111p.

MacFarlane, C., 1952. A survey of certain seaweeds of commercial importance in southwestern Nova Scotia. Can. J. Bot., vol. 30, pp. 78-97.

THE CANADIAN OPTICAL SENSOR WORKING GROUP

S.M. Till
Data Acquisition Division, Canada Centre for Remote Sensing
2464 Sheffield Road, Ottawa, Ontario K1A 0Y7
Telex: 053 3589

The Optical Sensor Working Group meets from time to time, to evaluate proposals for future optical remote sensing satellite systems and to provide preliminary specifications, conceptual designs and performance analyses for proposed optical systems as opportunities arise. Important considerations include the user requirements and the advances in technology and system design. The aim has been to satisfy both the user requirements for system performance, and the design constraints introduced by the state of technology and by the space-platform, or to find an acceptable compromise. During the past few years, the working group has considered and evaluated optical sensors for RADARSAT (References 1,2,3), and has recently considered the possibilities offered by a polar-orbiting platform (Reference 4). For this last activity, the working group members were drawn from the Canada Centre for Remote Sensing, the Communications Research Centre and the National Research Council, and had experience in remote sensing systems, optics and satellite systems. The group consulted the user agencies, such as the Departments of Fisheries and Oceans, of Environment, of Agriculture, and the Forestry Service and the Geological Survey, who provided input on the performance requirements to be considered in the system evaluation. The remote sensing advisory committees in Canada have also provided valuable input to these studies and discussions.

User Requirements

A major application of remote sensing in Canada is resource management, and the monitoring of renewable and non-renewable resources. User requirements for performance tend to be based on past experience with satellite data, such as the LANDSAT thematic mapper, with airborne data and with ground data. Data from airborne sensors such as the Canadian imaging spectrometer (the fluorescence line imager) and the pushbroom imager (MEIS) are characterised by high performance and spectral flexibility, and exposure to this type of data has led to new applications, and new expectations for satellite systems. Ground spectroscopic studies of targets result in the better understanding of spectral signatures and influence the requirements for spectral bands.

User applications related to agriculture include the monitoring of global and domestic crop condition and yield, the estimation of crop areas, and the documenting of catastrophic events such as floods. For these, the timeliness of the data (or frequency of coverage of

---

Presented at Canada-Germany Workshop, Ottawa, October 14-17, 1986

the target area) is an important feature, as is the spectral band selection which should be optimised for the specific crop/confusion crop. Of interest in forestry management is the identification of forest species, plus the mapping of clear cuts, and the detection and mapping of disease and damage; high spatial resolution and selectable high spectral resolution bands appear of major importance. The applications of ocean remote sensing range from the monitoring of primary productivity, to the monitoring of coastal processes and water quality. For these, critical factors are the radiometric responsivity because of the low reflectance of the ocean, and the dynamic range, if land or ice are also being imaged. These are just a few of the applications of an earth-observation optical sensor, and give an indication of the potential versatility of such a system.

Technical Considerations

The parameters of major interest to the user include: the geometric characteristics (spatial resolution or pixel size, geometric fidelity); the radiometric specifications (sensitivity, or signal-to-noise ratio at a specified target reflectance and solar elevation; dynamic range or, in user terms, the minimum and maximum scene radiance); the digitisation rate required to reflect this performance; the spectral channels (number, width, location); and the sensor look-angle. These parameters determine the engineering or design specifications, and it is necessary to calculate the impact upon sensor design of the various spatial geometric parameters, radiometric constraints and signal-to-noise ratios that are considered desirable from the applications viewpoint. These specifications should be realistic in terms of the state of the technology. For example the element size and well depth of ccd array detectors, the maximum analog to digital rate, and the imaging optics have certain limitations and design constraints. Similarly, as the number of elements across the swath is increased, mechanical or optical butting methods may be required with an array detector design to increase the swath, at the expense of more complex signal sampling, and/or increased optical train and mass, and more constraints on the optics focal plan design. The specifications should also be realistic in terms of the satellite platform; for example, there will be limitations on mass, volume, and power consumption, and on the data recording rate and downlink rate. Other considerations include the selection of on-board processing functions and post-flight processing, and the validation and calibration of the satellite system. An airborne system is considered an important component of a satellite system development; as part of the sensor development and testing program, as a satellite simulator to provide familiarity with the data characteristics, and to provide underflights and back-up to the satellite operation itself.

The optical systems considered by the working group have been of the multi-element array detector type (pushbroom imager, imaging spectrometer) which offer inherent advantages of radiometric sensitivity, and so spectral and spatial resolution. The members of the group were able to draw upon the considerable experience in Canada with this type of imaging sensor. Two advanced airborne optical imaging sensors have been successfully built in recent years by Canadian industry, the MEIS (References 5,6) and the Fluorescence Line Imager, whose design and operation are described in detail elsewhere in the Proceedings (by Gower, Borstad, Hollinger, etc.). These programmes have been accompanied by the development of real-time processors for such types of systems (Reference 7). The access of the user to such data has been accompanied by the development of processing techniques and new applications. The performance of an advanced optical system is to a great extent limited by detector performance, so that improvements are linked to detector improvements. Two items of note in this area in Canada have been the development of "mechanical butting" of detector arrays, and the development and patent of silicon detectors of enhanced blue response and dynamic range (Reference 8). The working group members were also able to draw upon experience in satellite data reception and data processing. The two Canadian ground receiving stations acquire LANDSAT, NOAA and SPOT data with plans for ERS-1 data, and the acquisition program has been accompanied for many years by an active programme in remote sensing applications, image analysis and methodology.

REFERENCES

1. Optical sensor for Radarsat, CCRS report 82-14, October 1982.

2. Optical sensor for Radarsat, J. Cihlar, R. O'Neil, F. Ahern, S.M. Till, Proceedings of 8th Canadian Symposium on Remote Sensing, 49-62, 1983.

3. The Radarsat RMOMS optical sensor, S.M. Till, F.J. Ahern, H. Werstiuk, and D. Meissner, Proceedings of 10th Canadian Symposium on Remote Sensing, 1985 (in press).

4. Preliminary specification for a space platform advanced optical sensor, CCRS Technical report, 1985, S.M. Till, R. Gauthier, R.A. Neville, R. Brown, J. Cihlar, H. Edel, D. Caswell, R. Wlochowicz, F. Ahern.

5. Evaluation of the prototype MEIS, Research report 78-5, H.H. Zwick, J.N. de Villiers and W.D. McColl, CCRS, Department of Energy, Mines and Resources, 1978.

6. Development and evaluation of the MEIS II imaging sensor, R.A. Neville, W.D. McColl, S.M. Till, Proceedings of SPIE, 395, 101-108, 1983.

7. Enhanced data acquisition capabilities, Remote Sensing in Canada, 13,4, 1985.

8. A novel wide dynamic range silicon photodetector and linear imaging array, S.G. Chamberlain and J.P.Y. Lee, IEEE Journal of solid-state circuits, SC-19, 41, 1984.

OPTICAL SENSOR WORKING GROUP

CANADA CENTRE FOR REMOTE SENSING
COMMUNICATIONS RESEARCH CENTRE
NATIONAL RESEARCH COUNCIL

CANADA-GERMANY WORKSHOP ON IMAGING SPECTROMETRY

S.M. TILL, OCTOBER 15, 1986

OPTICAL SENSOR WORKING GROUP

- SPACE OPTICAL SENSORS:
  - RADARSAT
    - "OPTICAL SENSOR FOR RADARSAT", 1982, 1984
    - "R-MOMS" , 1985, 1986
  - POLAR ORBITER

- CONSIDERATIONS:
  - USER REQUIREMENTS
  - ADVANCES IN TECHNOLOGY AND SYSTEM DESIGN

USER APPLICATIONS AND REQUIREMENTS

A) EXPERIENCE:

E.G. LANDSAT MSS, TM
CZCS
(SPOT)

AIRBORNE DATA MEIS, MSS, FLI

GROUND DATA

B) PARAMETERS:

E.G. SPATIAL RESOLUTION
SWATH WIDTH
SPECTRAL BANDS (WIDTH, LOCATION, NUMBER)
RADIOMETRIC SENSITIVITY
LOOK-ANGLE
DATA TIMELINESS

C) SAMPLE USER REQUIREMENTS:

RESOURCE MONITORING:

AGRICULTURE	GLOBAL CROP CONDITION/YIELD
	AREA ESTIMATES
	CATASTROPHIC EVENTS
FORESTRY	SPECIES IDENTIFICATION
	DISEASE DETECTION
	CLEAR CUT MAPPING
OCEANS	PRIMARY PRODUCTIVITY
	COASTAL PROCESSES
	WATER QUALITY
GEOLOGY	

TECHNOLOGY:

MULTI-SPECTRAL IMAGING SYSTEMS:

ROTATING MIRROR, "SINGLE" DETECTOR E.G. MSS, TM

- SENSITIVITY (SPECTRAL BANDWIDTH, SPATIAL RESOLUTION)
- MOVING PARTS

PUSHBROOM IMAGER

I) - LINEAR ARRAY E.G. MEIS, SPOT

II) - 2D ARRAY E.G. FLI

- MULTIPLEX ADVANTAGE
  SENSITIVITY, SPECTRAL BANDWIDTH, SPATIAL RESOLUTION
- SIMPLE OPTICAL DESIGN (I)
- SPECTRAL BAND SELECTION IN FLIGHT (II)
- NO MOVING PARTS (GEOMETRIC FIDELITY)
- CALIBRATION

SOME TECHNICAL CONSIDERATIONS

SPATIAL RESOLUTION AND SWATH WIDTH

DETECTOR ELEMENT SIZE

OPTICS (FOCAL LENGTH, FOCAL PLANE LENGTH, F/NUMBER)

DETECTOR ELEMENTS PER ARRAY

FIELD-OF-VIEW

SPECTRAL BANDS

INTERFERENCE FILTERS

DISPERSING ELEMENT

BANDWIDTH

NUMBER

RADIOMETRIC SPECIFICATIONS

I) MINIMUM SCENE RADIANCE (TARGET REFLECTANCE
SOLAR ELEVATION)

MAXIMUM SCENE RADIANCE (SATURATION LEVEL)

II) RADIOMETRIC RESOLUTION

RADIOMETRIC RANGE

(N.B. DIGITISATION RATE OF DATA, ANALOG TO DIGITAL, GAIN SWITCHING, LOOK-UP TABLES)

SOME TECHNICAL CONSIDERATIONS

DATA RATE

- SENSOR GROUND VELOCITY
- PIXEL SIZE, SWATH WIDTH
- DATA DIGITISATION RATE
- NUMBER OF SPECTRAL BANDS
- "HOUSEKEEPING"
- (DOWN-LINK)

ON-BOARD PROCESSING

CALIBRATION

POST-FLIGHT PROCESSING

AIRBORNE SYSTEM

- SATELLITE SENSOR DEVELOPMENT
- SATELLITE SIMULATION
- SATELLITE BACK-UP AND UNDERFLIGHTS

STATE-OF-THE-ART OPTICAL IMAGING SENSORS IN CANADA

E.G. MEIS I, II: FOR CCRS, BY MACDONALD, DETTWILER & ASSOCIATES, BRITISH COLUMBIA

MEIS II: 1982-1986, OPERATIONAL USE IN CCRS FALCON

- 200 AIRBORNE MISSIONS
- EVALUATION OF PUSHBROOM IMAGERY
- DEVELOPMENT OF DATA PROCESSING, CALIBRATION SYSTEM
- RESEARCH AND DEVELOPMENT OF REMOTE SENSING APPLICATIONS IN AGRICULTURE, FORESTRY, WATER QUALITY STEREO, CARTOGRAPHY, VEGETATION STRESS, GEOBOTANY, SATELLITE SIMULATIONS...
- HIGH SPECTRAL RESOLUTION DATA
- HIGH SPATIAL RESOLUTION DATA

FLI*: FOR FISHERIES AND OCEANS BY MONITEQ, ONTARIO, AND ITRES, ALBERTA

CANADIAN SATELLITE DATA EXPERIENCE

DATA ACQUISITION,
IMAGE ANALYSIS, METHODOLOGY
APPLICATION DEVELOPMENT

DETECTOR DEVELOPMENT IN CANADA

E.G. DYNAMIC RANGE
BLUE-RESPONSE
ARRAY BUTTING

* FOR DESIGN, EVALUATION, AIRBORNE MISSIONS AND RESULTS, SEE PRESENTATIONS BY GOWER, HOLLINGER, BORSTAD, ETC. ELSEWHERE IN WORKSHOP PROCEEDINGS.

Dark green = Laminaria
Pink = Laminaria-Chondrus
Red = Chondrus

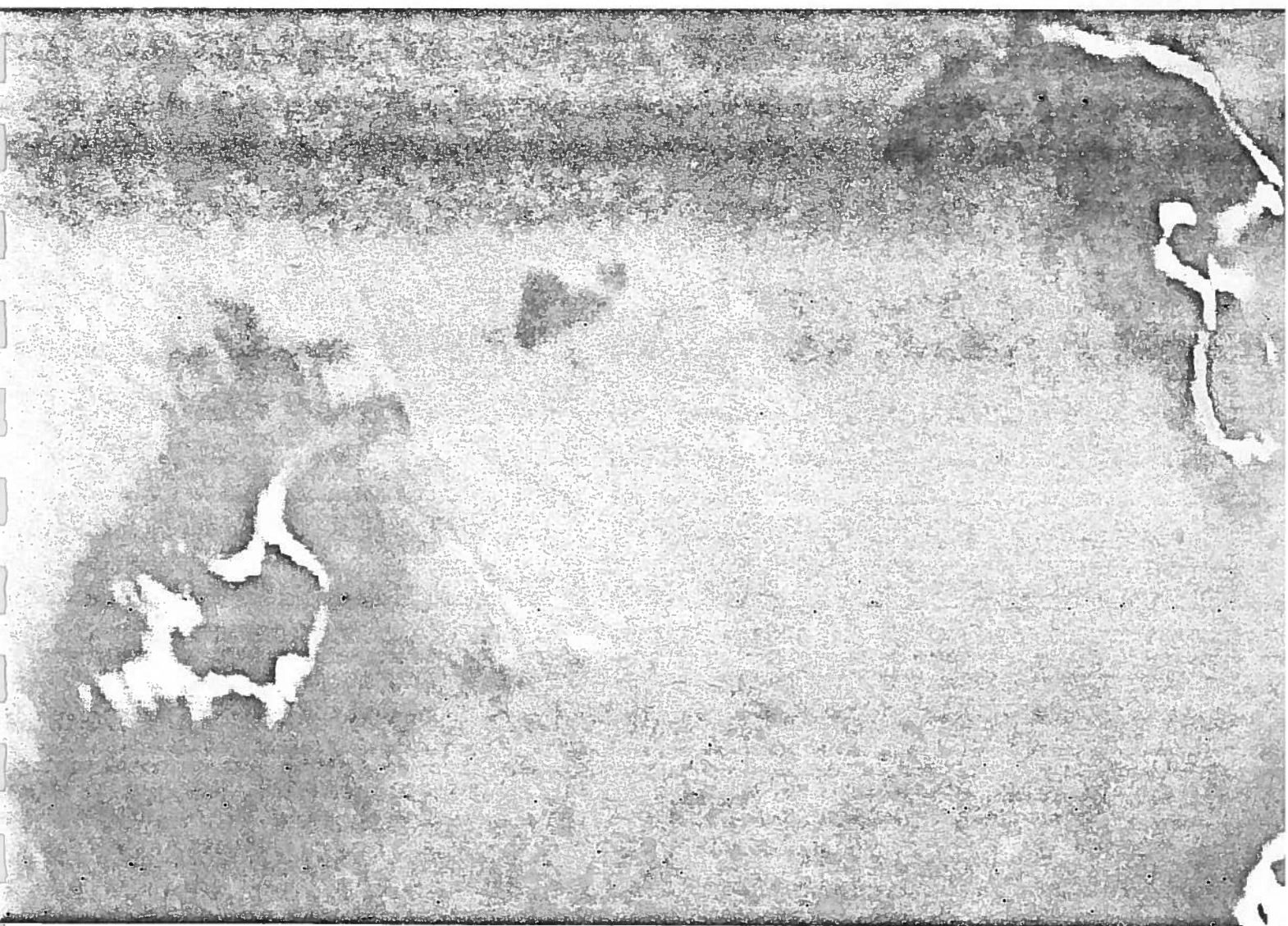

Photography 2. Color composite : area of St. John Ledge

LASER REMOTE SENSING OF THE MARINE ENVIRONMENT: RECENT RESULTS OBTAINED WITH THE OCEANOGRAPHIC LIDAR SYSTEM

D Diebel-Langohr, T Hengstermann & R Reuter

University of Oldenburg, FR Fermany

ABSTRACT

A lidar system was developed for research in the coastal zone. Based on spectroscopic methods data relevant for oceanographic studies and for marine pollution monitoring are obtained. Operated from aircraft, a nearly synoptic investigation of extended areas is achieved.
The system was utilized in experiments in the North Sea and the Adriatic. Data on the spectral light turbidity and on the concentration of dissolved organics (Gelbstoff) and chlorophyll a are reported. By use of nanosecond laser pulses and a fast signal receiver depth profiles of the attenuation coefficient down to 6 attenuation lengths were measured. Airborne measurements were performed over marine oil spills. They allowed a determination of the oil type, and of the oil film thickness in the micrometre range.

Keywords: laser remote sensing, lidar, depth profiling, Gelbstoff, chlorophyll, light attenuation, oil spill monitoring.

1. INTRODUCTION

In the past decade remote sensing methods have become an important tool in oceanographic research. The use of satellites for measurements of the colour of the sea by means of scanning optical radiometers has led to remarkable results over the open ocean. These systems allow a sensitive delineation of the primary production in the surface layer since water colour can be related to the presence of phytoplankton (Ref. 1). However, problems arise for the interpretation of data obtained over coastal waters where other substances such as suspended minerals and dissolved organics (Gelbstoff) optically compete with phytoplankton (Ref. 2). Because of the masking effect of the atmosphere a quantitative evaluation of these substances has not been achieved so far.

Another method of remote sensing makes use of lidar systems installed in aircraft. A closer distance of typically 100-500 m between the instrument and the water surface reduces atmospheric effects significantly. Laser spectroscopy enables a specific measurement of the spectral light turbidity and of the concentration of Gelbstoff and chlorophyll a. Some of these quantities can be detected as profiles down to depths corresponding to about 6 attenuation lengths.

Shipboard measurements with limited horizontal resolution can thus be extended by airborne lidar data of the surface layer obtained over larger areas. Moreover, synoptic satellite imagery can be calibrated along the flight line in terms of the water constituents which determine the water colour measured by the satellite.

In addition to the investigation of these parameters being of interest for oceanographic research, lidar allows monitoring of marine oil pollution. Due to the specific optical properties of mineral oils an identification of the oil type, a measurement of oil film thickness in the micrometre range, and detection of submerged oil volumes floating at depths up to a few attenuation lengths is achieved.

In this paper we describe the Oceanographic Lidar System (OLS) developed at the University of Oldenburg. Designed as a profiling system the instrument meets the requirements for oceanographic research, in particular with respect to a sensitive measurement of hydrographic parameters. Concerning oil spill investigations where a scanning system is far superior due to the high spill variability at scales of less than 100 m, only the principal capabilities of lidar can be demonstrated. Results of oceanographic experiments and of oil spill monitoring exercises performed in the North Sea and the Adriatic are discussed.

2. THE OCEANOGRAPHIC LIDAR

2.1 Principle of measurement

The oceanographic lidar is an active sensor by which an optical probing of the upper water layer from an airborne platform is achieved. Basically it consists of a high power laser emitting pulses at near UV or visible wavelengths where seawater shows good light transmission, and of a gated signal receiver for the investigation of laser-induced radiation from the water column.

Monochromatic irradiation of natural seawater yields spectral structures (Fig. 1) which are related to (i) elastic Rayleigh and Mie scattering, (ii) water Raman scattering being shifted by a wavenumber of 3400 cm^{-1} with respect to the excitation line, its intensity reflecting the penetration

Proceedings of the 3rd International Colloquium on Spectral Signatures of Objects in Remote Sensing, Les Arcs, France, 16—20 Dec. 1985 ESA SP-247)

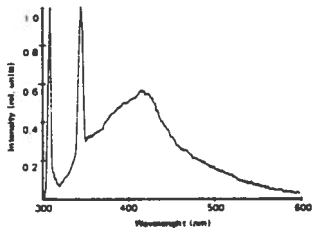

Figure 1. Emission spectrum of a natural water sample taken from the German Bight. Excitation wavelength 308 nm. The peaks at 308 and 344 nm are due to elastic and water Raman scattering. The fluorescence band centred at 420 nm is due to Gelbstoff. The curve is corrected for the spectral response of the instrument and normalized to the Raman scatter intensity.

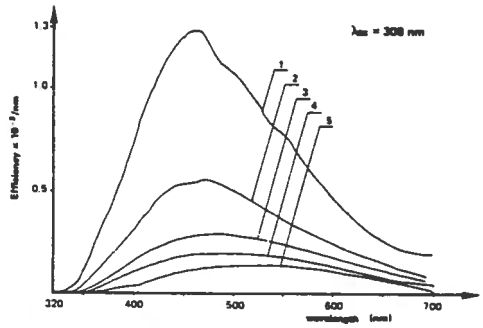

Figure 2. Emission spectra of (1) Statfjord crude oil, (2) Arabian light, (3) Arabian medium, (4) Arabian heavy crude oil, (5) fuel oil. The predominance of heavy or light oil fractions determines the intensity and shape of the spectrum from which information on the oil type is deduced. Excitation wavelength 308 nm.

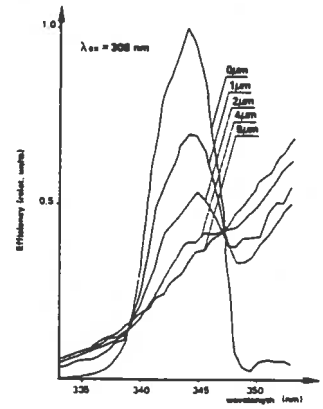

Figure 3. Depression of water Raman scatter due to absorption by a Statfjord crude oil film on the water surface. Excitation wavelength 308 nm.

depth of the laser beam into the water column and the attenuation of the Raman scattered light on its way back to the water surface, (iii) fluorescence of Gelbstoff and chlorophyll a (the latter, not shown in Figure 1, peaking at 685 nm with a half width of 20 nm).

It will be shown in Section 2.2 that the intensity of the detected water Raman scatter signal is proportional to the inverse sum of light attenuation coefficients at the laser and water Raman scatter wavelengths. Gelbstoff and chl a concentrations are derived from their fluorescence intensities normalized to the water Raman scatter signal (Ref. 3-4); systematic errors which are produced by the spectral light attenuation coefficient being generally different at water Raman and fluorescence detection wavelengths must be reduced by a spectrally close selection of the corresponding detection channels (Ref. 5). Concerning chl a the dependence of the specific fluorescence efficiency on the ambient light field and other factors must be taken into account (Ref. 6). Elastic scattering detected at the laser excitation wavelength principally contains information on the concentration and size distribution of hydrosols if bistatic lidar systems are utilized (Ref. 9). However, airborne investigations of this method have not been achieved so far.

The presence of mineral oil on the water surface drastically changes the clear water signature measured with lidar: water Raman scattering is damped due to the high absorption coefficient of oil, and oil fluorescence arises covering the whole visible spectrum (Figs. 2, 3). Both effects depend sensitively on the laser wavelength, on the oil type and the film thickness and provide thus a means for quantitative measurements of these oil parameters (Ref. 3, 10-13). Concerning film thickness, the sensitivity of lidar ranges between .1 and 50 μm; these values are characteristic of spills due to illegal release of mineral oil at sea, whereby lidar has a potential for the investigation of those pollutant contributions.

2.2 Theory of operation

The hydrographic lidar equation (Ref. 14) describing the signal dP received from a depth interval dz at depth z is written as

$$dP = A\,\eta\,\frac{\exp\left(-\int_0^z c\,dz'\right)}{(z+nH)^2}\,dz \qquad (1)$$

with z=0 on the water surface, η denoting the quantum efficiency of fluorescence or scattering, c the sum of light attenuation coefficients at the laser and detection wavelengths, H aircraft flight height, m refractive index of water, and A including instrumental factors, signal loss in the atmosphere and effects of the rough water surface on the beam propagation.

Integration of Eq. 1 over a homogeneous layer at $z_1<z<z_2$ yields (Ref. 5, 13)

$$P_{z_1 \to z_2} = A \exp\left(-\int_0^{z_1} c\,dz\right)\frac{\eta}{c}\left(\frac{1}{(z_1+nH)^2}-\frac{\exp\left(-c(z_2-z_1)\right)}{(z_2+nH)^2}\right) \qquad (2)$$

representing the general solution of the lidar equation for the response of a water or oil layer in an arbitrarily stratified water column. Assuming a homogeneous situation, integration between z=0 and $z \gg 1/c$ results in (Ref. 14)

$$P = \frac{A}{(mH)^2}\,\frac{\eta}{c} \qquad (3)$$

Normalization of a fluorescent signal P_F to the water Raman scatter signal P_R yields

$$\frac{P_F}{P_R} = \frac{\eta_F}{\eta_R} \Big/ \frac{c_R}{c_F} \qquad (4)$$

Assuming c_R/c_F = const. which holds approximately for a narrow spectral selection of fluorescence and

Raman detection wavelengths, Eq. 4 is proportional to the fluorescent matter concentration $n_F \eta_F$ since the water Raman efficiency η_R is a constant. For the same reason P_R describes the sum of the light attenuation coefficients c_R at the laser and the Raman scatter wavelength.

2.3 Instrument description

The Oceanographic Lidar System (OLS) has been designed for airborne investigations of hydrographic parameters. The instrument is a profiling sensor allowing a simultaneous application of two laser excitation and 7 detection wavelengths for a specific measurement of light turbidity, and of Gelbstoff and chl a concentrations as outlined in Section 2.1. Flight height during operation is typically 200 m.

An excimer laser serves as the main light source with 10 MW peak power and 12 ns pulse width at 308 nm. Front and rear laser output are utilized as lidar beam or as pumping beam for a dye laser with 1 MW peak power and 6 ns pulse length at 450 nm. Maximum pulse repetition rate is 20 Hz.

Signal receiver is a Schmidt-Cassegrain f/10 telescope with a 40 cm aperture diameter. The field of view, almost coaxial with the laser beams, is set to 5 mrad which corresponds to the excimer laser beam divergence. At 200 m flight height this results in a footprint diameter of 1 m.

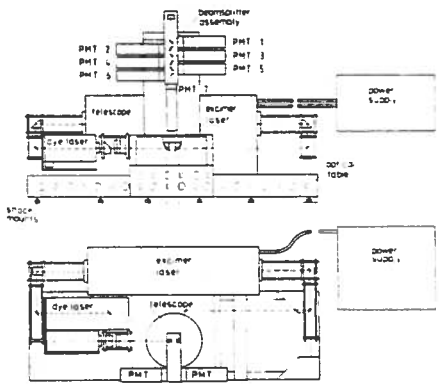

Figure 4. Optical part of the Oceanographic Lidar System. Position of the telescope is above a bottom hatch of the aircraft.

Dichroic beamsplitters deflect selected spectral ranges of the telescope output to optical filters with typical bandwidths of 10 nm, and gated photomultipliers. Detection channels at 344 and 533 nm correspond to the water Raman scatter wavelengths with 308 and 450 nm excitation, respectively. Chl a fluorescence is observed at 685 nm. Channels at 366, 380, 500 and 650 nm are used for the measurement of Gelbstoff and oil fluorescence spectra and for the identification of the baseline of water Raman scatter and chl a fluorescence (Figs. 1-3). A relative calibration of these channels is performed on the ground by use of a 1 m^2 plate of white teflon which has the advantage of possessing a fluorescence covering the near UV and visible spectrum when irradiated with the excimer laser, with an efficiency which corresponds well to the typical water column return. This enables a sensitive delineation of water turbidity and of fluorescent water column constituents in relative units. Attempts will be made to obtain an absolute calibration of OLS in future experiments. Based on absolute data of tne fluorescence efficiency of Gelbstoff and chl a and of the water Raman scatter efficiency this will allow to derive these parameters in absolute units.

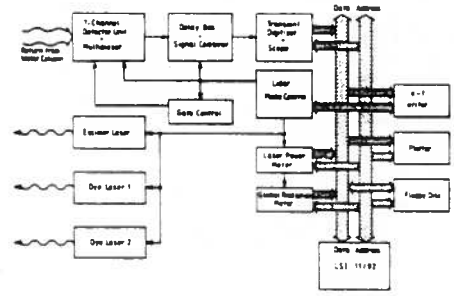

Figure 5. Schematic of the signal flow of the Oceanographic Lidar System.

Signal digitization is done with a transient recorder at a sampling rate of 500 MHz and a resolution of 6 bit. A fast logarithmic amplifier is used in the depth profiling mode for an enhancement of the dynamic range. Since the digitizer is a one-channel instrument, 3 photomultipliers selected by the operator are sequentially combined on one signal line and fed to the transient recorder.

The system is controlled by a microcomputer, by which laser selection and triggering, selection of different detection channels, quick-look data output and data storage are achieved.

3. OCEANOGRAPHIC APPLICATIONS

OLS was utilized in a number of experiments in cooperation with oceanographic institutions. Most of these experiments were carried out in the German Bight as part of an interdisciplinary research programme on characteristic water masses and fronts occurring in that area (Ref. 7, 5).

Here we present some of the results obtained during flights in the northern Adriatic Sea in August 1984. The goal of ADRIA 84 which was performed under the auspices of the Commission of the European Communities, ISPRA Establishment, was an investigation of the hydrographic processes present in this area in summer and an examination of the potential of remote sensing for their study (Ref. 15).

Results of a flight on August 30, 1984 are shown in Figure 6. From the excimer laser induced signals the Gelbstoff concentration, from those of the dye laser, the chl a concentration are derived according to Eq. 4, i.e. assuming the water column to be homogeneous within the penetration depth of the laser beams. The Po river plume with a high variability of the measured parameters, and the existence of different water masses with individual substance concentrations are obvious from the data. These water masses are separated by fronts with gradients of typically a factor of 10 over distances of 1-3 km.

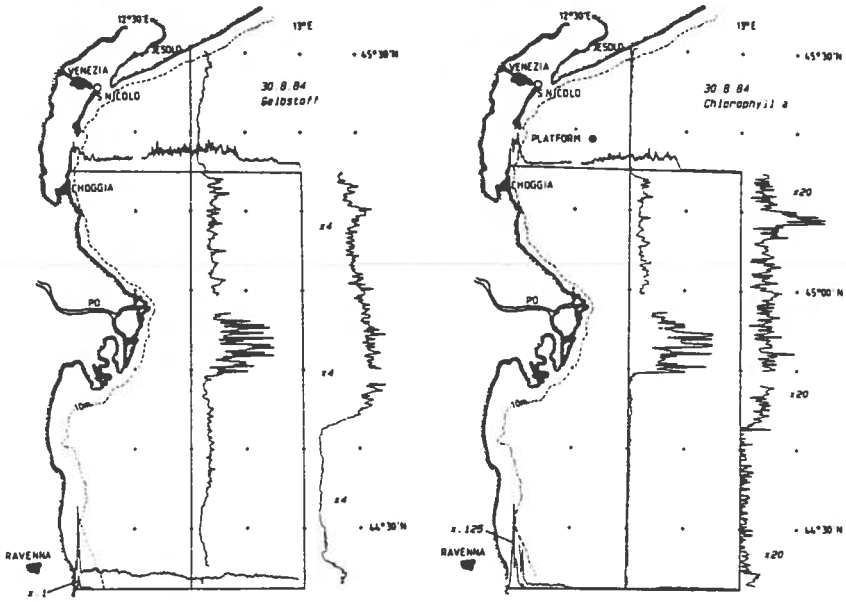

Figure 6. Distribution of Gelbstoff (left) and chl a (right) in the northern Adriatic Sea measured with lidar on August 30, 1984. Scaling of the profiles is identical except for the track on longitude 13°00'E which is given with higher resolution. Flight height was 200 m, signal repetition rate was 1 Hz.

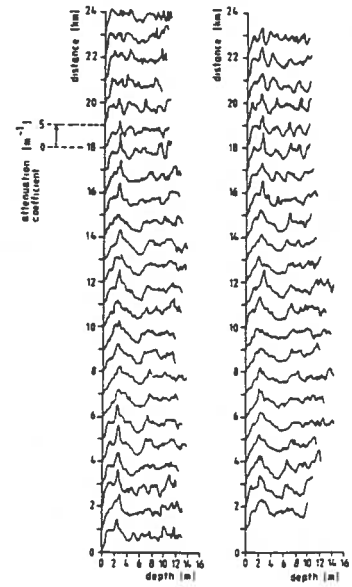

Figure 7. Depth profiles of the attenuation coefficient c(450 nm) + c(533 nm) derived from two identical flights. Averaging over 1 km was applied to the lidar data. Flight tracks from 12°57' to 12°39'E on 45°19'N, August 31, 1984.

A comparison with in situ findings obtained in the northern part of the flight track on longitude 13°00'E yields a Gelbstoff and chl a concentration of 0.15-0.20 mg/l and 1-2 µg/l to be characteristic of the water mass present in that area (Ref. 15). The lower sensitivity limit of OLS in limpid waters is thus in the order of 0.01 mg/l for Gelbstoff and 0.1 µg/l for chl a. With these results lidar provides a sensitivity which is comparable with that of laboratory instrumentation.

The depth profiling mode of OLS was tested for the first time during ADRIA 84. Results of a flight on August 31, 1984 on the latitude of the Lagoon of Venice are shown in Figure 7. Profiles of the light attenuation coefficient were derived from the time resolved lidar measurement of water Raman scattering by an algorithm which assumes tne laser pulse to be shorter than the 2 ns time resolution of the detector system (Ref. 8). A penetration depth which corresponds to about 6 attenuation lengths was achieved with a resolution of about 1 m.

4. OIL SPILL INVESTIGATIONS

Initiated and organized by the Commission of the European Communities, ISPRA Establishment, the oil spill remote sensing experiment ARCHIMEDES 1 was conducted in October 1983 off the coast of Holland. Goal of the exercise was an investigation of passive and active remote sensing methods at microwave and optical frequencies for detecting and analyzing marine oil pollution (Ref. 16). Two spills were produced consisting of fuel oil (40 m³) and of chocolat mousse (50 m³), monitored over a period of 30 hours, and finally removed by recovery ships.

Lidar measurements performed in this experiment (Ref. 13) reveal that the bulk of the spilled oil remained concentrated within small zones of 100-300 m diameter, surrounded by extended areas with films of micrometre thickness. The corresponding fluorescence spectra show that the oil had been decomposed into different fractions, the lighter ones being present in the thin peripheral films; this effect which is not caused by weathering seems to be characteristic of fuel and was not observed with crude oil. Data interpretation for the chocolat mousse spill indicates that most parts of the oil were floating below the water surface at depths of about 10-30 cm.

Data of a flight over the fuel oil spill about 3 hours after release are shown in Figure 8a. Aircraft altitude was 200 m. Signal repetition rate was 5 Hz resulting in fingerprints on the ground at distances of 10 m. The 344 nm signal represents water Raman scattering. It shows a drastic decrease in intensity at the edge of the spill when compared with the slightly varying signal received over clear water. The film thickness, Figure 8b, is calculated from this variation by appropriate algorithms (Ref. 3, 10-13) with an estimated accuracy of 50 % on the basis of light attenuation coefficients of the oil measured in the laboratory.

The other detection channels, Figure 8a, reflect fluorescence of Gelbstoff and oil. A closer inspection of the spectral signatures obtained at different locations of the spill, Figure 8c, illustrates the decomposition of the oil into different fractions with individual fluorescence characteristics as mentioned above. This is particularly evident when comparing the fluorescence of the oil with that received over clear water. The signal change calculated from Eq. 2 when passing from clear water to a surface oil film with thickness d is

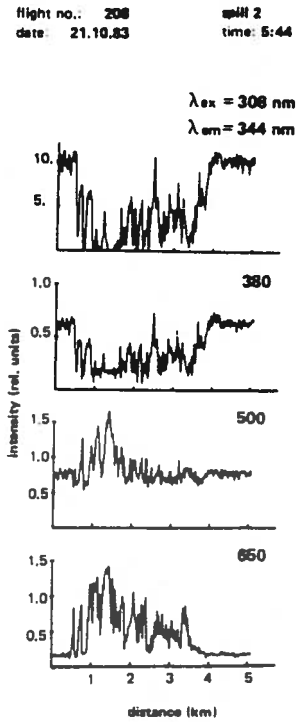

Figure 8a. Lidar data obtained over a fuel oil spill. Excitation wavelength 308 nm, detection wavelengths 344, 380, 500 and 650 nm. Flight height 200 m, signal repetition rate 5 Hz.

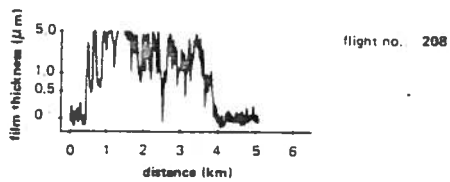

Figure 8b. Oil film thickness derived from water Raman scattering at 344 nm.

$$\Delta P \sim \left(\frac{\eta_w}{c_w} - \frac{\eta_o}{c_o}\right)(1 - \exp(-c_o d)) \qquad (5)$$

with η_w, η_o efficiency of water and oil, c_w, c_o the corresponding attenuation coefficients. Assuming the water column to be homogeneous the change in the sign of the signal variation observed at green wavelengths is thus attributed to a change of the oil type.

5. CONCLUSIONS

The Oceanographic Lidar System has shown its potential of remote measurements of oceanic parameters

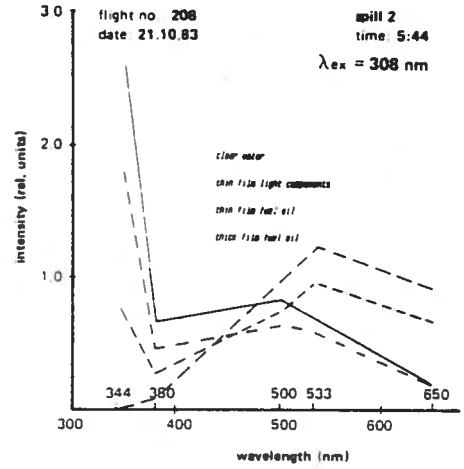

Figure 8c. Spectral signatures derived from different locations of the spill. Scaling of water Raman scattering (344 nm) is depressed by a factor of 3 due to its high intensity. Notation of the spectra refers to decreasing Raman scatter intensity.

in a number of airborne experiments. These cover a sensitive delineation of Gelbstoff and chlorophyll a distributions and of the spectral light turbidity of seawater, being of interest for oceanographic research. The capabilities of investigating marine oil spills with respect to an analysis of the oil type and the oil film thickness have been demonstrated.

Future activities will cover an application of OLS within oceanographic programmes where a sensor with large-scale monitoring capabilities is required. This concerns particularly research on transport and mixing, the investigation of frontal systems and their physical and biological dynamics.

Water depth resolved detection of hydrographic parameters will be studied in more detail. Theoretical investigations of the method will be compared with laboratory tests using a 10 m tank with controlled stratification of the water column and with airborne experiments.

Concerning water quality monitoring a signature catalogue of fluorescence and absorption properties of oils is now in progress. These data will provide a basis for operational oil spill survey. Moreover, the capabilities of detecting and identifying chemical pollutants in the water column with lidar are currently investigated.

Efforts will be made in order to establish procedures for an absolute calibration of hydrographic lidar data without the need of ground truth information. This will provide an important improvement of oceanographic lidar remote sensing.

6. ACKNOWLEDGEMENTS

The experiments ADRIA 84 and ARCHIMEDES I were initiated, realized and financially supported by the Commission of the European Communities, ISPRA Establishment. We wish to express our thanks to Dr. P. Schlittenhardt and Dr. R.H. Gillot, Ispra.

We are indebted to our colleagues Dr. K.P. Günther, K. Loquay and R. Zimmermann for their participation in developing OLS and for their support during the experiments.

We are also grateful to DFVLR Oberpfaffenhofen for making available the research aircraft. Our thanks go to H. Finkenzeller and P. Vogel for their comprehensive support during the experiments.

The development of the Oceanographic Lidar System is financed by a grant from the Bundesministerium für Forschung und Technologie, Bonn; research on water masses and frontal systems by a grant from the Deutsche Forschungsgemeinschaft, Bonn; research on lidar monitoring of oil spills by the Niedersächsisches Ministerium für Wissenschaft und Kunst, Hannover.

7. REFERENCES

1. Gordon H R, Clark D K, Brown J W, Brown O B, Evans R H & Broenkow W W 1983, Phytoplankton pigment concentrations in the Middle Atlantic Bight: comparison of ship determinations and CZCS estimates, *Appl Opt* vol 22, 20-36.

2. Fischer J 1985, On the information content of multispectral radiance measurements over an ocean, *Int J Rem Sens* vol 6, 773-786.

3. Kung R T V & Itzkan I 1976, Absolute oil fluorescence conversion efficiency, *Appl Opt* vol 15, 409-415.

4. Hoge F E & Swift R N 1982, Delineation of estuarine fronts in the German Bight using airborne laser-induced water Raman backscatter and fluorescence of water column constituents, *Int J Rem Sens* vol 3, 475-495.

5. Diebel-Langohr D, Hengstermann T & Reuter R 1986, Identification of hydrographic fronts by airborne lidar measurements of Gelbstoff distributions. In: Dynamic Biological Processes at Marine Physical Interfaces, J C J Nihoul (Ed.), Proc. 17. Int. Liège Coll. on Ocean Hydrodynamics, 13.-17. May 1985, Elsevier, Amsterdam (in press).

6. Günther K P 1986, A quantitative description of the chlorophyll a fluorescence reduction due to global irradiation in the surface layer, ibid.

7. Krause G, Budeus G, Gerdes D, Schaumann K & Hesse K 1986, Frontal systems in the German Bight and their physical and biological effects, ibid.

8. Diebel-Langohr D, Hengstermann T & Reuter R 1986, Water depth resolved determination of hydrographic parameters from airborne lidar measurements, ibid.

9. Freking B, Klattenhoff J & Reuter R 1984, Investigations of marine hydrosols by light scattering, *Verh Dt Phys Ges* (VI) vol 19, 1546-1558.

10. Visser H 1979, Teledetection of the thickness of oil films on polluted water based on the oil fluorescence properties, *Appl Opt* vol 18, 1746-1749.

11. O'Neill R A, Buja-Bijunas L & Rayner D M 1980, Field performance of a laser fluorosensor for the detection of oil spills, *Appl Opt* vol 19, 863-870.

12. Hoge F E & Swift R N 1983, Experimental feasibility of the airborne measurement of absolute oil fluorescence spectral conversion efficiency, *Appl Opt* vol 22, 37-47.

13. Diebel-Langohr D, Hengstermann T, Reuter R, Cecchi G & Pantani L 1985, Measuring oil at sea by means of an airborne laser fluorosensor, The Archimedes 1 Experiment, R H Gillot (Ed.), Commission of the European Communities, EUR 10216 EN, Luxemburg, 123-142.

14. Browell E V 1977, Analysis of laser fluorosensor systems for remote algae detection and quantification, National Aeronautics and Space Administration, Report NASA TN D-8447, 39 pp.

15. Schlittenhardt P 1985 (Ed.), ADRIA 84 - Data catalogue, Commission of the European Communities, JRC ISPRA, S.A. I. 05.E2.85.23.

16. Gillot R H 1985 (Ed.), The Archimedes 1 Experiment, Commission of the European Communities, EUR 10216 EN, Luxemburg, 223 pp.

Workshop on High Spectral Resolution Imaging for Land and Ocean Remote Sensing

Aspects of a Canadian German Cooperation under the ESA Earth Observation Programme

H. Winkenbach, DFVLR, Cologne (Federal Republic of Germany)

1) Introduction into the German Earth Observation Programme structure

To start with it might be useful to give a short overview about the elements of the German Earth Observation Programme.
Fig. 1 gives a survey of the entities which are involved in the planning and implementation of Space Programmes.
Planning is performed by the scientific institutes, the DFVLR, the industry and the government (BMFT) as far as national interests are involved and the programmes have to be funded by BMFT.
The decision about a programme lies within the responsibility of BMFT both on a national and international scale.
The Space Research/Project Executive Department of DFVLR implements the Programmes.

2) Goals and Instrument Development of the German Earth Observation Programme

Fig. 2-5 shows the main goals of the national Earth Observation Programme. These are in general mainly the provision and utilization of remotely sensed data for applications in the various fields. This means the two focal points in developing instruments and methods for data processing are addressed. It is important to say that the FRG does not intend to develop and operate any Earth Observation satellites within the national programme; therefore the programme is restricted to the development and operation of selected instruments.

As to the optoelectronic equipments up to now we have designed and tested in space a first version of a Modular Optoelectronic Multispectral Scanner (MOMS 01). As a starting point a Phase A study for a Chlorophyll-detecting imaging spectrometer for space (ROSIS) and a Phase B study for a high spatial resolution stereoscopic looking experiment have been performed (MOMS-Stereo). Also an airborne Scanner for short wave infrared detection is being under construction.

For the sake of completeness there should be mentioned developments for data processing and evaluation methods in every user's interest, e.g. the utilization of ERS-1.

3) Near future activities for further national planning in respect of optoelectronic instrument developments

At the end of this year a general discussion about further hardware development beyond MOMS 01 in the national frame is envisaged. The main arguments for the decisions to be taken for further experiment developments ought to be the needs of the user community in the middle to the end of the 90ies, not to duplicate the existing and planned equipments elsewhere and the chance to launch the instrument on a spacecraft, e.g. Polar Platform.

After the successful conduct of the mentioned study for Chlorophyll-detection from space the entities GKSS, DFVLR and MBB started with the joint development of an aircraft prototype which will permit not only a thorough tests of the feasibility of the instrument but will also open new applications (including land) because of the narrow spectral bands involved.

...

4) Earth Observation with Imaging Spectrometry within ESA's Earth Observation Programmes

It can be assumed that all persons present are aware of the objectives of ESA's Earth Observation Programmes.

Regarding the main topics of the programmes:

- to prepare operational systems in polar orbit tailored to the needs in the field of ocean, ice, coastal zones and meteorological applications
- to initiate the development of Satellites for experimental/ preoperational use in remote sensing land application
- to prepare potential future missions by advanced instrument studies and carry out pre-development of instruments,

a high spectral resolution imaging is a useful tool. Therefore an Imaging Spectrometer is in the list of ESA's Earth Observation Preparatory Programme (EOPP) as a "Possible Instrument" to be prepared for development.
Also the latest register for instruments which was handed over to the EUA Study Group for the Polar Platform as an output of the ESA workshop ESPOIR (European Symposium on Polar Platform Opportunities and Instrumentation for Remote Sensing) which recently took place includes such an equipment.
The objectives of ESA's programmes and the user requirements seems to be constraining for ESA to take into consideration a High Resolution Imaging Spectrometer.

5) Perspectives of German Canadian Cooperations under the ESA Earth Observation Programmes

As part of EOP, the Federal Republic of Germany and other member countries signed in thecourse of this year the Earth Observation Preparatory Programme (EOPP).

It is obvious that in connection with the discussion about the cooperation Germany-Canada the EOPP should be primarily regarded. Because of the potential and interests of various organizations within the Federal Republic of Germany it is expected that these will participate in special tasks of the EOPP such as

- mission concept and system studies
- instrument and feasibility studies
- measuring campaigns involving aircraft and ships
- predevelopment of critical technologies.

The accomplishment of the individual objectives of EOPP is to be reached by invitations of tender in the frame of a provided Procurement Plan.
From my point of view it may be possible that national institutions, university institutes and industry of both nations cooperate in the accomplishment, e.g. instrument and feasibility studies or measuring campaigns and so on.
At the time being cooperation between German and Canadian institutions is established which does not relate directly to the requirements of EOPP (e.g. in scientific fields), but it broadens the interests of the scientific community in ESA' programme. If possible, the cooperation frame should be enlarged.
As already mentioned it has not yet been decided whether and to which extend BMFT will provide financial support to the national development of an Imaging Spectrometer for the purpose of space flight. From today's view such a financial support is a prerequisite for a development.

Irrespective of the decissions yet to be taken by the two countries on the future technological approach and on a possible bilateral cooperation, the scenarions lending themselves under ESA's Earth Observation Programme could be discussed.

...

These scenarios include basically:

- Bilateral development of an Imaging Spectrometer to be made available to ESA (e.g. for the Polar Platform), with or without ESA's responsibility for the data management.

- Bilateral cooperation perhaps in Phase A of the development, but then to be taken over by ESA as a project.

"ROSIS-Reflective Optics System Imaging Spectrometer - a new multi-purpose Remote Sensing Instrument

by

Dr. H. Graßl & Dr. R. Doerffer
GKSS, Geesthacht, F.R.G.

Dr. H. van der Piepen
DFVLR-NE/OE, Oberpfaffenhofen, F.R.G.

B. Kunkel, F. Blechinger, Dr. R. Buschner, Dr. R. Lutz, R. Ziegler
Messerschmitt-Bölkow-Blohm GmbH
Space Systems Group, Ottobrunn, F.R.G.

The paper describes the results of a recent study on this subject leading to a detailed concept definition of a spaceborne chlorophyll fluorescence imaging spectrometer. This instrument apparently is suitable also for a variety of other applications, especially as an airborne version.
The technical concept is based on a novel type of an all-reflective optics system and a 1024^2 matrix CCD detector array and an advanced electronics concept.
The imaging spectrometer is designed to cover a spectral range from 425 to 960 nm in resolution steps of 5 nm per channel at 0.06 % albedo resolution. It will provide 108 spectral channels. The FOV amounts to ± 16.2° at 300 m ground pixel size. This corresponds to 1024 pixels in the spatially scanned (cross track) direction. Since at present no frame-transfer matrix CCD array with 1024^2 pixels is available, the initiated airborne version will use 512^2 only.

Imaging spectrometer, matrix CCD, chlorophyll fluorescence, grating spectrometer

1. INTRODUCTION

This paper is closely related to the preceding paper by Doerffer, Graßl and van der Piepen as regards the scientific mission background.

Accordingly, only the essentials of the mission requirements are briefly summarised here.

The emphasis of the above mentioned study /R1/ was on the measurement of ocean chlorophyll distribution from space (reference altitude 525 km) through its absorption (blue/green spectrum) and essentially its sun-stimulated fluorescence around 685 nm. Further channels were allocated to yellow substance and suspended matter detection, see Tab. 1. This requirements survey has been established by the a. m. scientists who accompanied the total study performance. Their involvement assured a permanent accordance of the instrument study with the user interests.

The study started with a tradė on the most suitable concept principle, i.e. a concept with discrete spectral channels realised with modular optics and interference filters for channel separation and linear detector arrays versus the imaging spectrometer concept as described in the following.

The first alternative had been studied 3 years ago by the team in a similar ESA Study on the Ocean Colour Monitoring instrument (OCM) /R2/. The results of that study were taken as an input to /R1/.

The main areas of trading both concepts against another were the radiometric performance analysis (parametric study) and the feasibility of the corresponding optical concept in line with the performance specifications.

In addition, a comparison has been carried out to existing or planned sensor systems and their performance. In simplification, the aim was to arrive at a kind of "improved CZCS" with better spatial resolution and radiometric performance and higher number of spectral channels plus more appropriate spectral allocation of these.

In general, the detection of chlorophyll in ocean surface and subsurface layers through its fluorescence can be seen as the most challenging spaceborne remote sensing task, since:

- the ocean surface represents the "darkest" natural surface on earth (typical albedos below 0.05)
- the ocean surface signal arriving at the sensor is buried in excessive contributions from the atmosphere (Rayleigh and Mie backscatter)
- the "fluorescence peak" at 683-685 nm represents a rather small "delta signal" or "delta albedo" of less than 1% at low chlorophyll concentration.

Despite these constraints, the imaging spectrometer concept turned out to be the favourite solution for this task: though the spatial resolution is slightly inferior compared to the linear array concept (more limited in terms of pixels per array, slightly lower dynamic range), its main advantage to offer an almost unlimited number of extremely narrow-band spectral channels made it superior. Note that spectral bandwidths of less than 10 nm impose severe optical transmission losses in case of the interference filter version.

The development (computer program) of a new, all-reflective optics concept enabling the wide spec-

tral range at the required FOV of ± 15° supported the decision towards the ROSIS concept considerably (ROSIS: Reflective Optics System Imaging Spectrometer).

2. ROSIS CONCEPT PRINCIPLE

The operation principle of an imaging spectrometer meanwhile is rather well known. The schematic drawing of Fig. 1 illustrates the functional principle of this particular design easily (see also Fig. 2 and 3):

- the image on ground is relayed via a deflection mirror (2 in the construction drawing, Fig. 3) the purpose of which is to vary the scan line forward or aft to avoid sun-glint on the ocean surface, onto the
- primary telescope mirrors 5 and 6 (Fig.3) which focuses the image onto the image slit (7) which represents the actual scan line on ground by cutting off the rest of the FOV
- the focused scan line image is expanded and parallized through the collimator system (8 & 9) for
- dispersion into the spectral components by the subsequent blazed grating, the main spectrometer element (reflective grating)
- the dispersed beams (dashed lines in Fig.3) are imaged onto the matrix CCD array (14) by the collimator optics, now used as imager optics, via another small deflection mirror (13) which becomes necessary since the physical dimension of the detector array does not allow its mounting aside the slit
- on top of the detector array, the detector array trigger and analog readout electronics PCB is mounted to avoid long connections between both, i.e. to avoid EMC problems and cross-talk.

The front end relay/deflection mirror also serves as a means to reflect diffused sun light into the instrument for calibration (the reversed side is covered with a diffuser). Furthermore, the same mirror is used in an intermediate position as a shutter to enable dark current correction measurements for the detector array.

Another calibration subunit is included in form of the cw laser diode underneath the front deflection mirror (19 in Fig.3) which serves as a spectral channel control reference, i.e. verification that the pre-launch channel allocation is maintained; in case of deviation, it will enable a reprogramming of the channel spectrum allocation.

3. TECHNICAL DESCRIPTION

The ROSIS instrument is subdivided into the optical module as shown in Fig. 3 and an electronics module, see Fig. 4.

The main features of the optics concept are summarised in Tab. 2. The main mirrors are aspheric elliptical mirrors and designed such that their residual curvature radius compensates the mean residual slit curvature (curved slit image by grating), see Fig. 5. The resulting maximum distortion per channel remains below 0.2 pixel size at the FOV limits even.

The mechanical concept for the optics module reflects the specific adjustment and tolerance requirements of ROSIS in view of the number of optical elements to be kept in alignment:

- the basic structure consists of two integrally milled shells, of which the bottom structure supports all essential optical components (mirrors, grating, internal baffles); it is made entirely of aluminum to avoid thermal gradients across the structure. The upper shell contains the detector array plus its adjustment devices (not shown) and a TE cooler for thermal control and dark current reduction.
- All optical components including the detector array can be precision adjusted to about ± 3 µm (requirements for the mirrors about ± 10 µm)
- The front deflection mirror will be driven by a stepper motor
- The relatively high thermal expansion coefficient of aluminum requires a rather stable semi-active thermal control (± 2 K) which is achieved by multi-layer thermal blankets and heating of the optics module during eclipse phases
- Heat generated within the optical module will be dissipated via a 150 mm² radiator which can point towards earth even (see shaded area on instrument in Fig. 2).

Considerable effort has been put into the ELECTRONICS CONCEPT as well in order to meet the high radiometric requirements and not deteriorate the focal plane assembly performance.

The overall electronics is subdivided into 4 main subunits which are:

- the analog control/readout electronics in the optical module (including a small power supply section for the TE cooler)
- the signal processing and correction electronics
- the processor/software part for operational control of the instrument and data readout organisation
- auxiliary electronics such as power supply, telemetry and telecommand, housekeeping, harness etc.

The overall block diagramm is shown in Fig. 7; the dashed line marks the the subunits which are accomodated within the elctronics box (altogether 25 PCB's).

The user (ground control) is able to select 28 spectral channels out of the available 256 channels (only 50% of the detector array are used as sensitive area, while the second half is used as an intermediate storage zone in the frame transfer mode). Every spectral channel provides 1024 (spaceborne version) resp. 512 (preliminary airborne version based on the Thomson-CSF TH 7884 device) pixels.

The detector array generates for each pixel a "reference" and a composite signal, i.e. the actual scene signal is superimposed to the reference signal. A special electronics subunit is provided to recover the scene video signal and to increase the dynamic range in form of the correlated double sampling technique. The resulting dynamic range is 4000:1, yet only 8 bit are transferred into the subsequent signal processing chain through gain control (programmable, to reduce the output data rate).

Each pixel is radiometrically corrected (dark current and sensitivity). The large number of correction values requires an appropriate memory size (256 lines x 1024/512 pixels per line x 2 correction values, equivalent to 512 resp. 256 kbyte memory.

In order to further reduce the data rate, the following data reduction schemes are foreseen:

- integration over adjacent pixels (data reduction), i.e. increased ground pixel size, as a moderate hardware supplement
- Arithmetric Logic Unit (ALU) for in-flight synthesis of spectral channels (e.g. ratioing of pre-determined channels with moderate hardware but higher software effort)
- data compression through DPCM techniques, the currently expected compression factor is 2.4; this unit needs experimental verification with the first test model.

In addition to the optical calibration references, see sect. 2, an internal electronic self-test and calibration is included to eliminate drift effects of the signal processing elements.

Subsequent to the signal correction and processing, the formatter transmits the serial digitized video data including header information (time, gain, attitude data, channel number, operational mode etc) to the mass storage or data handling system of the spacecraft or aircraft, i.e. telemetry for real-time transmission or on-board storage.

The processor system (data management system - DMS) consists of an 80C86 µP (space-qualified MBB processor) with an appropriate structure (number of general purpose registers, interrupt logic, bus organisation) and adequate speed. A highly developed hard- and software support is available for this system, including the capability for higher program languages (PL/M, Pascal,C). This enables full operational control of all possible operation modes as well as pre- and re-programming of channel allocations, selection, gain control, radiometric correction, data reduction modes etc..

The processor system is modularized to enable relatively simple adaptation to varying environment, operation modes (number of I/O ports, memory etc) and features:

- low power
- compact size
- radiation hard
- rugged system.

The electrical ground support system (EGSE) will be established in 1987 in the course of the first airborne test model.

The same applies for the Optical Ground Support Equipment (OGSE).

4. SUMMARY SPECIFICATIONS

The main instrument characteristics are summarised in the tables 2 (optical system), 3 (performance summary) and 4 (technical data, including the FPA (Focal Plane Assembly) specifications. These are still preliminary for the spaceborne version since at the time of this paper's presentation no directly applicable matrix CCD array exists which provides 1024 pixels in the spatial scanning direction (the only existing 1024^2 array of Texas Instruments (TI-VP1M) is available as a staring mode device only and not as frame-transfer array which would be needed for this purpose (i.e. with one half as intermediate storage zone).

According to the team's information, promising developments are under way in Japan, the USA and the United Kingdom; thus, for the time envisaged for the space version realisation, the availability of a suitable matrix CCD can be assumed.

As regards the performance data of the airborne version, the quoted 2.5 nm bandwidth can not be realised with either the total FOV of ± 16° and simultaneously with 0.2 pixel matching.

For concept verification purposes, the started airborne test version will have the CCD placed on one half of the ± 16° FOV (the TH 7884 covers 50% of the design FOV only) in order to demonstrate the ROSIS performance at larger view angles.

5. OUTLOOK, CONCLUSIONS

The herewith proposed ROSIS instrument represents the "first generation" of this imaging spectrometer type only.

The first model which is initiated already on the basis of internal funding by the DFVLR (inst. of Commun. Techn. and Remote Sensing, Oberpfaffenhofen) and the GKSS (Geesthacht near Hamburg) as users of the instrument and MBB-ERNO, Ottobrunn Space Systems Group, is to be considered as an airborne test version only which does not represent all electronics features as described above.

It is worthwhile to mention that for this particular instrument type an airborne version reveals an even broader application range than the space version, see as a preliminary overview Tab. 6. This results from the ground pixel size mainly since 2 m ground pixel size e.g. at 4 km flight altitude are considered sufficient for almost all kinds of applications. The nature and number of candidate applications is expected to extend in the course of the first flight test programme.

For spaceborne missions - with the exception of water colour measurements - typically the combination with a high-resolution (spatial) scanner is recommended.

An extension towards longer wavelengths is the apparent logical follow-on goal; the all-reflective optics concept clearly is favourite for such extension (even with some modifications of focal lengths and grating number). Especially the incorporation of SWIR channels in the range from 1.4 to about 2.5 µm is the next development goal since it represents rather attractive applications such as geological exploration, wider vegetation status studies or atmospheric measurements, in particular also cloud studies, ice and snow analysis etc..

The required detector array technology is not yet mature for spaceborne versions but promising for airborne test versions (e.g. matrix arrays based on Pd-Si Schottky Barrier techniques or hybrid arrays of InSb, CMT, with promising developments in Europe and the USA).

MBB plans to start with these spectral ranges in 1989.

An extension towards longer IR wavelengths, i.e. MIR (3.5-5 µm) and thermal IR (8-15 µm) is planned for the subsequent years, provided there is sufficient interest and suport for these spectral ranges.

6. ACKNOWLEDGEMENTS

The authors like to express their paricular acknowledgements to Dr. R. Doerffer, Prof. H. Graßl and Dr. H. van der Piepen for their support in the study /R1/ as well for the launching of the airborne test version, here including M. Schröder of the DFVLR, and the whole MBB team for their effort.

REFERENCES:

/R1/ Feasibility and Definition Study "Chlorophyll Mapping of the Ocean by means of Detector Array Sensors"; MBB Final Rep. for BMFT Contr. 01 QS 8508 8, June 1986

/R2/ Feasibility Study of "Advanced Optical Techniques for Ocean Colour Measurements"; MBB Final Report of the ESA Contr. 5235/F/CG(SC), June 83

/R3/ G. Cerutt-Maori/J.P. Durpaire: Un radiomètre optique multispectral pour l'etude des océans" ESA Journ. 1982, Vol. 6, p. 163f

/R4/ "Investigation of the Feasibility of Mapping Chlorophyll Fluorescence from Space", Can. Corp. for Univ. Space Science, March 81

/R5/ "Analysis of Flight Data from the Fluorescence line Imager", G.A. Borstad, May 85

NOTE:

Copies of the ROSIS brochure are available at this Conference at the MBB-ERNO Poster stand.

Tab. 1: Spectral Channels, Bandwidths and radiometric Resolution Requirements

Channel No.	Main Application	Central Wavel. λ_c (nm)	Bandwidth (nm)	Resolution (% of total signal per channel
1	Chlorophyll Absorption	440	20	$\leq$ 0.5
2	" "	480	20	"
3	Suspended Matter Conc. Correlation for 1+2	560	20	"
4	Fluorescence Correlation	675	10	$\leq$ 0.2
5	Fluorescence Channel	683	10	"
6	Fluorescence Correl. (atm.)	711	5	"
Option	Yellow Stuff (conc.,absorpt)	410	20	$\leq$ 0.5
Option	Atmospheric Correction	745	20	"

Tab. 2: Optical System Design Parameters

PRIMARY OPTICS	COLLIMATOR/IMAGER OPTICS	GRATING
Type: "Blechinger"	same	Blazed Grating
Focal Length: 31.5 mm	90 mm	Grating number: n = 40
f-number: 3.5	3.5	Blaze angle: 2°
FOV: $\pm$ 16	$\pm$ 4.2 (relay FOV)	Spectr. diverg. 5 nm
Distortion: 2 %	0.2 pixel (resid. slit curvature)	
Alignm. Toler. 0.3'	0.3' (arc min)	0.2'

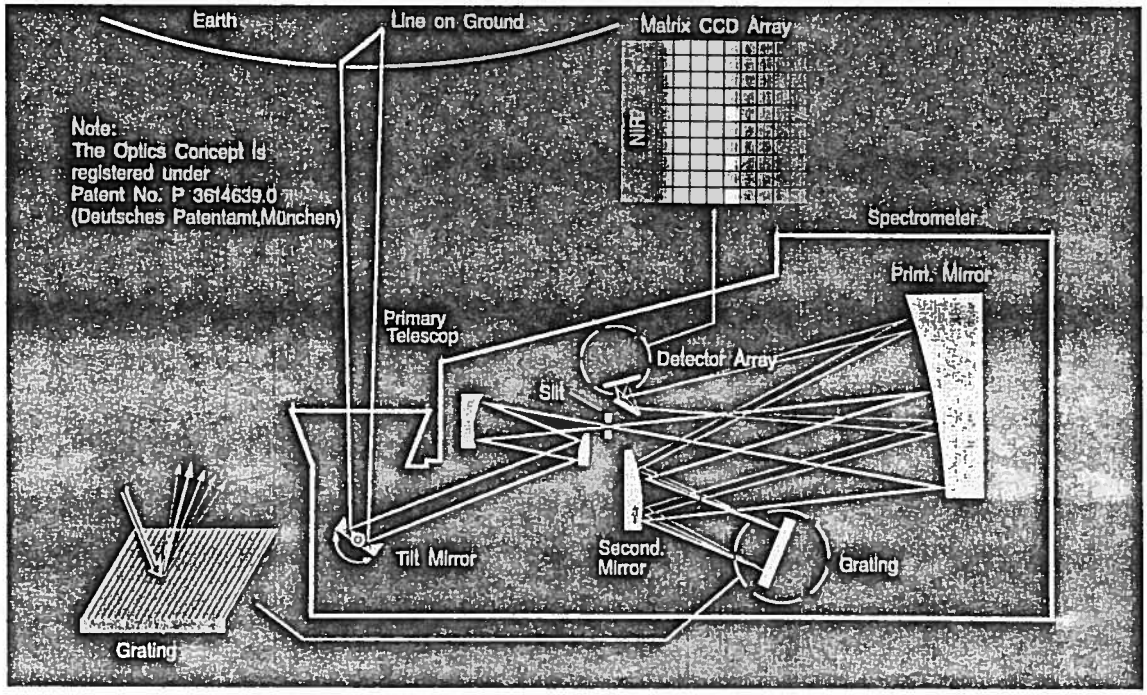

Fig. 1: ROSIS Imaging Spectrometer, functional Principle (Optical Module)

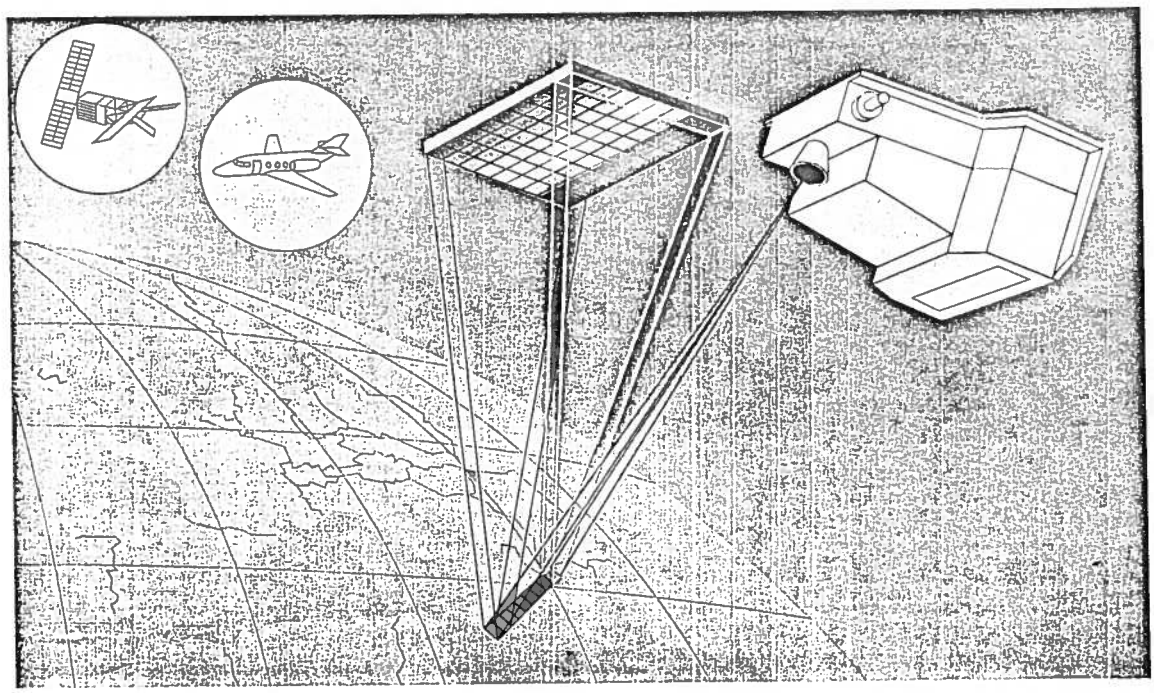

Fig. 2: ROSIS schematic Illustration

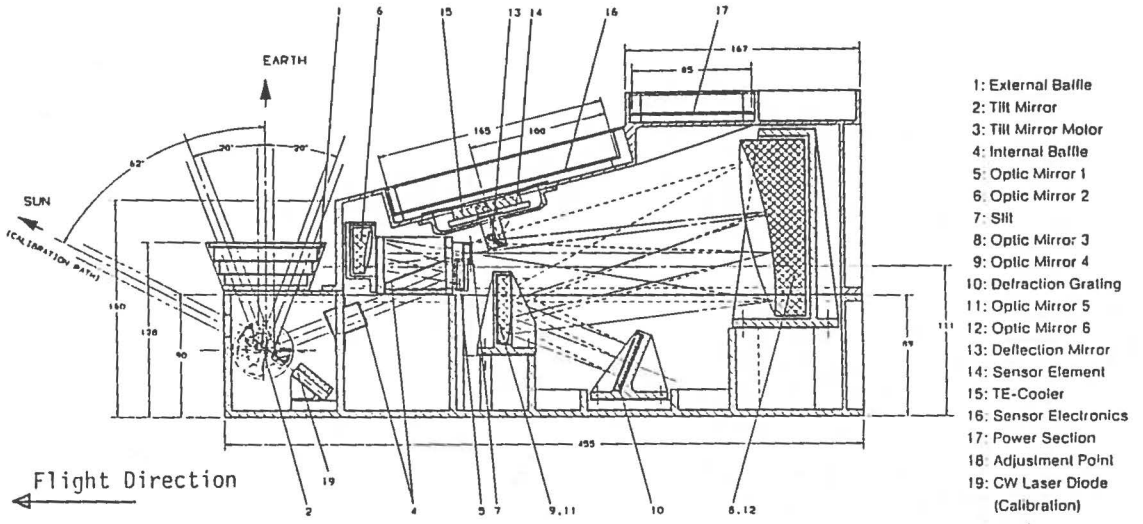

Note: The Optics Concept is registered under Patent No. 3614639.0 (Deutsches Patentamt, München)

Fig. 3: ROSIS Construction Drawing (Optical Module)

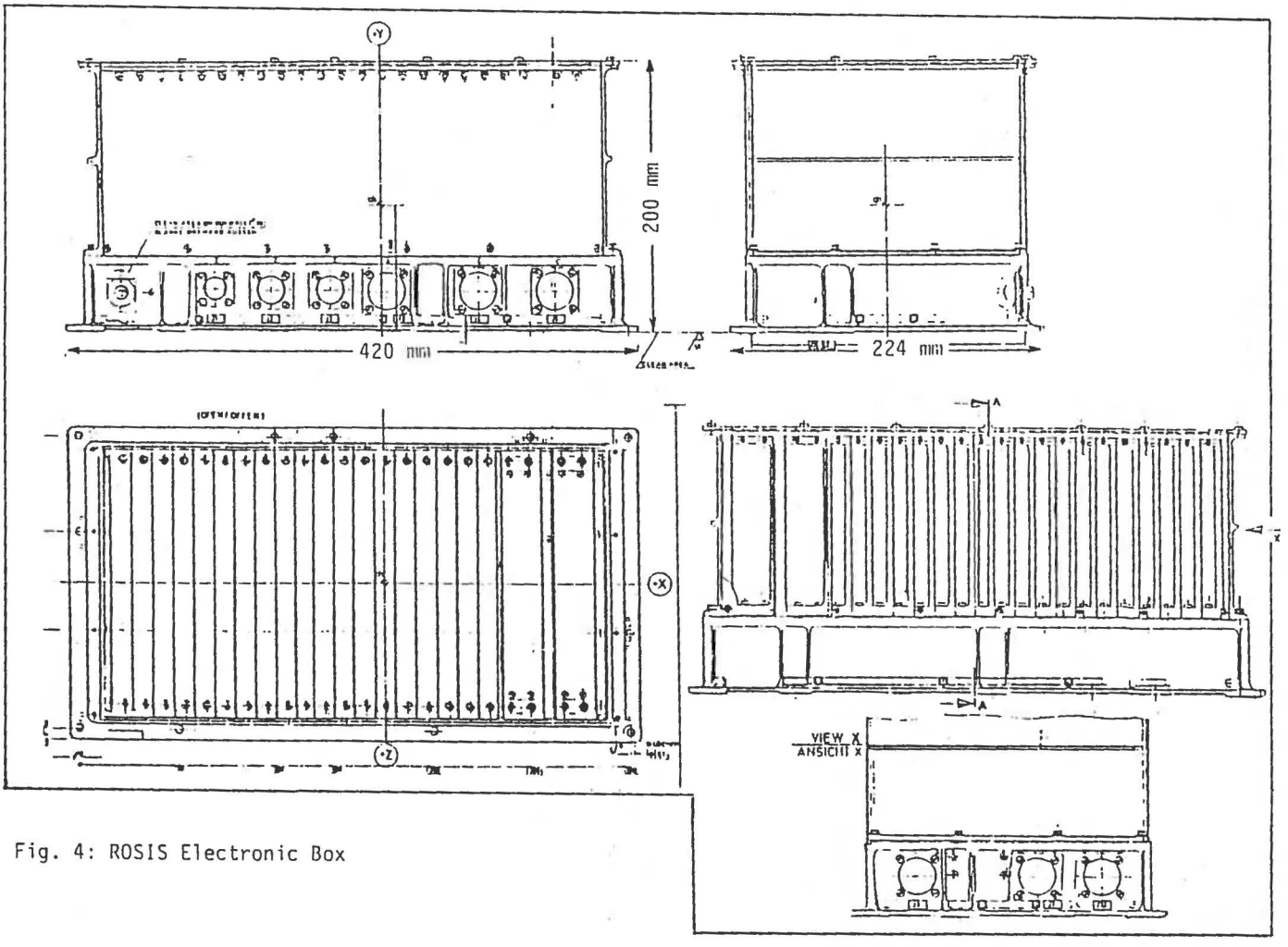

Fig. 4: ROSIS Electronic Box

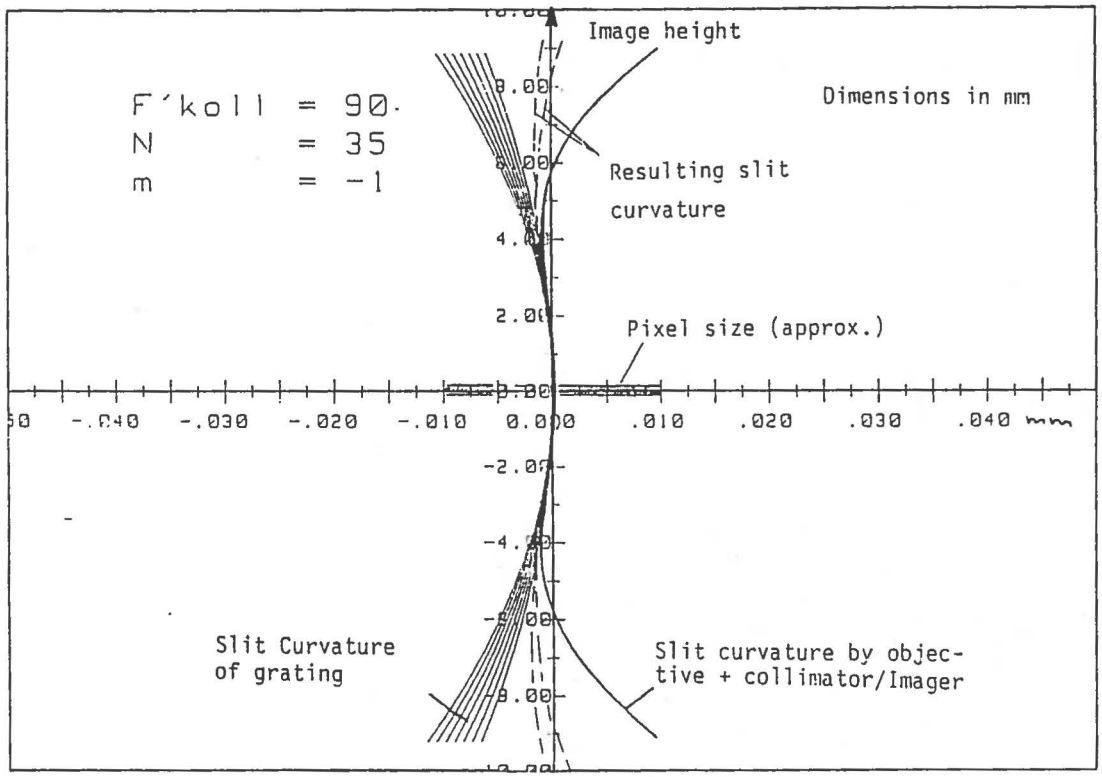

Fig. 4: ROSIS - Compensation of Grating/Slit Curvature by Collimator/Imager Optics

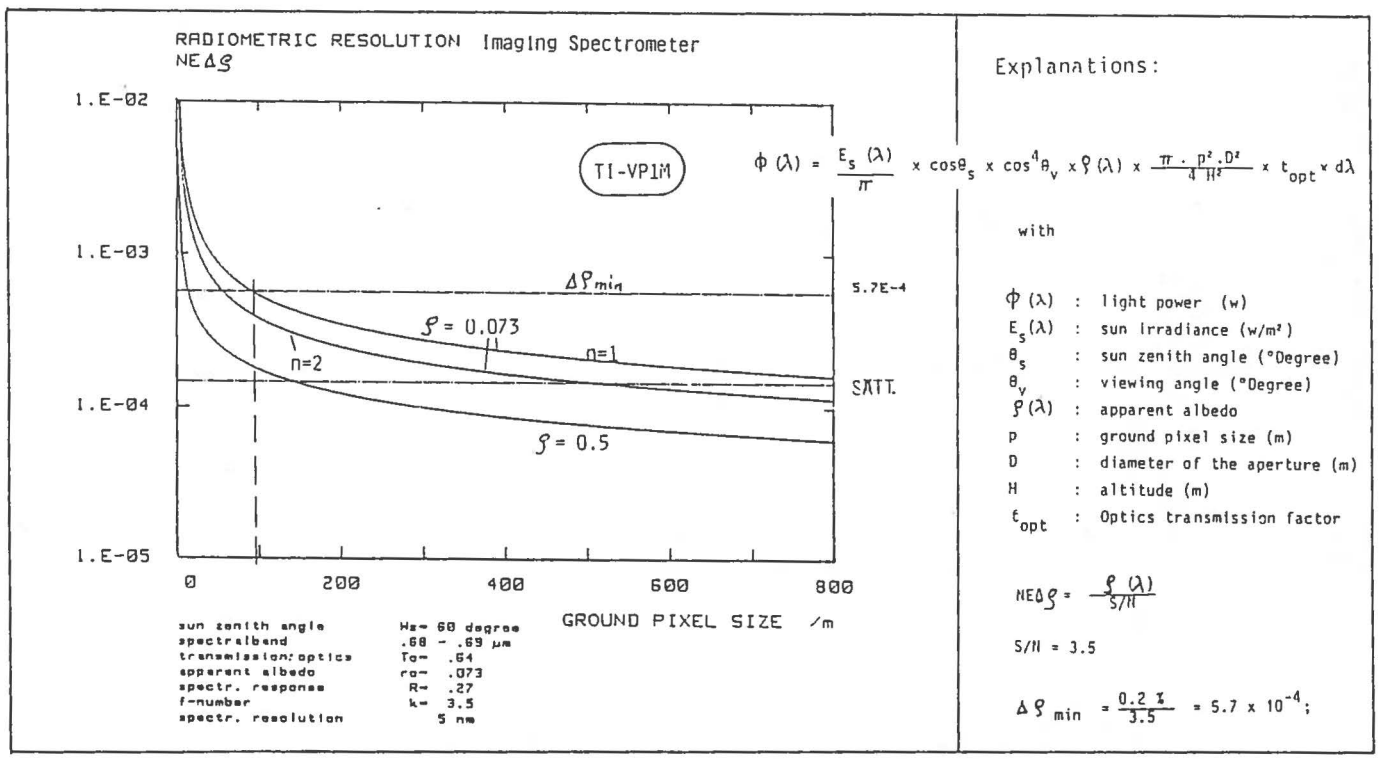

$$\Phi(\lambda) = \frac{E_s(\lambda)}{\pi} \times \cos\theta_s \times \cos^4\theta_v \times \rho(\lambda) \times \frac{\pi \cdot p^2 \cdot D^2}{4\,H^2} \times t_{opt} \times d\lambda$$

$$NE\Delta\rho = \frac{\rho(\lambda)}{S/N}$$

$$\Delta\rho_{min} = \frac{0.2\ \%}{3.5} = 5.7 \times 10^{-4};$$

Fig. 6: Example of radiometric Performance Analysis: Chlorophyll Fluorescence Channel at 685 nm
Note: Reference Detector Array TI-VP1M is not a frame transfer device but has been taken as the only available 1024² CCD detector array; the resulting feasible ground pixel size is about 100 m, however, this would require 3000 pixels per scan line and, thus, exceed current matrix detector array technology

$$S/N = \frac{n_s}{\sqrt{n_s + n_d^2 + n_{rms}^2}} \qquad n_s = \frac{\Phi(\lambda) \times R(\lambda) \times \tau}{e}$$

where $R(\lambda)$ is the spectral resonsivity of the detector (A/W)
τ is the integration time (s)
e the electronic charge ($e = 1.6 \times 10^{-19}$C)

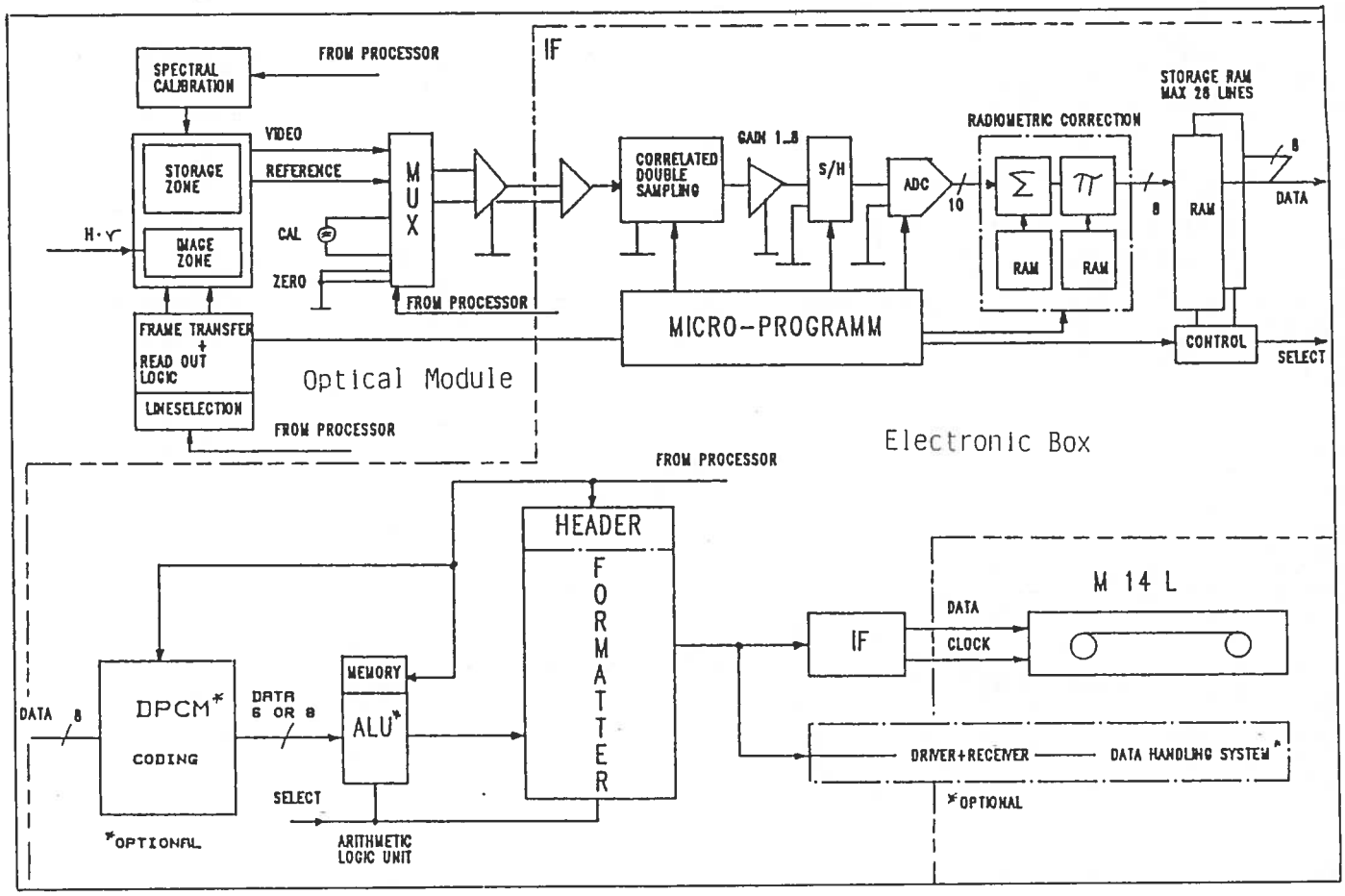

Fig. 7: ROSIS overall Electronics Block Diagramme

Tab. 3: Summary ROSIS Performance Data (Airborne and spaceborne Versions)

	Airborne Version		Spaceborne Version
	4km Altitude	8 km Altitude	(Altitude: 525 km)
Total FOV		± 16°	± 16°
Instantan. FOV		0.55 mrad	0.55 mrad
Swath Width (km)	± 1.15	± 2.3	± 150
Ground Pixel Size (m)	2.2	4.4	300
No. of Pixels/Scan Line	512		1024
No. of usable spectr. Channels		256	at a spectral range of 400nm ≤ λ ≤ 900nm
No. of selectable spectr. Channels		128	
No. of readout Channels		≤ 28	
Spectral Bandwidth per Channel	2/5 nm*)		5nm
Radiometr. Resolution Fluorescence Channel (685)	$< 10^{-4}$ of apparent albedo $\geq 2 \times 10^{-3}$		

*) 5 nm Baseline Concept, 2 nm feasible

Tab. 4: Summary ROSIS technical Specifications

Focal Plane Assembly Specifications (Detector Arrays)

Focal Plane Assembly:

Current detector array baseline: Thomson-CSF TH 7883 with:

- 512 (V) x 500 (H) pixels
- Pixel size: 23.5 x 18.5 µm
- > 3000 : 1 dynamic range
- 2 arrays (corresponding to 2 optics modules)

Preferred detector array:

- 1024 x 512 pixels (e.g. modified TI VPIM or extended TH 7883)
- 5000 : 1 dynamic range
- Current TI VPIM difficult to use because of virtual phase readout

Moderate TE cooling (-25° C) of FPA to reduce dark current noise

ROSIS overall technical Specifications

	Optics Module	Electronics Module	Total
Dimensions (cm)	24 x 28 x 45	22 x 21 x 42	
Weight	18	9.5	27.5
Electr. Power (W)			
- average	6	26	32
- peak	16 (heater)	36	52
Digital Data Rate (Mbps)			
- uncompr.	8.85 - 20 channels / 4.42 - 10 channels		
- compressed	3.7 - 20 channels / 1.85 - 10 channels		

Tab. 5: ROSIS Development Planning

MBB Imaging Spectrometer, Development Plan:	
Visible/NIR Version (0.4-1.0 μm):	
1985/86:	Concept definition (national funding)
1986/87:	Breadboard for laboratory verification (MBB inhouse funding)
1987/88:	Airborne test model, space compatible
1988/89:	In-orbit demonstration model for short-term ($\leq$30 d) verification in space
by 1993:	Operational version
SWIR Version (1.5-2.5 μm):	
1988/89:	Breadboard version (e.g. with MBB/IMEC arrays)
1990/91:	Airborne version
1992/93:	In-orbit demonstration model
MIR/TIR Version (3.5-15 μm):	
1989:	Concept definition
1994:	Spaceborne model

Tab. 6: Survey of preliminary candidate ROSIS Applications

Discipline/Application	Airborne Version $\Delta\lambda = 2.5$ nm	Spaceborne Version $\Delta\lambda = 5$ nm	Remarks
Oceanography			
- Chlorophyll Absorption/Fluorescence Monitoring	++ (regional)	++ (global)	Design Driver
• - Coastal Zone Water Quality	+ •	(+)	
Land Use			
- Vegetation Status Monitoring	++ •	+	• Combination with
• - Vegetation Disease Monitoring	++	+	high-resol. Scanner
- Vegetation Classific. Mapp	++	+	recommended
- Settlement Classific. + Mapp			
Hydrology			
• - Water Quality Monitoring	•	(+)	• Spatial resolution
- Chlorophyll Contents Monit.	++	(+)	limited for Spaceb.
- Sedimentation Mapping	+	(+)	version
Environmental Monitoring			
(*) - all above asterix applications			
- Air Quality Monitoring (Aerosol load)	+	+	
Glaciology			
- Snow/Ice Status (humidity, age . . .)	+	(+)	

++ fully applicable + valuable contributions (+) limitation through resolution/addit. sensors
• SWIR channel complementation

EUROPEAN SPACE AGENCY (ESA)

- AGREEMENT OF COOPERATION 9TH DECEMBER 1978

- RENEWED IN JANUARY 1984 FOR 5 YEARS

- CANADA CONTRIBUTES TO MANDATORY ACTIVITIES

- CANADA CAN JOIN OPTIONAL PROGRAMS: OLYMPUS, ERS-1

- REPRESENTATION AT COUNCIL AND PROGRAM BOARDS

PREVIOUS EXPERIENCE

GENERAL STUDIES

|

REMOTE SENSING PREPARATORY PROGRAM (RSPP)

1981-82

|

ERS-1 PHASE B

1983-84

|

ERS-1 PHASE C/D

1984-1989

|

ERS-1 PHASE E

1989-1990

ERS-1

- LAUNCH 1989 - PROBABLE SLIP TO 1990
- SPAR BUILDING RADAR X-BAND LINK
- COMDEV BUILDING RADAR COMPONENTS
- MDA BUILDING KIRUNA GROUND STATION
- GATINEAU GROUND STATION DESIGN PROCEEDING
- PROTOTYPE PROCESSOR COMPLETED
  - 1/50 REAL-TIME
- GROUND SYSTEM CONSTRUCTION TO START IN 1987
- RADAR APPLICATIONS FUNDING IN SPACE PLAN

EARTH OBSERVATION PREPARATORY PROGRAMME (EOPP)

OBJECTIVE

- TO ADVANCE THE DEFINITION STATUS AND PREPARATION OF FUTURE PROGRAMMES IN EARTH OBSERVATION SUCH THAT THE CORRESPONDING PHASES B, C/D AND E CAN BE APPROVED AND INITIATED.

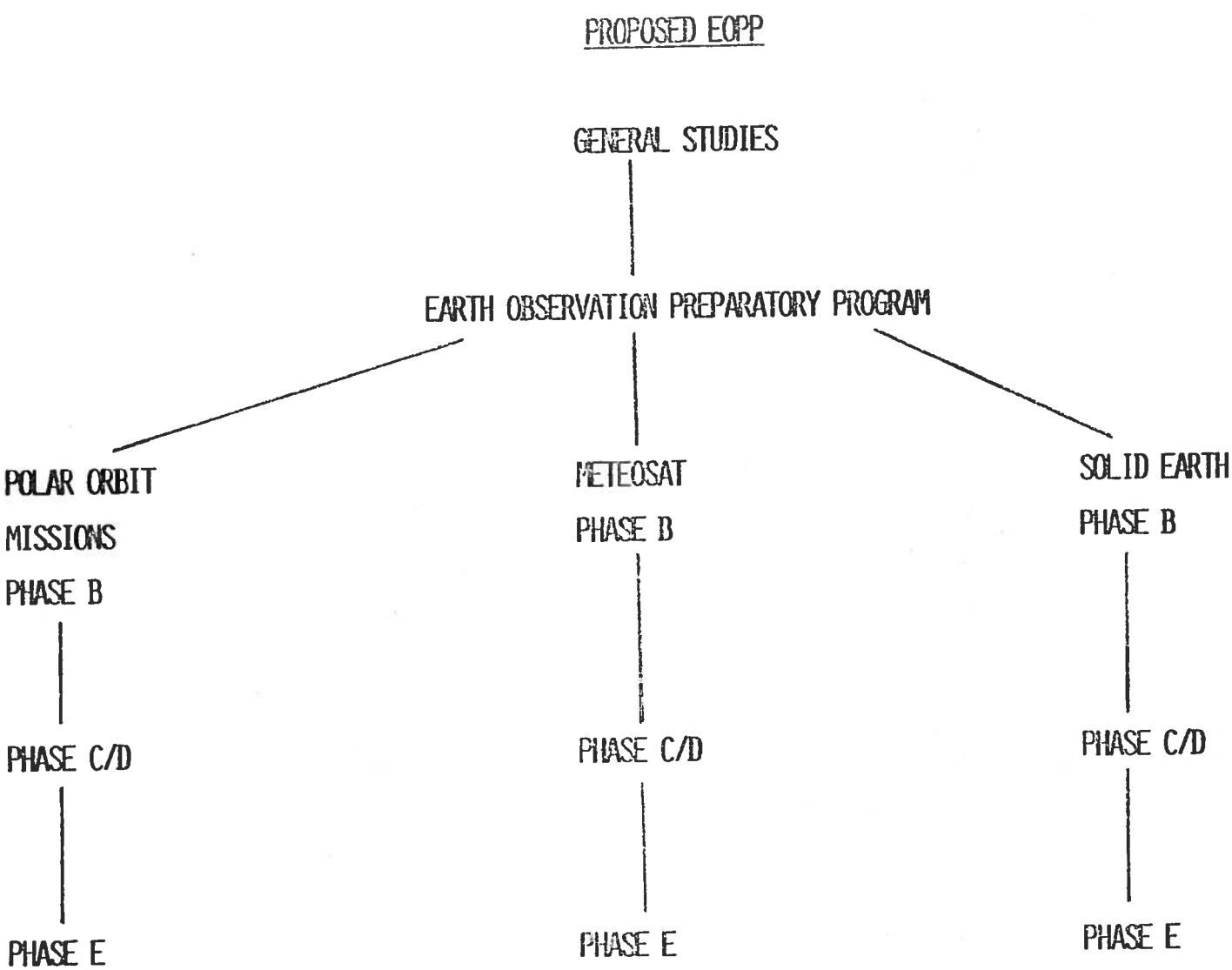
PROPOSED EOPP
GENERAL STUDIES
EARTH OBSERVATION PREPARATORY PROGRAM
POLAR ORBIT
MISSIONS
PHASE B
PHASE C/D
PHASE E
METEOSAT
PHASE B
PHASE C/D
PHASE E
SOLID EARTH
PHASE B
PHASE C/D
PHASE E

EOPP ACTIVITIES

- ESTABLISHMENT OF MISSION CONCEPTS
- SYSTEM STUDIES
- INSTRUMENT STUDIES
- FEASIBILITY STUDIES
- MEASUREMENT CAMPAIGNS
- INVESTIGATION OF BASIC TECHNOLOGY REQUIREMENTS
- PRE-DEVELOPMENT OF CRITICAL TECHNOLOGIES AND SUB-ASSEMBLIES
- ESTIMATION OF PROGRAM COSTS, SCHEDULES AND RISKS

OUTPUT OF EOPP

FOR EACH PREPARED PROGRAM:

- MISSION OBJECTIVES
- FEASIBILITY
- PROGRAM REQUIREMENTS
- ECONOMIC BENEFITS
- DEFINITION OF INSTRUMENTS
- DEFINITION OF GROUND SEGMENT
- RESULTS OF TRADE-OFFS
- LAUNCH AND SERVICING REQUIREMENTS
- FIRST COST ESTIMATE

EOPP

FINANCIAL

PARTICIPANT	%
BELGIUM	3.61
DENMARK	1.77
FRANCE	18.17
GERMANY	20.00
IRELAND	1.40
ITALY	11.00
NETHERLANDS	4.84
NORWAY	1.85
SPAIN	4.00
SWEDEN	3.78
SWITZERLAND	3.87
UNITED KINGDOM	15.18
CANADA	6.00
FINLAND	1.62
NOT YET COVERED	2.91
	100.00

	1986	1987	1988	1989	1990	TOTAL	
TOTAL (KAU)	6,447	13,104	13,736	14,286	11,230	58,803	[ASSUMES 4% P.A. INFLATION AND EXCHANGE RATE OF 1.27734]
CANADA 6% ($K)	338	1,004	1,053	1,095	861	4,401	

CANADIAN EOPP PRIORITIES

SYNTHETIC APERTURE RADAR	INSTRUMENT DEVELOPMENT
IMAGING SPECTROMETER	DATA PROCESSING
BREWER OZONE SPECTROPHOTOMETER	USER DEVELOPMENT

ECPP
PROCUREMENT PLAN

Issue No.: 2
Date: 1 SEP 1986

Page: 2 of Chapter 4

(Mid-1985 economic cond., 1986 exchange rates)

REF. NO.	TITLE OF ACTIVITY	PREV. REF. NO.	COST EST. (KAU) 1986	1987	1988	1989	1990	TOTAL	KEY EVENTS START	END	PROCUR. TYPE	POLICY PS	CONTRACT CATEGORY	PROCUR. STATUS	COMPANY/INSTITUTE/ REMARKS
I.2	* Advanced Instrument Studies (including adapt.to the PP)														
I.2.1	SAR		60	132				192	85/4	87/3	C		I		
I.2.2	Hi. Res. Opt. Imager		60	132				192	86/4	87/3	C		I		
I.2.3.	Wind Scatterometer		55	126				181	86/4	87/3	C		I		
I.2.4.	IMR		55	126				181	86/4	87/3	C		I		
I.2.5.	GC		55	126				181	86/4	87/3	C		I		
I.2.6.	Altimeter		55	126				181	86/4	87/3	C		I		
I.2.7.	Data Handling		30	77				107	86/4	87/3	C		DH		
I.2.8.	High res. thermal IR imager		50	100				150	86/4	87/3	C		I		
I.3.	* Longer term instr. studies														
I.3.1.	Imaging Spectrometer		55	126				181	86/4	87/3	C		I		
I.3.2.	Lidar		55	126				181	86/4	87/3	C		I		
I.3.3.	Limb Sounder		55	126				181	86/4	87/3	C		I		
I.4.	Unsolicited Proposals		75	165				240	-	-	-		-		
I.5.	Cooperative cost study (Expend./service.platform)		50	100				150	86/4	87/4	C		B		
	SUBTOTALS Page 2		710	1408	0	0	0	2118							

NOTES: Procurement policy:
C= Competitive
R= Restricted
D= Direct
PS= Participating State
Dates: Year/Quarter

NOTES: CONTRACT CATEGORY -See ANNEX

PROCUR. STATUS
A: AFP issued
P: Proposal received
I: Approved by IPC
S: Contract started
E: Contract ended

* Instrument studies are subject to finalization as a result of [PDR working

OVERVIEW OF THE TOTAL CANADIAN CIVILAN SPACE PROGRAM

Canadian Space Program expenditures for the next five years are summarized in the following table and chart.

Total Space Program Expenditures ($M)

CURRENT YEAR	NEXT FIVE YEARS				
1985/86	1986/87	1987/88	1988/89	1989/90	1990/91
158	148	160	170	166	180

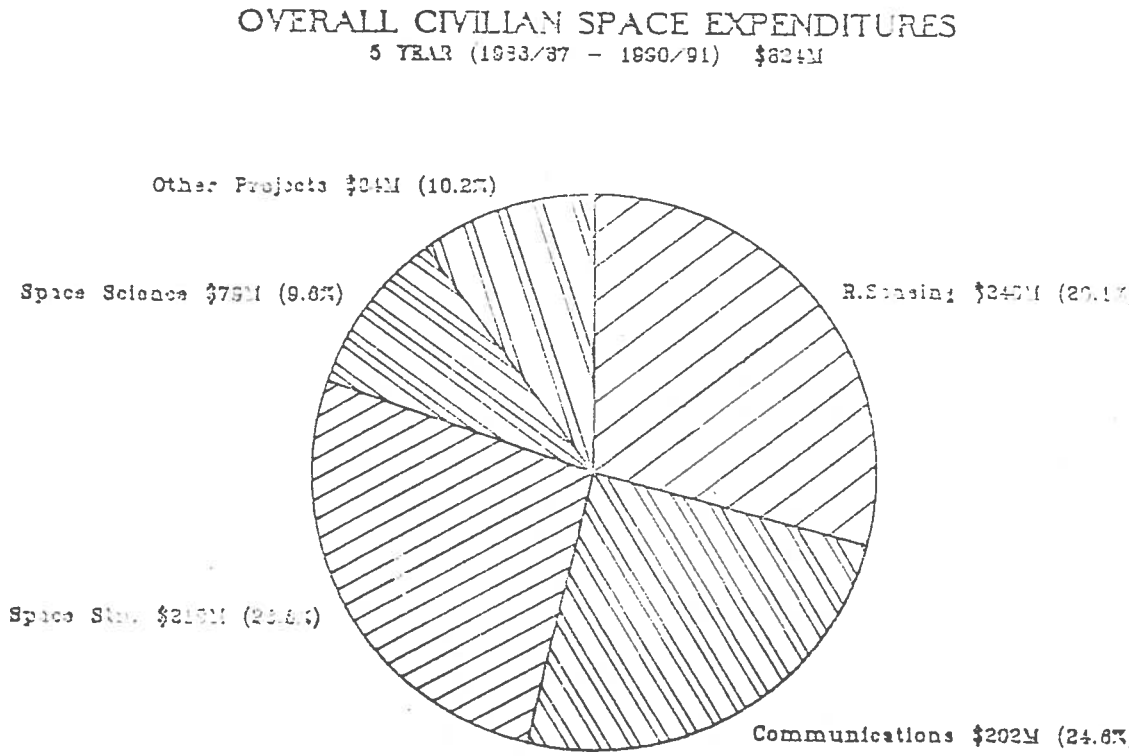

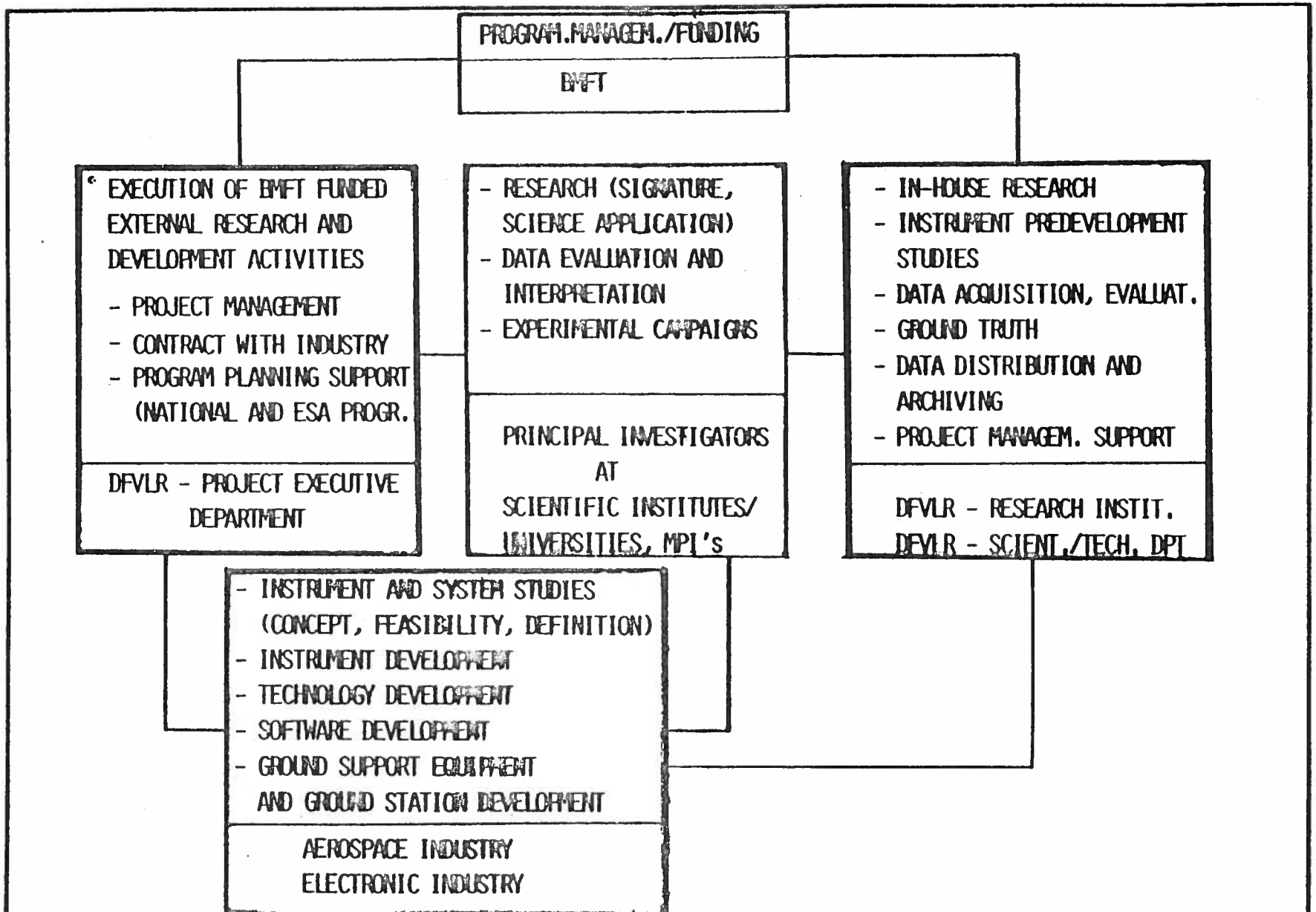

DFVLR
BPT

Fig.1 GERMAN EARTH OBSERVATION PROGRAM

PROGRAM STRUCTURE

SEP 1983

PROGRAMME GOALS

o THE GENERAL GOAL OF THE BMFT FUNDED PART OF THE NATIONAL EARTH OBSERVATION PROGRAMME IS

THE PROVISION AND UTILIZATION OF REMOTELY SENSED DATA FOR APPLICATIONS IN

- LAND OBSERVATION (AGRICULTURE, FORESTRY, GEOLOGY, REGIONAL PLANNING ...)
- PHYSICS OF THE SOLID EARTH
- PHYSICS OF THE OCEAN (INCL. MONITORING OF SEA ICE, COASTAL PHENOMENA ...)
- PHYSICS OF THE MIDDLE AND LOWER ATMOSPHERE, CLIMATE RESEARCH

o THE PROGRAMME INCLUDES TWO MAIN TASKS

I. INSTRUMENT DEVELOPMENT (~70 % OF THE BUDGET)

II. DEVELOPMENT OF METHODS FOR DATA PROCESSING AND DATA EVALUATION, DEMONSTRATION OF POTENTIAL USE OF REMOTELY SENSED DATA FOR GEOSCIENCE APPLICATION (~30 % OF THE BUDGET)
(TO OBTAIN SUCH DATA, SOURCES FROM ESA AND FOREIGN SPACE MISSION AS WELL AS FROM OWN EXPERIMENTAL INSTRUMENT FLIGHT WILL BE USED)

o BUDGET

PRESENTLY 16 MIODM, PLANNED MEDIUM TERM INCREASE UP TO 30 MIODM.

DFVLR RF-TN

Fig 2
ELEMENTS OF THE GERMAN EARTH OBSERVATION PROGRAMME

JULY 1986

PROGRAMME GOALS (CONT.)

- o IT IS NOT INTENDED TO DEVELOP AND OPERATE ANY EARTH OBSERVATION SATELLITES IN THE FRAMEWORK OF THE NATIONAL PROGRAMME.

  THEREFORE, IT IS RESTRICTED TO

  - THE DESIGN, DEVELOPMENT AND EXPERIMENTAL OPERATION OF SELECTED INSTRUMENTS WHICH PRIMARILY WILL TAKE FLIGHT OPPORTUNITIES IN SHUTTLE AND SPACELAB MISSIONS OR ESA SATELLITE MISSIONS

- o OBJECTIVES OF SUCH MISSIONS ARE
  - TO TEST NEW INSTRUMENT CONCEPTS AND MEASUREMENT METHODS,
  - TO DEVELOP AND APPLY NEW DATA PROCESSING TECHNIQUES AND INTERPRETATION METHODS
  - TO DEMONSTRATE POTENTIAL OF FUTURE OPERATIONAL USE

INSTRUMENT DEVELOPMENT

o LAND AND OCEAN OBSERVATION

OPTICAL IMAGING INSTRUMENTS:

- METRIC CAMERA
- MODULAR OPTO-ELECTRONIC MULTISPECTRAL SCANNER (MOMS)

TWO VIS CHANNEL IMAGER
SWIR IMAGER
STEREO IMAGER
IMAGING SPECTROMETER
} MOMS FAMILY

MICROWAVE RFMOTE SENSING INSTRUMENTS

- MICROWAVE REMOTE SENSING EXPERIMENT (MRSE)
- X-SAR

o PHYSICS OF SOLID EARTH

- PRECISE RANGE AND RANGE RATE EQUIPMENT (PRARE)

DFVLR RF-TN	Fig.3 ELEMENTS OF THE GERMAN EARTH OBSERVATION PROGRAMME	JULY 1986

INSTRUMENT DEVELOPMENT (CONT.)

o ATMOSPHERIC PHYSICS (STRATOSPHERE, MIDDLE ATMOSPHERE)
  - MILLIMETER WAVE ATMOSPHERIC SOUNDER (MAS)
  - MICHELSON INTERFEROMETER FOR PASSIVE ATMOSPHERIC SOUNDING (MIPAS)

o CLIMATOLOGY (RADIATION BUDGET)
  - CONICAL SCANNING RADIOMETER (CSR)

DFVLR RF-TN	Fig.3 ELEMENTS OF THE GERMAN EARTH OBSERVATION PROGRAMME	JULY 1986

DATA PROCESSING / DATA EVALUATION

o PARTICIPATION IN FOREIGN OR INTERNATIONAL MEASUREMENT CAMPAIGNS.

EXAMPLES:

- SAR 580
- AGRISAR

o PARTICIPATION IN FOREIGN EXPERIMENTAL MISSIONS.

EXAMPLE: SIR-B

o PREPARATION ON ERS-1 DATA EVALUATION FOR APPLICATIONS IN

- OCEANOGRAPHY, CLIMATOLOGY
- GEODESY, GEOPHYSICS
- SEA ICE MONITORING
- LAND OBSERVATION (AGRICULTURE, FORESTRY, GEOLOGY, REGIONAL PLANNING ...)

o DEVELOPMENT OF METHODS FOR DATA EVALUATION AND INTERPRETATION

EXAMPLES: UTILIZATION OF STEREOSCOPIC SPOT DATA FOR TOPOGRAPHIC MAPPING;
METHODS FOR MULTIDISCIPLINARY APPLICATION ORIENTED EVALUATION
OF REMOTE SENSING DATA

DFVLR RF-TN	Fig4ELEMENTS OF THE GERMAN EARTH OBSERVATION PROGRAMME	JULY 1986

OUTLOOK

- CONTINUING INSTRUMENT DEVELOPMENT ACTIVITIES.
  FLIGHTS/REFLIGHTS OF SELECTED INSTRUMENTS WILL MAINLY BE REALIZED IN NASA SHUTTLE MISSIONS/D-2 SPACELAB MISSION.
  THOSE MISSIONS WILL SERVE AS EXPERIMENTAL STEPS ON THE WAY TO FUTURE OPERATIONAL MISSIONS ⟶ POLAR PLATFORM

- MAIN AREAS OF FURTHER INSTRUMENT DEVELOPMENTS:
  - ACTIVE MICROWAVE REMOTE SENSING (X-SAR)
  - OPTICAL IMAGING WITH STEREO CAPABILITY AND/OR IMAGING SPECTROMETRY (MOMS-TYPE)
  - MILLIMETER WAVE RADIOMETRY AND INFRARED INTERFEROMETRY FOR ATMOSPHERIC RESEARCH (MAS, MIPAS)
  - REMOTE SENSING WITH LIDAR SYSTEMS
  - SCANNING IR RADIOMETRY FOR CLIMATE RESEARCH (CSR)

- DATA PROCESSING AND EVALUATION ACTIVITIES:
  PREPARATION OF FUTURE EARTH OBSERVATION SATELLITE DATA EVALUATION (DEVELOPMENT OF ALGORITHMS, DEVELOPMENT AND VALIDATION OF MODELS, PILOT AND DEMONSTRATION CAMPAIGNS).

DFVLR RF-TN	Fig.5ELEMENTS OF THE GERMAN EARTH OBSERVATION PROGRAMME	JULY 1986

German-Canadian Workshop on Chlorophyll Fluorescence
Ottawa, October 1986

SOME POSSIBLE METEOROLOGICAL APPLICATIONS OF AN IMAGING SPECTROMETER

Hartmut Graßl
Forschungszentrum Geesthacht
Max-Planck-Straße 1
D-2054 Geesthacht, FRG

1. Introduction

Imaging spectrometers allow a nearly simultaneous high resolution (spectral or/and spatial) imaging of natural surfaces. Depending on the choice of spectral channels different specific applications may be optimized. While the existing FLI (Fluorescence Line Imager, Moniteq) and the planned ROSIS (Reflective Optics System Imaging Spectrometer, MBB) were both primarily designed for water colour and are or could be used for vegetation stress monitoring also, a new application in atmospheric physics would surely boost both instruments.

This short note shall point to four applications of an imaging spectrometer with detector arrays sensitive at wavelength from 0.5 to 1.0 µm. The four uses are:

- cloud height
- optical depth of clouds and mean cloud droplet size
- spectral albedo of snow or mean crystal size
- water vapour column content.

All possible four uses will be characterized by only a short information on

- basic physical principle
- spectral channel position
- importance for meteorology and climatology.

2. Cloud Height

2.1 Principle

If optically thick clouds are replacing a partly reflecting natural solid surface if viewed from above the ratio R of upward spectral radiances within I_a and outside I_w an absorption band of an atmosphereic gas will grow with cloud height, since the absorption of the layers below the main reflecting upper part of a cloud is no longer so effective. If the absorbing gas is well mixed like molecular oxygen (O_2) the ratio R is a direct measure of the pressure within the backscattering cloud layers. Pressure in turn is easily changed into height if the pressure-height relationship is approximately known for an area.

2.2 Channels

The centre of the 0.76 µm O_2-band offers a position for the $I_{\lambda a}$ channels. One or preferably two nearby window channels allow a determination of R without any absolute calibration. The accuracy of cloud height determination is a weak function of the extinction coefficient $e_{\lambda w}$ in the window channels in the upper cloud layer, is also depending on spectral resolution of the O_2-channel and on sun elevation, however, is nearly independent on aerosol particle backscatterng. A computer simulation using an azimuthally dependent radiative transfer code has been started and should also show the possible use of one or two more O_2-channels in order to determine cloud height also for optically thin clouds.

2.3 Importance

Correct cloud height assignment within an image would - besides allowing global climatologies of cloud height - enhance a number of remotely sensed meteorological variables, however, most strongly

- temperature profile
- water vapour profile
- longwave net flux at cloud height

3. Clouds: Optical Depth and Droplet Size

3.1 Principle

The albedo of a water cloud is no simple function of the liquid water path. It is strongly varying - at fixed optical depth - with mean drop size. If, however, weak liquid water absorption bands in the 0.7 to 1.0 µm range are used both optical depth and droplet size distribution mode radius may be inferred.

The spectral albedo or radiance minima within the absorption bands become deeper both with increasing droplet size and increasing optical depth but differently for different drop sizes, thus possible enabling a separation of the optical depth and size effect.

3.2 Channels

The optimized channel positions are

- maximum liquid water absorption
- minimum liquid water absorption

leading to maximum upward radiance differences between absorption and window channels which contain the droplet size and optical depth information. Window and absorption channels should avoid water vapour absorption bands. At least two channels of each type should be available. Whether an absolute calibration is needed cannot be answered at present. A careful simulaton study is needed before answering.

Some disturbance might be caused by absorption of aerosol particles within, on or outside the droplets. The drop size retrieved would also be biased towards droplet size within the top layers of a cloud.

3.3 Importance

The knowledge of optical depth and mean droplet size in an aerial overview would extremely enhance our understanding of cloud physics and would also improve the remote detection of related parameter like solar radiation at the surface and liquid water path.

4. Spectral Albedo of Snow or Mean Snow Crystal Size

4.1 Principle

Ice, like liquid water, also has weak absorption bands in the 0.7 to 1.0 µm range, shifted to somewhat longer wavelengths. As for the size of cloud droplets also for crystal size these absorption bands mark minima in snow covered surface reflection.

The depth of these minima is firstly a function of crystal or floc size and secondly of crystal shape. Thus, the spectral near infrared albedo of snow also contains more than just a reflectivity information.

4.2 Channels

Compared to section 3 no drastic change in channel selection occurs. If the shift to longer wavelength is accounted for and if water vapour absorption is circumvented section 3.2 is also applicable. In both applications (section 3 and 4) a measurement above 1.0 µm within stronger liquid water and ice absorption bands would increase the accuracy of droplet or crystal size retrievals as long as the signal-to-noise ratio - thereby accounting for increased channel differences - is as high as in the shortest infrared range.

4.3 Importance

Over the inland ice sheets an information on mean crystal size in the uppermost layers of a snow pack increases the information on snow methamorphosis, enables the detection of fresh snow or may enable the discrimination of rime areas. If informatoin from visible channels is added, the contamination of snow by soot may be detected.

5. Water Vapour Column Content

5.1 Principle

The water vapour vibration rotation bands from 0.6 to 1.0 µm wavelength offer a way for day-time water vapour column content determination. The relative differences or ratios of upward radiances in and outside these

absorption bands are a strong function of water vapour column content, they are modified by geometry (sum elevation and remote sensing viewing angle) and they are weak functions of the temperature profile.

5.2 Channels

As for cloud height and cloud optical depth channels in and outside rather weak absorption bands are necessary. The spectral resolution is not really important since rather broad absorption features as well as windows exist within the 0.7 to 1.0 µm domain. In order to avoid too much temperature dependence of radiance ratios or relative radiance differences the least temperature dependent parts of the absorption bands should be chosen. Again a careful simulation accounting for geometry, channel number required for specific accuracies and temperature dependence is a prerequisite of an application.

5.3 Importance

Water vapour is the least known important meteorological variable in many areas of the globe. The present meteorological satellites with thermal IR channels derive water vapour information only after the determination of temperature profiles. Their accuracy reaches 0.2 - 0.3 gcm^{-2} water vapour content which is for most atmospheres accurate roughly to 10 %. The proposed method would be more accurate especially for cold atmospheres and would be nearly independent on a temperature profile information, however, would also fail in cloudy areas.

6. Combination of Applications

The above four applications - if combined - would not only add their specific retrieved parameters but would enhance the accuracy of all the parameters retrievable. As an example the knowledge of water vapour column content gives a correction of possible remaining influences on snow albedo and on optical depth of low lying clouds. No more than 10 channels would be sufficient for all tasks, since the window channels needed in all sections could remain the same.

For the above applications simulations have been (section 2) or will be (sections 3 to 5) started soon in order to be able to use optimized channels as soon as the airborne version of ROSIS is available.